# AN ABSTRACT OF A THESIS

## MODELING, ANALYSIS AND CONTROL OF SINGLE PHASE DC-AC MULTI-LEVEL CONVERTERS

Bhanu Naga Venkata Manideep Angirekula

Master of Science in Electrical and Computer Engineering

Multi-level cascaded H-bridge (CHBMC) single phase DC-AC converter with reduced voltage ripple can be an advantageous utility as an interface between the photovoltaic panels and the utility grid. The CHBMC is a DC-AC converter with multiple DC sources. When the individual converters are modulated using unipolar PWM scheme, in which the carrier waves are appropriately shifted, the output waveforms are known to be improved. The performance of this unipolar PWM scheme has not been investigated when the input DC voltages are unequal. Using the double Fourier series approximation of the converter switching functions, a model was derived that enables the elimination of certain harmonic components in the output voltage. This method is proposed for two, three, four and five cell cascaded H-bridge converters. The proposed method also considers the maximum utilization of input DC sources to determine the appropriate modulation signals. Simulation results obtained using a MATLAB/Simulink platform and compared with experimental results validate the proposed method.

Multi-string multi-level inverter topologies similar to two, three and four cells cascaded H-bridge inverters are presented as they reduce the required number of switches than CHB to obtain the same desired output voltage. Moreover, the modeling and analysis of the multi-string multi-level inverter have not been presented anywhere else. Hence, a Karnaugh mapping technique which is rarely used in power electronics is proposed to model the converter. The Fourier series analysis which was used to determine the expression for modulation signals is also proposed. Computer simulation results obtained using a MATLAB/Simulink platform verify the proposed double Fourier series analysis and experimental results validate the proposed method.

The active and reactive power control schemes of single phase multi string multi-level converter with LCL filter connected to the grid are designed in $qd$ synchronous reference frame. The transformation to $qd$ synchronous reference frame from single phase is not well established as the Park's transformation requires a minimum of two orthogonal signals to transform. Hence, a fictitious orthogonal signal is generated using the all pass filter (APF) method to transfer the two signals into $qd$ reference frame. Using the APF, a three phase $qd$ phase locked loop (PLL) control scheme is applied to the single phase system. The scheme to control the active and reactive powers going into the grid is set forth. Computer simulation results obtained using a MATLAB/Simulink platform verifies the proposed control scheme.

**MODELING, ANALYSIS AND CONTROL OF SINGLE PHASE DC-AC MULTI-**

**LEVEL CONVERTERS**

A Thesis

Presented to

the Faculty of the Graduate School

Tennessee Technological University

by

Bhanu Naga Venkata Manideep Angirekula

In Partial Fulfillment

of the Requirements of the Degree

MASTER OF SCIENCE

Electrical Engineering

May 2014

**CERTIFICATE OF APPROVAL OF THESIS**

**MODELING, ANALYSIS AND CONTROL OF SINGLE PHASE DC-AC MULTI-LEVEL CONVERTERS**

by

Bhanu Naga Venkata Manideep Angirekula

Graduate Advisory Committee:

| | |
|---|---|
| Joseph Ojo, Chairperson | Date |
| Periasamy Rajan | Date |
| Ghadir Radman | Date |
| Ahmed Kamal | Date |

Approved for the Faculty:

Mark Stephens
Senior Associate Provost
for Academic Affairs

Date

ii

**DEDICATION**


    This work is dedicated to my father Angirekula Raghunadha Rao, my mother Angirekula Lakshmi, my eldest sister Mayuri and her husband Megharaju Bandaru, my elder sister Madhuri and her husband Maganti Venkata Chandrakanth.

# ACKNOWLEDGEMENTS

# TABLE OF CONTENTS

# LIST OF FIGURES

# LIST OF TABLES

# CHAPTER 1

# INTRODUCTION

## 1.1 Introduction

This chapter gives a brief overview on the renewable energy resources available, and introduces the cascaded H bridge multi-level converter, which is one of the topic of this thesis. This thesis focuses on the Karnaugh mapping technique, modulation schemes, Fourier series analysis of cascaded H bridge multi-level converter and multi string multi-level converter. The objectives of this work are clearly described. Finally, the organization of the thesis is presented.

## 1.2 Renewable Energy Resources

A study of renewable energy resources is presented in [1]. The Fossil fuel-based technologies have advanced our quality of life based on fossil fuel. The use of fossil fuel in our day to day life comes at a very high price. The use of fossil fuels must be controlled and the usage of renewable energy resources has to be increased to save the fossil fuels – oil, natural gas, and coal - for the future and to reduce the cost on the middle class person. The usage of renewable energy resources will also minimize global warming. The empowerment of every energy user in a new energy economy based on

renewable sources is to make him/her an energy manager by conserving energy, reducing carbon footprints, and installing distributed renewable energy sources.

To meet the carbon reduction targets, it is important to use the sources of energy that are renewable and sustainable. There is a need to replace the traditional fossil fuel based vehicles with electric cars, and the stationary power from traditional fuels, coal, gas and oil, with green sources for sustainable energy fuel for the future. Some of the renewable energy resources are discussed in [1]. The most important renewable energy resources are discussed here.

### 1.2.1    Fuel Cell

Apart from the renewable energy resources, such as wind and the sun, hydrogen ($H_2$) is an important source of renewable energy. Hydrogen is abundantly available in the universe. When hydrogen is used as a source of energy, it gives off only water and heat with no carbon emissions. Hydrogen fuel cells are used to generate electric energy at stationary electric power-generating stations for residential, commercial, and industrial loads. Figure 1.1 shows the equivalent circuit of fuel cell.

### 1.2.2    Solar and Photovoltaic

Solar and photovoltaic (PV) energies are very important renewable energy sources. The heat energy from the sun - solar thermal energy – can be used to heat water

to a high temperature and pressurized in a conventional manner to run a turbine generator.

Solar PV sources are arrays of cells of silicon materials that convert solar radiation into direct current electricity. The cost of a crystalline silicon wafer is very high, but new light absorbent materials have significantly reduced the cost. The manufacture of PV cells is based on two different types of material:
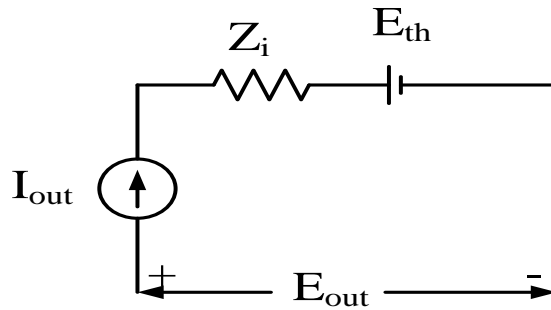
Figure 1.1 Equivalent circuit of a fuel cell.
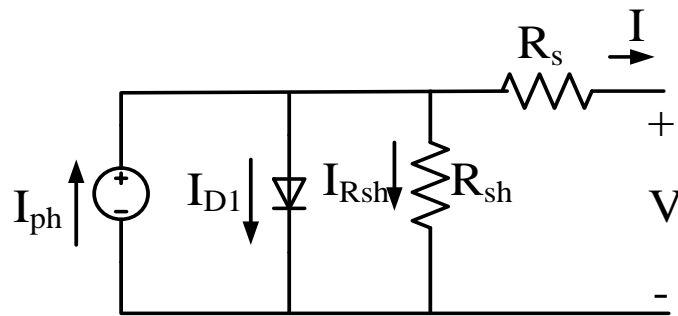
Figure 1.2: The single exponential model of a Photovoltaic module.

- a semiconductor material that absorbs light and converts it into electron-hole pairs, and

- a semiconductor material with junctions that separate photo generated carriers into electrons and electron holes.

The single exponential model of a PV module is shown in Figure 1.2.

The face of the PV module is designed to allow maximum light energy to be captured by the silicon materials. In the above model, the PV module is represented by a current source $I_{ph}$ in parallel with the shunt resistance $R_{sh}$. The single exponential model is given by (1.1).

$$I = I_{ph} - I_o \left\{ \exp\left[ \frac{q(V + IR_s)}{n_c AKT} \right] - 1 \right\} - \frac{V + IR_s}{R_{sh}} \qquad (1.1)$$

where A is the diode quality factor,

$n_c$ is the number of cells in the module,

$k$ is the Boltzmann's constant,

$q$ is the electronic charge,

$T$ is the ambient temperature in Kelvin.

### 1.3 Multi-level Converters

The multi-level voltage source inverters in the medium voltage energy management market provide a cost effective solution for industries [2]. In multi-level converters, the desired output voltage is synthesized by combining one or more separate DC sources depending on the type of the multi-level converter. The most common independent sources used are photovoltaic panels, fuel cells, batteries and ultra-capacitors

[3]. The main advantages of multi-level converters are low harmonic distortion of the desired output voltage, low electromagnetic interference, high efficiency and the ability to operate at high voltages.

A multilevel converter has several advantages over a conventional two-level converter that uses high switching frequency pulse width modulation (PWM). The attractive features of a multilevel converter can be briefly summarized as follows.

- Multilevel converters not only can generate the output voltages with very low distortion, but also can reduce the dv/dt stresses; therefore electromagnetic compatibility (EMC) problems can be reduced.

- Multilevel converters produce smaller common mode voltage; therefore, the stress in the bearings of a motor connected to a multi-level motor drive can be reduced.

- Multilevel converters can draw input current with low distortion.

- Multilevel converters can operate at both fundamental switching frequency and high switching frequency PWM. It should be noted that lower switching frequency usually means lower switching loss and higher efficiency.

The multi-level converters in general are categorized into three commercial topologies

- Diode clamped multi-level converter.

- Capacitor clamped multi-level converter.

- Cascaded H-bridge multi-level converter.

The applications of diode clamped multi-level converters include high power AC motor drives in fans, mills and pumps. The capacitor clamped multi-level converters have

been used in high-bandwidth high-switching frequency applications such as medium voltage traction drives. The cascaded H-bridge multi-level converter which will be discussed further has been applied to high power and high quality applications such as reactive power compensators, photovoltaic power conversion, and uninterruptible power supplies [4].

The topologies of the four classical types of multi-level converters are discussed below.

### 1.3.1    Diode Clamped Multi-level converter

Since the voltages across the semiconductor switches are limited by the conduction of diodes connected to various DC levels, this type of multi-level inverters is termed as diode clamped multi-level inverters. It has been shown that the principle of diode-clamping to DC link voltages can be extended to any number of voltage levels [4]. The simple topology of diode clamped multi-level converter is shown in Figure 1.3. The advantages of 'm' level diode clamped multi-level inverters are as follows:

- A large number of levels 'm' yields a small harmonic distortion.

- All phases share the same DC Bus.

- Reactive power flow can be controlled.

- High efficiency for fundamental switching frequency.

- The control method is relatively simple.

The disadvantages of 'm' level diode clamped multi-level inverters are as follows:

- Excessive clamping diodes (*m-1*)(*m-2*) are required per phase.

- Real power flow is difficult because of the unbalancing of capacitors.

- Different current ratings for switch devices are required due to their conduction duty cycle.
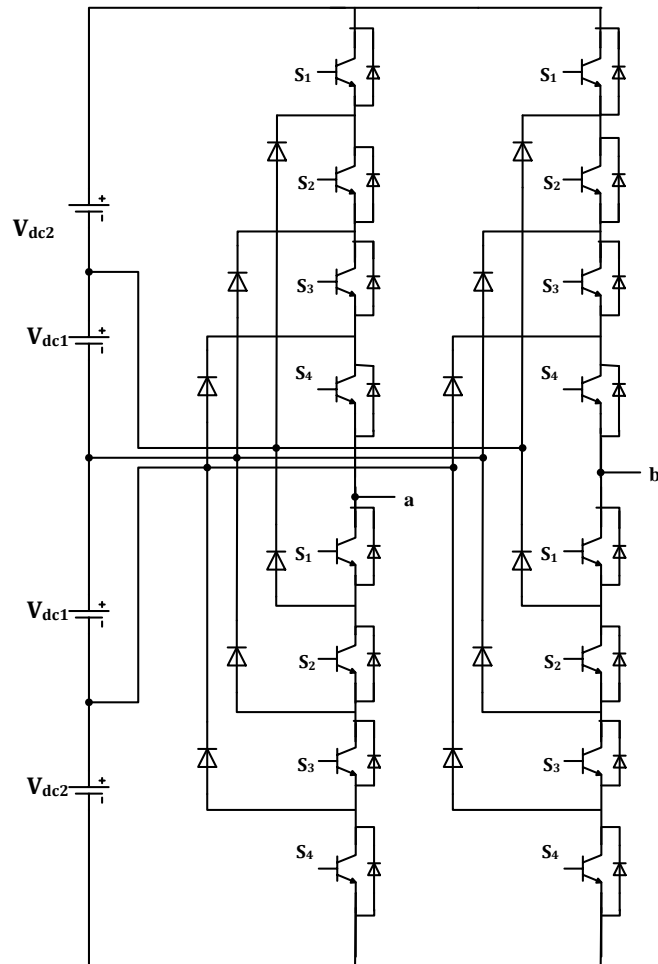


Figure 1.3: Single phase five level diode clamped inverter.

### 1.3.2 Capacitor Clamped Multi-level converter

The capacitor clamped, alternatively known as flying capacitor has several advantages and disadvantages. The simple topology of a three level capacitor clamped inverter is shown in Figure 1.4.

The advantages of '$m$' level capacitor clamped Multi-level converter are as follows:

- Large '$m$' allows the capacitors extra energy during long discharge transient.

- Flexible switch redundancy for balancing different voltage levels.

- Lower total harmonic Distortion when the levels $m$ is high.

- Real and Reactive power flow can be controlled.

The disadvantages of $m$ - level capacitor clamped multi-level converter are as follows:

- Large numbers of capacitors are bulky and generally more expensive than the clamping diodes used in the diode-clamped multi-level converter.

- Complex control is required to maintain the balance of capacitor voltages.

- Poor switching utilization and efficiency for real power transmission.
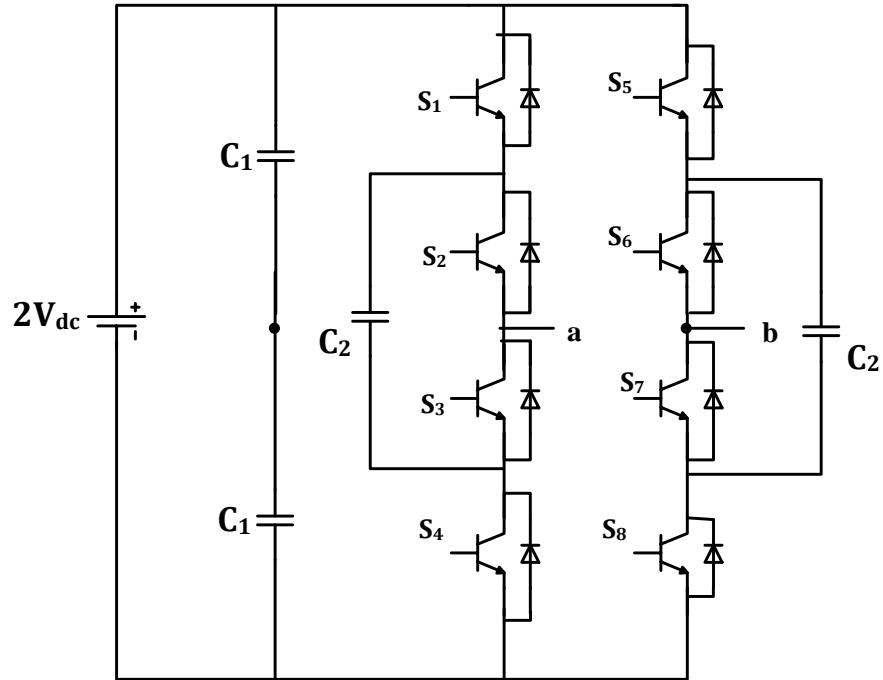
Figure 1.4: Single phase five level capacitor clamped inverter.

### 1.3.3    Cascaded H-bridge Multi-level converter

The cascaded H-bridge multi-level inverter is generally used when there are more than one DC source. Because of this limitation, this converter is mostly used for renewable energy resources like photovoltaic panel or fuel cell. The advantages of a cascaded H-bridge multi-level converter with 's' separate DC sources per phase are as follows:

• The series structure allows a scalable, modularized circuit layout and packaging since each H-bridge has the same structure.

- Different DC voltage source ratios can be applied in order to achieve different voltage levels in the output signals.

- Requires the least number of components considering that there are no extra clamping diodes or voltage balancing capacitors.

- Switching redundancy for inner voltage levels is possible because the phase output voltage is the sum of the each bridge's output.

- Potential of electrical shock is reduced due to the separate DC sources.

- The fact that multilevel converters need several DC sources in the DC side makes them attractive for Photovoltaic (PV) applications.

- Device voltage sharing is automatic and there is no restriction on switching patterns.

- Cascaded multi-level converter (CMC) has smaller dv/dt compared to series connected 2-level.

-  The modularity of this topology is an important feature, and because of that some redundancy is possible by using more cells per phase than is actually required.

- Because of its modular structure, control strategy is relatively easy.

- Compared to other multilevel topologies, CMC requires least number of components, since there is no need for clamping diodes and flying capacitors.

- The CMC has redundant Inverter Operation and Scalability.

The main disadvantage of a cascaded H-bridge multi-level converter is that this converter is limited to certain application where separate DC Sources are available.
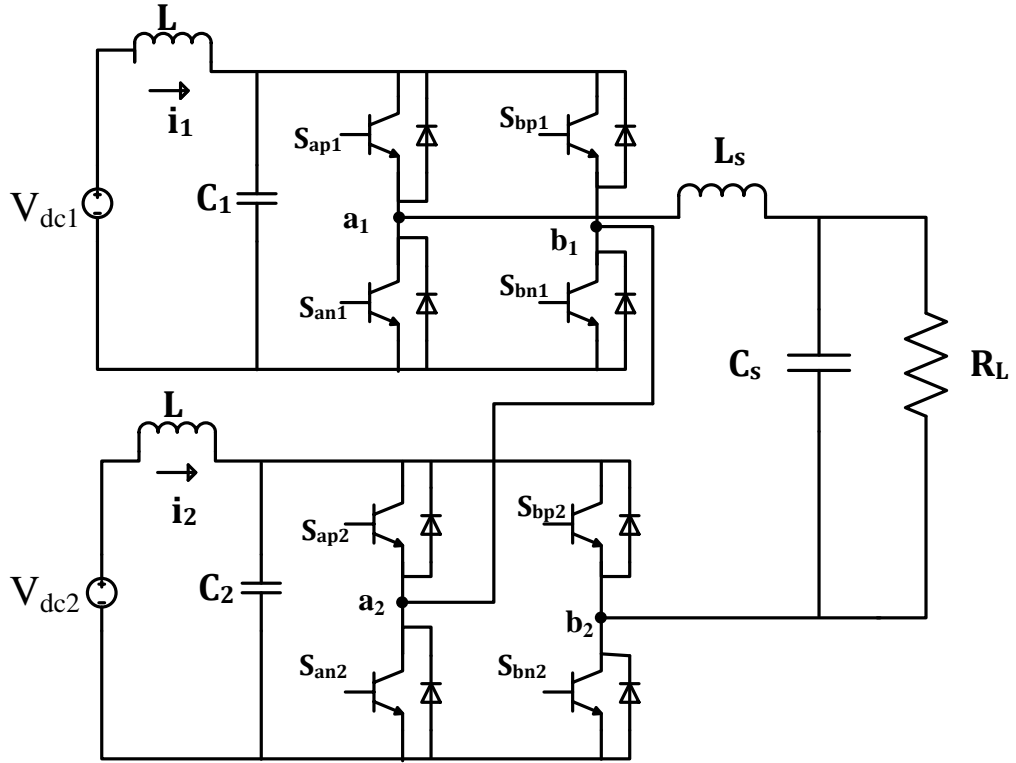
Figure 1.5: Single phase five level cascaded H bridge converter connected to 'R' load through an LC filter.

## 1.3.4 Modular Multi-level Converter (MMC)

Recently, a multilevel converter topology based on cascaded modular cells that do not require a multi pulse transformer has been proposed [5]. This topology, called the modular multilevel converter (MMC), uses series-connected modular cells fed by floating dc capacitors and can manage dc or ac input voltages, generating controlled output currents [6]. One of the main challenges of the MMC control system is the simultaneous control of the output currents, the generation of a proper input current reference to

provide the power required by the load and also keep the dc voltages at the reference

value, and the balance of the capacitor voltage among cells [7].

Figure 1.6 illustrates the single phase modular multilevel inverter consisting of

'8' individual cells in each leg. By switching a number of cells in the upper and lower

arm of each leg, the voltage $V_d$ is adjusted. In a similar manner, the voltage $V_{AB}$ can be

adjusted to a desired value.
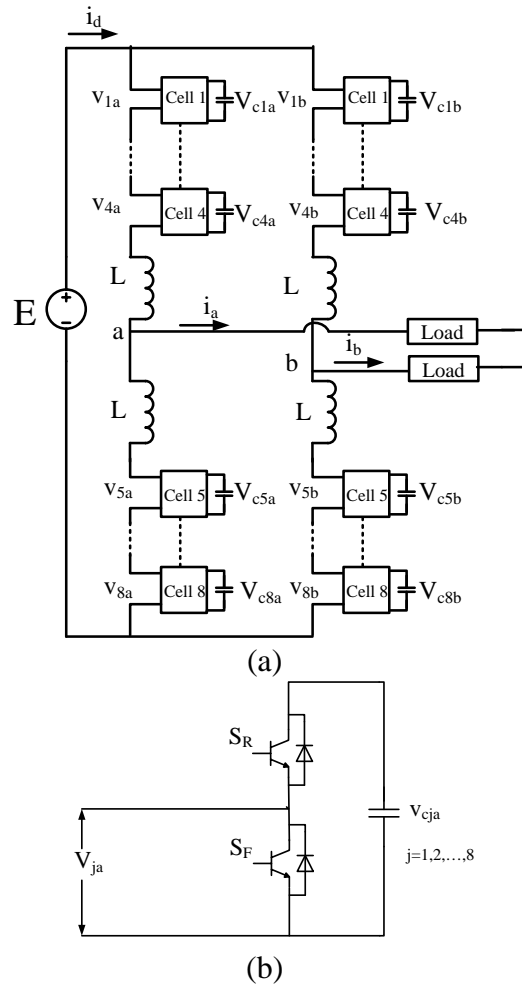


Figure 1.6: Single phase Modular Multilevel converter (a) Topology, (b) Individual Cell

The structural characteristics of the MMC topology offer many technical and economic advantages.

- Due to its modular construction, the life-cycle maintenance and operating costs could be more economic than those of other multilevel converters.

- It is also relatively easier to adjust the voltage and power levels because its scalable voltage level can implement the staircase output waveforms.

- The more steps enable the lower switching frequency, leading to lower total harmonic distortions and switching losses.

The MMC topology is often featured with its robustness for component failures. Low-level VSC topologies generally require high-voltage (HV) switching devices where several semiconductors are connected in series and work simultaneously for desired HV blocking ability. When one of the semiconductors is faulted, it may cause critical system failure. In the case of MMC, more reliable LV semiconductor devices are used as switches in a sub module so that the fail-safe functionality can be easily implemented merely by bypassing a corresponding faulted sub module. However, it is interesting to note that this well-known fail-safe functionality on device failures of MMC due to its topology and operational redundancy has neither been detailed with a commonly used simulation tool nor evaluated regarding its operational influence on the components inside or outside the MMC [8].

## 1.4 Objectives of the Thesis

The major objectives of the thesis are as follows:

- To model and analyse multi cell cascaded H-bridge multi-level converter especially two cell, three cell and four cell.

- To eliminate the dominant harmonics in the output voltage waveforms the using double Fourier series analysis.

- To determine the expressions of the unipolar PWM modulation signals for two cell, three cell and four cell cascaded H-bridge inverters using the double Fourier series analysis.

- To develop a novel multi-string multi-level inverter topology for distributed energy resources.

- To design, model and analyse the multi-string multi-level inverter topology especially for five, seven and nine levels.

- To demonstrate the use of the Karnaugh Mapping Technique (KMT) in power electronic converters.

- To determine the expressions for the modulation signals of multi-string multi-level inverter using the double Fourier series.

- To compare the switching losses between cascaded H-bridge multi-level converters and multi-string multi-level converter.

- To generate the switching pulses required from the Digital Signal Processor (DSP) for experimental hardware setup.

- To control the active and reactive powers going into the grid when the multi string multi-level inverter is connected to the grid.

- To achieve the phase synchronization of grid voltage and frequency with the filtered voltage and frequency, a Phase Locked Loop (PLL) control for the single phase system is to be implemented in the grid connected systems.

## 1.5 Thesis Outline

This thesis is categorized in ten chapters. Chapter 1 presents the overview of the renewable energy resources used in multi-level converters and brief discussion on the multi-level converters. This chapter also presents the types of multi-level converters by giving a clear view using their respective topologies. Some of the main advantages and disadvantages of each type of multi-level converter are also introduced. This chapter also gives clear research objectives of the thesis followed by the organization of the thesis. Then, reviews of previous work for the cascaded H bridge multi-level converter are addressed in Chapter 2.

In Chapter 3, the generalization of 'q' cell single phase cascaded H-bridge multi-level inverters is presented. The pulse width modulation techniques, the modeling and analysis of 'q' cell CHBCM are presented.

Chapter 4 presents the modeling and analysis of two-cell, three-cell and four-cell cascaded H-bridge multi-level converter using both Harmonic Balance Technique (HBT) and Double Fourier Series (DFS) analysis. The elimination of dominant harmonics in the output voltage is implemented using the DFS analysis. This method enables a method to determine the expressions of the unipolar modulation signals. The transient results of output voltage, input source currents, switching pulses are also presented along with experimental results. The study of over modulation region of operation is also presented.

Chapter 5 presents a novel multi-string multi-level inverter topology. Chapter 5 focusses on two DC input sources to produce a five-level of desired output voltage. This chapter also introduces the Karnaugh Mapping Technique (KMT) to derive the voltage equation in terms of switching functions in power electronic converters. The Karnaugh Mapping Technique is not well used in the analysis of power electronic converters, but it is an efficient way to find the expression for output voltage. The modes of operation of this converter are also presented. The expression for modulation signal is found using the instantaneous approximation of switching functions as modulation signals and also using the DFS analysis. This chapter also presents the modulation technique and the comparison of switching losses between the cascaded H-bridge five-level converter and the multi-string five-level converter topologies. Simulation and experimental results are also presented at the end of the chapter.

Chapter 6 presents the novel multi-string seven-level inverter topology. This chapter also follows the Karnaugh Mapping Technique which was discussed in Chapter 5. The modes of operation of this converter are also presented. The expression for modulation signal is found using the instantaneous approximation of switching functions.

The approximation of switching functions are written in terms of modulation signals and the DFS analysis is used to decompose these approximations. This chapter also presents the modulation technique and the comparison of switching losses between cascaded H-bridge seven-level converter and multi-string seven-level converter topologies. Simulation and experimental results are also presented at the end of the chapter.

Chapter 7 presents the multi-string nine-level inverter topology which is an extension of the multi-string seven-level inverter which will be presented in Chapter 6. This chapter presents the modes of operation, determination of the expression for the modulation signals, modulation technique and also compares the switching losses with cascaded H-bridge nine-level converter. Simulation and experimental results are also presented at the end of the chapter. This chapter also discusses the generalized modulation technique for 'n' level converter.

Chapter 8 presents the multi-string nine-level inverter topology with the LCL filter connected to the grid. The main objective of this topology is to control the active and reactive powers going into the grid. The design of the LCL filter including Bode plots are presented in this chapter. The Harmonic Balance Technique is used to determine the dynamic equations of the system in the qd synchronous reference frame. The steady state analysis of this systems is also presented.

Chapter 9 presents the design of the controller designs of both the 'L' and 'LCL' filters of the multistring nine-level inverter connected to the grid. The control schemes are designed in qd synchronous reference frame. The phase locked loop control similar to both the filters are set forth. The simulation results of both the filter types verify the proposed control schemes.

Finally, the concluding remarks and summary of the work are presented in Chapter 10. Moreover, the contributions of this research work and future suggestions are also included in this chapter.

# CHAPTER 2

## LITERATURE REVIEW

A survey of the literature reviews related to this thesis are presented in this chapter. The review consists of three sections. In Section 2.1, the topologies of multi-level converter and their modulation techniques are reviewed. Section 2.2 presents the review on harmonic elimination in the output voltage of multi-level converter. The different research works related to the single phase *qd* synchronous reference frame control of multi-level converters are reviewed in Section 2.3.

## 2.1 Review on Multi-Level Converters and their Modulation Techniques

It is very important to study the types of multi-level converters and their applications [9], [10]. These multi-level converters and their advantages and disadvantages were discussed in chapter 1. The cascaded multi-level inverters have several features and advantages such as high degree of modularity, the possibility of connecting directly to medium voltage, high input and output power quality, high availability, and the control of power flow in the regenerative version [2]. In [2], the recent developments and applications of these inverters, including new proposed topologies, modulation techniques, and control strategies are discussed. The most relevant control and modulation methods developed for the three main types of multi-level converters are discussed [11]. The modulation methods are multi-level sinusoidal pulse-width modulation, multi-level selective harmonic elimination, and space-vector

19

modulation [12]. The review from these papers reveals the proper shifting in the carrier waveforms to reduce the harmonics in output voltage [13], [14].

In [15], it was shown that the stand-alone photovoltaic (PV) systems still require a battery storage with improved efficiency and robustness, which can be achieved using multilevel topologies. A compilation of the most common topologies of multilevel converters is presented.

In [16], the traditional nine level converter is converted to a 31 level inverter using the same number of switches. The choice of the voltage ratio, 1:2:4:8, ensures that all electrolytic capacitors used in the multilevel inverter will not be connected in the reverse polarity, therefore guaranteeing the reliability of the separate dc voltage sources.

A topology of hybrid cascade converter with series-connected symmetrical and asymmetrical diode-clamped h-bridge cells are presented in [17] and [18]. Also the converters are designed to increase efficiency with high output voltage resolution. The dc link voltage rating is proposed for the multilevel diode-clamped and three-level H-bridge inverters to improve the output voltage and current quality. Some new hybrid topologies similar to [17] are proposed based on different needs. In [19] and [20], a hybrid cascaded multi-level inverter is proposed to drive a motor. Similarly in [21], the new multilevel topology with the bidirectional auxiliary switch, generating the required five-level output using only five power switches is proposed. In [22], cascaded multilevel converter-based transmission STATCOM is proposed. The system design methodology and development of power stages are also presented in [22].

Cascaded multilevel inverters with regeneration capability and reduced number of switches is presented in [23]. This paper proposes the use of a single-phase reduced cell

suitable for cascaded multilevel converters. This cell uses a reduced single phase active rectifier at the input and an H-bridge inverter at the output side, as it produces a very good performance, effectively controlling the waveform of the input current and of the output voltage.

Currently available power inverter systems for Hybrid Electric Vehicles (HEVs) use a dc–dc boost converter to boost the battery voltage for a traditional three-phase inverter. The present HEV traction drive inverters have low power density, are expensive, and have low efficiency because they need a bulky inductor. Reference [24] presents a cascaded H-bridge multilevel boost inverter for electric vehicle (EV) and hybrid EV (HEV) applications implemented without the use of inductors.

Reference [25] is a dissertation on design and control of a cascaded H-bridge converter based solid state transformer (SST). In [26] a solution for using only one dc source in asymmetric cascaded multilevel inverters with high frequency link is presented. Different multi-level PWM methods with low modulation indices are proposed in [27]. Generally a phase shifted multi-carrier PWM method is used in cascaded multi-level converter [28], but a level shifted multi-carrier PWM (LS-PWM) method is proposed in [29]. The results have also shown that LS-PWM leads to worse THD but better efficiency than phase shifted PWM (PS-PWM).

Recently, several researchers have focused on the cascaded multilevel inverter whereby two multilevel inverters are series connected to a motor load by splitting the neutral connection. The resulting performance is exceptional in terms of power quality since the overall number of voltage levels is effectively the product of the two cascaded inverters. Reference [30] demonstrates that it is possible to extend this performance to an

21

even higher number of voltage levels referred to as overdistended operation. This form of operation is desired since it effectively increases the available voltage converting levels in spite of some missing levels. In [31], an improved carrier-based SVPWM method using leg voltage redundancies in generalized cascaded multilevel inverter topology is proposed.

In [32], synthesis of multilevel converters based on single and three-phase converter building blocks is presented. This paper synthesized a family of multilevel converters that is constructed by using multiple well-developed single- and/or three-phase converter building blocks. The resulting advantages include a modular structure that leads to convenient construction and maintenance as well as easy extension to higher voltage levels.

An active power filter and a static var compensator with active power generation capability have been implemented using a 27-level inverter in [33]. The filter can compensate for load currents with a high harmonic content and a low power factor, resulting in sinusoidal currents from the source.

Modular multilevel converter (MMC) is one of the next-generation multilevel converters intended for high- or medium-voltage power conversion without transformers [34]. The MMC is based on cascade connection of multiple bidirectional chopper-cells per leg, thus requiring voltage-balancing control of the multiple floating dc capacitors.

## 2.2 Harmonic Elimination in Cascaded Multi-Level Converters

The elimination of harmonics or low Total Harmonic Distortion (THD) is important in the case of multi-level converters. In [35], a complete method selective-harmonic-elimination pulse width modulation scheme that is used to solve limitation of switching losses and balancing of DC capacitor voltages is presented. In general, the most significant low-frequency harmonics are chosen for elimination by properly selecting angles among different level inverters, and high-frequency harmonic components can be readily removed by using additional filter circuits. This method is called selective harmonic elimination PWM. Similarly in [36], active harmonic elimination in multi-level converters is proposed. Output voltage harmonic elimination in case of cascaded three cell, four cell and five cell converters are shown in [37].

A five-level symmetrically defined multilevel selective harmonic elimination pulse width modulation (MSHE–PWM) strategy is proposed in [38]. In [39], the control of seven-level hybrid cascaded multi-level inverter with fundamental frequency switching control is proposed. This paper also shows that the modulation index range can be extended using harmonic compensation technique.

In [40], a generalized analysis of a multistate switching cells-based single-phase multilevel power factor correction (PFC) rectifier is presented. Harmonic distortion optimization of cascaded H-bridge inverters considering device voltage drops and non-integer dc voltage ratios is presented in [41]. The minimal THD values, together with the corresponding step angles and dc voltage source ratios, have been obtained for the 5-, 7-,

23

9-, 11-, and 13-level cases; accounting for the device voltage drops when the load is resistive or inductive. Harmonic elimination of cascade multilevel inverters with non-equal dc sources using particle swarm optimization is presented in [42]. In [43], a modulation-based method for generating pulse waveforms with selective harmonic elimination is proposed. Harmonic elimination, traditionally digital, is shown to be achievable by comparison of a sine wave with modified triangle carrier.

In general, it is now accepted that natural or asymmetrical regular sampled PWM with a third harmonic injected or a space-vector centered reference waveform gives the best harmonic performance, with discontinuous modulation having some advantages for higher modulation ratios. Hence, in [44] a general analytical solution for the carrier-based PWM to mathematically identify the harmonic cancellation that occurs in various PWM implementations and converter topologies is proposed.

Reference [45] presents a reduced switching-frequency active-harmonic-elimination method (RAHEM) to eliminate any number of specific order harmonics of multilevel converters. The method of triangular carrier switching control of two-level inverters is extended to cascaded multilevel inverters using phase-shifted multicarrier unipolar pulse width modulation (PWM) is presented in [46].

When controlling the grid current, the injected current in the grid should not have a total Harmonic Distortion (THD) larger than 5%. In the design of the controllers of PV inverters connected to the grid, the maximum voltage THD is 8% [47].

## 2.3 Control of Multi-Level Converters

A variety of control schemes have been used in the past for the control of multi-level converters. Two different types of controllers have been used in the single phase system. They are resonant controllers and qd synchronous reference frame controllers. The main control variables in the cascaded multi-level converters are the input capacitor DC voltages as it is difficult to keep them balanced. Several control schemes on balancing of DC capacitor voltages are presented in [48]. The methods in [48], [3], [49], [29, 50], [51] ensure that the dc bus capacitor voltages converge to the reference value, even when the loads attached to them are extracting different amounts of power. In [52], a control method applicable to single dc-source cascaded H-bridge multi-level inverters to improve their capacitor voltage regulation is proposed. In this method, two cells are connected in cascade, one is the auxiliary H-bridge and the other is the main H-bridge inverter. The main H-bridge inverter switches at fundamental frequency and the auxiliary inverter switches at the PWM frequency.

In [53], a switching strategy for multilevel cascade inverters, based on the space-vector theory is presented. The proposed high-performance strategy generates a voltage vector across the load with minimum error with respect to the sinusoidal reference. In addition, it generates a very low harmonic distortion operating with reduced switching frequency, without the use of traditional sinusoidal pulse width modulation techniques or more sophisticated vector modulation methods.

In [54], the control is based on compensating the real and reactive (P-Q) power difference between the bulk inverter and the load. The new control explicitly commands the power into the conditioning inverter so that its capacitor voltage remains constant. The new control method eliminates the PWM switching in the bulk inverter while the conditioning inverter capacitors are regulated at the commanded voltage without the need for a real-power dc source.

Cascaded H-bridge multi-level inverters are needed for hybrid electric vehicles. In summary, the main advantages of using multilevel converters for hybrid electric drives include the following [55].

- They are suitable for large VA-rated and/or high-voltage motor drives.

- These multilevel converter systems have higher efficiency compared to other types of multi-level converters because the devices can be switched at minimum frequency.

- No EMI problem or common-mode voltage/current problem exists.

- Charge imbalance problem results when the converters are in either charge mode (rectification) or drive mode (inversion).

In [56], a control method to stabilize a multiple of capacitor voltages without an equilibrium state is proposed. Power balancing is guaranteed by varying the common-mode voltage, using an online nonlinear model-predictive controller. The controller predicts the system evolution as a function of the control inputs.

In [57], two types of control were developed. One relies on controlling the two three-level inverters jointly and the other uses separate controls. Both controls included

capacitor voltage balancing so that a dc source was needed for only one three-level inverter.

A simple and generalized feed-forward SVM (1D-FFSVM) technique for multilevel single-phase cascade converters (CHB) has been presented in [58]. Using the proposed modulation strategy, any dc voltage ratio in the CHB converter can be accommodated in the modulation process to generate the reference voltage. The controller determines the best output voltage of the power converter, and this voltage will be generated by the modulator even under extreme dc-link voltage unbalance situations.

In [59], [60], a high performance fixed switching frequency sliding mode controller is proposed for a single-phase unipolar inverter. Sliding mode control (SMC) is recognized as robust controller with a high stability in a wide range of operating conditions, although it suffers from chattering problem. The proposed frequency-domain method of switching characterization for cascaded H-bridge multi-level inverter (CHBMLI) has estimated accurately the hysteresis bandwidth for the desired maximum switching frequency.

A novel PWM control scheme for PV applications is presented in multi string five level inverter in [61]. The analysis of a multi cell topology that is implemented with single-phase non-regenerative cells under an unbalanced ac mains is presented in [62]. In [63], a new low-frequency predictive current control is proposed for a single-phase cascaded H-bridge multilevel rectifier.

The choice of single-phase PWM rectifiers for the input of the cells results in a reduced number of power switches and a simpler input transformer than the three phase equivalent. However, its control is not as straightforward. Reference [64] proposes the

use of higher order resonant controllers in the classical control structure of the single-phase PWM rectifier. This ensures zero steady-state tracking error of the reference current at fundamental frequency.

Instead of using the resonant controllers, the qd synchronous reference frame controls for single phase multi-level inverters are presented in [65], [66]. In order to generate the q and d axes voltages and currents for single phase inverters, a fictitious second signal is needed. The different methods for generation of fictitious second signal are presented in [67], [68], [69]. For the control of grid connected multi-level inverters, a qd single phase synchronous reference frame PLLs are presented in [66], [70].

# CHAPTER 3

# GENERALIZATION OF SINGLE PHASE CASCADED H-BRIDGE DC-AC MULTI LEVEL CONVERTER

## 3.1 Introduction

Multilevel cascaded H-bridge (CHB) converters have received much research interest than other multilevel converter configurations. This interest is due to their merits as compared to other topologies in terms of minimum number of devices, modularity and reliability. A multilevel CHB is composed of a series connection of H-bridges, also called cells. Each cell has an independent dc-link, which can be controlled to a different dc voltage, providing a high degree of freedom [49].

The 'q' cell cascaded H-bridge multi-level converter consists of 'q' conventional single-phase, H-bridge, 3-level inverters, herein referred to as cells, connected in series. Hence, the output voltage of the system is the sum of the individual voltage levels produced by the 'q' cells. Since the modes of operation of the 'q' cells are same, only need to consider one of them is considered in demonstrating the principle of operation.

Multi-level cascaded H-bridge single phase DC-AC converter with reduced voltage ripple can be an advantageous utility as an interface between the photovoltaic panels and the utility grid. When the individual converters are modulated using unipolar PWM scheme in which the carrier waves are appropriately shifted, the output waveforms are known to be very improved. The performance of this unipolar PWM scheme has not

been investigated when the input DC voltages are not the same. Using the Double Fourier

Series approximation of the converter switching functions; a model was derived that

enables the elimination of certain harmonic components in the output voltage. The

topology of single phase 'q' cell CHBMC is shown in Figure 3.1 and an example of two

cell cascaded H-bridge single phase DC-AC converter is shown in Figure 3.2. Let $S_{ijk}$ be

the switching functions of switches $T_{ijk}$, where $i = a,b$, $j = p,n$ and $k = 1,2,3,...q$

respectively. $V_1, V_2,..., V_q$ are input DC sources, $V_{dc1}, V_{dc2},..., V_{dcq}$ are the respective 'q' DC

capacitor voltages, $I_1, I_2,..., I_q$ are respective input currents, and $I_o$ is output current.
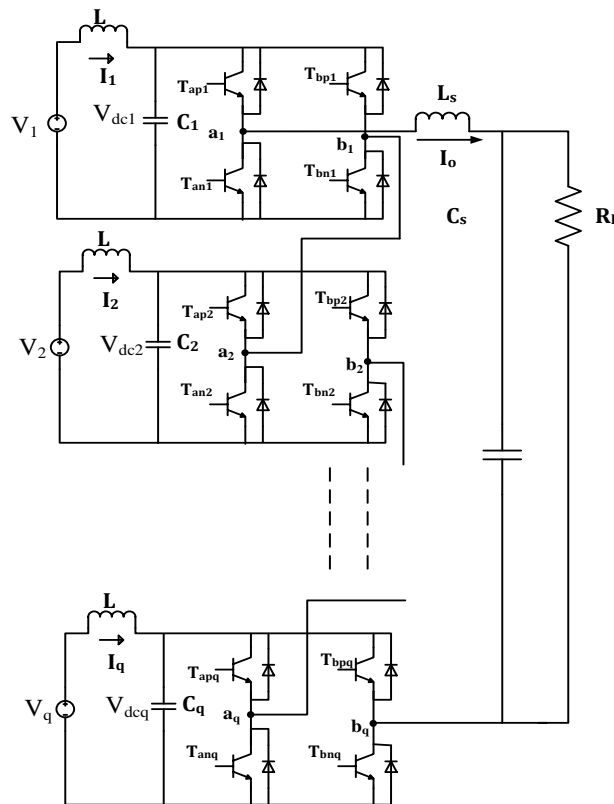


Figure 3.1 Single phase two cell CHB inverter connected to resistive load.
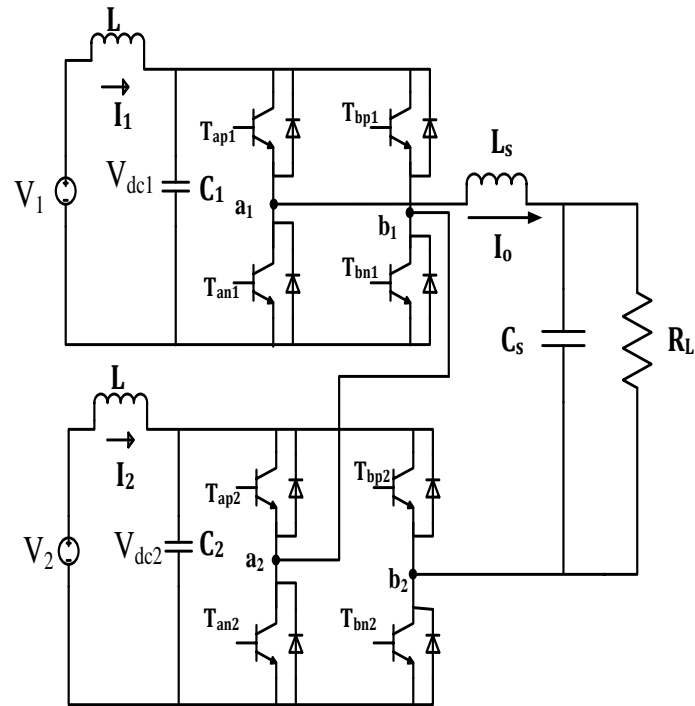
Figure 3.2 Single phase two cell CHB inverter connected to resistive load.

## 3.2 Modulation Techniques

### 3.2.1    Existence Function or Switching Function

Two related sets of parameters are of interest, when approaching the design of a
switching power converter [71].

- The external terminal performance, defined by the dependent quantities, will
  determine how well the converter meets application needs.

- The internal currents and voltages of the converter's switching loops will determine the selection of the active switching devices to be used.

Both sets of parameters can be obtained from the dependent quantities, which are determined by the defined quantities and the switching pattern. To obtain a precise, quantitative definition of the dependent quantities, some means of formally and quantitatively describing the switching pattern is needed.

The mathematical expressions used for that purpose are herein called existence functions. The existence function for a single switch assumes unit value whenever the switch is closed and is zero whenever the switch is open. In a converter, each switch is closed and opened in a repetitive pattern. Hence, its existence function will take the form shown in Figure 3.3 (a) - a train of pulses of unit amplitude. The simplest, or unmodulated, existence functions have pulses all of the same time duration and zero intervals with the same property. The pulses of the same time duration are generally used in DC-DC converters when a constant signal is compared with a carrier waveform. The more complex variety, which has differing pulse durations and various interspersed zero times, is called a modulated existence function. The example of modulated existence function is shown in Figure 3.3 (a), when a modulation signal (sine wave) is compared with the carrier waveform, the switching pulses are generated based on their comparison techniques.

The use of existence functions to derive dependent quantities and internal converter stresses is relatively easy. Let's consider a switch in a converter matrix. The switch is connected to $V_i$, the i$^{th}$ set of M-defined voltages, and to $I_j$, the j$^{th}$ set of N-defined currents. It's existence function is $H_{ij}$. Now, whenever the switch is closed, $V_j$,

the voltage impressed on $I_j$ must be $V_i$ because the switch supports no voltage and no other switch connected to $I_j$ can be closed without violating KVL. Whenever the switch is open, voltage $V_i$ is removed from $I_j$ with the switch supporting the difference between $V_i$ and $V_j$ existing at that time. Hence,

$$V_j = H_{ij}V_i + Contributions\ of\ remainder\ of\ sources\ and\ switches. \quad (3.1)$$

$$I_s = H_{ij}I_j \quad (3.2)$$

The current flowing in $V_i$ is clearly the current in this switch plus the currents in all other switches connected to this same voltage. Hence it can be written as:

$$I_i = H_{ij}I_j + Contributions\ of\ remainder\ of\ sources\ and\ switches. \quad (3.3)$$

The equations of voltage and current give the contributions of this individual switch to the dependent quantities. The voltage impressed on a switch $V_s$ is the difference between its voltage and source, $V_i$ and the voltage impressed on its current source while it is open.
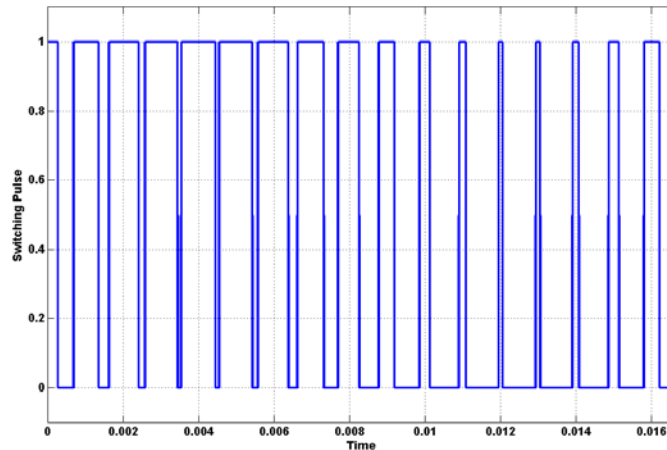
Figure 3.3 Switching Function.

Thus the dependent quantities and the switch stresses can be completely defined using the existence functions.

As can be seen from Figure 3.3 (a), the existence functions are trains of unit value pulses interspersed by periods of zero value. Since switching patterns are invariably repetitive, existence functions are periodic. They can be mathematically represented in various ways; Laplace transforms can be used, as can Z-transforms.

Since the converter consists solely of switches, which have only two possible states, such control can be effected only by changes in the switching pattern. The variables that are available to implement such control are:

1. the duty cycle of the pulse train.

2. the repetition frequency of the pulse train can be varied.

3. the phase or time displacement of the existence function relative to some fixed external reference can be varied.

34

In dc-to-dc converters, the defined quantities are perfectly smooth dc. The dependent quantities are obtained by multiplying the defined quantities by the existence functions of the switches. The average component of switching function is the only term that can be controlled in effect to dc-to-dc converters.

The alternative control technique that can be used is using the modulating function $M(t)$. The existence functions for ac-to-dc and dc-to-ac converters must be complete sets in order to avoid violation of KCL and KVL, and so the dc component becomes an invariant integer which is modulation signal.

### 3.2.2    Pulse Width Modulation Control:

The fundamental magnitude of the output voltage from an inverter can be controlled to be constant by exercising control within the inverter itself that is no external control circuitry is required. The most efficient method of doing this is by Pulse Width Modulation (PWM) control used within the inverter. In this scheme the inverter is fed by a fixed input voltage and a controlled ac voltage is obtained by adjusting the on and the off periods of the inverter components. The advantages of the PWM control scheme are:

a) The output voltage control can be obtained without addition of any external components.

b) PWM minimizes the lower order harmonics, while the higher order harmonics can be eliminated using a filter.

The disadvantage possessed by this scheme is that the switching devices used in the inverter are expensive as they must possess low turn on and turn off times, nevertheless

PWM operated are very popular in all industrial equipments. PWM techniques are characterized by constant amplitude pulses with different duty cycles for each period. The width of these pulses are modulated to obtain inverter output voltage control and to reduce its harmonic content. There are different PWM techniques which essentially differ in the harmonic content of their respective output voltages, thus the choice of a particular PWM technique depends on the permissible harmonic content in the inverter output voltage.

### 3.2.3     Sinusoidal Pulse Width Modulation Control:

The sinusoidal PWM (SPWM) method also known as the triangulation, sub harmonic, or sub-oscillation method, is very popular in industrial applications. The SPWM is explained with reference to first half of Figure 3.6, which is the half-bridge circuit topology for a single-phase inverter.

For realizing SPWM, a high-frequency triangular carrier wave $v_c$ is compared with a sinusoidal reference $v_r$ of the desired frequency. The intersection of $v_c$ and $v_r$ waves determines the switching instants and commutation of the modulated pulse. The PWM scheme is illustrated in Figure 3.4, in which $v_c$ is the peak value of triangular carrier wave and $v_r$ that of the reference, or modulating signal. The figure shows the triangle and modulation signal with some arbitrary frequency and magnitude. In the inverter of Figure 3.6, the switches $T_{ap1}$ and $T_{an1}$ are controlled based on the comparison of control signal and the triangular wave which are mixed in a comparator. When

sinusoidal wave has magnitude higher than the triangular wave the comparator output is high, otherwise it is low.

If $v_r > v_c$, then $T_{ap1}$ will be on and the output voltage will be $V_{out} = \frac{V_d}{2}$. Similarly, if $v_r < v_c$, then $T_{an1}$ will be on and the output voltage will be $V_{out} = -\frac{V_d}{2}$.

The comparator output is processed in a trigger pulse generator in such a manner that the output voltage wave of the inverter has a pulse width in agreement with the comparator output pulse width. The magnitude ratio of $\frac{v_r}{v_c}$ is called the modulation index $(m_i)$ and it controls the harmonic content of the output voltage waveform.

The magnitude of fundamental component of output voltage is proportional to $m_i$. The amplitude $v_c$ of the triangular wave is generally kept constant. The frequency–modulation ratio $m_f$ is defined as

$$m_f = \frac{f_t}{f_m}.$$  (3.4)
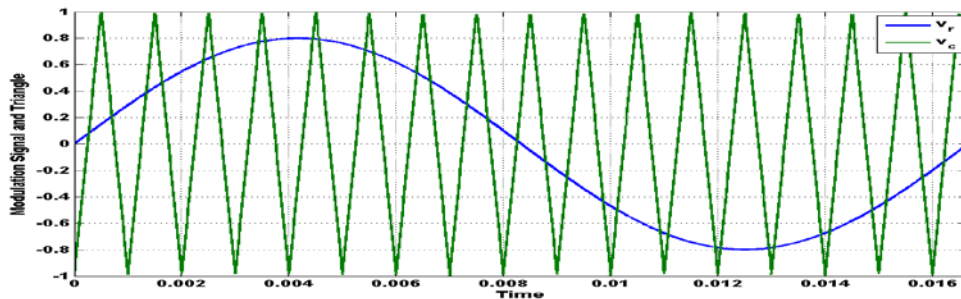


(a)
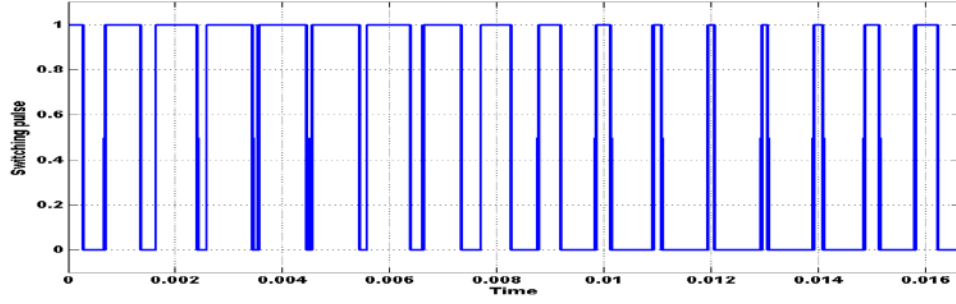
(b)

Figure 3.4: Sinusoidal Pulse Width Modulation: a) Illustration, (b) Switching pulse

generation.

### 3.2.4 SPWM with Bipolar switching

In this scheme the diagonally opposite transistors $T_{ap1}$, $T_{bn1}$ and $T_{bp1}$ and $T_{an1}$ are turned on or turned off at the same time. The output of leg A is equal and opposite to the output of leg B. The output voltage is determined by comparing the control signal, $v_r$ and the triangular signal, $v_c$ as shown in Figure 3.5 to get the switching pulses for the devices, and the switching pattern is as follows.

$$V_r > V_c, \qquad T_{ap1} \text{ is ON} \Rightarrow V_{ao} = \frac{V_d}{2} \text{ and } T_{bn1} \text{ is ON} \Rightarrow V_{bo} = -\frac{V_d}{2} \qquad (3.5)$$

$$V_r < V_c, \qquad T_{an1} \text{ is ON} \Rightarrow V_{ao} = -\frac{V_d}{2} \text{ and } T_{bp1} \text{ is ON} \Rightarrow V_{bo} = \frac{V_d}{2}. \qquad (3.6)$$

38

(a)



(b)
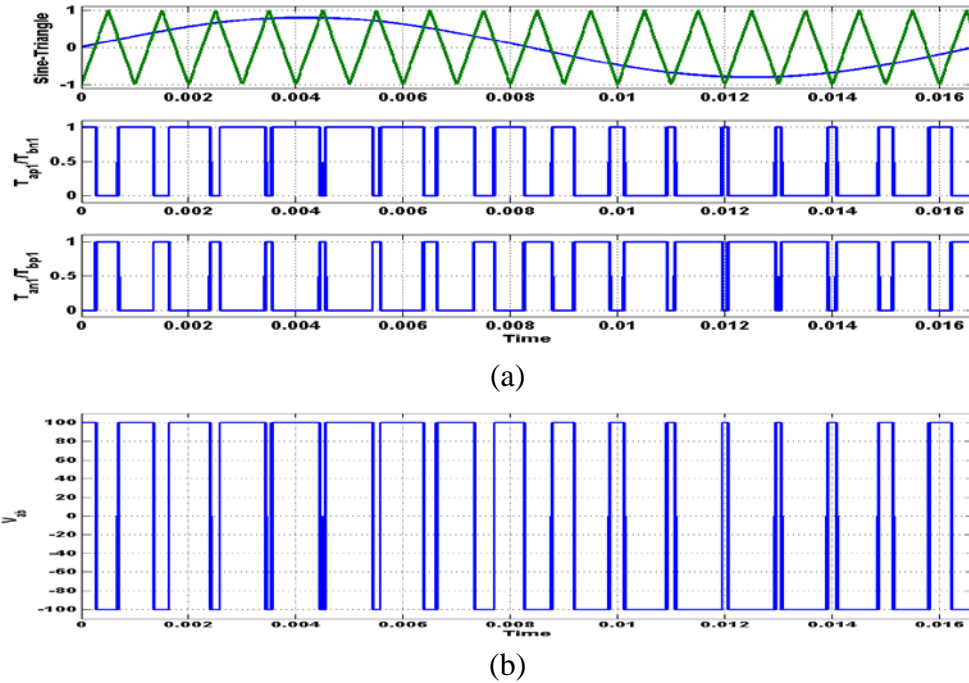
Figure 3.5: SPWM with Bipolar switching a) Illustration, (b) Switching pulse generation.

### 3.2.5    SPWM with Unipolar Switching

In this scheme, the devices in one leg are turned on or off based on the comparison of the modulation signal $V_r$ with a high frequency triangular wave. The devices in the other leg are turned on or off by the comparison of the modulation signal $-V_r$ with the same high frequency triangular wave. Figure 3.6 show the unipolar scheme for a single –phase full bridge inverter, with the modulation signals for both legs and the associated comparison to yield switching pulses for both the legs.

The logic behind the switching of the devices in the leg connected to 'a' is given as:

$$V_r > V_c \; ; T_{ap1} \text{ is } ON \text{ and } V_{ao} = \frac{V_d}{2} \tag{3.7}$$

$$V_r < V_c \; ; T_{an1} \text{ is } ON \text{ and } V_{ao} = -\frac{V_d}{2} \tag{3.8}$$

and that in the leg connected to 'b' is given as

$$-V_r > V_c \; ; T_{bp1} \text{ is } ON \text{ and } V_{bo} = \frac{V_d}{2} \tag{3.9}$$

$$-V_r < V_c \; ; T_{bn1} \text{ is } ON \text{ and } V_{bo} = -\frac{V_d}{2}. \tag{3.10}$$



(a)



(b)

40
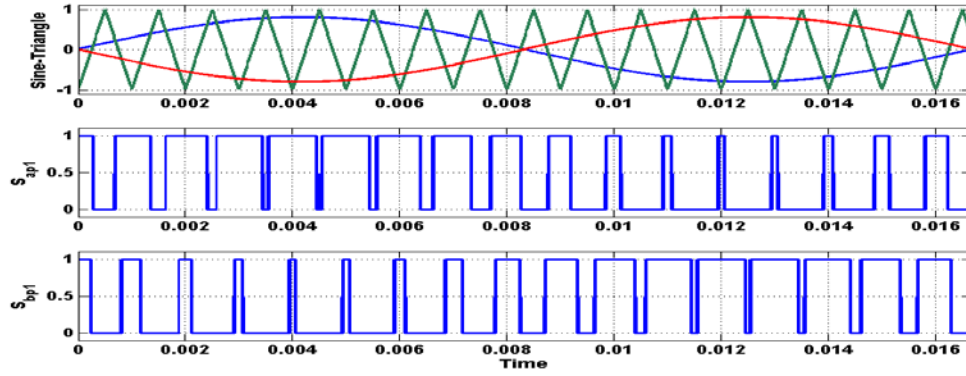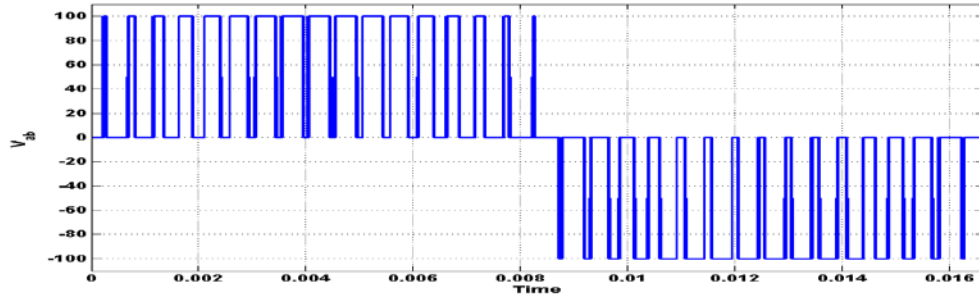
Figure 3.6: SPWM with Unipolar switching a) Illustration, (b) Switching pulse generation.

## 3.3 Determination of the expressions for the output voltage and input currents

The Kirchoff's current law (KCL) and Kirchoff's voltage law (KVL) are applied on the circuit shown in Figure 3.1.

According to KCL and KVL, only one switch must be turned on at any time. Therefore

$$S_{apk} + S_{ank} = 1.$$

$$S_{bpk} + S_{bnk} = 1.$$

(3.11)
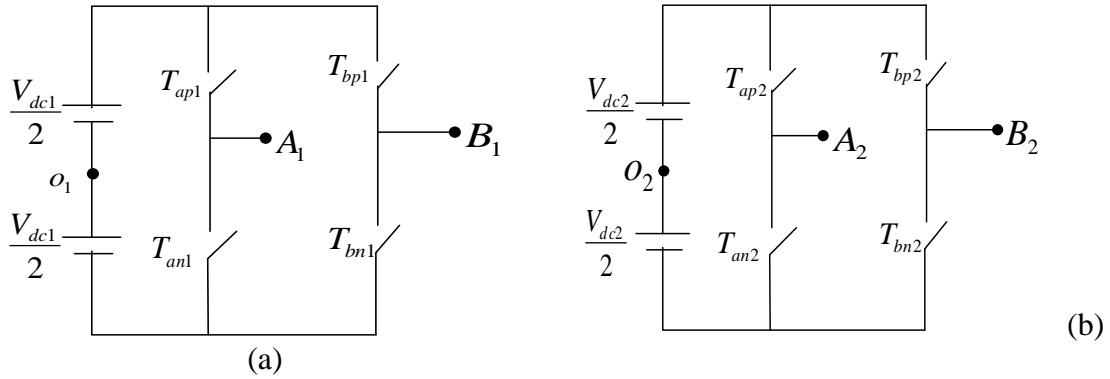


Figure 3.7: (a) Cell 1, (b) Cell 2, (c) SPWM, (d) Switching pulse generation.

Let $V_{ABk}$ be the output voltage of $k^{th}$ cell, where $k$ is the number of cells, $k = 1, 2, \ldots, q$, $I_{ok}$ be the output current of each cell respectively and $V_{AB}$ be the output voltage of the combined 'q' cell cascaded H-bridge converter. Then

$$V_{AB} = V_{AB1} + V_{AB2} + ... + V_{ABq}. \tag{3.12}$$

Based on q-cell cascaded H-bridge multilevel inverter topology, $V_{AO1} = \dfrac{V_{dc1}}{2}$ when $T_{ap1}$ is

on and $V_{AO1} = -\dfrac{V_{dc1}}{2}$ when $T_{an1}$ is on for first cell.

Therefore, $V_{AO1} = \dfrac{V_{dc1}}{2}\left(S_{ap1} - S_{an1}\right).$ \hfill (3.13)

Using (3.11), $V_{AO1} = \dfrac{V_{dc1}}{2}\left(2S_{ap1} - 1\right).$ \hfill (3.14)

Similarly, $V_{BO1} = \dfrac{V_{dc1}}{2}\left(S_{bp1} - S_{bn1}\right) = \dfrac{V_{dc1}}{2}\left(2S_{bp1} - 1\right).$ \hfill (3.15)

Therefore

$$V_{AB1} = V_{AO1} - V_{BO1} = \frac{V_{dc1}}{2}\left(2S_{ap1} - 1\right) - \frac{V_{dc1}}{2}\left(2S_{bp1} - 1\right) = V_{dc1}\left(S_{ap1} - S_{bp1}\right) \tag{3.16}$$

Similarly.

$$V_{AB2} = V_{AO2} - V_{BO2} = \frac{V_{dc2}}{2}\left(2S_{ap2} - 1\right) - \frac{V_{dc2}}{2}\left(2S_{bp2} - 1\right) = V_{dc2}\left(S_{ap2} - S_{bp2}\right) \tag{3.17}$$

$$V_{ABq} = V_{AOq} - V_{BOq} = \frac{V_{dcq}}{2}\left(2S_{apq} - 1\right) - \frac{V_{dcq}}{2}\left(2S_{bpq} - 1\right) = V_{dcq}\left(S_{apq} - S_{bpq}\right) \tag{3.18}$$

From (3.16-3.18),

$$V_{AB} = V_{dc1}\left(S_{ap1} - S_{bp1}\right) + V_{dc2}\left(S_{ap2} - S_{bp2}\right) + ... + V_{dcq}\left(S_{apq} - S_{bpq}\right) \tag{3.19}$$

Similarly the expression for output currents can also be derived to be

$$I_1 = I_{o1}\left(S_{ap1} - S_{bp1}\right)$$

$$I_2 = I_{o2}\left(S_{ap2} - S_{bp2}\right)$$

$$...$$ 

(3.20)

$$I_q = I_{oq}\left(S_{apq} - S_{bpq}\right)$$

$I_{o1} = I_{o2} = ... = I_{oq}$, when the cells are connected in cascade. (3.21)

## 3.4 Modulation Scheme

For general 'q' cell cascaded H-bridge multi-level converter, the number of triangles will be 'q'. The number of modulation signals will be '2q', where two modulation signals are required for each cell to generate the desired output voltage. The carrier waveforms of 'q' cell cascaded H-bridge multi-level inverter have to be shifted by $\dfrac{\pi}{q}$ in order to get the desired output voltage.

As shown in Figure 3.8, $M_{ak}, M_{bk}$ are the modulation signals for each leg of the single inverter for 'q' cells where $k = 1,2,...,q$. $Tri_1, Tri_2,...,Tri_q$ are the triangle carrier signals corresponding to each H-bridges and they all are displaced by $\dfrac{\pi}{q}$ from each other. Each switching pulse is generated as follows.

43
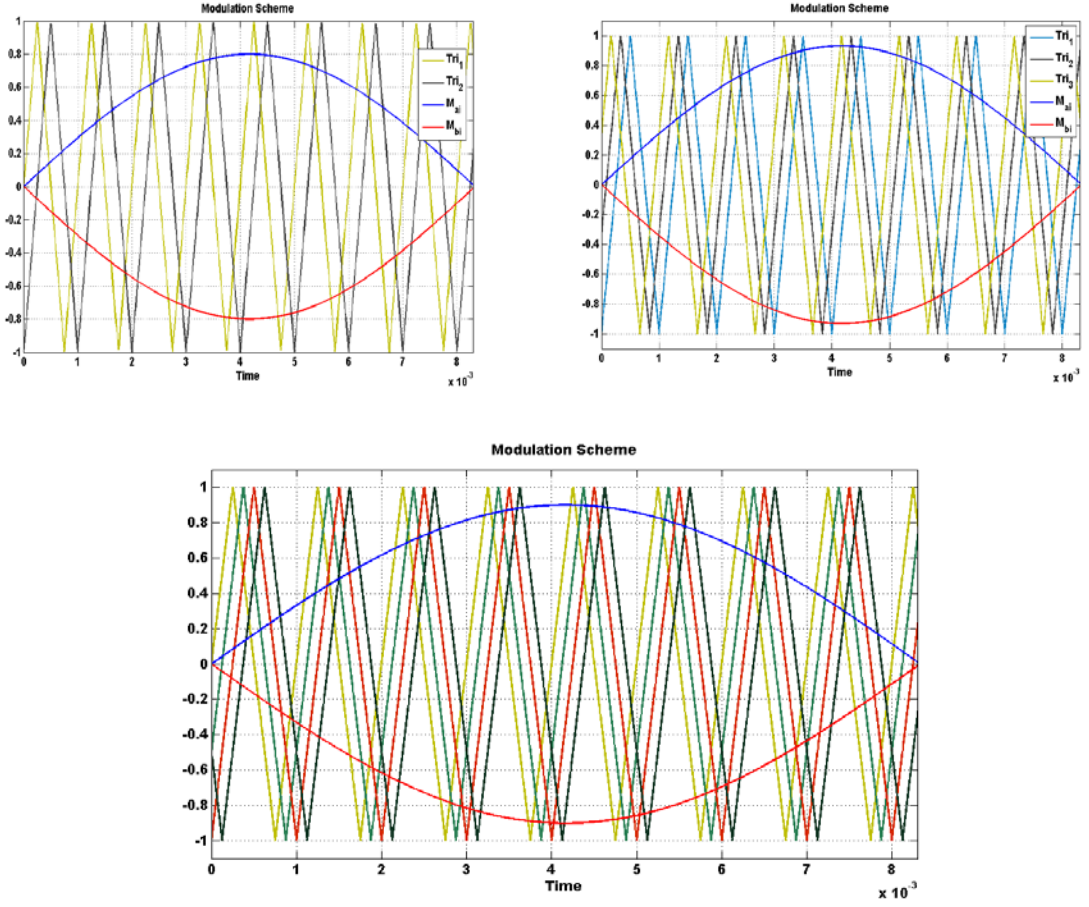
Figure 3.8 Modulation Scheme for two, three and four cell cascaded H-bridge DC-AC

converters.

$$S_{apk} = \begin{cases} 1 \text{ if } & M_{ak} > Tri_k \\ 0 \text{ if } & M_{ak} < Tri_k \end{cases}.$$   (3.22)

$$S_{ank} = \begin{cases} 0 \text{ if } & M_{ak} \geq Tri_k \\ 1 \text{ if } & M_{ak} < Tri_k \end{cases}.$$   (3.23)

$$S_{bpk} = \begin{cases} 1 \text{ if } & M_{bk} \geq Tri_k \\ 0 \text{ if } & M_{bk} < Tri_k \end{cases}. \tag{3.24}$$

$$S_{bnk} = \begin{cases} 0 \text{ if } & M_{bk} \geq Tri_k \\ 1 \text{ if } & M_{bk} < Tri_k \end{cases}. \tag{3.25}$$

where $k = 1, 2, ..., q$.

## 3.5 Determination of Unipolar PWM Modulation Signals

The principle of Fourier series expansion tells that any periodic function $f(t)$ can be decomposed into infinite series of sinusoidal harmonics [4].

$$f(t) = \frac{a_0}{2} + \sum_{m=1}^{\infty} a_m \cos(m\omega t) + b_m \sin(m\omega t). \tag{3.26}$$

$$a_m = \frac{1}{\pi} \int_{-\pi}^{\pi} f(t) \cos(m\omega t) \, d(\omega t). \tag{3.27}$$

$$m = 0, 1, 2, 3, ..., \infty.$$

$$b_m = \frac{1}{\pi} \int_{-\pi}^{\pi} f(t) \sin(m\omega t) \, d(\omega t). \tag{3.28}$$

$$m = 1, 2, 3, ..., \infty.$$

Consider a waveform $f(x, y)$ which varies as a function of carrier frequency and fundamental frequency, in which $x(t)$ and $y(t)$ are defined in (3.29) and (3.30).

$$x(t) = \omega_c t + \theta_c. \tag{3.29}$$

$$y(t) = \omega_o t + \theta_o. \tag{3.30}$$

Fourier series at a particular value of $y = y_1$ can be written as

$$f(x, y_1) = \frac{a_0(y_1)}{2} + \sum_{m=1}^{\infty} a_m(y_1) \cos mx + b_m(y_1) \sin mx. \tag{3.31}$$

where $a_m(y_1) = \frac{1}{\pi} \int_{-\pi}^{\pi} f(x, y_1) \cos mx \, dx.$ \hfill (3.32)

$$m = 0,1,2,3, \dots, \infty.$$

$$b_m(y_1) = \frac{1}{\pi} \int_{-\pi}^{\pi} f(x, y_1) \sin mx \, dx. \tag{3.33}$$

$$m = 1,2,3, \dots, \infty.$$

The coefficients $a_m(y_1)$ and $b_m(y_1)$ are particular values of two functions $a_m(y)$ and $b_m(y)$ which vary over the entire range of $y$. These functions can also be decomposed as

$$a_m(y) = \frac{c_{mo}}{2} + \sum_{n=1}^{\infty} c_{mn} \cos ny + d_{mn} \sin ny. \tag{3.34}$$

$$m = 0,1,2,3, \dots, \infty.$$

$$b_m(y) = \frac{e_{mo}}{2} + \sum_{n=1}^{\infty} e_{mn} \cos ny + f_{mn} \sin ny. \tag{3.35}$$

$$m = 1,2,3, \dots, \infty.$$

where

$$c_{mn} = \frac{1}{\pi} \int_{-\pi}^{\pi} a_m(y) \cos ny \, dy = \frac{1}{\pi^2} \int_{-\pi}^{\pi} \int_{-\pi}^{\pi} f(x, y) \cos mx \cos ny \, dx \, dy. \tag{3.36}$$

$$m = 0, 1,2,3, \dots, \infty.$$

$$n = 0,1,2,3, \dots, \infty.$$

$$d_{mn} = \frac{1}{\pi} \int_{-\pi}^{\pi} a_m(y) \sin ny \, dy = \frac{1}{\pi^2} \int_{-\pi}^{\pi} \int_{-\pi}^{\pi} f(x, y) \cos mx \sin ny \, dx \, dy. \tag{3.37}$$

$$m = 0, 1,2,3, \dots, \infty.$$

$$n = 1,2,3, \dots, \infty.$$

46

$$e_{mn} = \frac{1}{\pi} \int_{-\pi}^{\pi} b_m(y) \cos ny \, dy = \frac{1}{\pi^2} \int_{-\pi}^{\pi} \int_{-\pi}^{\pi} f(x,y) \sin mx \cos ny \, dx \, dy. \tag{3.38}$$

$$m = 1,2,3, \dots, \infty.$$

$$n = 0,1,2,3, \dots, \infty.$$

$$f_{mn} = \frac{1}{\pi} \int_{-\pi}^{\pi} b_m(y) \sin ny \, dy = \frac{1}{\pi^2} \int_{-\pi}^{\pi} \int_{-\pi}^{\pi} f(x,y) \sin mx \sin ny \, dx \, dy. \tag{3.39}$$

$$m = 1,2,3, \dots, \infty.$$

$$n = 1,2,3, \dots, \infty.$$

Using trigonometric identities in Table 3.1,

$$c_{mn} = \frac{1}{2\pi^2} \int_{-\pi}^{\pi} \int_{-\pi}^{\pi} f(x,y) \cos(mx + ny) \, dx \, dy$$

$$+ \frac{1}{2\pi^2} \int_{-\pi}^{\pi} \int_{-\pi}^{\pi} f(x,y) \cos(mx - ny) \, dx \, dy. \tag{3.40}$$

$$m = 0, 1,2,3, \dots, \infty.$$

$$n = 0,1,2,3, \dots, \infty.$$

$$d_{mn} = \frac{1}{2\pi^2} \int_{-\pi}^{\pi} \int_{-\pi}^{\pi} f(x,y) \sin(mx + ny) \, dx \, dy$$

$$- \frac{1}{2\pi^2} \int_{-\pi}^{\pi} \int_{-\pi}^{\pi} f(x,y) \sin(mx - ny) \, dx \, dy. \tag{3.41}$$

Table 3.1 Trigonometric Identities

| |
|---|
| $\cos(A + B) = \cos A \cos B - \sin A \sin B$ |
| $\sin(A + B) = \sin A \cos B + \cos A \sin B$ |
| $\cos(A - B) = \cos A \cos B + \sin A \sin B$ |

$$\boxed{\sin(A - B) = \sin A \cos B - \cos A \sin B}$$

$$m = 0, 1, 2, 3, \ldots, \infty.$$

$$n = 1, 2, 3, \ldots, \infty.$$

$$e_{mn} = \frac{1}{2\pi^2} \int_{-\pi}^{\pi} \int_{-\pi}^{\pi} f(x, y) \sin(mx + ny) \, dx \, dy$$

$$+ \frac{1}{2\pi^2} \int_{-\pi}^{\pi} \int_{-\pi}^{\pi} f(x, y) \sin(mx - ny) \, dx \, dy. \qquad (3.42)$$

$$m = 1, 2, 3, \ldots, \infty.$$

$$n = 0, 1, 2, 3, \ldots, \infty.$$

$$f_{mn} = \frac{1}{2\pi^2} \int_{-\pi}^{\pi} \int_{-\pi}^{\pi} f(x, y) \cos(mx + ny) \, dx \, dy$$

$$- \frac{1}{2\pi^2} \int_{-\pi}^{\pi} \int_{-\pi}^{\pi} f(x, y) \cos(mx - ny) \, dx \, dy. \qquad (3.43)$$

$$m = 1, 2, 3, \ldots, \infty.$$

$$n = 0, 1, 2, 3, \ldots, \infty.$$

The general Fourier component form for $f(x, y)$ can now be written as

$$f(x, y) = \frac{c_{00}}{4} + \frac{1}{2} \sum_{n=1}^{\infty} [c_{0n} \cos ny + d_{0n} \sin ny]$$

$$+ \frac{1}{2} \sum_{m=1}^{\infty} [c_{m0} \cos mx + e_{mo} \sin mx]$$

$$+ \sum_{m=1}^{\infty} \sum_{n=1}^{\infty} \begin{bmatrix} (c_{mn} \cos ny + d_{mn} \sin ny) \cos mx \\ +(e_{mn} \cos ny + f_{mn} \sin ny) \sin mx \end{bmatrix}. \qquad (3.44)$$

Using trigonometric identities mentioned in Table 3.1,

$$f(x,y) = \frac{c_{00}}{4} + \frac{1}{2}\sum_{n=1}^{\infty}[c_{0n}\cos ny + d_{0n}\sin ny]$$

$$+ \frac{1}{2}\sum_{m=1}^{\infty}[c_{m0}\cos mx + e_{mo}\sin mx]$$

$$+ \sum_{m=1}^{\infty}\sum_{n=1}^{\infty}\left[\begin{array}{l}\frac{1}{2}[c_{mn}\cos(mx+ny) + c_{mn}\cos(mx-ny)] \\ +\frac{1}{2}[d_{mn}\sin(mx+ny) - d_{mn}\sin(mx+ny)] \\ +\frac{1}{2}[e_{mn}\sin(mx+ny) + e_{mn}\sin(mx-ny)] \\ +\frac{1}{2}[f_{mn}\cos(mx-ny) - f_{mn}\cos(mx+ny)]\end{array}\right]. \tag{3.45}$$

which can be combined to form

$$f(x,y)$$

$$= \frac{c_{00}}{4} + \frac{1}{2}\sum_{n=1}^{\infty}[c_{0n}\cos ny + d_{0n}\sin ny] + \frac{1}{2}\sum_{m=1}^{\infty}[c_{m0}\cos mx + e_{mo}\sin mx]$$

$$+ \sum_{m=1}^{\infty}\sum_{n=1}^{\infty}\left[\begin{array}{l}\frac{1}{2}[(c_{mn}-f_{mn})\cos(mx+ny) + (c_{mn}+f_{mn})\cos(mx-ny)] \\ +\frac{1}{2}[(d_{mn}+e_{mn})\sin(mx+ny) + (e_{mn}-d_{mn})\sin(mx-ny)]\end{array}\right] \tag{3.46}$$

$$\frac{1}{2}(c_{mn}-f_{mn}) = \frac{1}{2\pi^2}\int_{-\pi}^{\pi}\int_{-\pi}^{\pi}f(x,y)\cos(mx+ny)\,dx\,dy. \tag{3.47}$$

$$\frac{1}{2}(c_{mn}+f_{mn}) = \frac{1}{2\pi^2}\int_{-\pi}^{\pi}\int_{-\pi}^{\pi}f(x,y)\cos(mx-ny)\,dx\,dy. \tag{3.48}$$

$$\frac{1}{2}(e_{mn}+d_{mn}) = \frac{1}{2\pi^2}\int_{-\pi}^{\pi}\int_{-\pi}^{\pi}f(x,y)\sin(mx+ny)\,dx\,dy. \tag{3.49}$$

$$\frac{1}{2}(e_{mn}-d_{mn}) = \frac{1}{2\pi^2}\int_{-\pi}^{\pi}\int_{-\pi}^{\pi}f(x,y)\sin(mx-ny)\,dx\,dy. \tag{3.50}$$

It can be seen from (3.37) and (3.39) that for any given value of $n$, $d_{mn} = -d_{m(-n)}$ and

$f_{mn} = -f_{m(-n)}$ so that the $(mx - ny)$ terms in (3.46) can alternatively be obtained by

summing the $(mx + ny)$ terms over negative $n$.

Hence, the complete solution for $f(x, y)$ becomes

$$f(x,y) = \frac{c_{00}}{4} + \frac{1}{2}\sum_{n=1}^{\infty}[c_{0n}\cos ny + d_{0n}\sin ny]$$

$$+ \frac{1}{2}\sum_{m=1}^{\infty}[c_{m0}\cos mx + e_{mo}\sin mx]$$

$$+ \frac{1}{2}\sum_{m=1}^{\infty}\sum_{n=-\infty}^{\infty}[(c_{mn} - f_{mn})\cos(mx + ny)$$ 

(3.51)

$$+ (d_{mn} + e_{mn})\sin(mx + ny)].$$

The resultant coefficients are defined as

$$\overline{C_{mn}} = A_{mn} + jB_{mn} = \frac{(c_{mn} - f_{mn})}{2} + \frac{j(d_{mn} + e_{mn})}{2}.$$

(3.52)

$$A_{mn} + jB_{mn} = \frac{1}{2\pi^2}\int_{-\pi}^{\pi}\int_{-\pi}^{\pi}f(x,y)[\cos(mx + ny)$$

$$+ j\sin(mx + ny)]dx\,dy$$

$$A_{mn} + jB_{mn} = \frac{1}{2\pi^2}\int_{-\pi}^{\pi}\int_{-\pi}^{\pi}f(x,y)e^{j(mx+ny)}dx\,dy.$$

(3.53)

$$f(x,y) = \frac{A_{00}}{2} + \sum_{n=1}^{\infty} [A_{0n} \cos ny + B_{0n} \sin ny]$$

$$+ \sum_{m=1}^{\infty} [A_{m0} \cos mx + B_{mo} \sin mx]$$

(3.54)

$$+ \sum_{m=1}^{\infty} \sum_{\substack{n=-\infty \\ n \neq 0}}^{\infty} [A_{mn} \cos(mx + ny) + B_{mn} \sin(mx + ny)].$$

(3.54) can be expressed in terms of time by substituting from (3.29) and (3.30) to become

$$f(t) = \frac{A_{00}}{2} + \sum_{n=1}^{\infty} [A_{0n} \cos(n[\omega_o t + \theta_o]) + B_{0n} \sin(n[\omega_o t + \theta_o])]$$

$$+ \sum_{m=1}^{\infty} [A_{m0} \cos(m[\omega_c t + \theta_c]) + B_{mo} \sin(m[\omega_c t + \theta_c])]$$

(3.55)

$$+ \sum_{m=1}^{\infty} \sum_{\substack{n=-\infty \\ n \neq 0}}^{\infty} \begin{bmatrix} A_{mn} \cos(m[\omega_c t + \theta_c] + n[\omega_o t + \theta_o]) \\ +B_{mn} \sin(m[\omega_c t + \theta_c] + n[\omega_o t + \theta_o]) \end{bmatrix}.$$

where $$m = 1,2,3, \dots, \infty.$$

$$n = 0,1,2,3, \dots, \infty.$$

$$A_{mn} = \frac{1}{2\pi^2} \int_{-\pi}^{\pi} \int_{-\pi}^{\pi} f(x,y)[\cos(mx + ny)] dx \, dy$$

$$B_{mn} = \frac{1}{2\pi^2} \int_{-\pi}^{\pi} \int_{-\pi}^{\pi} f(x,y)[\sin(mx + ny)] dx \, dy$$

Using $A_{mn}$ and $B_{mn}$, the coefficients, $A_{00}$, $A_{0n}$, $A_{m0}, A_{mn}$, $B_{m0}$, $B_{0n}$, $B_{mn}$ can be determined.

The harmonic spectrum of a general carrier-based PWM wave can be expressed in its most general form. The first term defines the DC component, the second term defines

51

the fundamental component (when $n = 1$) and baseband harmonic components which are integer multiples of the fundamental component. The third term defines carrier harmonic components as multiples of the carrier frequency. The fourth term defines sideband harmonic components displaced either side of the main carrier harmonics by integer multiples of the fundamental frequency component.



(a)
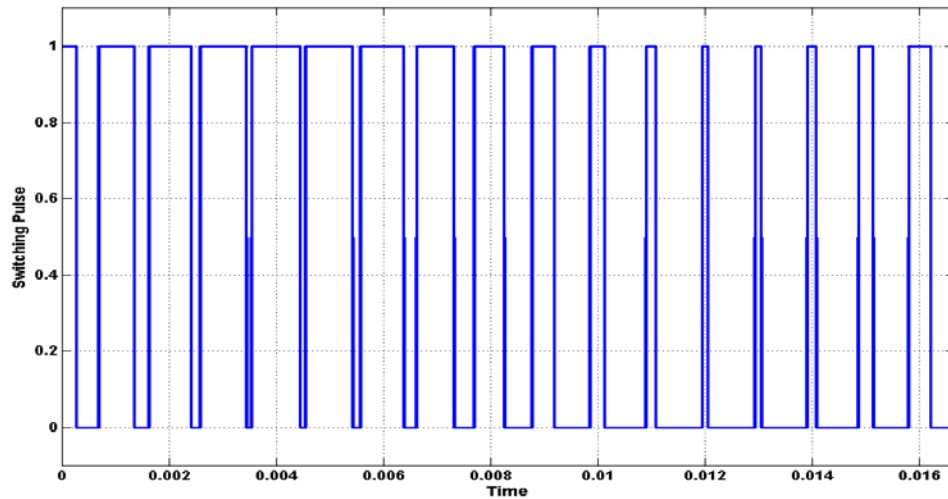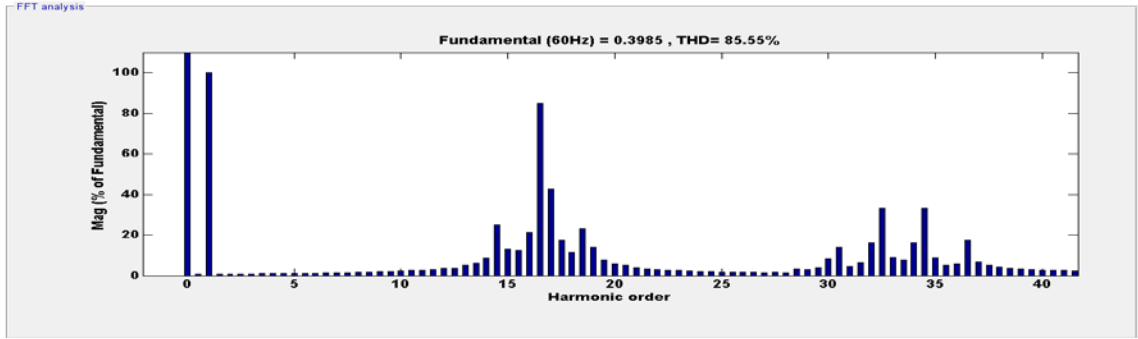
Figure 3.9 FFT analysis of switching pulse

The switching pulse and its FFT spectrum are shown in Figure 3.9 (a) and (b) respectively. As can be seen from the Figure 3.9 (b), the switching function has an average component similar to the first term in (3.55). It has a fundamental frequency component which is given in the second term and harmonics around switching frequency and around carrier frequency which are mentioned in terms three and four in (3.55).



(a)

53
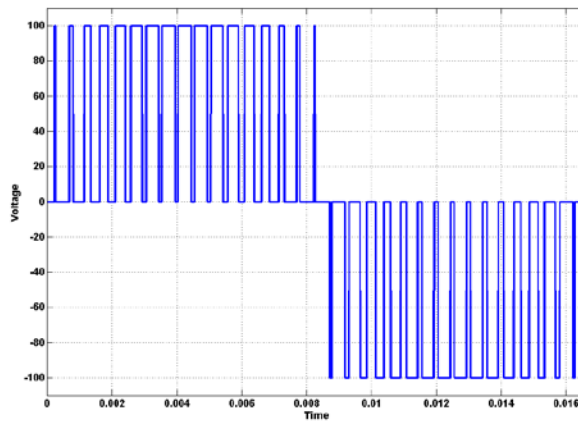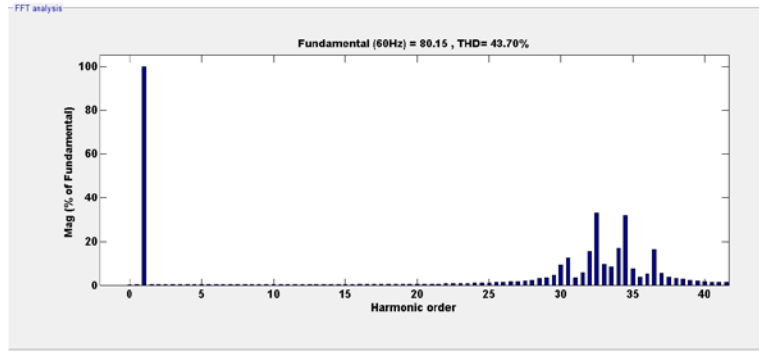
(b)
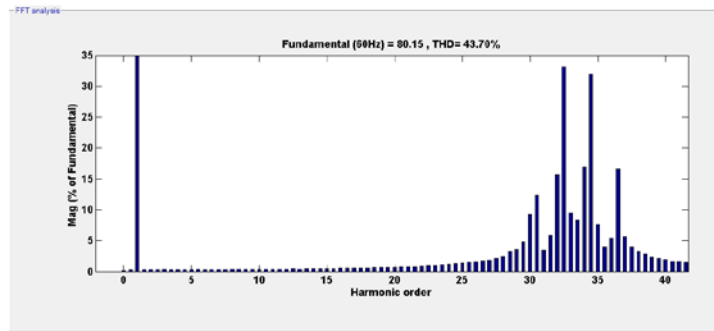


(c)

Figure 3.10 (a) Output Phase Voltage, (b) FFT spectrum showing Fundamental

component, (c) FFT spectrum showing harmonics.

Similarly, the FFT spectrum of single phase output voltage waveform is shown in Figure 3.10. The FFT waveform of the output voltage can be compared with the voltage spectrum shown in (3.58). As can be seen from the voltage spectrum in (3.58), the fundamental frequency component and the odd side band harmonics around an even carrier are presented. The Figure also shows the same frequency components as expressed in (3.58). The fundamental frequency component and odd side band harmonics around even carrier $(2\omega_c \pm \omega_s)$ can be seen in Figure 3.10 (c).

54

where $\omega_c = 1 \ kHz$, $\omega_s = 60 \ Hz$.

Therefore $2\omega_c \pm \omega_s = 2060 \ Hz \ or \ 1940 \ Hz$. The harmonic order will be 32 and 34.

Hence, the Double Fourier Series approximation of the converter switching functions is given as

$$f(\omega_s,\omega_c,t) = \left\{ \begin{array}{l} \left| \dfrac{A_{00}}{2} + \displaystyle\sum_{n=1}^{\infty}\left(A_{0n}\cos(n(\omega_s t + \theta_o)) + B_{0n}\sin(n(\omega_s t + \theta_o))\right) \right| \\[2em] + \displaystyle\sum_{m=1}^{\infty}\left(A_{m0}\cos(m(\omega_c t + \gamma_c)) + B_{m0}\sin(m(\omega_c t + \gamma_c))\right) \\[2em] + \displaystyle\sum_{m=1}^{\infty}\sum_{\substack{n=-\infty \\ n\neq 0}}^{\infty}\left( \begin{array}{l} A_{mn}\cos(m(\omega_c t + \gamma_c) + n(\omega_s t + \theta_o)) \\ + B_{mn}\sin(m(\omega_c t + \gamma_c) + n(\omega_s t + \theta_o)) \end{array}\right) \end{array}\right\}. \qquad (3.56)$$

where $i = a,b$; $j = p,n$; $k = 1,2,3,...,q$, and $\gamma_c$ the be initial angle of the carrier signal Consider the desired single phase output voltage,

$$V_s(t) = V_s\cos(\theta_e + \theta_o). \qquad (3.57)$$

where $\theta_e = \omega t$,

$V_s$ is the magnitude of the output voltage,

and $\theta_o$ is the initial angle.

The output voltage spectrum for a full bridge single phase leg is shown in (3.58) [4].

$$V_k = \left\{ V_{dck} M_k \cos(\theta_e + \theta_k) + \frac{4V_{dck}}{\pi}\sum_{m=2}^{\infty}\sum_{n=-\infty}^{\infty} \begin{array}{l} \dfrac{1}{m}J_n(\dfrac{m\pi}{2}M_k)\sin\left(\dfrac{\pi}{2}(m+n)\right) \\ \cos(m(\omega_c t + \gamma_k) + n(\theta_e + \theta_k)) \end{array} \right\}. \qquad (3.58)$$

$$\text{where } J_n(x) = \sum_{m=0}^{\infty} \frac{(-1)^m}{m!(m+n)!} \left(\frac{1}{2}x\right)^{2m+n}. \tag{3.59}$$

In this voltage odd carrier (triangular) and associated harmonics as well as even base band and side band harmonics are cancelled. As a result, the only harmonics which exist are the odd side band harmonics around an even carrier. The proof of cancellation of these harmonics are given in Appendix G. $M_k$ denotes the modulation index of the $k_{th}$ H-bridge.

In the 'q' cell CHB multi-level converter, the fundamental component of the total output voltage is expressed as

$$V_{s,fund} = V_{dc1}M_1\cos(\theta_e + \theta_1) + V_{dc2}M_2\cos(\theta_e + \theta_2) + ... + V_{dcq}M_q\cos(\theta_e + \theta_q). \tag{3.60}$$

The first dominant harmonic component which is the first side band harmonic around the second carrier frequency is given in (3.61).

$$V_{o1}^+ = \left\{ \begin{array}{l} -\dfrac{2V_{dc1}}{\pi} J_1(\pi M_1)\cos\big(2(\theta_c + \gamma_1) + (\theta_e + \theta_1)\big) \\[2ex] -\dfrac{2V_{dc2}}{\pi} J_1(\pi M_2)\cos\big(2(\theta_c + \gamma_2) + (\theta_e + \theta_2)\big) + ... \\[2ex] -\dfrac{2V_{dcq}}{\pi} J_1(\pi M_q)\cos\big(2(\theta_c + \gamma_q) + (\theta_e + \theta_q)\big) \end{array} \right\}. \tag{3.61}$$

where $\gamma_1, \gamma_2, \gamma_3, ..., \gamma_q$ are the initial angles of carrier waveforms,

$\theta_1, \theta_2, \theta_3, ..., \theta_q$ are the initial angles of fundamental signal.

If all the phase angles of modulation signals are the same and equal to the phase angle of the desired output voltage, the relationship between the modulation indices in terms of the input dc voltages and output desire voltage magnitude is shown in (3.62).

$$V_{dc1} M_1 + V_{dc2} M_2 + ... + V_{dcq} M_q = V_s.$$  (3.62)

Using $J_n(x) = \sum_{m=0}^{\infty} \dfrac{(-1)^m}{m!(m+n)!} \left(\dfrac{1}{2} x\right)^{2m+n}$, $J_1(\pi M_k) = \dfrac{\pi M_k}{2}$,  (3.63)

where $k = 1,2,3,...,q$

Therefore equation (3.61) becomes,

$$V_{o1}^+ = \begin{bmatrix} \left[ -M_1 V_{dc1} \cos(2(0) + \alpha) - M_2 V_{dc2} \cos\left(2\left(\dfrac{\pi}{q}\right) + \alpha\right) - ... \right] \\ -M_q V_{dcq} \cos\left(2\left(\dfrac{q\pi}{q}\right) + \alpha\right) \end{bmatrix}.$$  (3.64)

Equating sine and cosine terms in (3.64) will give some equations in terms of '$q$' unknown modulation signals $(M_1, M_2, ..., M_q)$. The addition of required number of constraints will give enough equations to solve for all the modulation indices of '$q$' cell CHBMC. For example, the modulation indices of two cells can be determined as given below.

$$V_{o1}^+ = -M_1 V_{dc1} \cos(2(0) + \alpha) - M_2 V_{dc2} \cos\left(2\left(\dfrac{\pi}{2}\right) + \alpha\right).$$  (3.65)

$$V_{o1}^+ = -M_1 V_{dc1} \cos\alpha + M_2 V_{dc2} \cos\alpha.$$  (3.66)

To eliminate the dominant harmonics given in (3.66), the modulation indices are selected in such a way that they satisfy the following equation,

$$-M_1 V_{dc1} \cos\alpha + M_2 V_{dc2} \cos\alpha = 0.$$  (3.67)

$$\Rightarrow M_1 V_{dc1} = M_2 V_{dc2}.$$  (3.68)

Substituting (3.68) in (3.62), the expression for each modulation index then becomes

$$M_1 = \frac{V_s}{2V_{dc1}} \tag{3.69}$$

$$M_2 = \frac{M_1 V_{dc1}}{V_{dc2}} = \frac{V_s V_{dc1}}{2V_{dc1} V_{dc2}} = \frac{V_s}{2V_{dc2}} \tag{3.70}$$

### 3.6 Over-modulation Region of Operation

The region of operation between the loss of linear control and complete loss of control is called the over modulation region [4]. Since the modulator effectively loses control of the output voltage waveform during the saturation period, the output voltage waveform becomes progressively distorted and includes low frequency harmonics of the fundamental component.

The double Fourier series approximation of the fundamental component of converter output voltage in the case of over modulation is given as [4]

$$V_{ab}(t) = \left[ \begin{array}{l} \dfrac{2V_{dc}}{\pi} \left[ 4\sin\psi + M\left(\pi - 2\psi - \sin 2\psi\right) \right] \cos\omega_o t \\ + \displaystyle\sum_{m=1}^{\infty} \sum_{n=-\infty}^{\infty} C_{mn} \cos\left(2m\omega_c t + [2n-1]\omega_o t\right) \end{array} \right]. \tag{3.71}$$

$$\text{where } C_{mn} = \frac{4V_{dc}}{m\pi^2} \left[ \begin{array}{l} J_{2n-1}(m\pi M)\cos\left[(m+n-1)\pi\right]\left[\pi - 2\psi - \dfrac{\sin 2(2n-1)\psi}{2n-1}\right] \\ + \displaystyle\sum_{\substack{k=1 \\ 2k-1\neq 2n-1}}^{\infty} \left[ \begin{array}{l} J_{2k-1}(m\pi M)\cos\left[(m+k)\pi\right] \\ \left(\dfrac{\sin 2(n+k-1)\psi}{n+k-1} + \dfrac{\sin 2(n-k)\psi}{n-k}\right) \end{array} \right] \end{array} \right]. \tag{3.72}$$

$$\psi = \cos^{-1}\left(\frac{1}{M}\right).$$

The gain from the fundamental component of (3.67) is

58

$$V_{ab} = \frac{2V_{dc}}{\pi} \left[ 4\sin\psi + M\left(\pi - 2\psi - \sin 2\psi\right) \right]. \tag{3.73}$$

For 'q' cell cascaded H bridge multi-level converter, the expression for gain from fundamental component is given as

$$V_{ab} = \sum_{k=1}^{q} \frac{2V_{dc_k}}{\pi} \left[ 4\sin\psi_k + M_k\left(\pi - 2\psi_k - \sin 2\psi_k\right) \right]. \tag{3.74}$$

where $\psi_k = \cos^{-1}\left(\frac{1}{M_k}\right)$, $k = 1,2,3,...,q$.

### 3.7 Summary

A method for the determination of the modulation signals for the multilevel cascaded single phase inverters which eliminate the dominant harmonics in the desired output voltage is proposed for both the linear and over-modulation operating regions. This method is applicable to the cases when the DC input voltages are either equal or unequal. This method can be extended for the determination of the modulation signals for higher multilevel cascaded single-phase converters. This chapter therefore provides an analytical method to determine the modulation signals required for unipolar PWM modulation of cascaded multi-level single-phase DC-AC converters. This chapter also provides the expression for output voltage gain for the over modulation operating region.

# CHAPTER 4

# SINGLE PHASE TWO, THREE, FOUR AND FIVE CELL CASCADED H-BRIDGE DC-AC CONVERTER

## 4.1 Introduction

In chapter 3, the full modeling and analysis of 'q' cell cascaded H-bridge multi-level converter was studied. In this chapter, the modeling and analysis of two, three, and four cells cascaded H-bridge multilevel converter are presented.



(a)

(b)
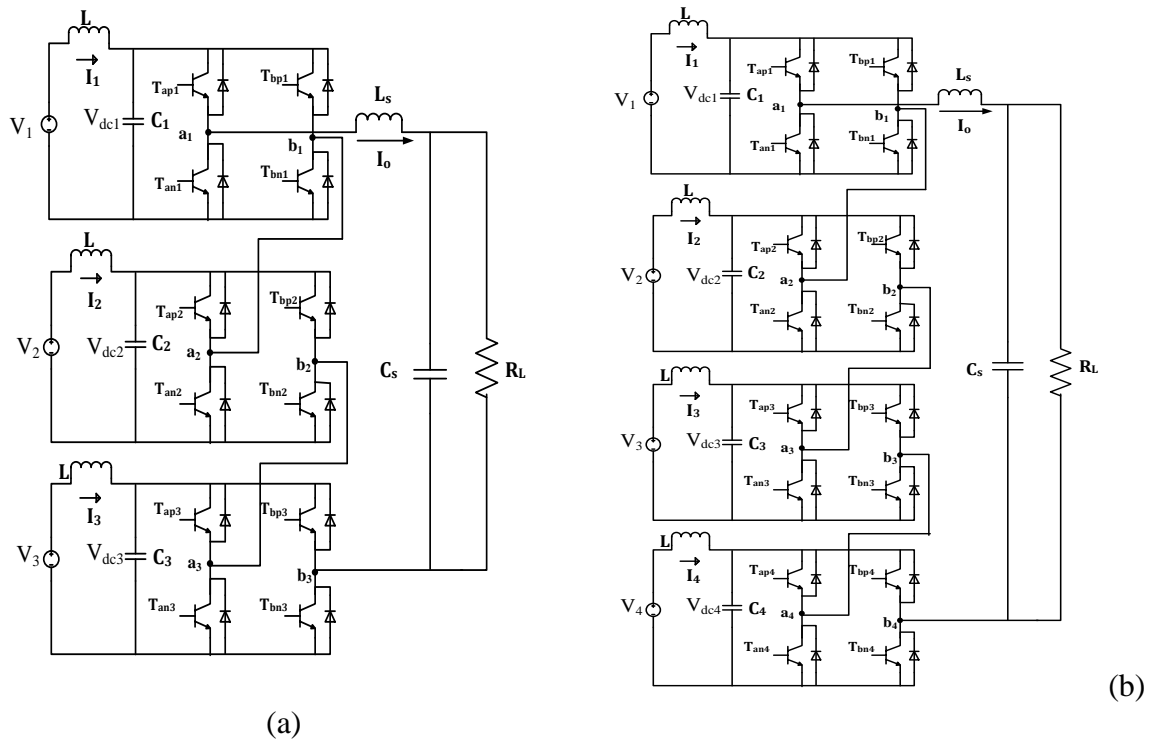
Figure 4.1 Single phase three cell and four cell CHB inverter connected to resistive load.

The simulation and experimental results are also presented in this chapter. The topology of single-phase 2-cell CHB multi-level inverter has already been shown in Figure 3.1. The topologies of single-phase 3-cell and 4-cell CHB multi-level inverter are shown in Figure 4.1 and 4.2, respectively.

## 4.2 Determination of Unipolar PWM Modulation Signals

The double Fourier series approximation of the switching functions given in (3.45) as

$$S_{ij}(\omega_s, \omega_c) = \left\{ \begin{array}{l} \dfrac{A_{00}}{2} + \displaystyle\sum_{n=1}^{\infty}\left(A_{0n}\cos(n\omega_s t) + B_{0n}\sin(n\omega_s t)\right) \\[2ex] + \displaystyle\sum_{m=1}^{\infty}\left(A_{m0}\cos(m\omega_c t) + B_{m0}\sin(m\omega_c t)\right) \\[2ex] + \displaystyle\sum_{m=1}^{\infty}\sum_{\substack{n=-\infty \\ n\neq 0}}^{\infty}\left(A_{mn}\cos(m\omega_c t + n\omega_s t) + B_{mn}\sin(m\omega_c t + n\omega_s t)\right) \end{array} \right\}. \tag{4.1}$$

where $i = a, b; \ j = p, n$

### 4.2.1    Two Cell Cascaded H-bridge DC-AC converter

The expression for each modulation index for two cell was given in chapter 3 as

$$M_1 = \frac{V_s}{2V_{dc1}}. \tag{4.2}$$

$$M_2 = \frac{M_1 V_{dc1}}{V_{dc2}} = \frac{V_s V_{dc1}}{2V_{dc1} V_{dc2}} = \frac{V_s}{2V_{dc2}}. \tag{4.3}$$

### 4.2.2 Three Cell Cascaded H-bridge DC-AC converter

The fundamental component of the total output voltage is expressed as

$$V_{s,fund} = V_{dc1} M_1 \cos(\theta_e + \theta_1) + V_{dc2} M_2 \cos(\theta_e + \theta_2) + V_{dc3} M_3 \cos(\theta_e + \theta_3). \qquad (4.4)$$

The first dominant harmonic component which is the first side band harmonic around the second carrier frequency is given in (4.5).

$$V_{o1}^+ = \left\{ \begin{array}{l} -\dfrac{2V_{dc1}}{\pi} J_1(\pi M_1) \cos\left(\begin{array}{l} 2(\theta_c + \gamma_1) \\ + (\theta_e + \theta_1) \end{array}\right) - \dfrac{2V_{dc2}}{\pi} J_1(\pi M_2) \cos\left(\begin{array}{l} 2(\theta_c + \gamma_2) \\ + (\theta_e + \theta_2) \end{array}\right) \\ -\dfrac{2V_{dc3}}{\pi} J_1(\pi M_3) \cos\left(\begin{array}{l} 2(\theta_c + \gamma_3) \\ + (\theta_e + \theta_3) \end{array}\right) \end{array} \right\}. \qquad (4.5)$$

If all the phase angles of modulation signals are the same and equal to the phase angle of the desired output voltage, then

$$\theta_1 = \theta_2 = \theta_3 = \theta_0.$$

The relationship between the modulation indices in terms of the input dc voltages and output desire voltage magnitude is shown in (4.6).

$$V_{dc1} M_1 + V_{dc2} M_2 + V_{dc3} M_3 = V_s. \qquad (4.6)$$

Using $J_n(x) = \sum_{m=0}^{\infty} \dfrac{(-1)^m}{m!(m+n)!} \left(\dfrac{1}{2} x\right)^{2m+n}$,

we get $J_1(\pi M_k) = \dfrac{\pi M_k}{2}$, $\qquad (4.7)$

where $k = 1,2,3.$

Therefore equation (4.5) becomes,

$$V_{o1}^+ = -M_1 V_{dc1} \cos(\gamma) - M_2 V_{dc2} \cos\left(\frac{2\pi}{3} + \gamma\right) + M_3 V_{dc3} \cos\left(\frac{4\pi}{3} + \gamma\right). \qquad (4.8)$$

To eliminate the dominant harmonics given in (4.8), the modulation indices are selected in such a way that they satisfy the following equations,

$$2M_1 V_{dc1} = M_2 V_{dc2} + M_3 V_{dc3}. \qquad (4.9)$$

$$M_2 V_{dc2} = M_3 V_{dc3}. \qquad (4.10)$$

Substituting (4.9), (4.10) in (4.6), the expression for each modulation index then becomes,

$$M_1 = \frac{V_s}{3V_{dc1}}; \; M_2 = \frac{V_s}{3V_{dc2}}; \; M_3 = \frac{V_s}{3V_{dc3}}. \qquad (4.11)$$

### 4.2.3    Four Cell Cascaded H-bridge DC-AC converter

The fundamental component of the total output voltage is expressed as

$$V_{s,fund} = \left[ \begin{array}{l} V_{dc1} M_1 \cos(\theta_e + \theta_1) + V_{dc2} M_2 \cos(\theta_e + \theta_2) \\ + V_{dc3} M_3 \cos(\theta_e + \theta_3) + V_{dc4} M_4 \cos(\theta_e + \theta_4) \end{array} \right] \qquad (4.12)$$

And the first dominant harmonic component which is the first side band harmonic around the second carrier frequency is given in (4.13).

$$V_{o1}^+ = \left[ \begin{array}{l} -\frac{2V_{dc1}}{\pi} J_1(\pi M_1) \cos\left(\begin{array}{l} 2(\theta_c + \gamma_1) \\ +(\theta_e + \theta_1) \end{array}\right) - \frac{2V_{dc2}}{\pi} J_1(\pi M_2) \cos\left(\begin{array}{l} 2(\theta_c + \gamma_2) \\ +(\theta_e + \theta_2) \end{array}\right) \\ -\frac{2V_{dc3}}{\pi} J_1(\pi M_3) \cos\left(\begin{array}{l} 2(\theta_c + \gamma_3) \\ +(\theta_e + \theta_3) \end{array}\right) - \frac{2V_{dc4}}{\pi} J_1(\pi M_4) \cos\left(\begin{array}{l} 2(\theta_c + \gamma_4) \\ +(\theta_e + \theta_4) \end{array}\right) \end{array} \right]. \qquad (4.13)$$

If the all the phase angles of the each modulation signals are the same and equal to the phase angle of the desired output voltage, the relationship between the modulation indices in terms of the input dc voltages and output desired voltage magnitude is shown in (4.14).

$$V_{dc1} M_1 + V_{dc2} M_2 + V_{dc3} M_3 + V_{dc4} M_4 = V_s .$$ (4.14)

(4.15)

Using $J_n(x) = \sum_{m=0}^{\infty} \frac{(-1)^m}{m!(m+n)!} \left(\frac{1}{2}x\right)^{2m+n}$ ,

we get $J_1(\pi M_k) = \frac{\pi M_k}{2}$ .

where $k = 1,2,3$.

Therefore equation (4.13) becomes,

(4.16)

$$V_{o1}^+ = \left\{ \begin{array}{l} -M_1 V_{dc1} \cos(2(0)+\gamma) - M_2 V_{dc2} \cos\left(2\left(\frac{\pi}{4}\right)+\gamma\right) \\[3mm] -M_3 V_{dc3} \cos\left(2\left(\frac{2\pi}{4}\right)+\gamma\right) - M_4 V_{dc4} \cos\left(2\left(\frac{3\pi}{4}\right)+\gamma\right) \end{array} \right\} .$$

$$V_{o1}^+ = -M_1 V_{dc1} \cos(\gamma) + M_2 V_{dc2} \sin(\gamma) + M_3 V_{dc3} \cos(\gamma) - M_4 V_{dc4} \sin(\gamma).$$ (4.17)

To eliminate the dominant harmonics given in (4.17), the modulation indices are selected in such a way that they satisfy the following equations,

$$M_3 V_{dc3} = M_1 V_{dc1} ;$$ (4.18)

$$M_4 V_{dc4} = M_2 V_{dc2}$$ (4.19)

These equations result in one more degree of freedom to specify the four modulation indices. Define the magnitudes of the first two cells to be related by a fraction, α

$$M_2 = \alpha M_1$$ (4.20)

Substituting (4.18), (4.19), and (4.20) in (4.14)

The expression for each modulation index then becomes,

$$M_1 = \frac{V_s}{2(V_{dc1} + \alpha V_{dc2})}$$

(4.21)

$$M_2 = \frac{\alpha V_s}{2(V_{dc1} + \alpha V_{dc2})}$$

(4.22)

$$M_3 = \frac{V_{dc1} V_s}{2V_{dc3}(V_{dc1} + \alpha V_{dc2})}$$

(4.23)

$$M_4 = \frac{\alpha V_{dc2} V_s}{2V_{dc4}(V_{dc1} + \alpha V_{dc2})}$$

(4.24)

## 4.3 Results and Discussion

### 4.3.1 Two cell CHBMC

The proposed modulation technique is derived and implemented on two cell cascaded H bridge multi-level converter. Experimental validation of proposed method on the laboratory prototype is set forth on a two cell cascaded H-bridge single phase DC-AC converter. The two cell CHBMC has to generate an AC voltage of $V_{out} = 80\cos(\omega t)$ when each of the two cells is fed with 50V dc voltage and the modulation indices are computed based on (4.2) and (4.3). The switching pulses of all the eight switches are shown in Figure 4.2. Figure 4.3 shows the simulation result of four input source currents. Figure 4.4 and Figure 4.5 show the simulation results of individual output voltage of each cell

and the overall output voltage of the inverter based on the proposed method. The Fourier spectrum analysis of the overall output voltage is seen in Figure 4.6. The fundamental frequency of the system is 60Hz. The peak value of fundamental component of output voltage is 79.99V.
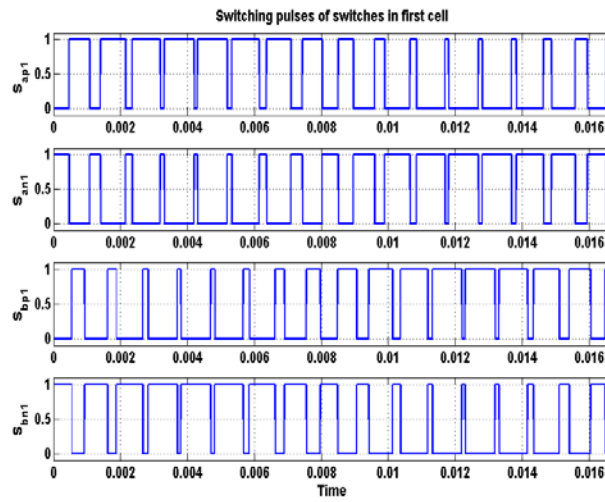


(a)
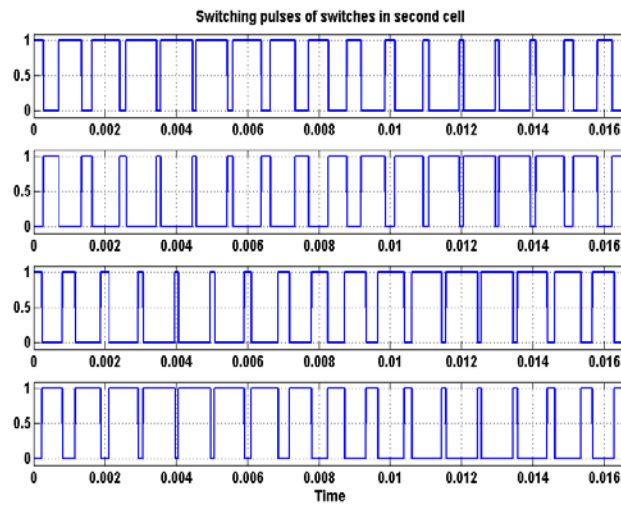


(b)

Figure 4.2. Simulation results: (a) Cell 1 switching pulses, (b) Cell 2 switching pulses

Therefore, this result verifies that the modulation indices calculated based on the proposed technique results in the minimization of harmonics. The three cell cascaded H bridge converter is connected to R load through an LC filter, with parameters $L_f = 100mH$, $C_f = 16\mu F$ and $R_o = 42\Omega$. Figure 4.7 shows the waveforms of load current and load voltage.
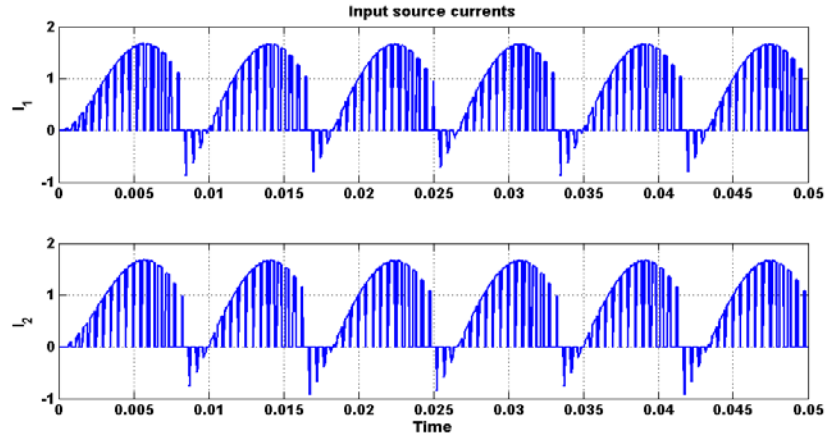
Figure 4.3. Simulation result of input source currents
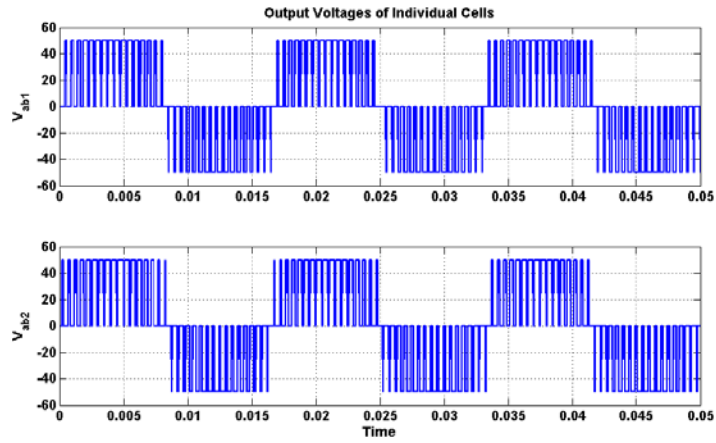


Figure 4.4. Simulation result of individual cell output phase voltages.
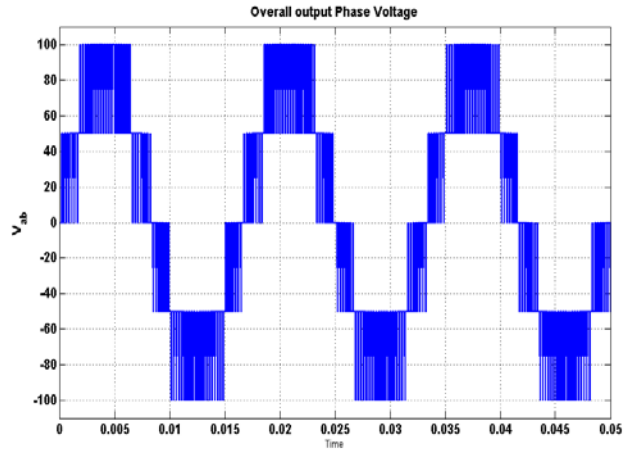
Figure 4.5. Simulation result of overall output phase voltage for two cell cascaded multi-

level inverter.
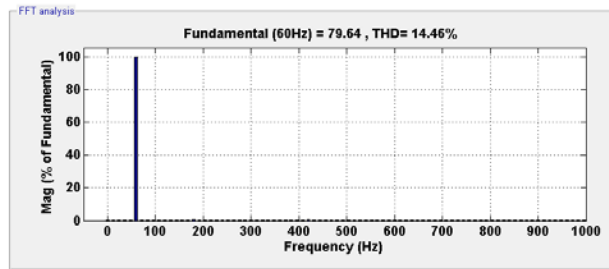


(a)
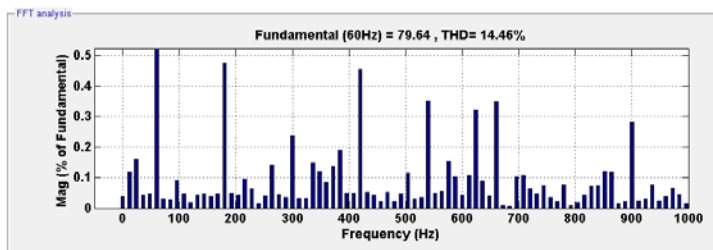


(b)

Figure 4.6. FFT analysis of simulated waveform of output voltage (a) Fundamental

component, (b) Harmonic components.

69
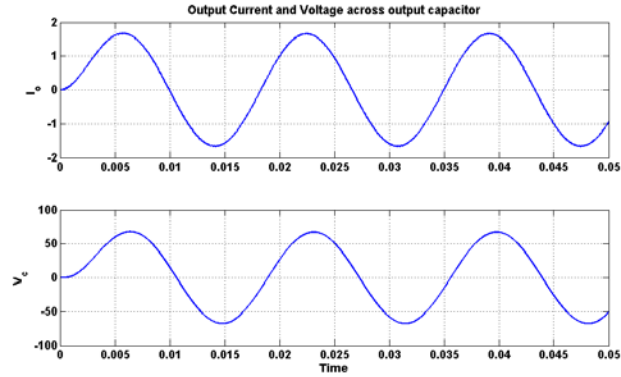
Figure 4.7 Output current and load voltage waveforms.

The experimental results of the two cell cascaded H-bridge multilevel inverter are also presented to compare with the computer simulation results. The waveforms of switching pulses of all the eight switches can be seen in Figure 4.8. Similarly, the output voltages of each individual cell are shown in Figures 4.9.



(a)                                                                (b)
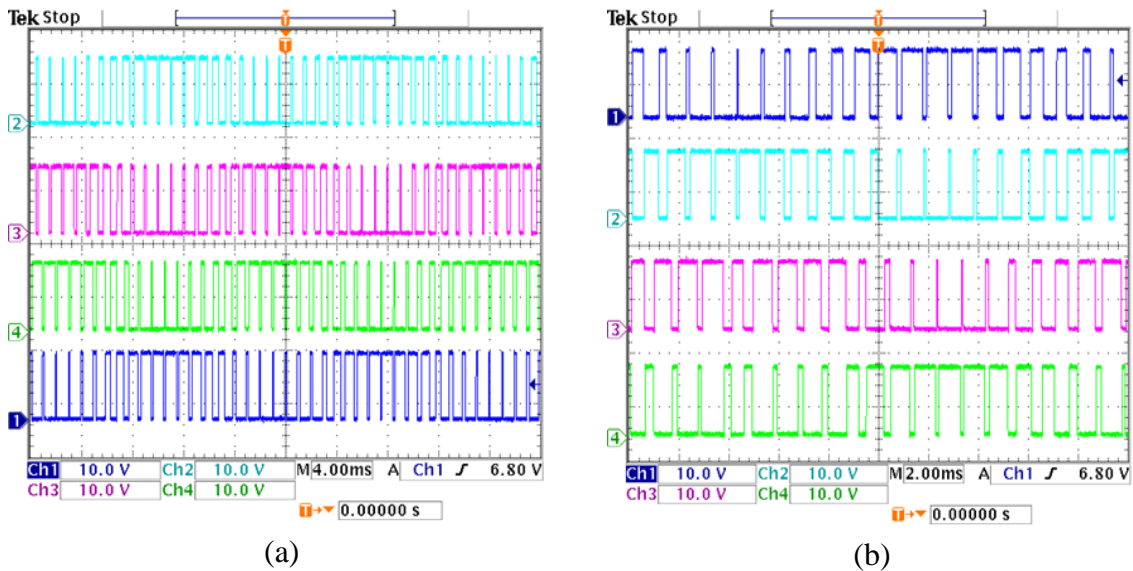
Figure 4.8 Experimental results of switching pulses: (a) Cell 1, (b) Cell 2.

70

(a)

(b)
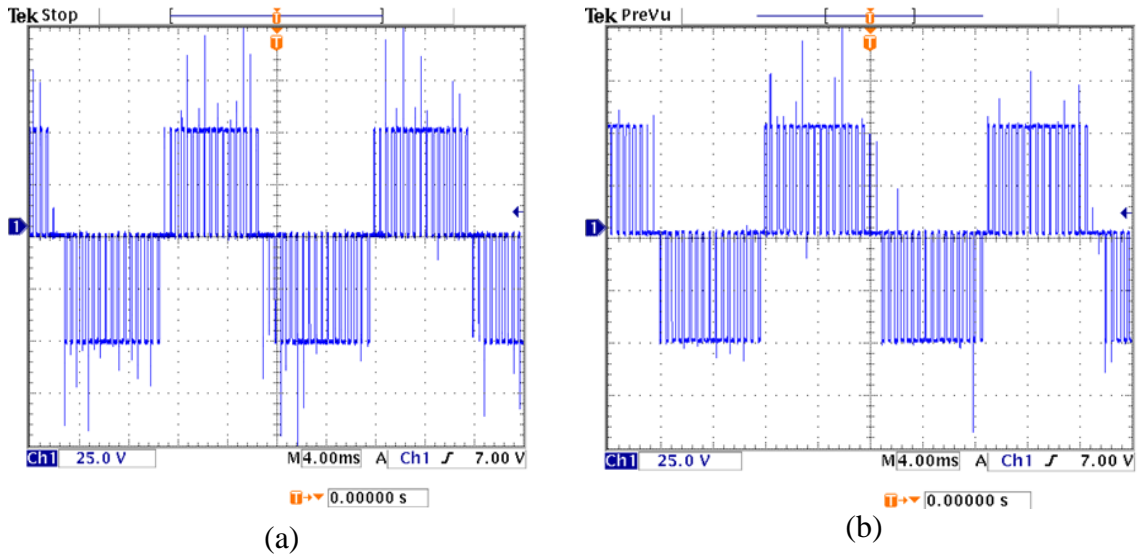
Figure 4.9 Experimental results of output voltage: (a) Cell 1, (b) Cell 2 (25V/div).

Figure 4.10 and Figure 4.11 show the experimental results of individual output voltage of each cell and the overall output voltage of the inverter based on the proposed method. So we can conclude from these results that the experimental results are in good validation with the simulation results.
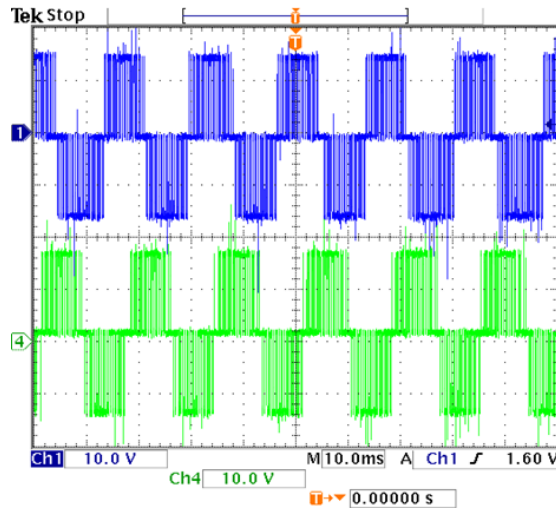


Figure 4.10 Experimental results of individual Output voltages together (10V/div).
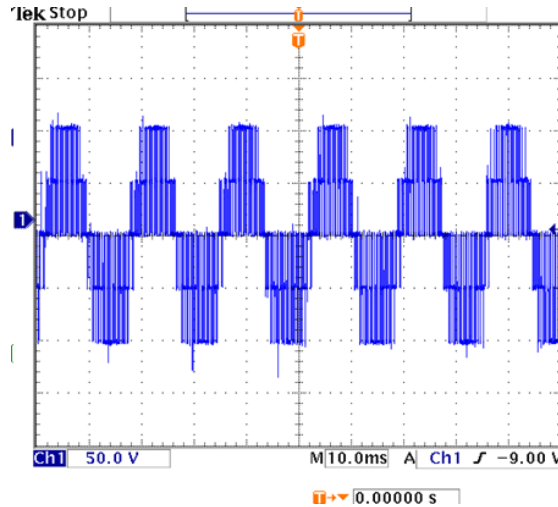
Figure 4.11 Experimental results of overall output voltage for two cell cascaded multi-level inverter (50V/div).

### 4.3.2    Three cell CHBMC:

The proposed modulation technique is derived and implemented on three cell cascaded H bridge multi-level converter also. Experimental validation of proposed method on the laboratory prototype is set forth on a three cell cascaded H-bridge single phase DC-AC converter. The three cell CHBMC has to generate an AC voltage of $V_{out} = 140\cos(\omega t)$ when each of the three cells is fed with 50V dc voltage and the modulation indices are computed based on (4.12). The switching pulses of all the 12 switches are shown in Figures 4.12, 4.13 and 4.14 respectively. Figure 4.15 shows the simulation result of four input source currents. Figure 4.16 and 4.17 show the simulation results of individual output voltage of each cell and the overall output voltage of the inverter based on the proposed method. The Fourier spectrum analysis of the overall

72

output voltage is seen in Figure 4.18. All the harmonic components of the output voltage are less than or equal to 0.03% of fundamental component. The peak value of the fundamental component of output voltage that can be seen from Figure 4.18 is 126.5V.Therefore, this result verifies that the modulation indices calculated based on the proposed technique results in the minimization of harmonics. The three cell cascaded H bridge converter is connected to R load through an LC filter, with parameters $L_f = 100mH$, $C_f = 16\mu F$ and $R_o = 42\Omega$. Figure 4.19 shows the waveforms of load current and load voltage.
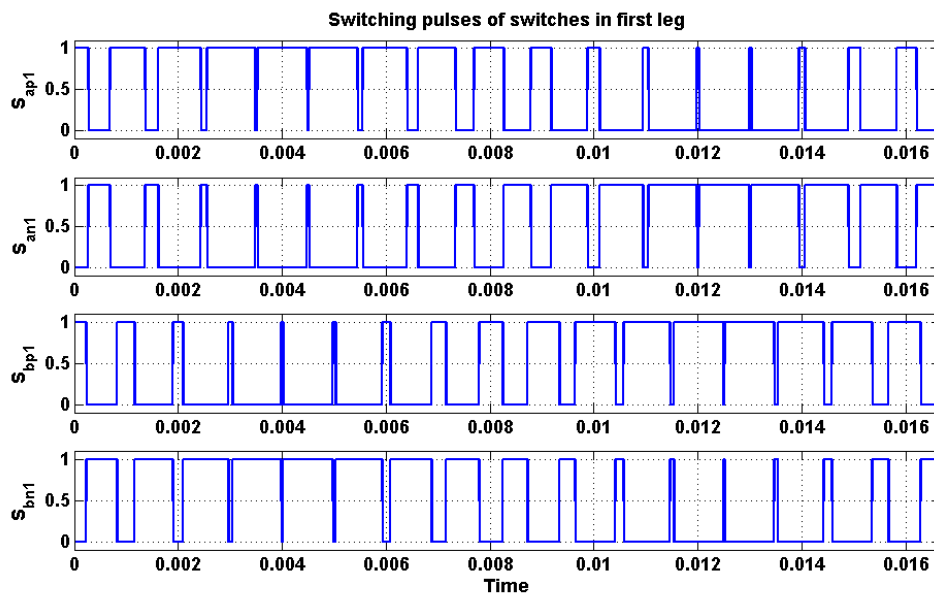


Figure 4.12 Simulation result of switching pulses of switches in first cell.
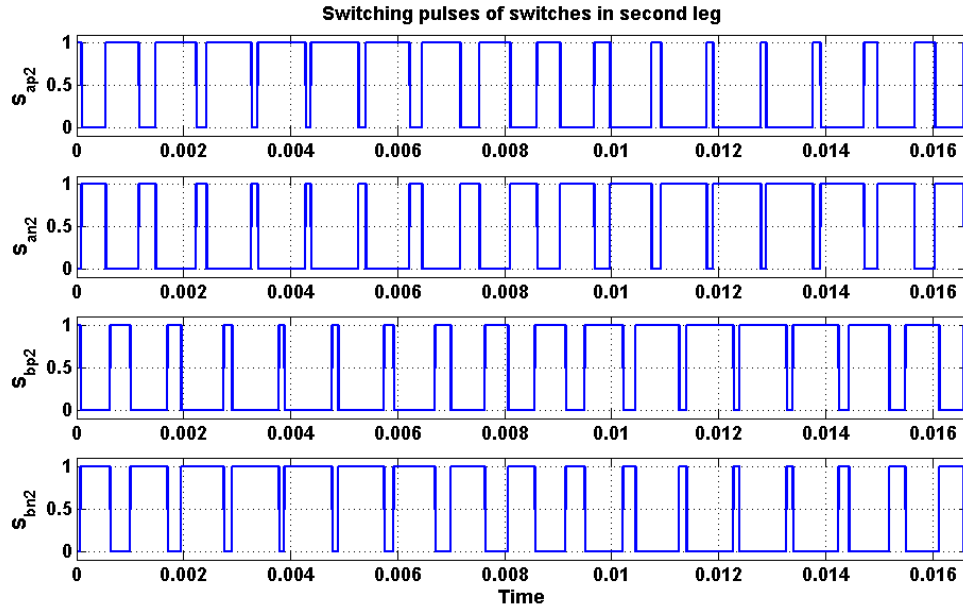
Figure 4.13 Simulation result of switching pulses of switches in second cell.
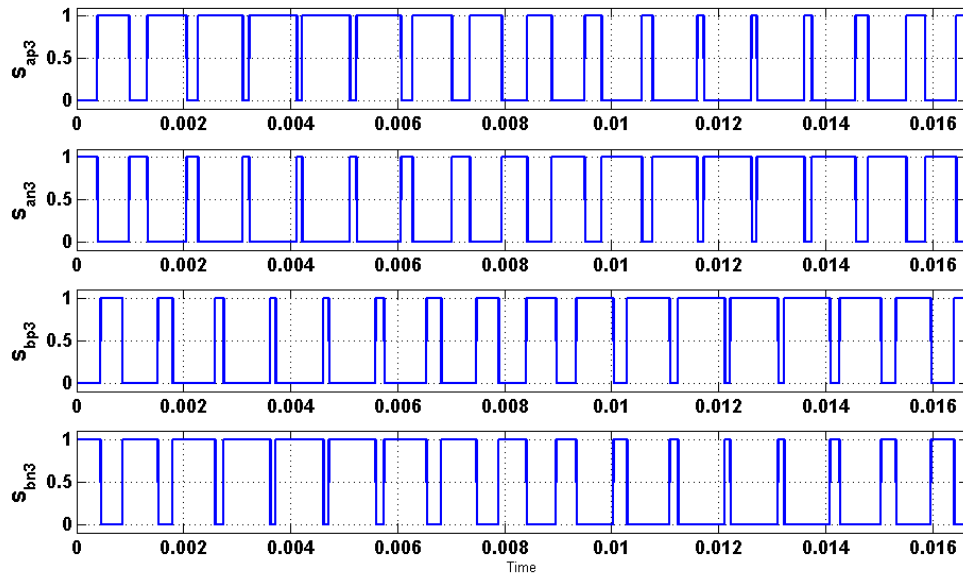


Figure 4.14 Simulation result of switching pulses of switches in third cell.

74
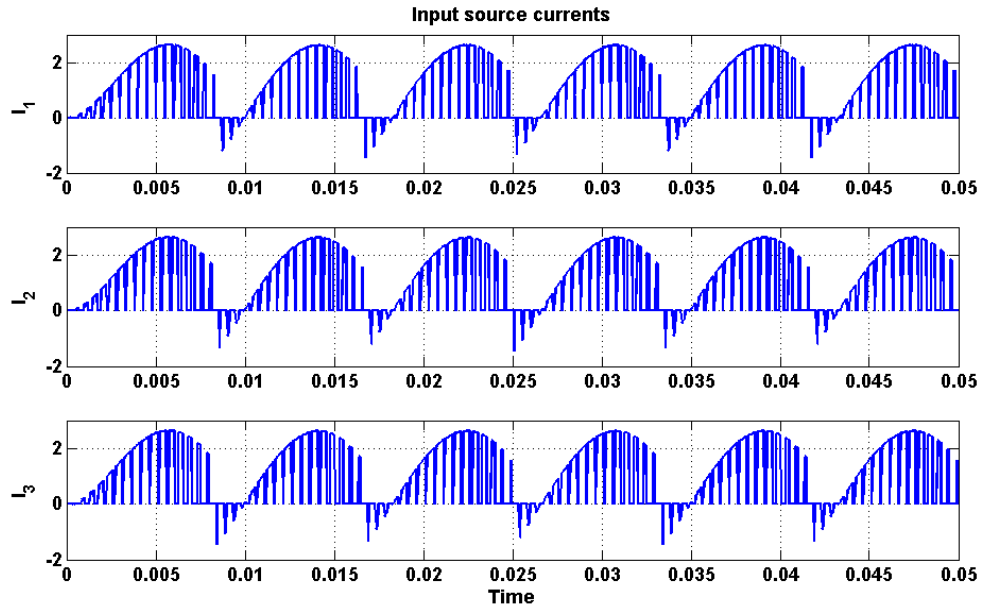
Figure 4.15 Simulation result of input source currents.
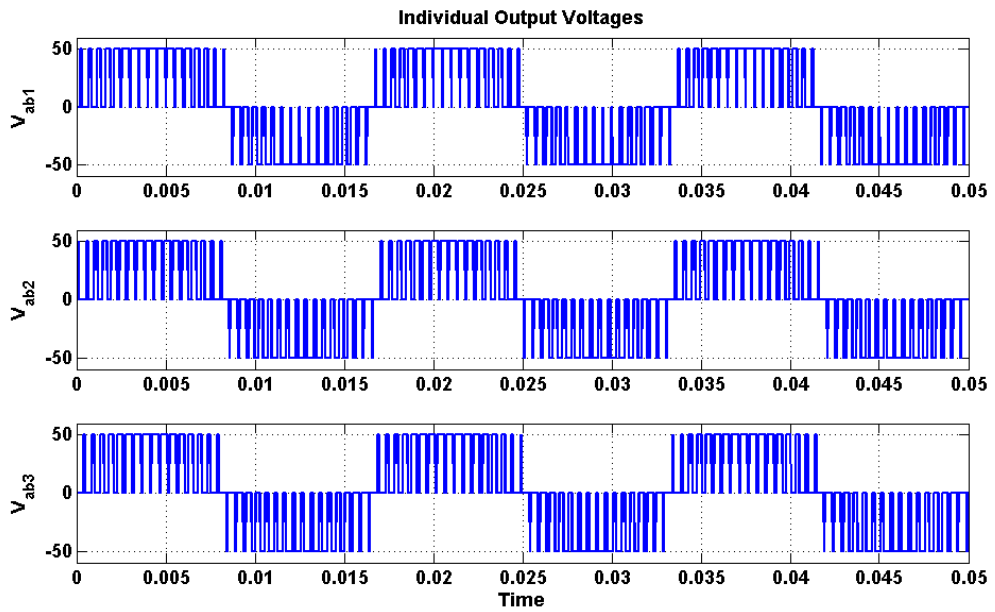


Figure 4.16 Simulation result of individual cell output phase voltages.
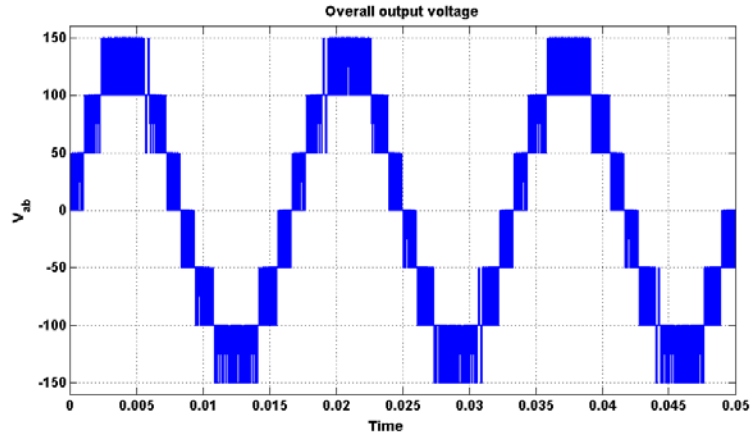
Figure 4.17 Simulation result of overall output phase voltage for three cell cascaded

multi-level inverter.
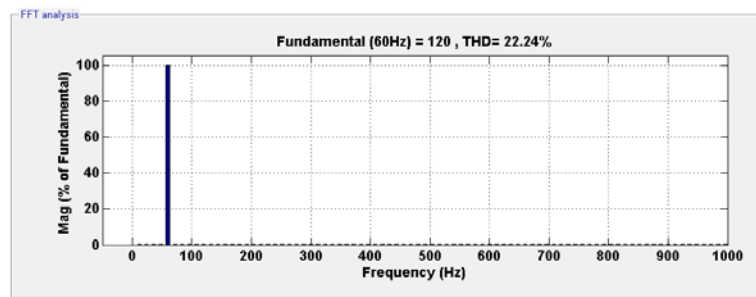


(a)
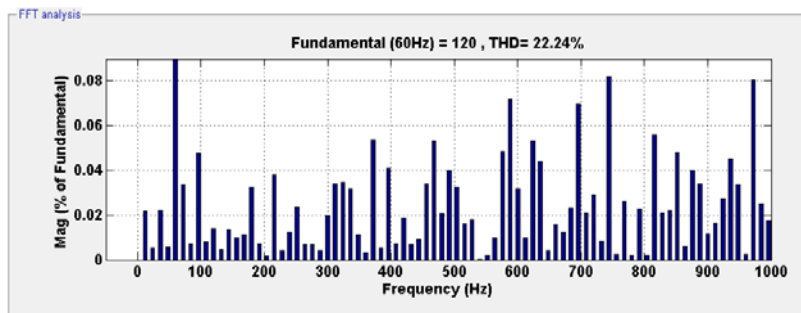


(b)

Figure 4.18 FFT analysis of simulated waveform of overall output phase voltage (a)

Normal spectrum, (b) Zoomed in to see harmonics.
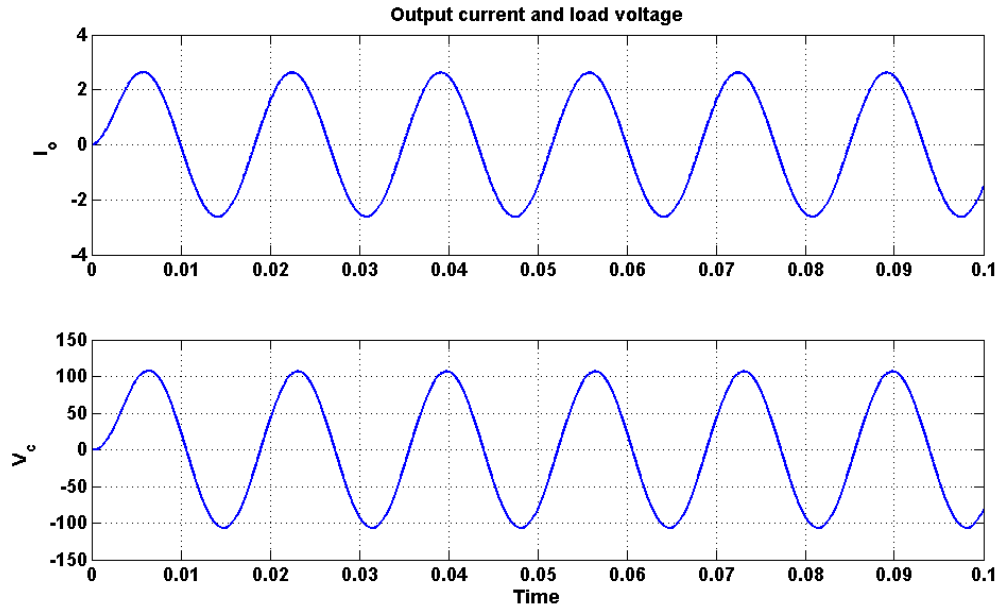
Figure 4.19 Output current and load voltage waveforms when inverter is connected to resistive load.

The experimental results of the overall system are also presented. The waveforms of switching pulses of all the twelve switches can be seen in Figures 4.20, 4.21, and 4.22. Similarly, the output voltages of each individual cell are shown in Figures 4.23, 4.24 and 4.25 respectively. Figures 4.26 and 4.27 show the experimental results of individual output voltage of each cell and the overall output voltage of the inverter based on the proposed method. So we can conclude from these results that the experimental results are in good validation with the simulation results.
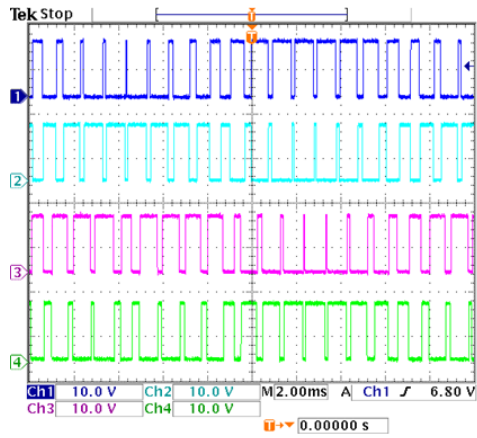
Figure 4.20 Experimental result of switching pulses of switches in first cell (10V/div).
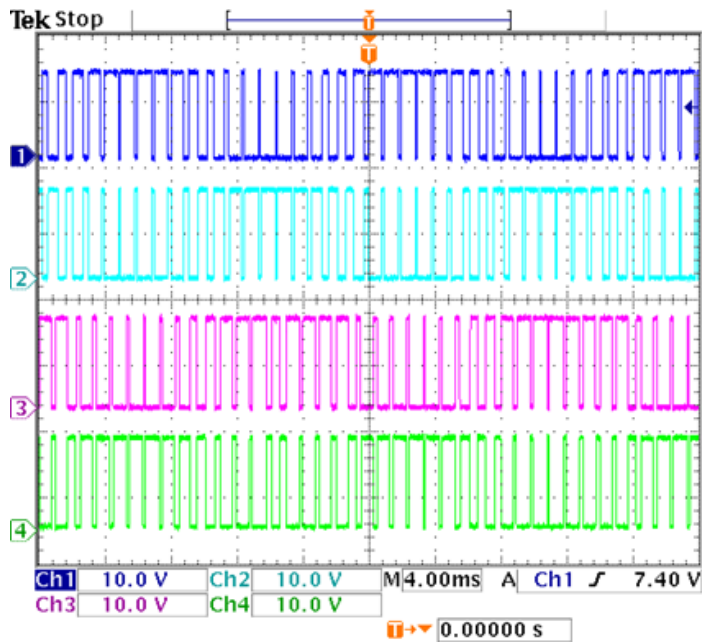


Figure 4.21 Experimental result of switching pulses of switches in second cell (10V/div).
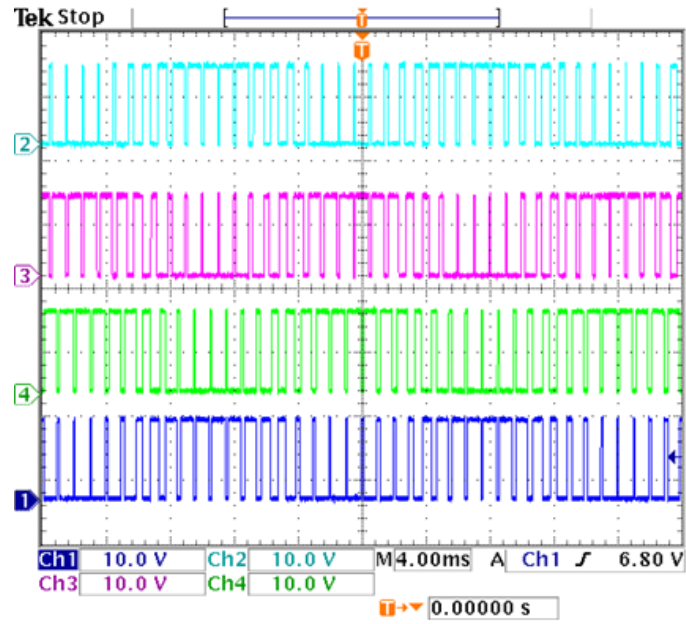
Figure 4.22 Experimental result of switching pulses of switches in third cell (10V/div).
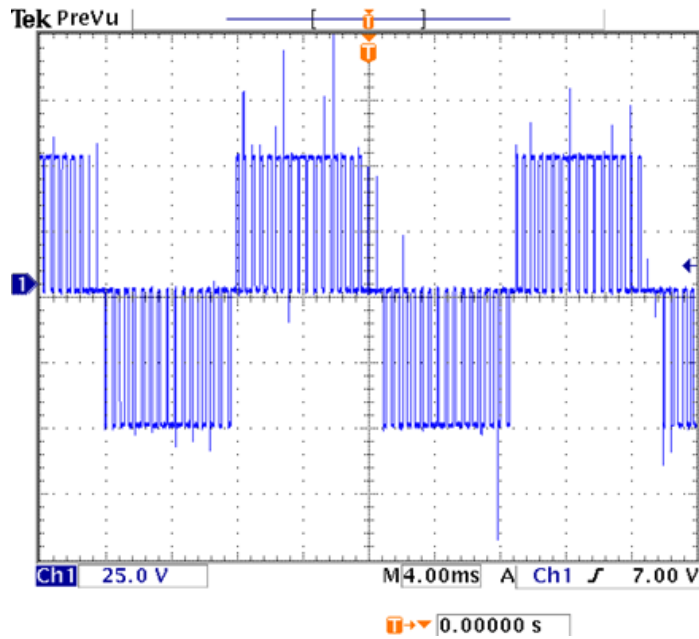


Figure 4.23 Experimental result of output voltage of inverter cell 1 (25V/div).
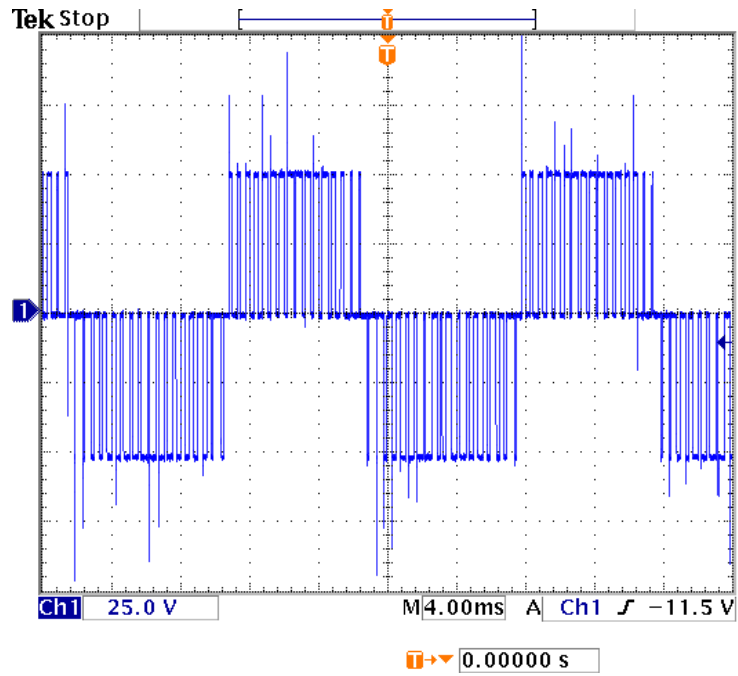
Figure 4.24 Experimental result of output voltage of inverter cell 2 (25V/div).
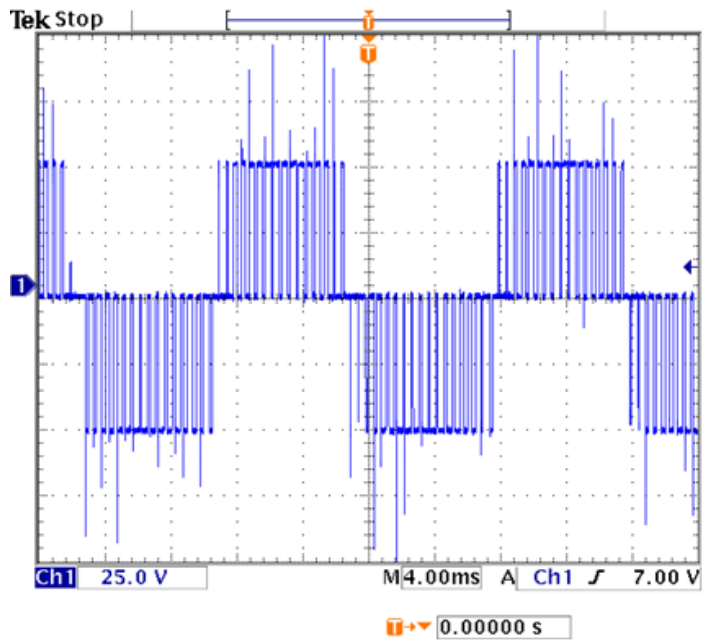


Figure 4.25 Experimental result of output voltage of inverter cell 3 (25V/div).
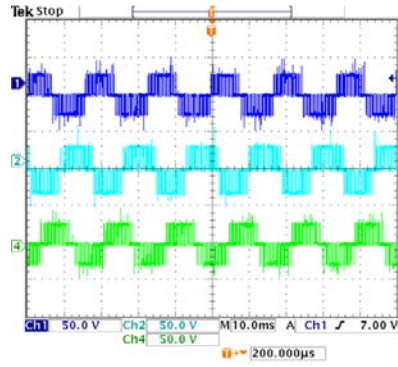
Figure 4.26 Experimental result of individual Output voltages together (50V/div).
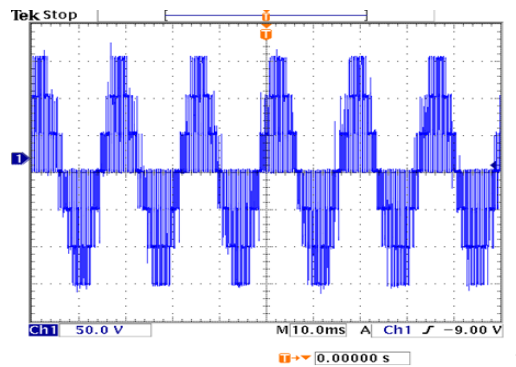


(a)
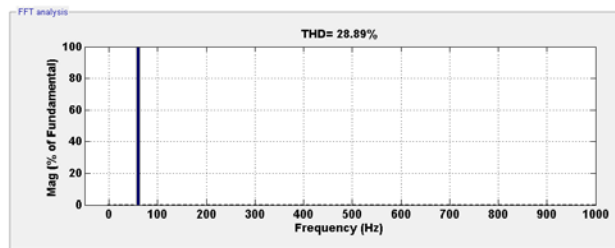


(b)
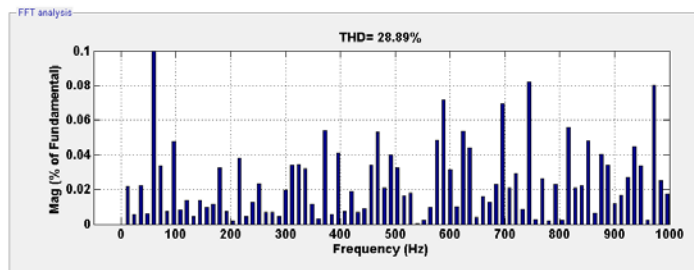


(c)

Figure 4.27 Experimental results: (a) Overall output voltage for three cell cascaded multi-

level inverter (50V/div), (b) Fundamental component, (c) Harmonic components.

### 4.3.3 Four Cell CHBMC

The proposed modulation technique is derived and implemented on four cell cascaded H bridge multi-level converter also. Experimental validation of proposed method on the laboratory prototype is set forth on a four cell cascaded H-bridge single phase DC-AC converter. The four cell CHBMC has to generate an AC voltage of $V_{out} = 180\cos(\omega t)$ when each of the four cells is fed with 50V dc voltage and the modulation indices are computed based on (4.21), (4.22), (4.23), and (4.24) respectively. Figures 4.28, 4.29, 4.30 and 4.31 show the simulation results of switching pulses of switches in cells 1, 2, 3 and 4 respectively. Figure 4.32 shows the simulation result of four input source currents. Figures 4.33 and 4.34 shows the simulation results of individual output voltage of each cell and the overall output voltage of the inverter based on the proposed method. The Fourier spectrum analysis of the overall output voltage is seen in Figure 4.35. All the harmonic components of the output voltage are less than or equal to 0.03% of fundamental component. The peak value of the fundamental component of output voltage that can be seen from Figure 4.18 is 180V. Therefore, this result verifies that the modulation indices calculated based on the proposed technique results in the minimization of harmonics. The four cell cascaded H bridge converter is connected to R load through an LC filter, with parameters $L_f = 100mH$, $C_f = 16\mu F$ and $R_o = 42\Omega$. Figure 4.36 shows the waveforms of load current and load voltage.
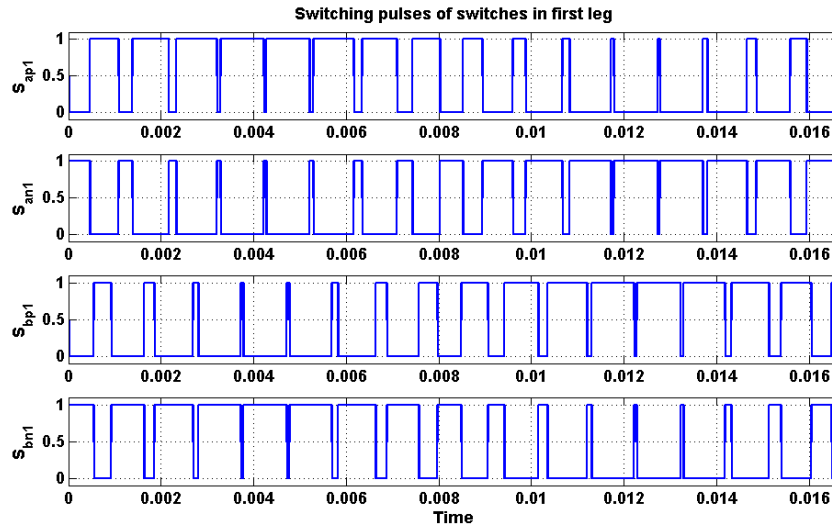
Figure 4.28 Simulation result of switching pulses of switches in first cell.
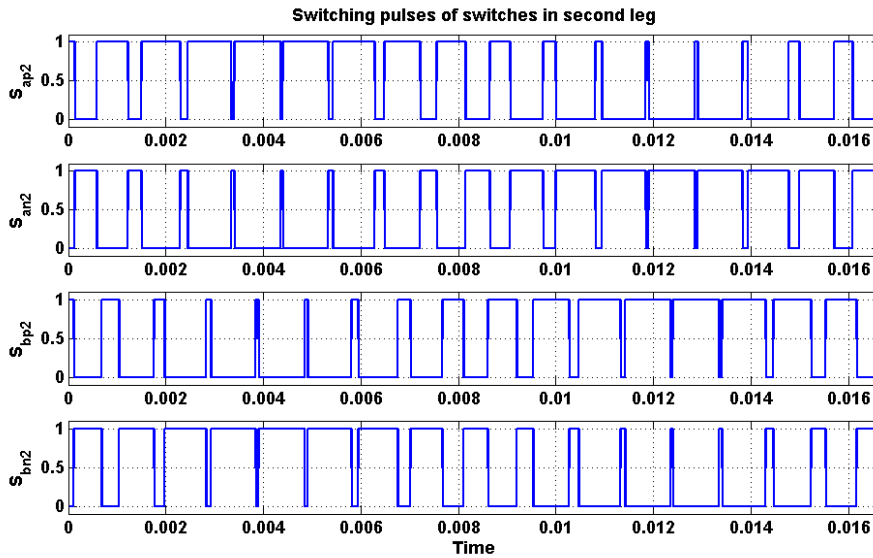


Figure 4.29 Simulation result of switching pulses of switches in second cell.
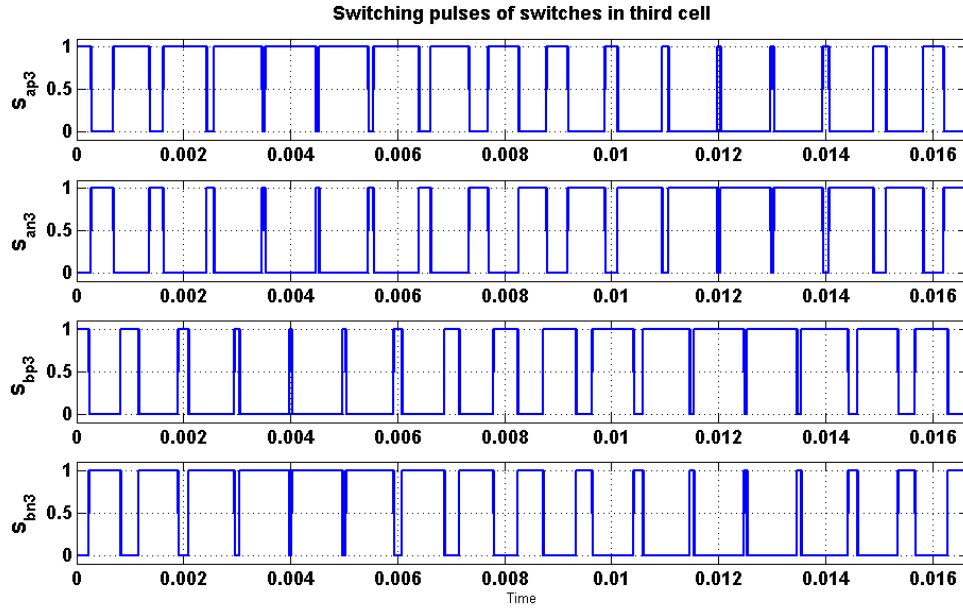
Figure 4.30 Simulation result of switching pulses of switches in third cell.
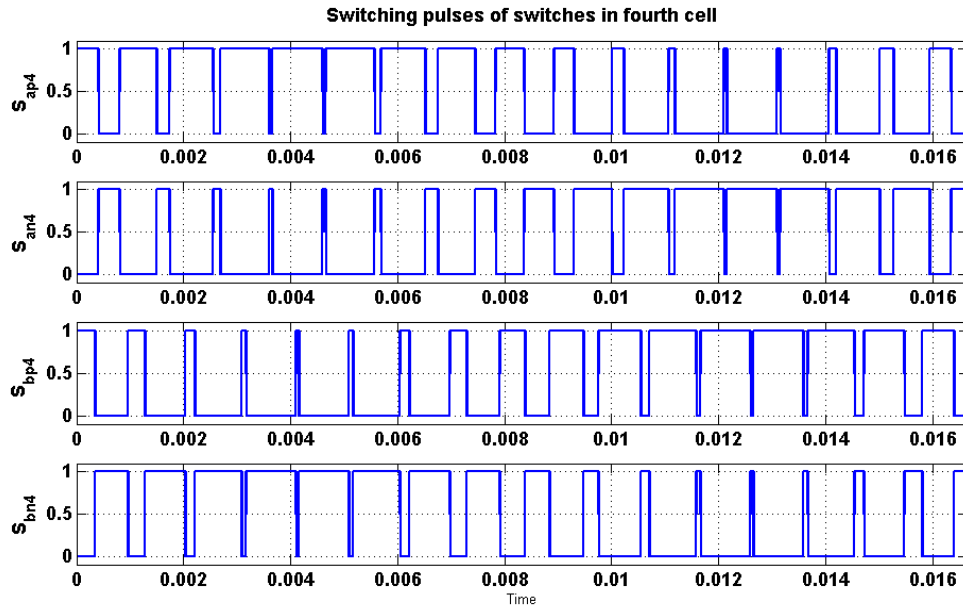


Figure 4.31 Simulation result of switching pulses of switches in fourth cell.
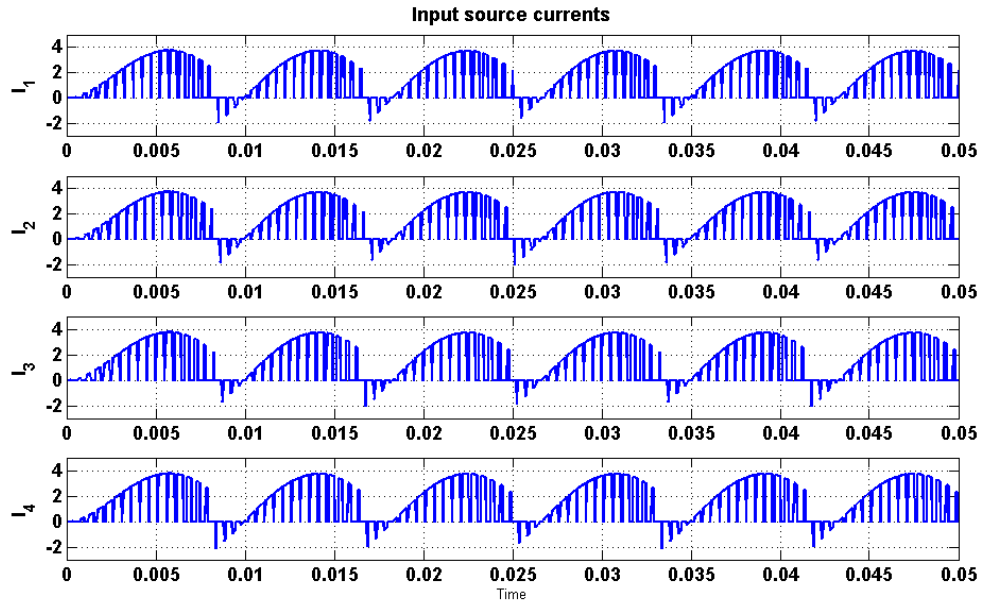
Figure 4.32 Simulation result of input source currents.
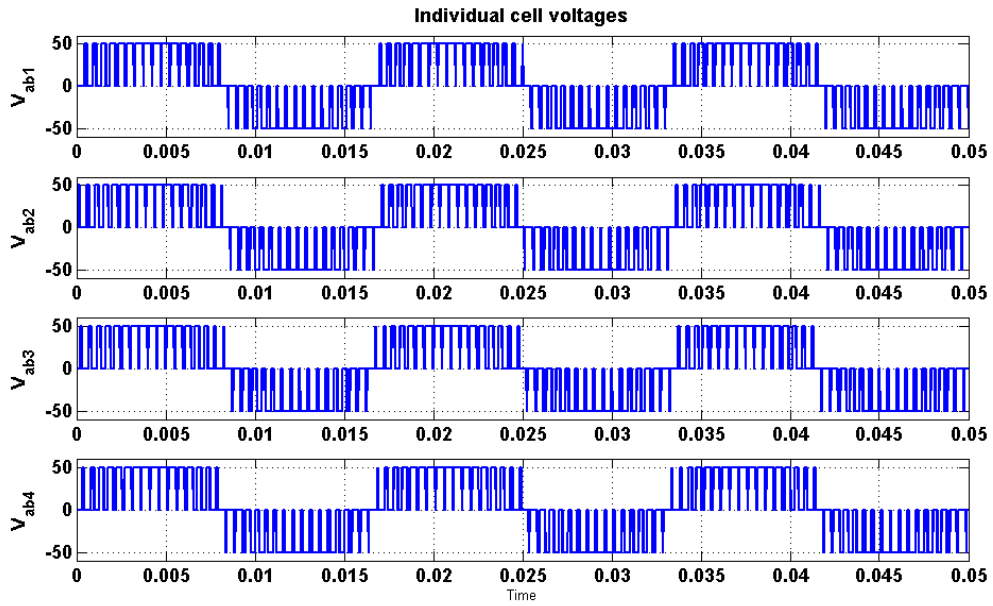


Figure 4.33 Simulation result of individual cell output phase voltages.
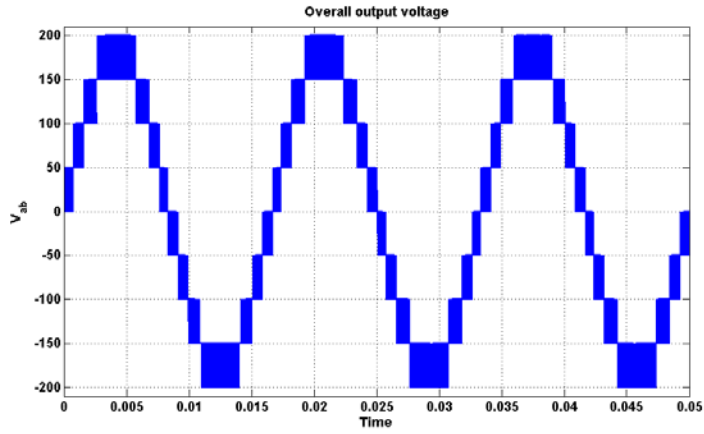
Figure 4.34 Simulation result of overall output phase voltage for four cell cascaded multi-level inverter.
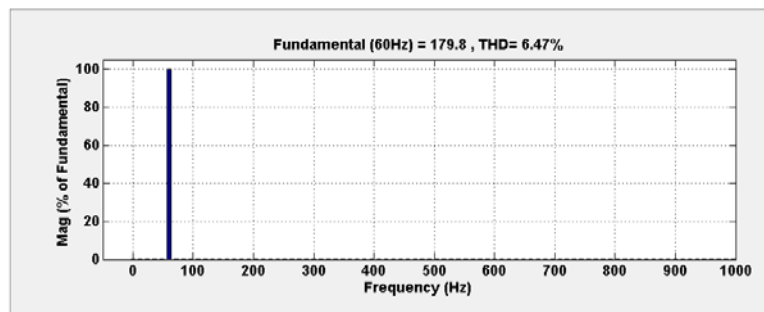


(a)



(b)

Figure 4.35 FFT analysis of the simulated waveform of overall output phase voltage for four cell CHBMC, (a) Fundamental component, (b) Harmonic components.
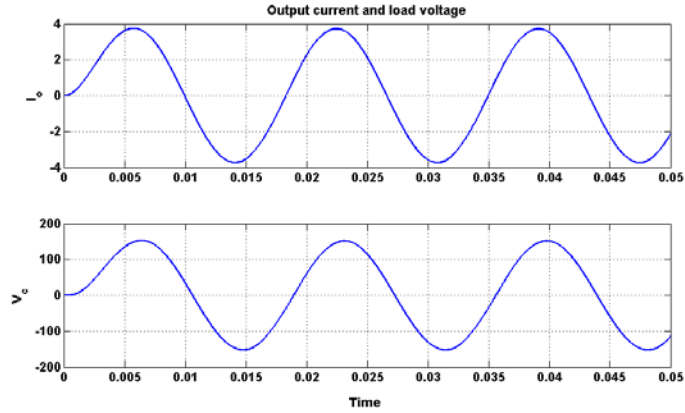
Figure 4.36 Output current and load voltage waveforms.
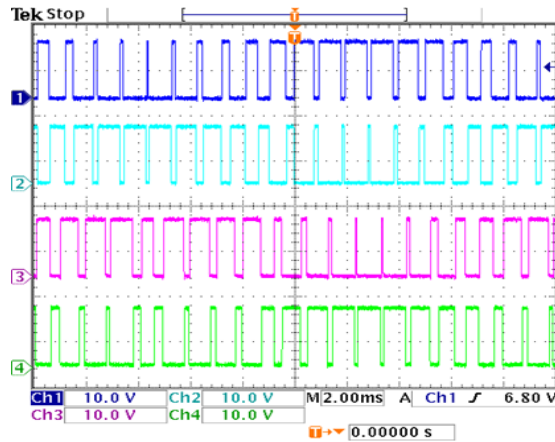


Figure 4.37 Experimental result of switching pulses of switches in first cell (10V/div).

The experimental results of the overall system are also presented. The waveforms of switching pulses of all the four cells can be seen in Figures 4.37, 4.38, 4.39, and 4.40 respectively. Figure 4.41 and 4.42 show the experimental results of individual output voltage of each cell and the overall output voltage of the inverter based on the proposed method. So we can conclude from these results that the experimental results are in good validation with the simulation results.

87
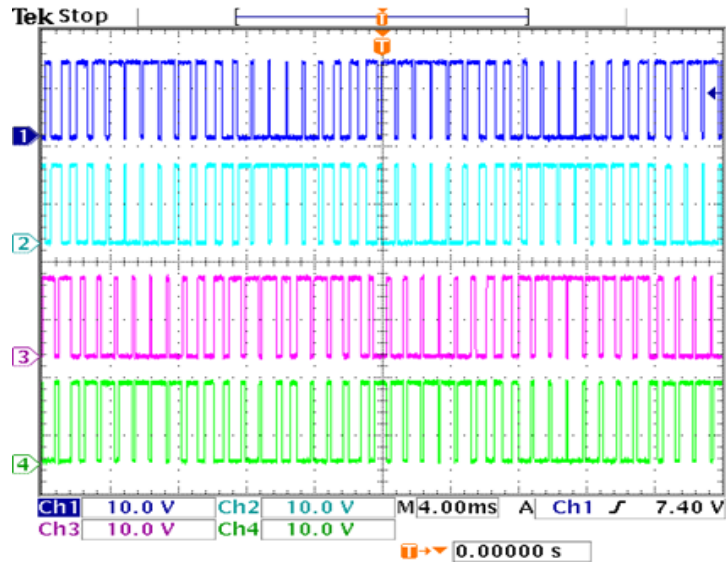
Figure 4.38 Experimental result of switching pulses of switches in second cell (10V/div).
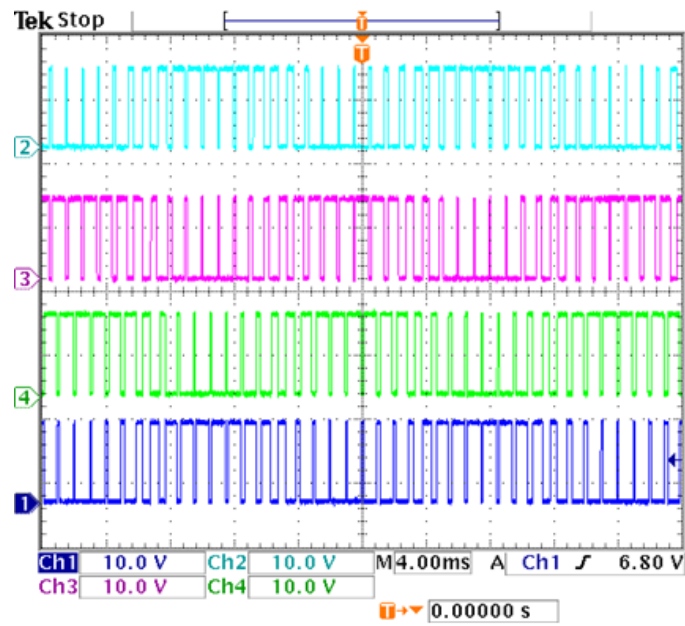


Figure 4.39 Experimental result of switching pulses of switches in third cell (10V/div).
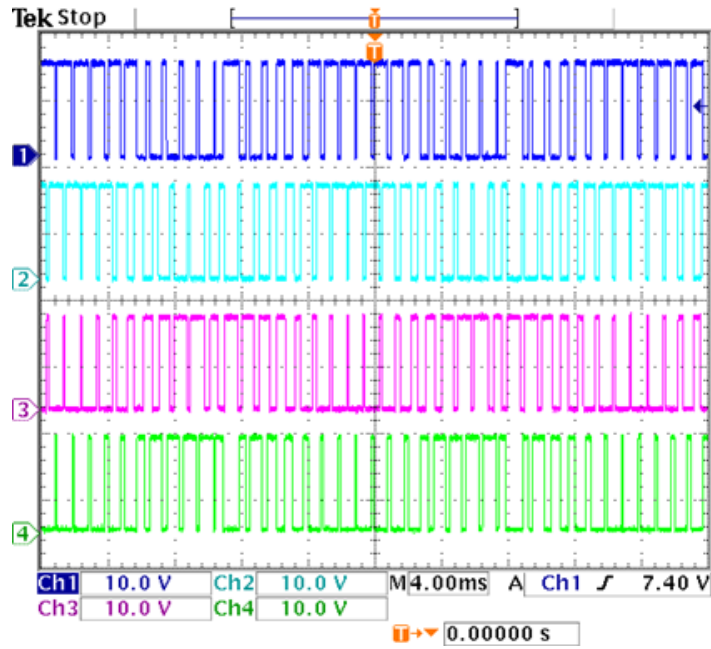
Figure 4.40 Experimental result of switching pulses of switches in fourth cell (10V/div).
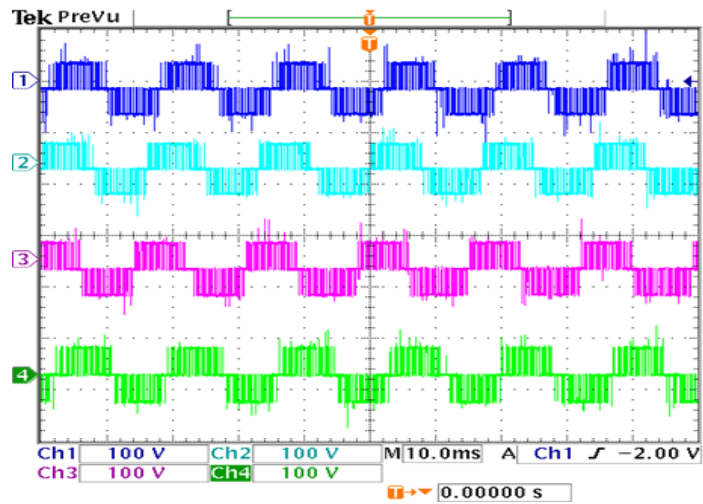


Figure 4.41 Experimental result of individual Output voltages together (100V/div).
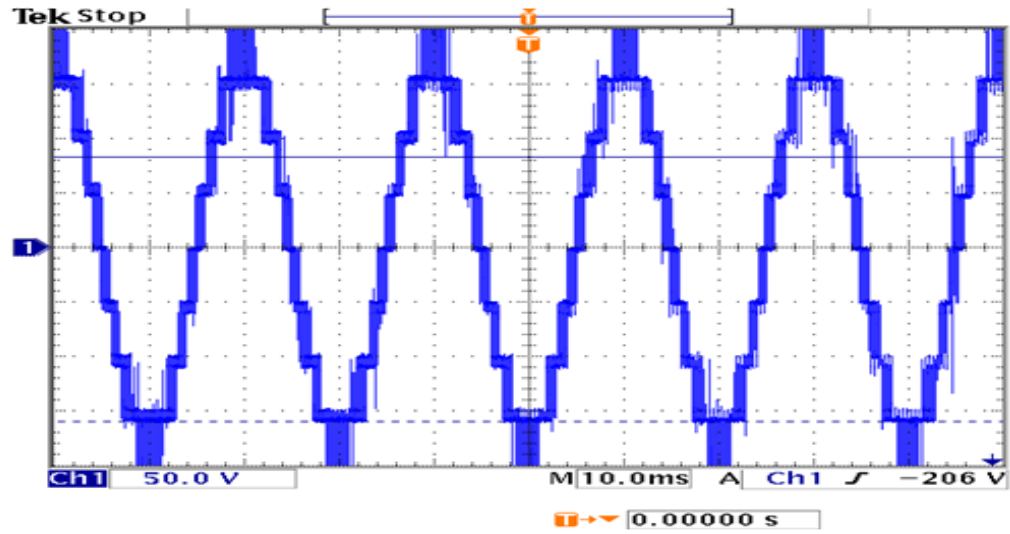
(a)
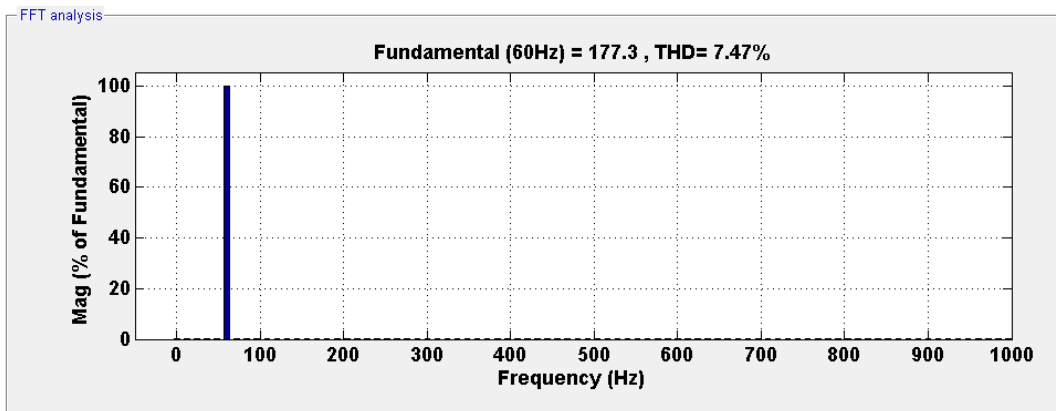


(b)
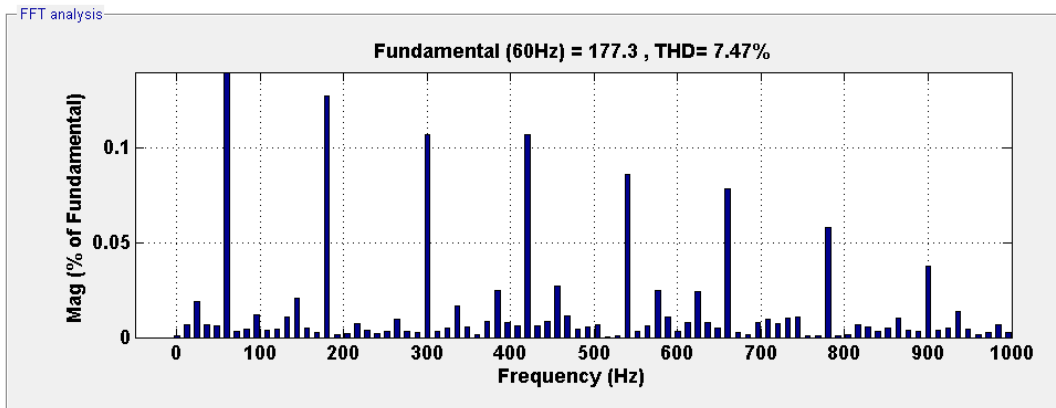


(c)

Figure 4.42 Experimental results: (a) Overall output voltage (50V/div), (b) FFT Normal

spectrum, (c) Zoomed in to see harmonics.

90

## 4.4 Over-modulation Region of Operation

### 4.4.1    Two Cell CHBMC

The region of operation between the loss of linear control and complete loss of control is called the over modulation region [4]. Since the modulator effectively loses control of the output voltage waveform during the saturation period, the output voltage waveform becomes progressively distorted and includes low frequency harmonics of the fundamental component.

Using (3.63), for the two cell cascaded H-bridge inverter contours of output voltage with variation in modulation indices are plotted for unequal DC input voltages in Figure 4.43. The parameters used for plotting the contour plots are $V_{d1} = 60V$, $V_{d2} = 40V$, $0.4 < M_1 < 1.4$, $0.4 < M_2 < 1.4$. This contour plot reveals the linearity between the output voltage magnitude and the modulation indices in the linear region (when the modulation indices are less or equal to unity) and thereafter deviate from the linear relationship in the over-modulation region, resulting in decreasing voltage gains.

Figures 4.44 and 4.45 respectively show the simulation results of individual output voltage and overall output voltages. Figure 4.46 (a) shows the FFT waveform of the overall output phase voltage in the over-modulation range. Figures 4.47 and 4.48 respectively show the experimental results of individual output voltage and overall output voltages operating in the over-modulation range. By comparing the FFT waveforms, Figure 4.6 (a) and Figure 4.46 (a), the lower order harmonics (3rd, 5th and 7th) can be seen

in the spectrum. The magnitude of harmonics (as a percentage of fundamental component) for linear modulation region case is less when compared to the case of over modulation operation. The parameters used for simulation and experimental results are $V_{d1} = V_{d2} = 50$, and $M_1 = M_2 = 1.15$.



Figure 4.43 Contour plot of output voltage with variation of modulation indices for two cell cascaded inverter for the case of over modulation.
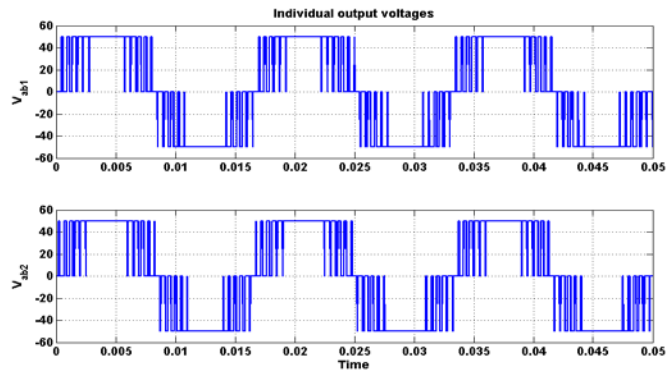


Figure 4.44 Simulation result of individual output voltages for the case of over modulation.
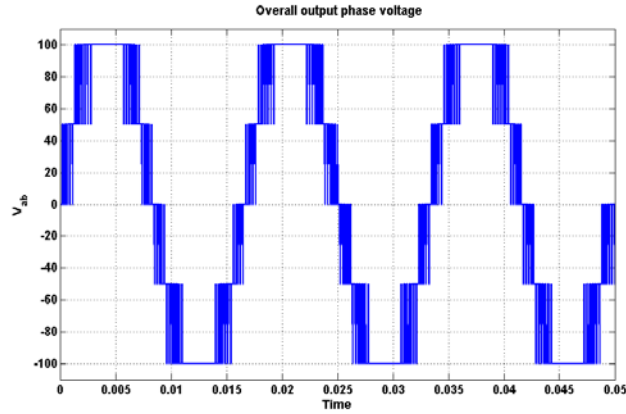
Figure 4.45 Simulation result of overall output voltage for the case of over modulation.
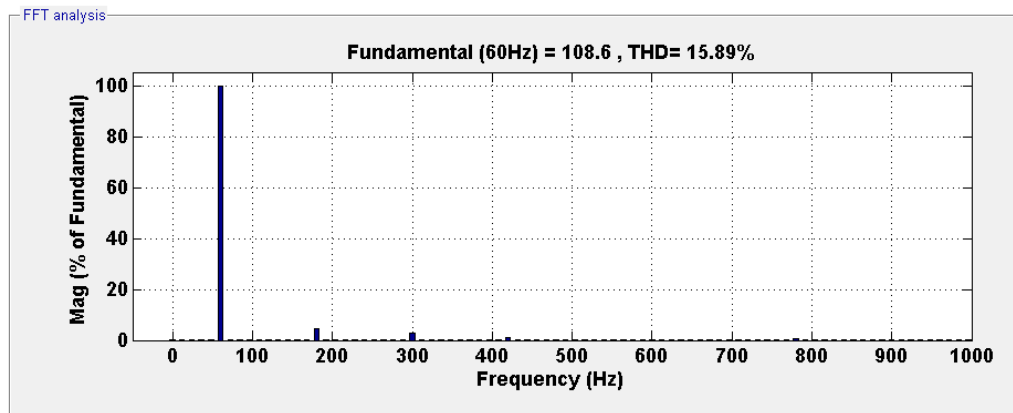


(a)
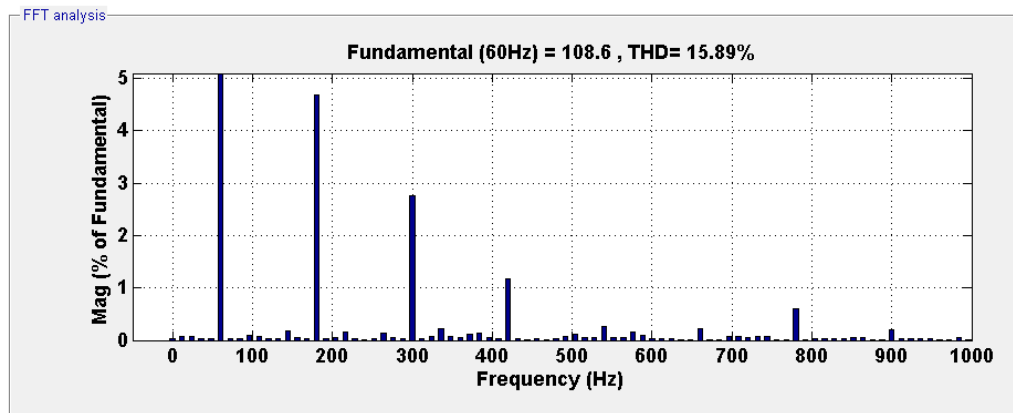


(b)

Figure 4.46 FFT waveform of simulated overall output phase voltage for the case of over

modulation. (a) Fundamental component, (b) Harmonic components.

93
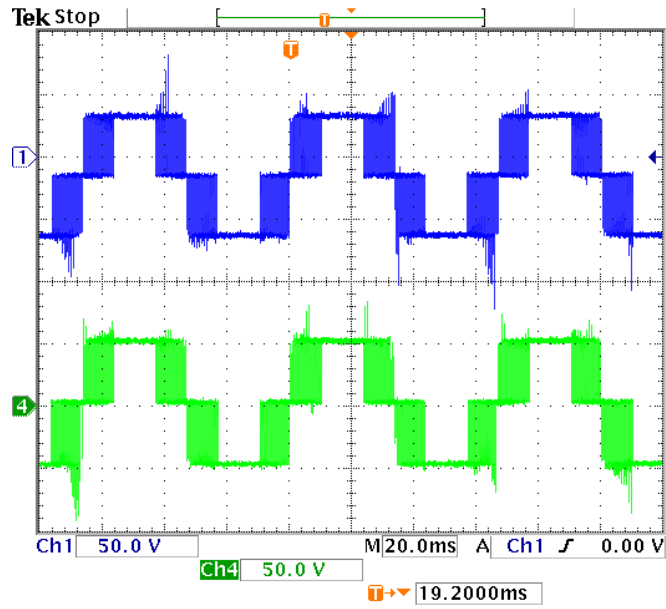
Figure 4.47 Experimental result of individual output voltages for the case of over
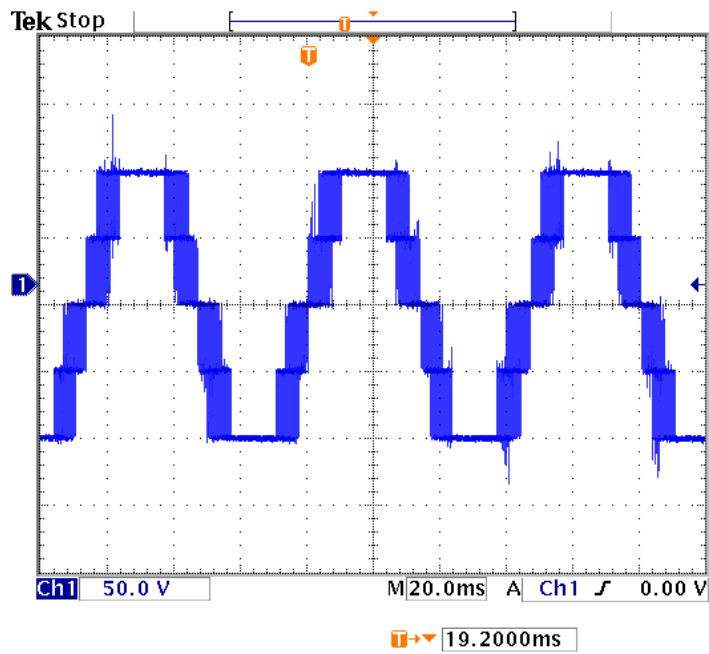
modulation (50V/div).



Figure 4.48 Experimental result of overall output voltage for the case of over modulation

(50V/div).

## 4.4.2      Three Cell CHBMC

Using (3.63), for the three cell, contours are plotted for unequal DC input voltages in Figure 4.49. The parameters used for plotting the contour are $V_{d1} = 60V$, $V_{d2} = 40V$, $V_{d3} = 50V$, $0.4 < M_1 < 1.4$, $0.4 < M_3 < 1.4$, $M_2 = 0.93$. This contour plot reveals the linearity between the output voltage magnitude and the modulation indices in the linear region (when the modulation indices are less or equal to unity) and thereafter deviate from the linear relationship in the over-modulation region, resulting in decreasing voltage gains.

Figures 4.50 and 4.51 respectively show the simulation results of individual output voltage and overall output voltages.
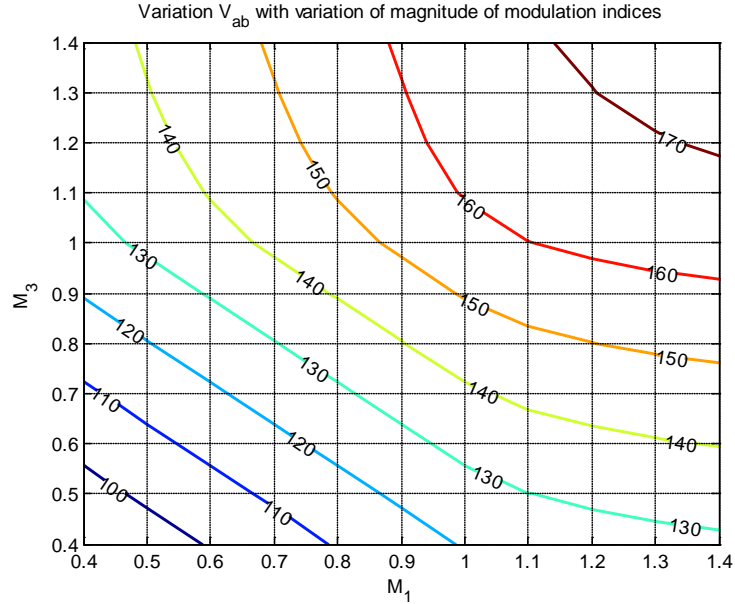
Figure 4.49 Contour plot of output voltage with variation in modulation indices of three cell cascaded inverter for the case of over modulation.

Figure 4.52 shows the FFT spectrum of the overall output phase voltage in the over-modulation range. Figures 4.53 and 4.54 respectively show the experimental results of individual output voltage and overall output voltages operating in the over-modulation range.

By comparing the FFT waveforms, Figure 4.18 (a) and Figure 4.52 (a), the lower order harmonics ($3^{rd}$, $5^{th}$ and $7^{th}$) can be seen in the spectrum. The magnitude of harmonics (as a percentage of fundamental component) for linear modulation region case is less when compared to the case of over modulation operation.

The parameters used for simulation and experimental results are $V_{d1} = V_{d2} = V_{d3} = 50$, $M_1 = M_2 = M_3 = 1.15$.
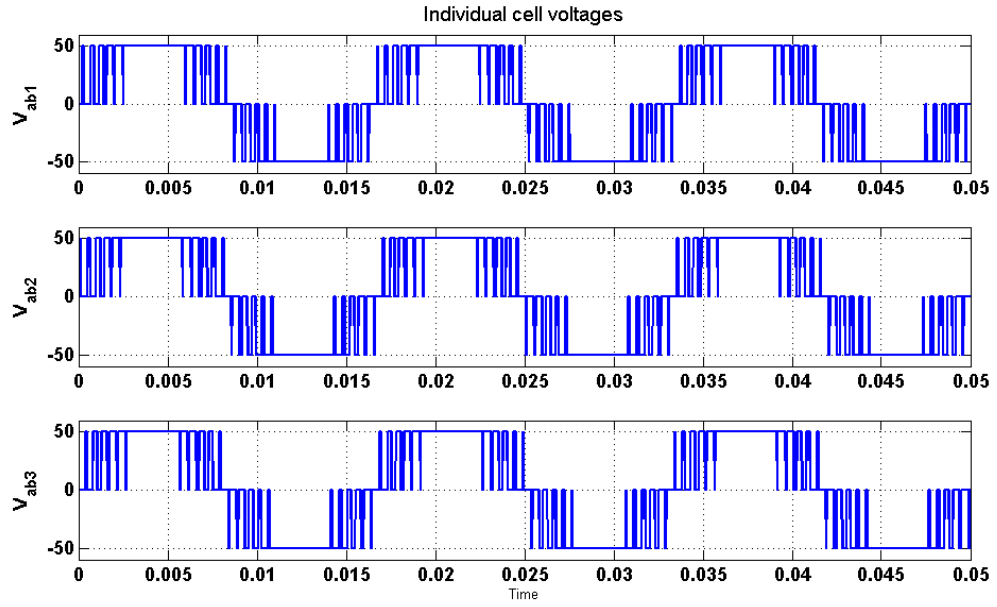
Figure 4.50 Simulation result of individual output voltages for the case of over
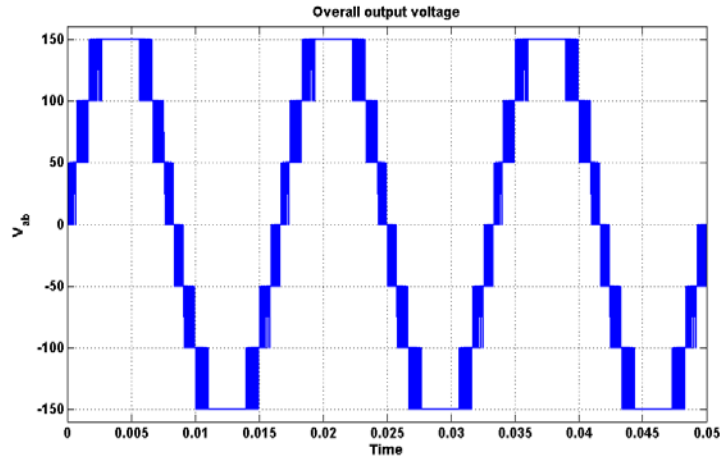
modulation.

Figure 4.51 Simulation result of overall output voltage for the case of over modulation.
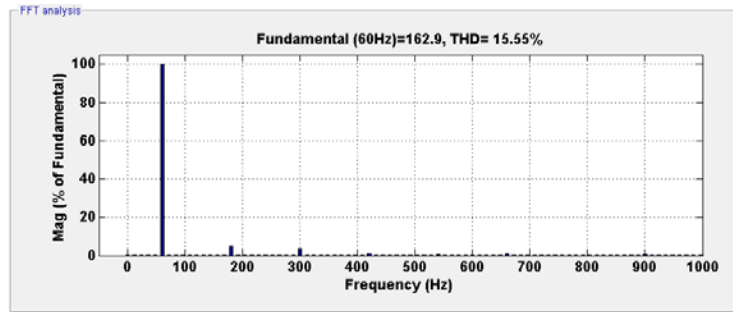


(a)
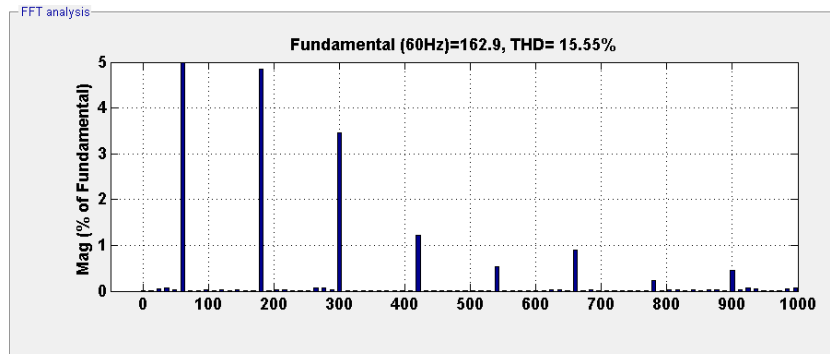


(b)

Figure 4.52 FFT analysis of simulated waveform of overall output phase voltage for the

case of over modulation. (a) Fundamental component, (b) Harmonic components.
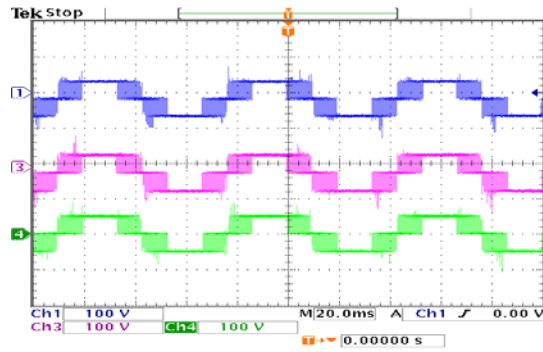
Figure 4.53 Experimental result of individual output voltages for the case of over

modulation (100V/div).
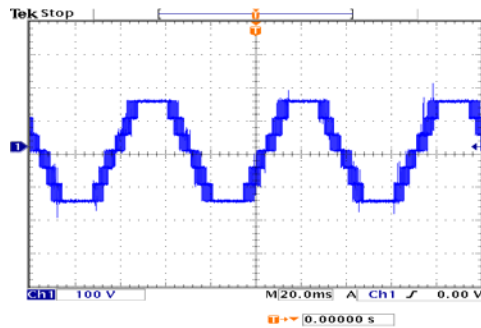


(a)
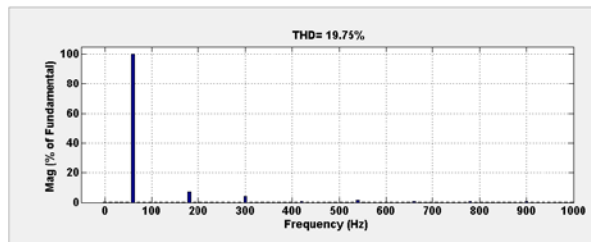


(b)
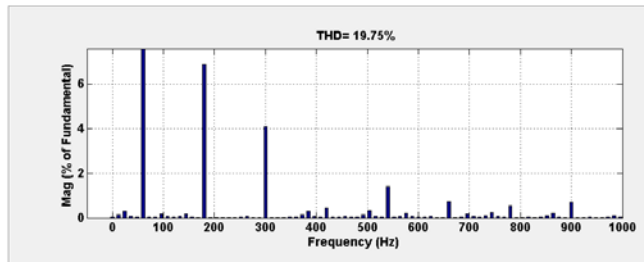


(c)

Figure 4.54 Experimental results: (a) Overall output voltage for the case of over

modulation (100V/div), (a) Fundamental component, (b) Harmonic components..

99

### 4.4.3 Four Cell CHBMC

Using (3.63), for four cell, contours are plotted for unequal DC input voltages in Figure 4.55. The parameters used for plotting the contour are $V_{d1} = 60V$, $V_{d2} = 35V$, $V_{d3} = 45V$, $V_{d4} = 50V$, $0.4 < M_1 < 1.4$, $0.4 < M_4 < 1.4$, $M_2 = 0.947$, $M_3 = 0.865$ the corresponding contour plot of output voltage magnitude can be seen in Figure 4.55.

This contour plot reveal the linearity between the output voltage magnitude and the modulation indices in the linear region (when the modulation indices are less or equal to unity) and thereafter deviate from the linear relationship in the over-modulation region, resulting in decreasing voltage gains.

Figures 4.56 and 4.57 respectively show the simulation results of individual output voltage and overall output voltages.
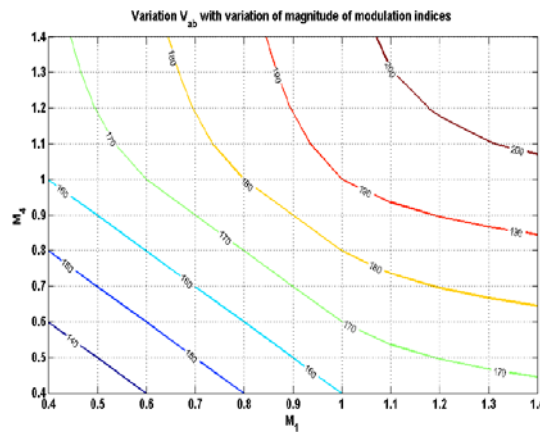


Figure 4.55 Contour plots of unknown modulation signals of four cell cascaded inverter for the case of over modulation.

100
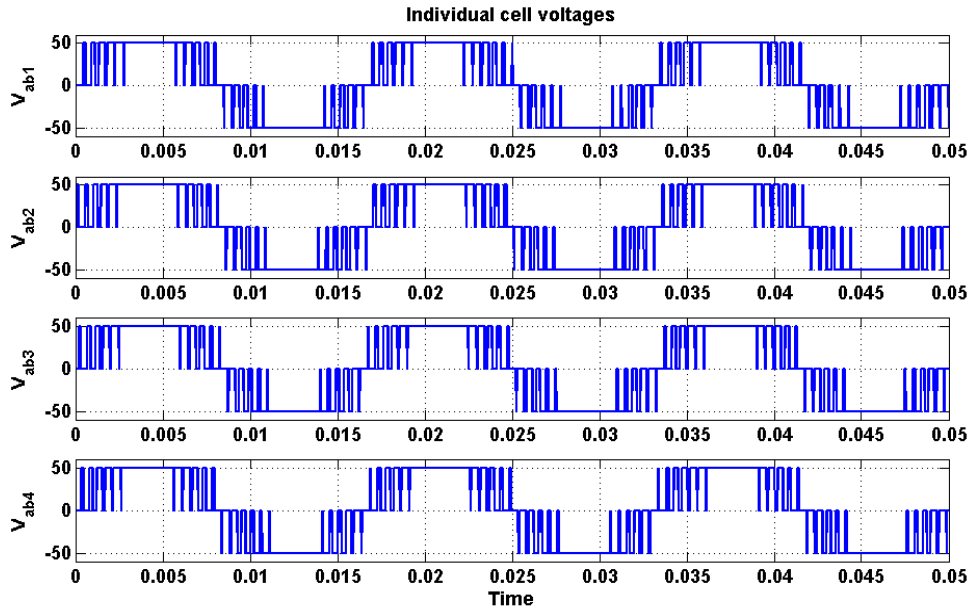
Figure 4.56 Simulation result of individual output voltages for the case of over
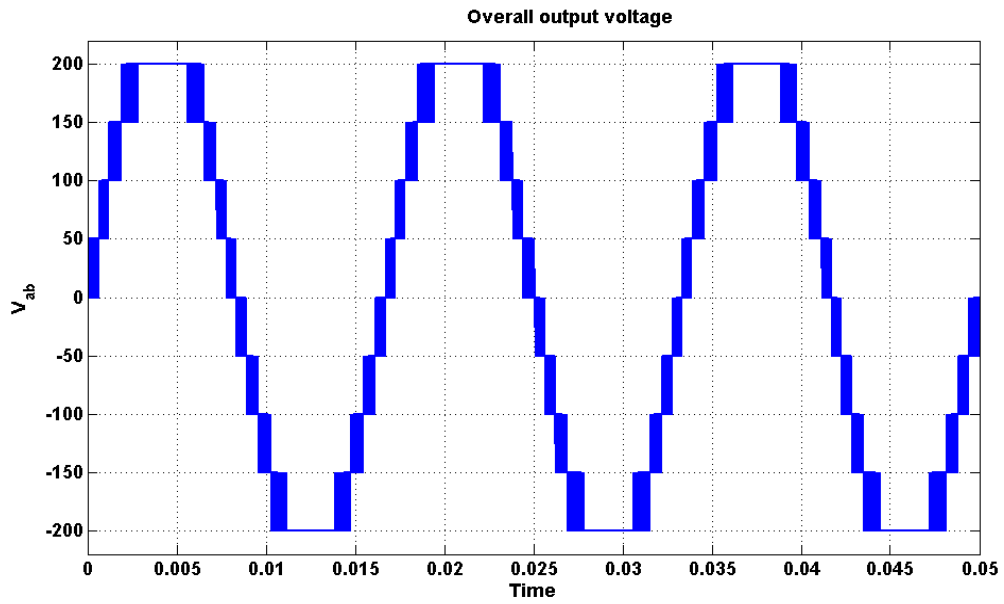
modulation.



Figure 4.57 Simulation result of overall output voltage for the case of over modulation.
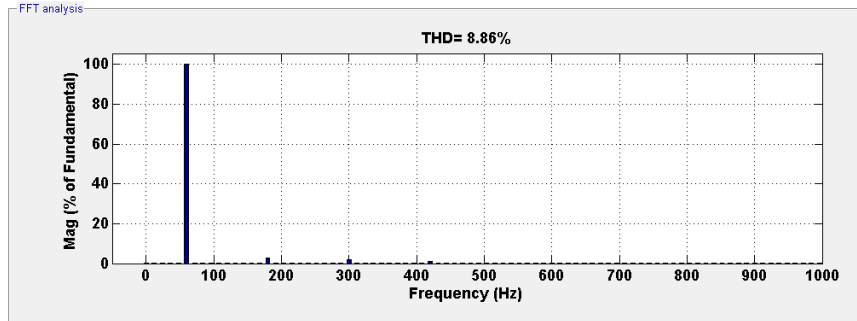
(a)
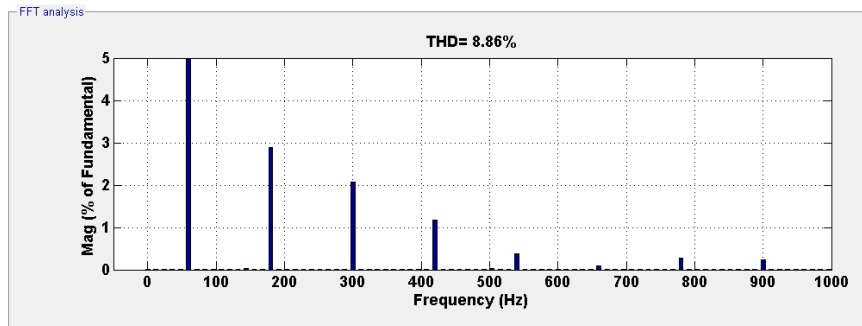


(b)

Figure 4.58 FFT spectrum of simulated waveform of overall output phase voltage for the

case of over modulation.
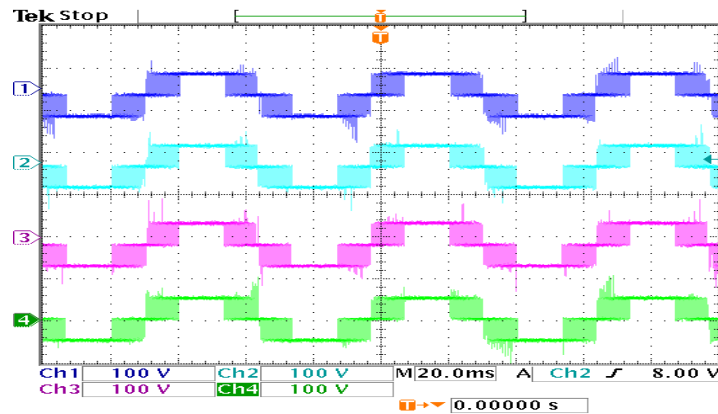


Figure 4.59 Experimental result of individual output voltages for the case of over

modulation (100V/div).
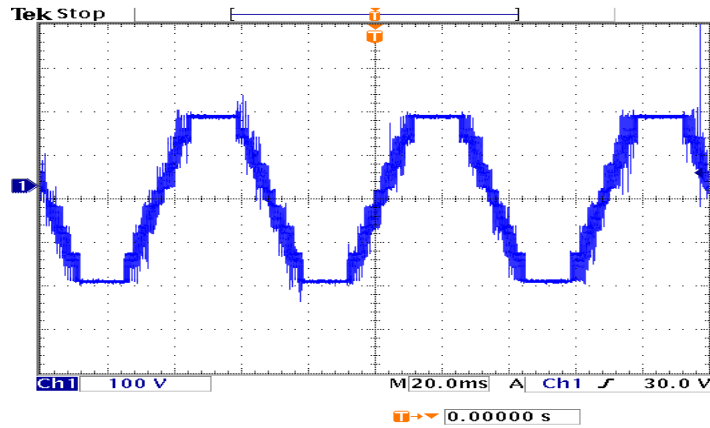
(a)
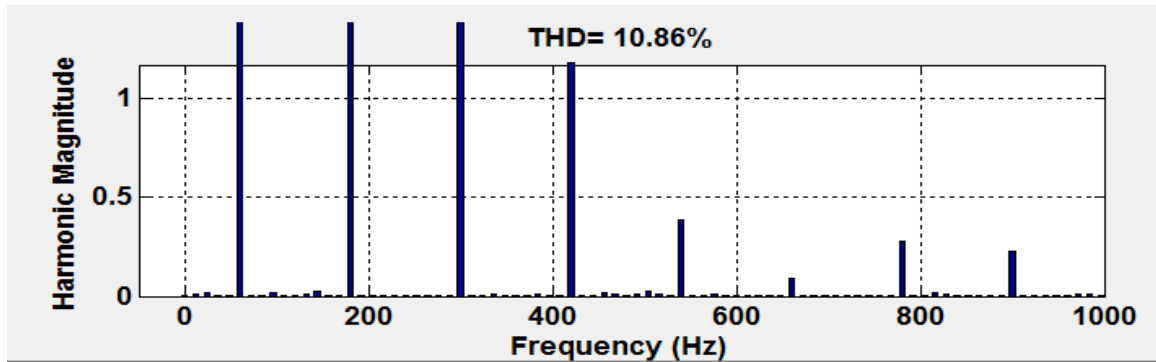


(b)

Figure 4.60 Experimental results: (a) Overall output voltage for the case of over

modulation (100V/div), (b) FFT analysis of experimental waveform.

Figure 4.58 shows the FFT spectrum of the overall output phase voltage in the over-modulation range. Figures 4.59 and 4.60 respectively show the experimental results of individual output voltage and overall output voltages operating in the over-modulation range.

By comparing the FFT waveforms, Figure 4.35 (a) and Figure 4.58 (a), the lower order harmonics (3$^{rd}$, 5$^{th}$ and 7$^{th}$) can be seen in the spectrum. The magnitude of

harmonics (as a percentage of fundamental component) for linear modulation region case is less when compared to the case of over modulation operation.

The parameters used for simulation and experimental results are $V_{d1} = V_{d2} = V_{d3} = V_{d4} = 50V$, $M_1 = M_2 = M_3 = M_4 = 1.15$.

## 4.5 Five Cell Cascaded H-bridge Multilevel DC-AC converter

The modulation technique which eliminates the dominant harmonics in the output voltage is also extended to five cell cascaded H- bridge inverter. The analysis of five cell cascaded H-bridge inverter is categorized into two regions.

- Linear operation region and
- Over-modulation region

The steady state contours and simulation results for both these regions are presented in this chapter.

### 4.5.1 Linear Operation Region

The double Fourier series approximation of the converter switching functions given in (3.45) as

$$
S_{ij}(\omega_s, \omega_c) = \left\{
\begin{aligned}
&\frac{A_{00}}{2} + \sum_{n=1}^{\infty} \left( A_{0n} \cos(n\omega_s t) + B_{0n} \sin(n\omega_s t) \right) \\
&+ \sum_{m=1}^{\infty} \left( A_{m0} \cos(m\omega_c t) + B_{m0} \sin(m\omega_c t) \right) \\
&+ \sum_{m=1}^{\infty} \sum_{\substack{n=-\infty \\ n \neq 0}}^{\infty} \left( A_{mn} \cos(m\omega_c t + n\omega_s t) + B_{mn} \sin(m\omega_c t + n\omega_s t) \right)
\end{aligned}
\right\} . \tag{4.25}
$$

where $i = a, b;\ j = p, n$

Consider the desired single phase output voltage represented in (4.26). $V_s$ is the magnitude of the output voltage and $\Theta_o$ is the initial angle.

$$
V_s(t) = V_s \cos(\theta_e + \theta_o) \text{ where } \theta_e = \omega_t \tag{4.26}
$$

The output voltage spectrum for a full bridge single phase leg is shown in (4.27). In this voltage odd carrier and associated harmonics as well as even base band and side band harmonics are cancelled.

As a result, the only harmonics which exist are the odd side band harmonics around an even carrier. $M_k$ denotes the modulation index of the $k_{th}$ H-bridge.

$$
V_k = \left\{ V_{dck} M_k \cos(\theta_e + \theta_k) + \frac{4 V_{dck}}{\pi} \sum_{m=2}^{\infty} \sum_{n=-\infty}^{\infty} \frac{1}{m} J_n(\frac{m\pi}{2} M_k) \sin\left( \frac{\pi}{2}(m+n) \right) \\ \cos(m(\theta_c + \gamma_k) + n(\theta_e + \theta_k)) \right\} \tag{4.27}
$$

where $J_n(x) = \sum_{m=0}^{\infty} \frac{(-1)^m}{m!(m+n)!} \left( \frac{1}{2} x \right)^{2m+n}$ . \tag{4.28}

In the four cell CHB multi-level converter, the fundamental component of the total output voltage is expressed as

$$
V_{s,fund} = \left\{
\begin{aligned}
&V_{dc1} M_1 \cos(\theta_e + \theta_1) + V_{dc2} M_2 \cos(\theta_e + \theta_2) \\
&+ V_{dc3} M_3 \cos(\theta_e + \theta_3) + V_{dc4} M_4 \cos(\theta_e + \theta_4) + V_{dc5} M_5 \cos(\theta_e + \theta_5)
\end{aligned}
\right\} \tag{4.29}
$$

The first dominant harmonic component which is the first side band harmonic around the second carrier frequency is given in (4.30).

$$V_{o1}^+ = \left\{ \begin{array}{l} \left[ -\dfrac{2V_{dc1}}{\pi} J_1(\pi M_1) \cos\!\left( \begin{array}{l} 2(\theta_c + \gamma_1) \\ +(\theta_e + \theta_1) \end{array} \right) - \dfrac{2V_{dc2}}{\pi} J_1(\pi M_2) \cos\!\left( \begin{array}{l} 2(\theta_c + \gamma_2) \\ +(\theta_e + \theta_2) \end{array} \right) \right. \\ \left. -\dfrac{2V_{dc3}}{\pi} J_1(\pi M_3) \cos\!\left( \begin{array}{l} 2(\theta_c + \gamma_3) \\ +(\theta_e + \theta_3) \end{array} \right) - \dfrac{2V_{dc4}}{\pi} J_1(\pi M_4) \cos\!\left( \begin{array}{l} 2(\theta_c + \gamma_4) \\ +(\theta_e + \theta_4) \end{array} \right) \right. \\ \left. -\dfrac{2V_{dc5}}{\pi} J_1(\pi M_5) \cos\!\left( \begin{array}{l} 2(\theta_c + \gamma_5) \\ +(\theta_e + \theta_5) \end{array} \right) \right] \end{array} \right\} \tag{4.30}$$

If phase angles of all the modulation signals are the same and equal to the phase angle of the desired output voltage, the relationship between the modulation indices in terms of the input dc voltages and output desired voltage magnitude is shown in (4.32).

$$V_s = V_{dc1} M_1 + V_{dc2} M_2 + V_{dc3} M_3 + V_{dc4} M_4 + V_{dc5} M_5 \tag{4.31}$$

Using (4.28), $J_1(\pi M_i) = \dfrac{\pi M_i}{2}$, where $i = 1,2,3,4,5$. $\tag{4.32}$

Substituting the phase shift angle of the carrier waves in (4.31),

$$V_{o1}^+ = \left\{ \begin{array}{l} \left[ -M_1 V_{dc1} \cos(\gamma) - M_2 V_{dc2} \cos\!\left( 2\!\left(\dfrac{\pi}{5}\right) + \gamma \right) \right. \\ \left. -M_3 V_{dc3} \cos\!\left( 2\!\left(\dfrac{2\pi}{5}\right) + \gamma \right) - M_4 V_{dc4} \cos\!\left( 2\!\left(\dfrac{3\pi}{5}\right) + \gamma \right) \right. \\ \left. -M_5 V_{dc5} \cos\!\left( 2\!\left(\dfrac{4\pi}{5}\right) + \gamma \right) \right] \end{array} \right\} . \tag{4.33}$$

To eliminate the dominant harmonics from the above equation, the modulation indices are selected in such a way that they satisfy the following two equations,

$$V_{dc1} M_1 + \left( V_{dc2} M_2 + V_{dc5} M_5 \right) \cos\!\left(\dfrac{2\pi}{5}\right) + \left( V_{dc3} M_3 + V_{dc4} M_4 \right) \cos\!\left(\dfrac{4\pi}{5}\right) = 0 . \tag{4.34}$$

$$\left(V_{dc2}M_2 - V_{dc5}M_5\right)\sin\left(\frac{2\pi}{5}\right) + \left(V_{dc3}M_3 - V_{dc4}M_4\right)\sin\left(\frac{4\pi}{5}\right) = 0. \tag{4.35}$$

There are three equations (4.31), (4.34) and (4.35) and there are five unknowns. Therefore, after specifying $M_2$ and $M_4$, the other three modulation signals magnitudes are expressed as

$$M_5 = \frac{V_s - \alpha_1 V_{dc2}M_2 - 2\alpha_3 V_{dc4}M_4}{\alpha_2 V_{dc5}}. \tag{4.36}$$

$$M_3 = \frac{1}{V_{dc3}}\left(V_{dc4}M_4 - \left(V_{dc2}M_2 - V_{dc5}M_5\right)\frac{\sin\left(\frac{2\pi}{5}\right)}{\sin\left(\frac{4\pi}{5}\right)}\right). \tag{4.37}$$

$$M_1 = \frac{1}{V_{dc1}}\left(V_s - V_{dc2}M_2 - V_{dc3}M_3 - V_{dc4}M_4 - V_{dc5}M_5\right). \tag{4.38}$$

where $\alpha_1 = 1 - \dfrac{\sin\left(\frac{2\pi}{5}\right)}{\sin\left(\frac{4\pi}{5}\right)} - \cos\left(\frac{2\pi}{5}\right) + \dfrac{\sin\left(\frac{2\pi}{5}\right)}{\tan\left(\frac{4\pi}{5}\right)}$.

$$\alpha_2 = 1 + \frac{\sin\left(\frac{2\pi}{5}\right)}{\sin\left(\frac{4\pi}{5}\right)} - \cos\left(\frac{2\pi}{5}\right) - \frac{\sin\left(\frac{2\pi}{5}\right)}{\tan\left(\frac{4\pi}{5}\right)} ; \alpha_3 = 1 - \cos\left(\frac{4\pi}{5}\right)$$

and $M = \dfrac{V_s}{V_{dc1} + V_{dc2} + V_{dc3} + V_{dc4} + V_{dc5}}$ where $M$ is the effective modulation $\tag{4.39}$

index of the converter.

Since we assume that we know the modulation indices $M_2$ and $M_4$, by varying $M_2$ and $M_4$ in the operable range, we can find the solutions for $M_1$, $M_3$ and $M_5$. The contour plots display the modulation indices of $M_1$, $M_3$ and $M_5$ for the two cases considered.

107

## Case I: Equal DC Input Voltages

Consider $V_s = 220V$, $V_{dc1} = V_{dc2} = V_{dc3} = V_{dc4} = V_{dc5} = 50V$. By varying $M_2$ and $M_4$ from 0 to $1.2M$, where M is given in (4.39), the contour of $M_1$, $M_3$ and $M_5$ is given in Figure 4.61.



(a)



(b)



(c)
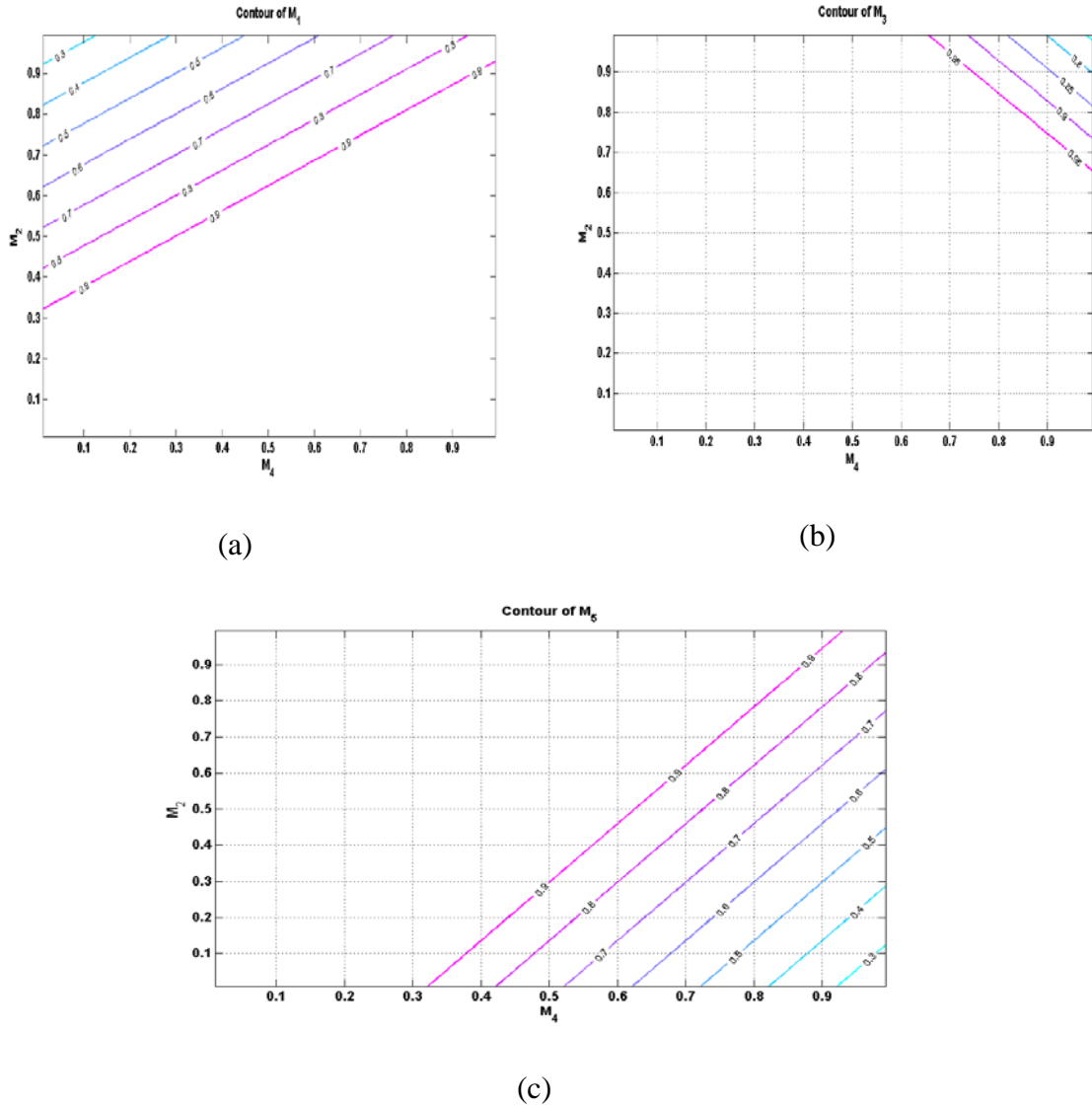
Figure 4.61 Linear operation regions for case I of (a) $M_1$, (b)$M_3$, (c)$M_5$.

### Case II: Unequal DC Input Voltages

Consider $V_s = 220V$, $V_{dc1} = 50V$, $V_{dc2} = 45V$, $V_{dc3} = 55V$, $V_{dc4} = 60V$, $V_{dc5} = 70V$.

By varying $M_2$ and $M_4$ from 0 to $1.2M$, where M is given in (4.39), the contour of $M_1$, $M_3$ and $M_5$ is shown given in Figure 4.62.



(a)

(b)

(c)
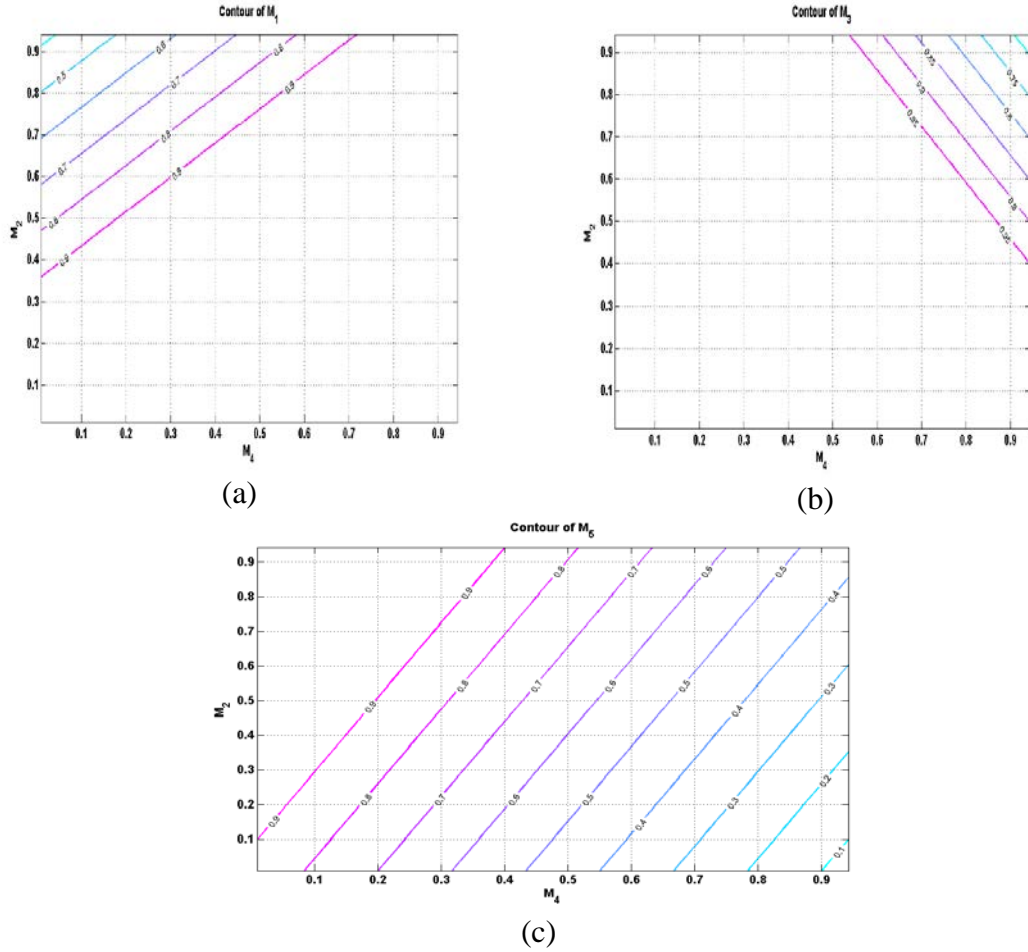
Figure 4.62 Linear operation regions for case II of (a) $M_1$, (b)$M_3$, (c)$M_5$.

For the first set of simulations (equal DC voltages), the modulation indices used are $M_1 = 0.97$, $M_2 = 0.85$, $M_3 = 0.88$, $M_4 = 0.7$, $M_5 = 0.6$. For the second set of simulations (for unequal DC voltages), the modulation indices selected are $M_1 = 0.95$, $M_2 = 0.95$, $M_3 = 0.69$, $M_4 = 0.9$, $M_5 = 0.48$.
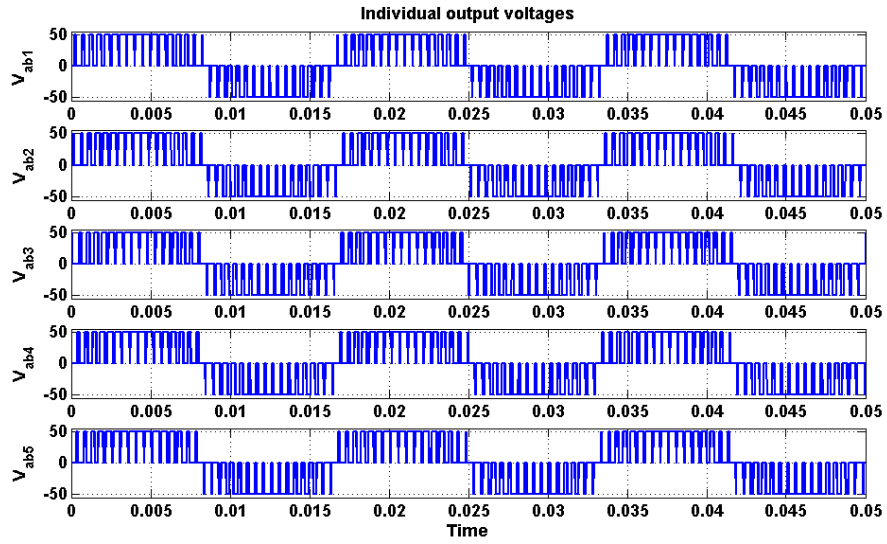
Figure 4.63 Simulation result of individual cell output voltages for equal DC voltages.
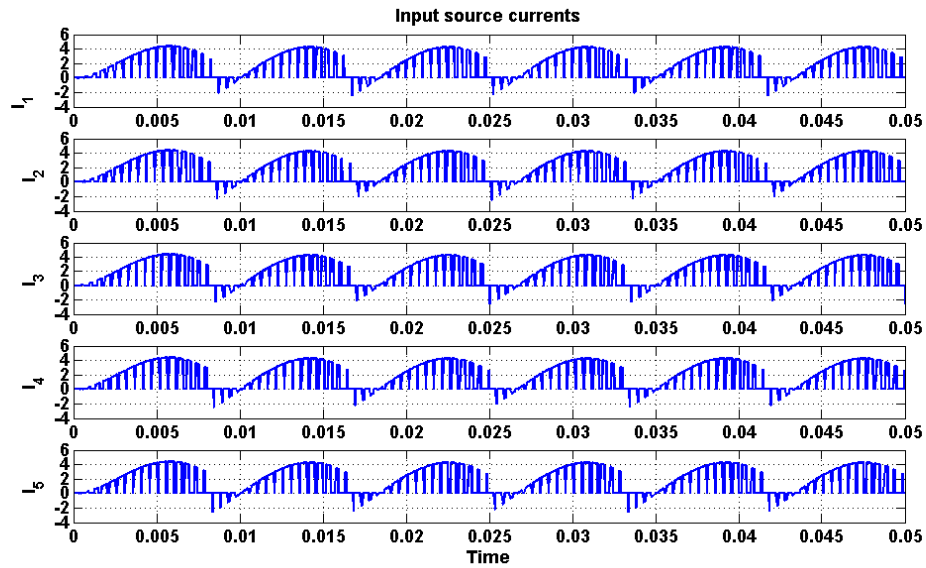


Figure 4.64 Simulation result of input source currents for equal DC voltages.

110
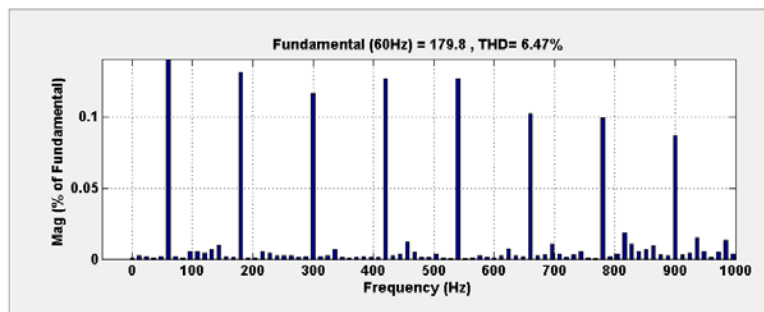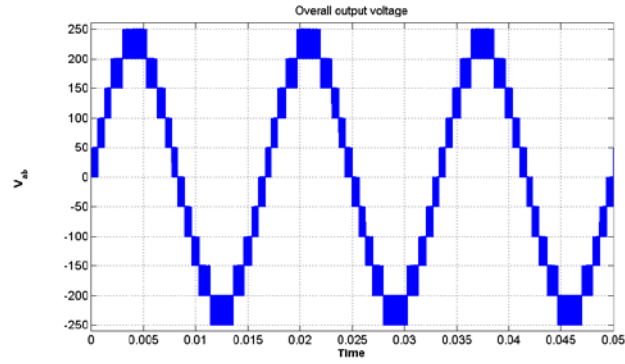
Figure 4.65 Simulation result of overall output voltage for equal DC voltages.
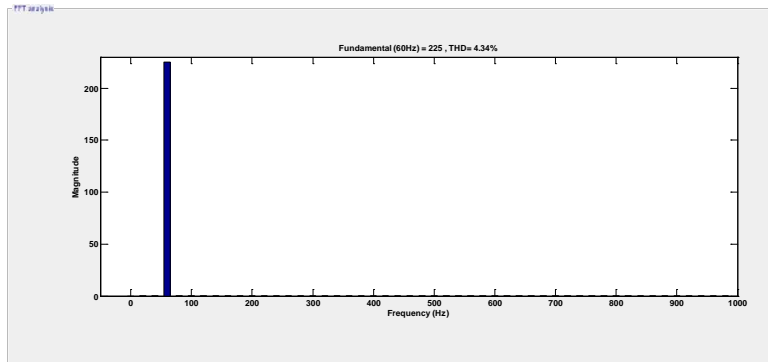


(a)
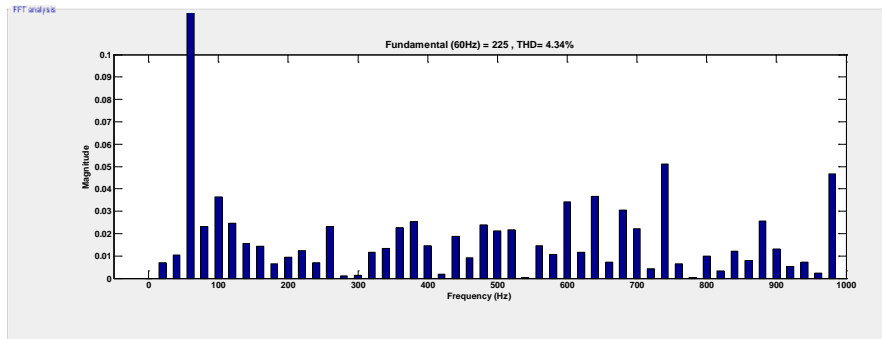


(b)

Figure 4.66 FFT waveform of simulated waveform of overall output voltage for equal DC

voltages (a) Showing fundamental component, (b) Showing harmonic components
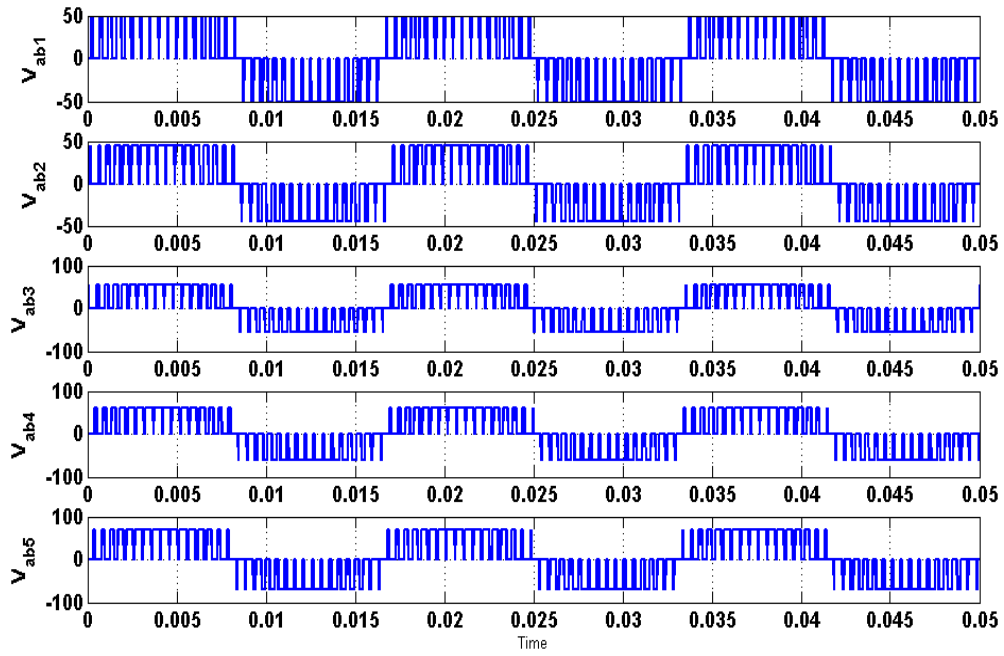
Figure 4.67 Simulation of individual output voltages for unequal DC voltages.
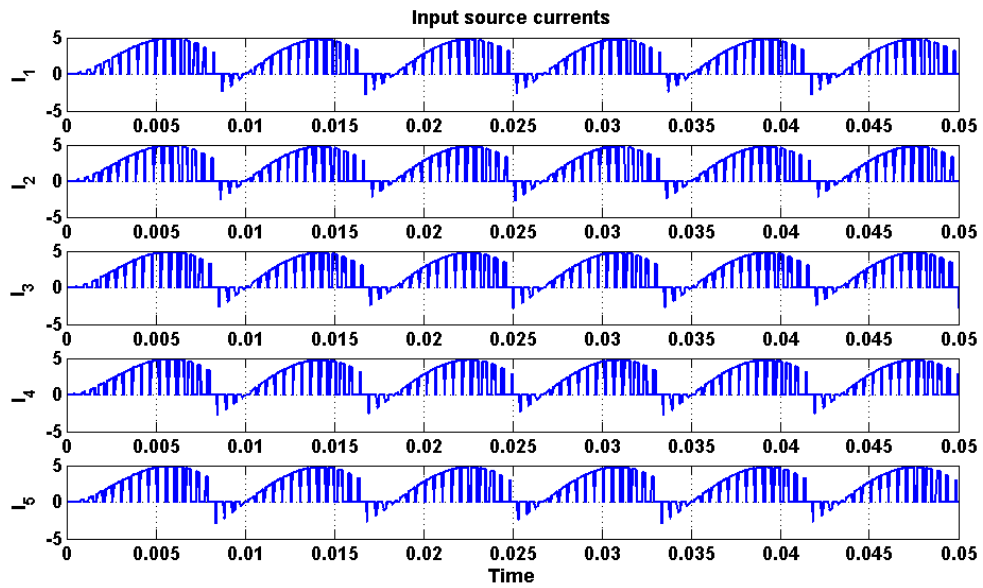


Figure 4.68 Simulation of input source currents for unequal DC voltages.
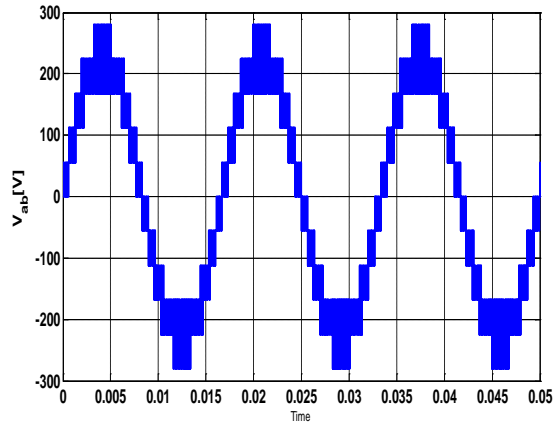
Figure 4.69 Simulation of overall output voltage for unequal DC voltages.
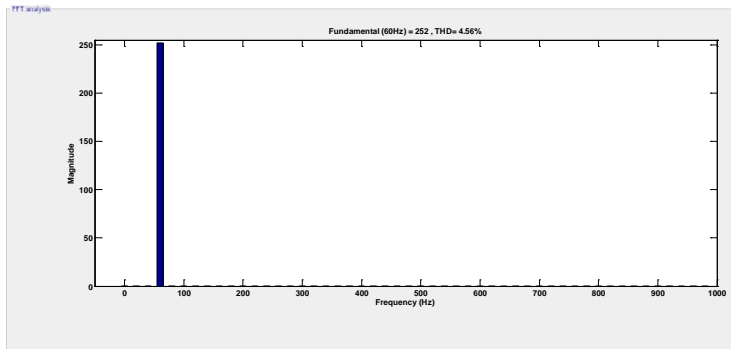


(a)
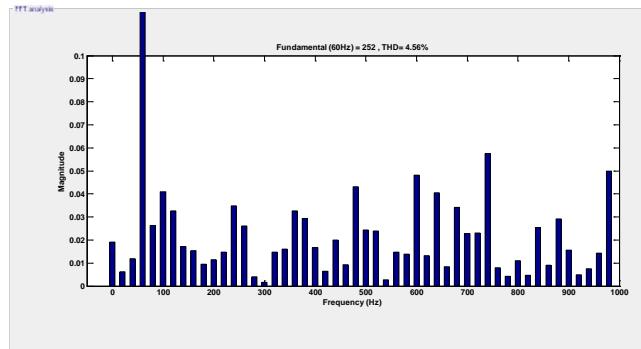


(b)

Figure 4.70 FFT spectrum of simulated waveform of overall output voltage for unequal

DC voltages. (a) Showing fundamental component, (b) Showing harmonic components

**4.5.2      Over-modulation region**

The region of operation between the loss of linear control and complete loss of control is called the over modulation region [4]. Since the modulator effectively loses control of the output voltage waveform during the saturation period, the output voltage waveform becomes progressively distorted and includes low frequency harmonics of the fundamental component.

The double Fourier series approximation of the fundamental component of converter output voltage in case of over modulation given in [4] as

$$
V_{ab}(t) = \begin{bmatrix} \dfrac{2V_{dc}}{\pi} \left[4\sin\psi + M\left(\pi - 2\psi - \sin 2\psi\right)\right]\cos\omega_o t \\[2mm] + \displaystyle\sum_{m=1}^{\infty}\sum_{n=-\infty}^{\infty} C_{mn}\cos\left(2m\omega_c t + [2n-1]\omega_o t\right) \end{bmatrix}. \tag{4.40}
$$

$$
C_{mn} = \frac{4V_{dc}}{m\pi^2}\begin{bmatrix} J_{2n-1}(m\pi M)\cos\left[(m+n-1)\pi\right]\left[\pi - 2\psi - \dfrac{\sin 2(2n-1)\psi}{2n-1}\right] \\[3mm] + \displaystyle\sum_{\substack{k=1 \\ 2k-1\neq 2n-1}}^{\infty}\begin{bmatrix} J_{2k-1}(m\pi M)\cos\left[(m+k)\pi\right] \\[2mm] \left(\dfrac{\sin 2(n+k-1)\psi}{n+k-1} + \dfrac{\sin 2(n-k)\psi}{n-k}\right) \end{bmatrix} \end{bmatrix}. \tag{4.41}
$$

$$
\psi = \cos^{-1}\left(\frac{1}{M}\right).
$$

The gain from the fundamental component of (4.40) is

$$
V_{ab} = \frac{2V_{dc}}{\pi}\left[4\sin\psi + M\left(\pi - 2\psi - \sin 2\psi\right)\right]. \tag{4.42}
$$

For '$q$' cell cascaded H bridge multi-level converter, the expression for gain is given as

$$V_{ab} = \sum_{i=1}^{q} \frac{2V_{dc_i}}{\pi} \left[ 4\sin\psi_i + M_i \left( \pi - 2\psi_i - \sin 2\psi_i \right) \right].$$

(4.43)

where $\psi_k = \cos^{-1}\left( \dfrac{1}{M_k} \right)$, $k = 1,2,3,..q$.

Using (4.43), contours are plotted for unequal DC input voltages in Figure 4.71. For five cell CHB, $V_{d1} = 50V$, $V_{d2} = 45V$, $V_{d3} = 55V$, $V_{d4} = 60V$, $V_{d5} = 70V$, $0.4 < M_1 < 1.4$, $0.4 < M_5 < 1.4$, $M_2 = 0.85$, $M_3 = 0.88$, $M_4 = 0.7$, the contour plot of output voltage magnitude is presented in Figure 4.71. This contour plot reveal the linearity between the output voltage magnitude and the modulation indices in the linear region (when the modulation indices are less or equal to unity) and thereafter deviate from the linear relationship in the over-modulation region, resulting in decreasing voltage gains.
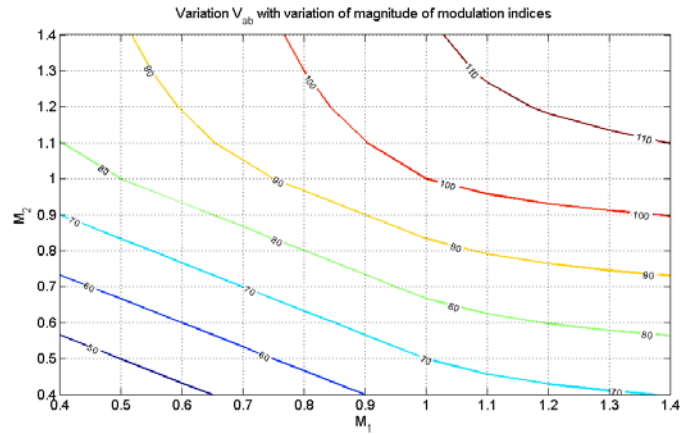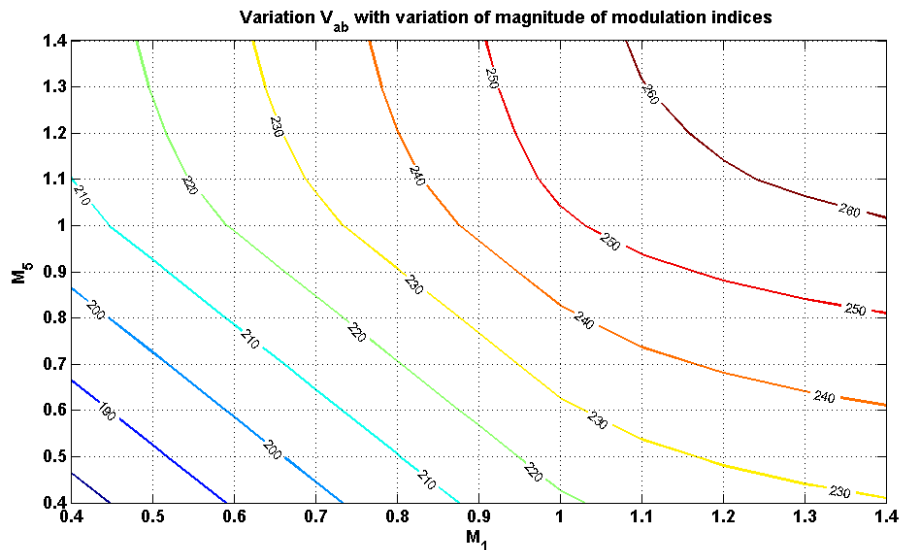


Figure 4.71 Contour plot of output voltage with variation of modulation indices for five cell cascaded inverter for the case of over modulation.

## 4.6 Summary

A method for the determination of the modulation signals for the multilevel cascaded single phase inverters which eliminate the dominant harmonics in the desired output voltage is proposed for both the linear and over-modulation operating regions. This method is applicable to the cases when the DC input voltages are either equal or unequal. This method was implemented on two, three, four and five cell cascaded H-bridge multilevel converters but it still can be extended for the determination of the modulation signals for higher multilevel cascaded single-phase converters. Computer simulation results, contour plots and experimental results are provided to demonstrate the utility of the proposed approach. This chapter therefore provides an analytical method to determine the modulation signals required for unipolar PWM modulation of cascaded multi-level single-phase DC-AC converters.

# CHAPTER 5

## SINGLE PHASE MULTI STRING FIVE LEVEL DC-AC CONVERTER

### 5.1 Introduction

This chapter presents the modeling and analysis of a novel multi-string multilevel DC-AC converter influenced by five level inverter presented in [72]. This multi-level inverter is called multi-string as it is mainly designed for strings of PV cells. In this chapter, modeling and analysis has been done considering the PV cells as DC sources.

The topology of single phase multi string five level inverter can be seen in Figure 5.1. This topology offers strong advantages like improved output voltage waveforms, smaller filter size and low electromagnetic interference and THD [72], . This topology requires DC sources like two cell cascaded H-bridge inverter which also gives five level output voltage. So, this topology can be compared with the conventional cascaded H-bridge multi-level inverter.

This topology requires two less switches than the two cell cascaded H-bridge inverter. And moreover, two of the switches are operated at line frequency. As a result, the switching losses when compared with two cell cascaded converter are considerably less. The carrier based PWM is used to generate PWM signals for the switches.
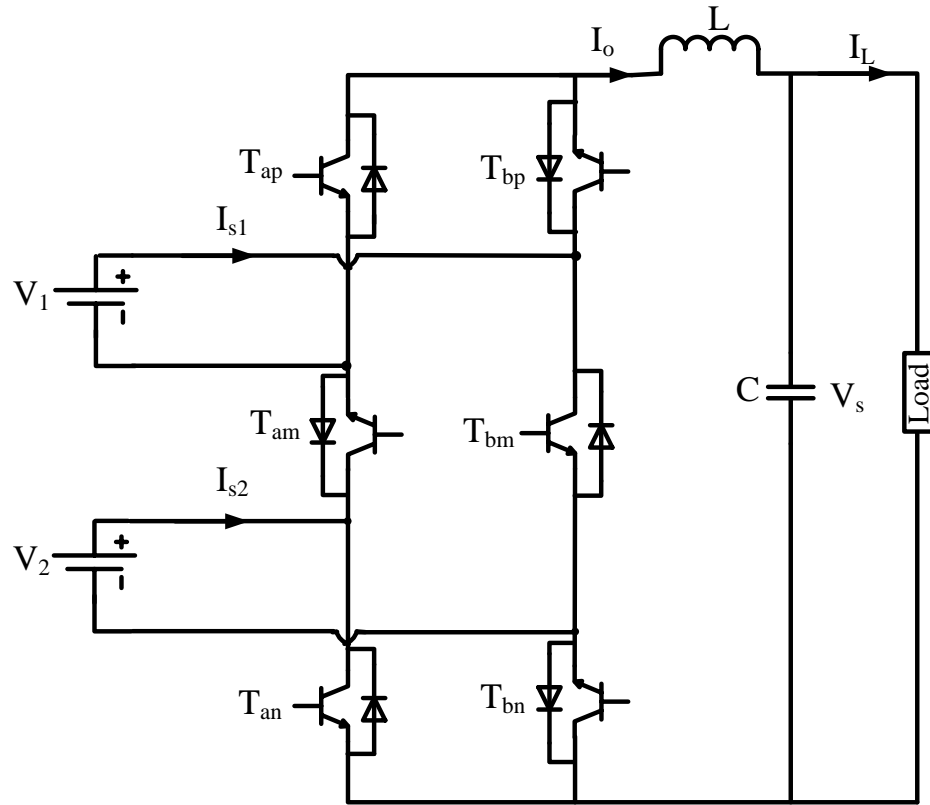
Figure 5.1 Schematic diagram of single phase multi string five level inverter.

From the Figure 5.1, $S_{ip}, S_{im}, S_{in}$, are the switching functions of switches $T_{ip}, T_{im}, T_{in}$, $i = a, b$ respectively. $V_1, V_2$ are input DC sources, $I_{s1}, I_{s2}$ are respective input currents, and $I_o$ is output current.

## 5.2 Modes of Operation

The different modes of operation of multi-string five level inverter are shown in Table 5.1. Each mode shown in Table 5.1 is described in terms of output voltage.

.

Table 5.1 Switching modes of multi string five level converter.

| Mode | $S_{ap}$ | $S_{am}$ | $S_{an}$ | $V_{AB}$ | $I_{s1}$ | $I_{s2}$ |
|------|------|------|------|------|------|------|
| 1 | 0 | 1 | 0 | $V_1+V_2$ | $I_0$ | $I_0$ |
| 2 | 0 | 1 | 1 | $V_1$ | $I_0$ | 0 |
| 3 | 1 | 1 | 0 | $V_2$ | 0 | $I_0$ |
| 4 | 1 | 1 | 1 | 0 | 0 | 0 |
| 5 | 0 | 0 | 0 | 0 | 0 | 0 |
| 6 | 1 | 0 | 0 | $-V_1$ | $-I_0$ | 0 |
| 7 | 0 | 0 | 1 | $-V_2$ | 0 | $-I_0$ |
| 8 | 1 | 0 | 1 | $-V_1-V_2$ | $-I_0$ | $-I_0$ |

- **Maximum positive output, $V_1+V_2$:** When the switches $T_{am}$, $T_{bp}$, and $T_{bn}$ are ON; the output voltage $V_{AB}$ is $V_1+V_2$. This mode of operation can be seen in Figure 5.2 (a).

- **Half-level positive output, $V_1$:** This output condition is possible for two different switching combinations. One switching combination is such that active switches $T_{am}$, $T_{bp}$, and $T_{an}$ are ON; the other combination is such that switches $T_{am}$, $T_{ap}$, and $T_{bn}$ are ON. During these operating stages, output voltage $V_{AB}$ is $V_1$ or $V_2$. These modes of operation can be seen in Figure 5.2 (c) and Figure 5.2 (d).
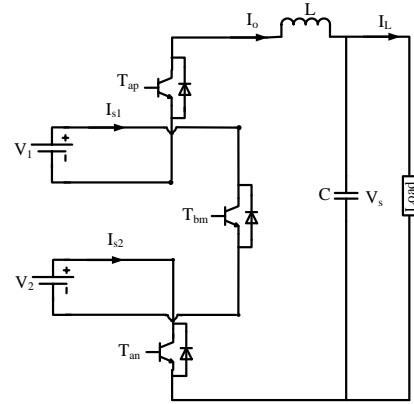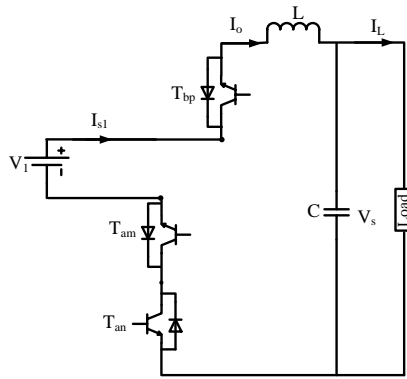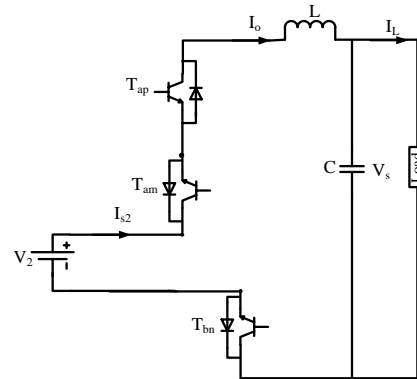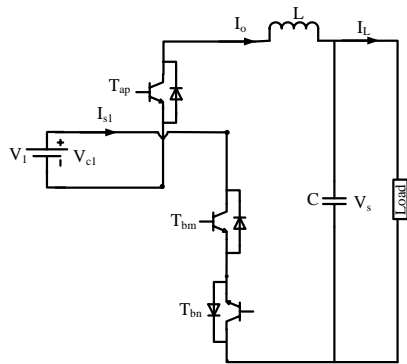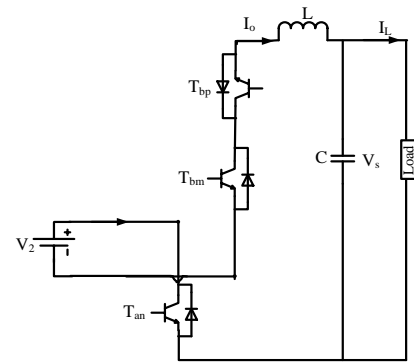
Figure 5.2 Modes of operation of the multi string five level converter.

- **Minimum output, $V_1$-$V_2$:** This output condition is possible for two different switching combinations, either when whole first leg is ON or whole second leg is ON. At that instant, load will be short-circuited, and voltage applied to load terminals will be $V_1$-$V_2$.

- **Half-level negative output,$-V_1$, -$V_2$:** This output condition is possible for two different switching combinations. One switching combination is such that active switches $T_{bm}$, $T_{ap}$, and $T_{bn}$ are ON; the other combination is such that switches $T_{bm}$, $T_{bp}$, and $T_{an}$ are ON. During this operating stage, output voltage $V_{AB}$ is $-V_1$, -$V_2$. These modes of operation can be seen in Figure 5.2 (e) and Figure 5.2 (f).

- **Maximum negative output, $-V_1$-$V_2$ :** When switches $T_{ap}$ , $T_{bm}$ , and $T_{an}$ are ON; the output voltage $V_{AB}$ is $-V_1$-$V_2$ . This mode of operation can be seen in Figure 5.2 (b).

### 5.3 Logic Realization

Karnaugh mapping technique is the logic realization technique used to solve the truth tables [73]. In this case, solving the truth table of modes of operation, an expression for output voltage in terms of switching function can be derived.

According to Kirchoff's Current Law (KCL) and Kirchoff's Voltage Law (KVL),

$$S_{bj} = 1 - S_{aj}, j = p, m, n .\tag{5.1}$$

where $S_{aj}, S_{bj}$ are the switching functions of switches $T_{aj}, T_{bj}$ , $j = p, m, n$ respectively.

121

According to Karnaugh mapping, any output 'y' can be written as the sum of all operating modes. From Truth Table 5.1, the voltage equation using Karnaugh mapping is written as

$$V_{AB} = \sum (1,2,3,6,7,8). \tag{5.2}$$

where $1,2,3,... =$ Operating Modes .

$$V_{AB} = \begin{bmatrix} (V_1 + V_2)(S_{bp}S_{am}S_{bn}) + (V_1)(S_{bp}S_{am}S_{an}) + (V_2)(S_{ap}S_{am}S_{bn}) \\ + (-V_1)(S_{ap}S_{bm}S_{bn}) + (-V_2)(S_{bp}S_{bm}S_{an}) + (-V_1 - V_2)(S_{ap}S_{bm}S_{an}) \end{bmatrix}. \tag{5.3}$$

$$V_{AB} = \begin{bmatrix} V_1(S_{bp}S_{am}S_{bn} + S_{bp}S_{am}S_{an} - S_{ap}S_{bm}S_{bn} - S_{ap}S_{bm}S_{an}) \\ + V_2(S_{bp}S_{am}S_{bn} + S_{ap}S_{am}S_{bn} - S_{bp}S_{bm}S_{an} - S_{ap}S_{bm}S_{an}) \end{bmatrix}. \tag{5.4}$$

$$V_{AB} = \begin{bmatrix} V_1(S_{bp}S_{am}(S_{bn} + S_{an}) - S_{ap}S_{bm}(S_{bn} + S_{an})) \\ + V_2(S_{am}S_{bn}(S_{bp} + S_{ap}) - S_{bm}S_{an}(S_{bp} + S_{ap})) \end{bmatrix}. \tag{5.5}$$

Using (5.1) in (5.5),

$$V_{AB} = V_1(S_{bp}S_{am} - S_{ap}S_{bm}) + V_2(S_{am}S_{bn} - S_{bm}S_{an}). \tag{5.6}$$

$$V_{AB} = V_1((1 - S_{ap})S_{am} - S_{ap}(1 - S_{am})) + V_2(S_{am}(1 - S_{an}) - (1 - S_{am})S_{an}). \tag{5.7}$$

$$V_{AB} = V_1(S_{am} - S_{ap}) + V_2(S_{am} - S_{an}). \tag{5.8}$$

The expression for voltage equation in terms of switching functions is given in (5.8). Similarly, the expressions for input currents $I_{s1}$, $I_{s2}$ can also be found and are given in (5.14) and (5.20) respectively.

$$I_{s1} = \sum (1,2,6,8) = \text{Sum of operating modes.} \tag{5.9}$$

$$I_{s1} = I_o [(S_{bp}S_{am}S_{bn}) + (S_{bp}S_{am}S_{an}) - (S_{ap}S_{bm}S_{bn}) - (S_{ap}S_{bm}S_{an})]. \tag{5.10}$$

$$I_{s1} = I_o [S_{bp}S_{am}(S_{bn} + S_{an}) - S_{ap}S_{bm}(S_{bn} + S_{an})]. \tag{5.11}$$

122

$$I_{s1} = I_o \left[ S_{bp} S_{am} - S_{ap} S_{bm} \right]. \tag{5.12}$$

$$I_{s1} = I_o \left[ \left(1 - S_{ap}\right) S_{am} - S_{ap} \left(1 - S_{am}\right) \right]. \tag{5.13}$$

$$I_{s1} = I_o \left( S_{am} - S_{ap} \right). \tag{5.14}$$

$$I_{s2} = \sum(1,3,7,8) = \text{Sum of operating modes.} \tag{5.15}$$

$$I_{s2} = I_o \left[ \left( S_{bp} S_{am} S_{bn} \right) + \left( S_{ap} S_{am} S_{bn} \right) - \left( S_{bp} S_{bm} S_{an} \right) - \left( S_{ap} S_{bm} S_{an} \right) \right]. \tag{5.16}$$

$$I_{s2} = I_o \left[ S_{am} S_{bn} \left( S_{bp} + S_{ap} \right) - S_{bm} S_{an} \left( S_{bp} + S_{ap} \right) \right]. \tag{5.17}$$

$$I_{s2} = I_o \left[ S_{am} S_{bn} - S_{bm} S_{an} \right]. \tag{5.18}$$

$$I_{s2} = I_o \left[ S_{am} \left(1 - S_{an}\right) - \left(1 - S_{am}\right) S_{an} \right]. \tag{5.19}$$

$$I_{s2} = I_o \left[ S_{am} - S_{an} \right]. \tag{5.20}$$

Therefore the dynamic model equations of the system are given as

$$V_1 \left( S_{am} - S_{ap} \right) + V_2 \left( S_{am} - S_{an} \right) = L_o p I_o + V_c. \tag{5.21}$$

$$Cp V_c = I_o - I_L. \tag{5.22}$$

## 5.3.1    Voltage stress calculations

Voltage stress is defined as the voltage across each switch at any time. Since the voltage across each switch is different, the voltage stresses are calculated and are given from (5.23) to (5.28).

$$V_{Sap} = S_{bp} V_{c1}. \tag{5.23}$$

$$V_{Sbp} = S_{ap} V_{c1}. \tag{5.24}$$

$$V_{Sam} = S_{bm}(V_{c1} + V_{c2}).$$ (5.25)

$$V_{Sbm} = S_{am}(V_{c1} + V_{c2}).$$ (5.26)

$$V_{San} = S_{bn}V_{c2}.$$ (5.27)

$$V_{Sbn} = S_{an}V_{c2}.$$ (5.28)

## 5.4 Modulation Scheme

For modulation scheme, level shifted carrier based PWM is used. In level shifted PWM, the carrier waveforms are in phase but are level shifted as shown in Figure 5.3.
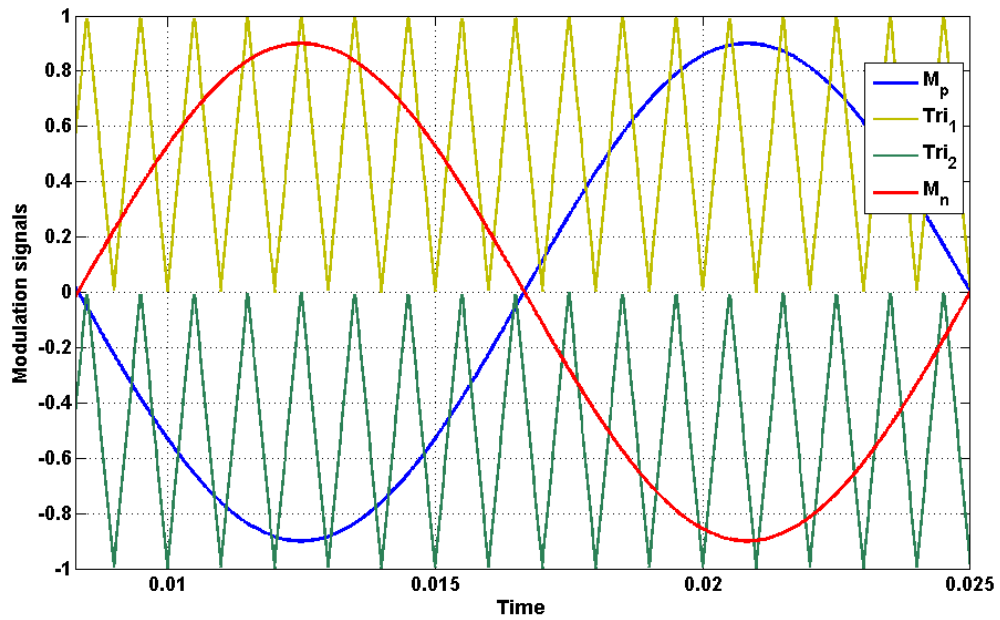


Figure 5.3 Modulation scheme.

If the switching pulses of switches in one leg are generated, then their complementary will be respectively the switching pulses of switches in another leg. Here $S_{bp}$, $S_{am}$, $S_{an}$ are considered as main switches and $S_{ap}$, $S_{bm}$, $S_{bn}$ are generated by complementing $S_{bp}$, $S_{am}$, $S_{an}$ respectively. The generation of switching pulses is as follows:

$$S_{ap} = \begin{bmatrix} 1 \text{ when } M_p < Tri_1 \text{ for } M_p > 0, M_p < Tri_2 \text{ for } M_p < 0 \\ 0 \text{ when } M_p > Tri_1 \text{ for } M_p > 0, M_p > Tri_2 \text{ for } M_p < 0 \end{bmatrix}. \tag{5.29}$$

$$S_{bp} = \begin{bmatrix} 1 \text{ when } M_p > Tri_1 \text{ for } M_p > 0, M_p > Tri_2 \text{ for } M_p < 0 \\ 0 \text{ when } M_p < Tri_1 \text{ for } M_p > 0, M_p < Tri_2 \text{ for } M_p < 0 \end{bmatrix}. \tag{5.30}$$

$$S_{am} = \begin{bmatrix} 1 \text{ when } M_p > 0 \\ 0 \text{ when } M_p < 0 \end{bmatrix}. \tag{5.31}$$

$$S_{bm} = \begin{bmatrix} 1 \text{ when } M_p < 0 \\ 0 \text{ when } M_p > 0 \end{bmatrix}. \tag{5.32}$$

$$S_{an} = \begin{bmatrix} 1 \text{ when } M_n > Tri_2 \text{ for } M_n < 0, M_n > Tri_1 \text{ for } M_n > 0 \\ 0 \text{ when } M_n < Tri_2 \text{ for } M_n < 0, M_n < Tri_1 \text{ for } M_n > 0 \end{bmatrix}. \tag{5.33}$$

$$S_{bn} = \begin{bmatrix} 1 \text{ when } M_n < Tri_2 \text{ for } M_n < 0, M_n < Tri_1 \text{ for } M_n > 0 \\ 0 \text{ when } M_n > Tri_2 \text{ for } M_n < 0, M_n > Tri_1 \text{ for } M_n > 0 \end{bmatrix}. \tag{5.34}$$

where $M_p$ and $M_n$ are the modulation signals and $Tri_1$ and $Tri_2$ are the two carrier waveforms used to generate switching pulses by level shifted carrier based PWM. The modulation signals and carrier waveforms can be seen in Figure 5.3.

### 5.4.1    Determination of expressions for modulation signals

The expressions for modulation signals are determined using double Fourier series analysis. At any time, if the carrier frequency is much larger than the frequency of modulation signals, the switching functions are approximated based on the instantaneous values of modulation signal [74].
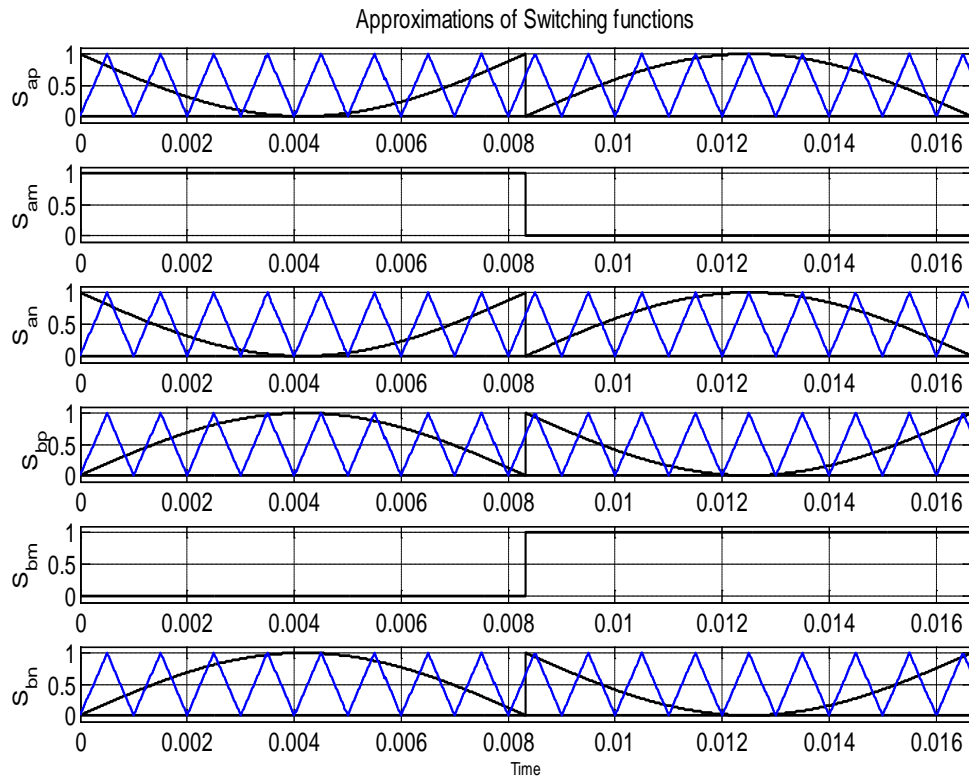


Figure 5.4 Approximations of switching functions in terms of instantaneous values of modulation signals.

Let the two modulation waveforms used be of the form $M_p = M_1 \sin(\theta + \psi_1)$ and

$M_n = M_2 \sin(\theta + \psi_2)$, where $\psi_1$ and $\psi_2$ are the initial phase angles of modulation signals

respectively and $\theta = \omega t$, where $\omega$ is the frequency of the reference voltage waveform.

From Figure 5.4, the switching functions are approximated by their instantaneous values

of modulation signal.

$$
S_{ap} = \begin{cases} 1 - M_p & \psi_1 \le \theta_1 < \pi + \psi_1 \\ -M_p & \pi + \psi_1 \le \theta_1 \le 2\pi + \psi_1 \end{cases} \tag{5.35}
$$

$$
S_{am} = \begin{cases} 1 & \psi_1 \le \theta_1 < \pi + \psi_1 \\ 0 & \pi + \psi_1 \le \theta_1 \le 2\pi + \psi_1 \end{cases} \tag{5.36}
$$

$$
S_{an} = \begin{cases} 1 - M_n & \psi_2 \le \theta_2 < \pi + \psi_2 \\ -M_n & \pi + \psi_2 \le \theta_2 \le 2\pi + \psi_2 \end{cases} \tag{5.37}
$$

$$
S_{bp} = \begin{cases} M_p & \psi_1 \le \theta_1 < \pi + \psi_1 \\ 1 + M_p & \pi + \psi_1 \le \theta_1 \le 2\pi + \psi_1 \end{cases} \tag{5.38}
$$

$$
S_{bm} = \begin{cases} 0 & \psi_1 \le \theta_1 < \pi + \psi_1 \\ 1 & \pi + \psi_1 \le \theta_1 \le 2\pi + \psi_1 \end{cases} \tag{5.39}
$$

$$
S_{bn} = \begin{cases} M_n & \psi_2 \le \theta_2 < \pi + \psi_2 \\ 1 + M_n & \pi + \psi_2 \le \theta_2 \le 2\pi + \psi_2 \end{cases} \tag{5.40}
$$

Using Fourier series analysis, the expressions for switching functions are given in (5.41-

5.46). The detailed derivations are given in Appendix A.

The expressions for $S_{ap}$, $S_{am}$, $S_{an}$, $S_{bp}$, $S_{bm}$, $S_{bn}$ are given as

$$
S_{ap} = \frac{1}{2} - M_p - \frac{2}{\pi}\left(\sin(\psi_1 - \theta)\right). \tag{5.41}
$$

$$S_{am} = \frac{1}{2} - \frac{2}{\pi}\left(\sin(\psi_1 - \theta)\right). \tag{5.42}$$

$$S_{an} = \frac{1}{2} - M_n - \frac{2}{\pi}\left(\sin(\psi_2 - \theta)\right). \tag{5.43}$$

$$S_{bp} = \frac{1}{2} + M_p + \frac{2}{\pi}\left(\sin(\psi_1 - \theta)\right). \tag{5.44}$$

$$S_{bm} = \frac{1}{2} + \frac{2}{\pi}\left(\sin(\psi_1 - \theta)\right). \tag{5.45}$$

$$S_{bn} = \frac{1}{2} + M_n + \frac{2}{\pi}\left(\sin(\psi_2 - \theta)\right). \tag{5.46}$$

The equations (5.41), (5.42), (5.43), (5.44), (5.45), (5.46) verify the basic equation (5.1). Substituting those equations into (5.8), then the output voltage equation becomes

$$V_{AB} = V_1 M_p - V_2 M_n. \tag{5.47}$$

In output voltage, odd carrier and associated harmonics as well as even base band and side band harmonics are cancelled. As a result, the only harmonics which exist are odd side band harmonics around an even carrier. $M_i$ denotes the modulation index of $i_{th}$ H-bridge.

$$V_i = \begin{bmatrix} V_i M_i \sin(\theta + \psi_i) \\ + \frac{4V_{ci}}{\pi} \sum_{m=2}^{\infty} \sum_{n=-\infty}^{\infty} \frac{1}{m} J_n\left(\frac{m\pi}{2}M_i\right)\sin\left(\frac{\pi}{2}(m+n)\right) \\ \cos(m(\theta_c + \gamma_i) + n(\theta + \psi_i)) \end{bmatrix}. \tag{5.48}$$

where $J_n(x) = \sum_{m=0}^{\infty} \frac{(-1)^m}{m!(m+n)!}\left(\frac{1}{2}x\right)^{2m+n}.$ \tag{5.49}

The first dominant harmonic component which is first side band harmonic around second carrier frequency is given below.

$$V_{o1}^+ = -\frac{2V_1}{\pi} J_1(\pi M_1) \cos(2(\theta_c + \gamma_1) + (\theta + \psi_1)) + \frac{2V_2}{\pi} J_1(\pi M_2) \cos(2(\theta_c + \gamma_2) + (\theta + \psi_2)). \tag{5.50}$$

Using $J_n(x) = \sum\limits_{m=0}^{\infty} \frac{(-1)^m}{m!(m+n)!} \left(\frac{1}{2} x\right)^{2m+n}$ , $J_1(\pi M_i) = \frac{\pi M_i}{2}$, where $i = 1,2$ .

Therefore (5.50) becomes,

$$V_{o1}^+ = -M_1 V_1 \cos(2(\theta_c + \gamma) + (\theta + \psi_1)) + M_2 V_2 \cos(2(\theta_c + \gamma) + (\theta + \psi_2)). \tag{5.51}$$

To eliminate dominant harmonics, modulation indices are selected in such a way that

$$[M_1 V_{c1} \cos(\theta + \psi_1) - M_2 V_{c2} \cos(\theta + \psi_2)] \cos(2(\theta_c + \gamma)) = \tag{5.52}$$
$$[M_1 V_{c1} \sin(\theta + \psi_1) - M_2 V_{c2} \sin(\theta + \psi_2)] \sin(2(\theta_c + \gamma))$$

$$\Rightarrow M_1 V_{c1} \cos(\theta + \psi_1) - M_2 V_{c2} \cos(\theta + \psi_2) = 0. \tag{5.53}$$

and $M_1 V_{c1} \sin(\theta + \psi_1) - M_2 V_{c2} \sin(\theta + \psi_2) = 0$.

$$\Rightarrow Tan(\theta + \psi_1) = Tan(\theta + \psi_2). \tag{5.54}$$

$$\Rightarrow \theta + \psi_1 = 2n\pi + (\theta + \psi_2). \tag{5.55}$$

$$\Rightarrow \psi_1 = 2n\pi + \psi_2. \tag{5.56}$$

Let $M_2 = -\alpha M_1$, then from (5.8) and (5.56)

$$M_p = \frac{V_{AB}}{V_{c1} + \alpha V_{c2}}. \tag{5.57}$$

$$M_n = \frac{-\alpha V_{AB}}{V_{c1} + \alpha V_{c2}}, \text{ where } 0 < \alpha \le 1. \tag{5.58}$$

## 5.5 Switching Loss Comparison with Two Cell Cascaded H-bridge inverter

The switching power loss for this proposed topology is compared with the cascaded H bridge multilevel Inverter topology. The average switching power loss $P_s$ in the switch caused by these transitions [75] can be defined as

$$P_s = 0.5 V_S I_o f_s \left( t_{(on)} + t_{(off)} \right). \tag{5.59}$$

where $t_{(on)}$ and $t_{(off)}$ are the turn-on and turn-off times, respectively; $V_S$ is the voltage stress across the switch; and $I_o$ is the current flowing through the switch.

Let both the proposed circuit and cascaded H bridge multi-level converter are operated at the same turn-on and turn-off times and at the same load current $I_o$. Then the average switching power loss $P_s$ is proportional to $V_S$ and $f_s$. So in general

$$P_s \propto V_S f_s. \tag{5.60}$$

The voltage stresses of the eight switches of the conventional cascaded H-bridge inverter are all equal to $V_s$. According to Figure 5.5, the switching loss of cascaded H-bridge inverter from eight switches can be obtained as

$$P_{s,H-bridge} \propto 8 V_s f_s. \tag{5.61}$$

Similarly the switching power loss of multi string five-level inverter shown in Figure 5.1 with six switches can also be obtained as

$$P_{s,\text{multi string}} \propto 4 V_s f_s + 2(2 V_s) f_m. \tag{5.62}$$

$$P_{s,\text{multi string}} \propto 4 V_s (f_s + f_m). \tag{5.63}$$

where $f_m$ is the line frequency.
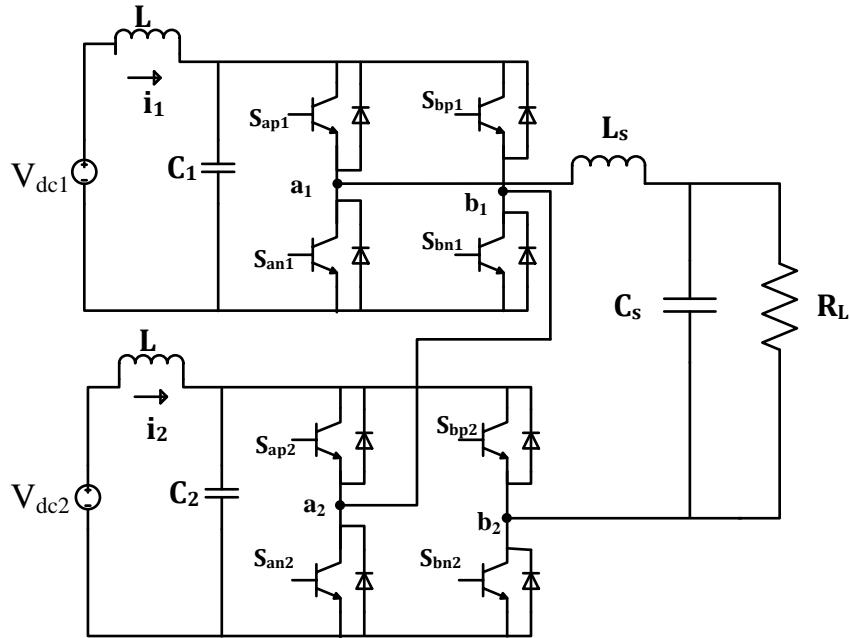
Figure 5.5 Two cell cascaded H-bridge inverter.

Because the switches $S_{am}$, $S_{bm}$ are operated at line frequency and switching frequency is larger than line frequency $f_m \ll f_s$, the switching losses of the proposed circuit is approximated to

$$P_{s,\text{multi string}} \propto 4V_s f_s . \tag{5.64}$$

Comparing equations (5.61) and (5.64), switching losses in multi string multi-level converter are almost 50% less than cascaded H bridge multi-level converter in this case.

## 5.6 Simulation Results and Discussions

The simulation of multi string five-level inverter topology was carried out using Matlab/Simulink software. The parameters used for simulation are, $V_{AB} = 80V$ , $V_1 = 50V$ ,

$V_2 = 50V$ and $\alpha = 1$. $M_1, M_2$ are derived from (5.57) and (5.58) respectively. Figure 5.3 shows the modulation scheme that was used to generate switching pulses shown in Figure 5.6. From Figure 5.6, the switching pulses of the middle switches can be seen at line frequency. Figure 5.7 shows the voltage across each switch, as can be seen from Figure 5.7, the voltage stress of middle two switches $T_{am}, T_{bm}$ are twice that of other four switches. Figure 5.9 shows the waveforms of output phase voltage $V_{AB}$ and. Figure 5.8 shows the waveforms of two input source currents.
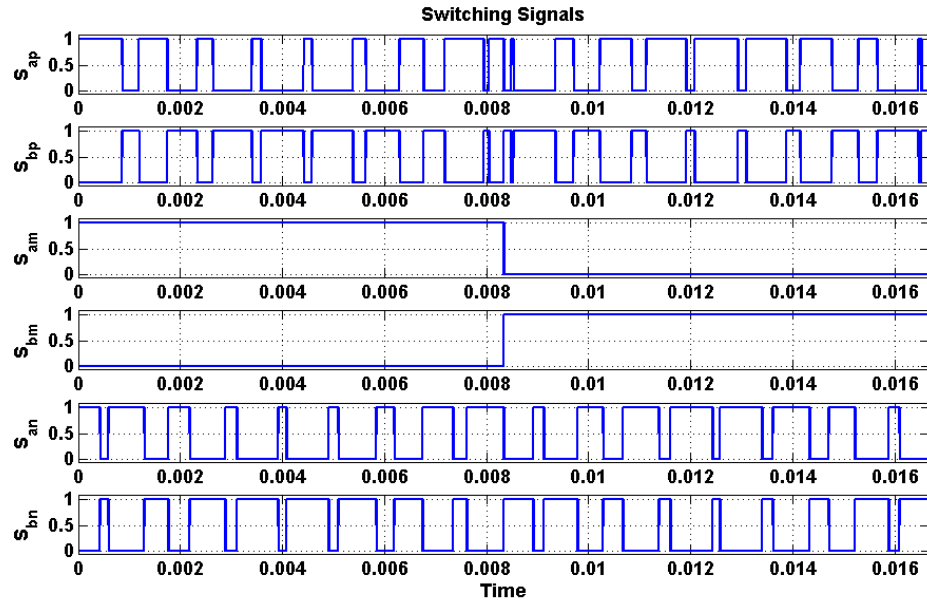
Figure 5.6 Simulation results of switching pulses of all the switches.
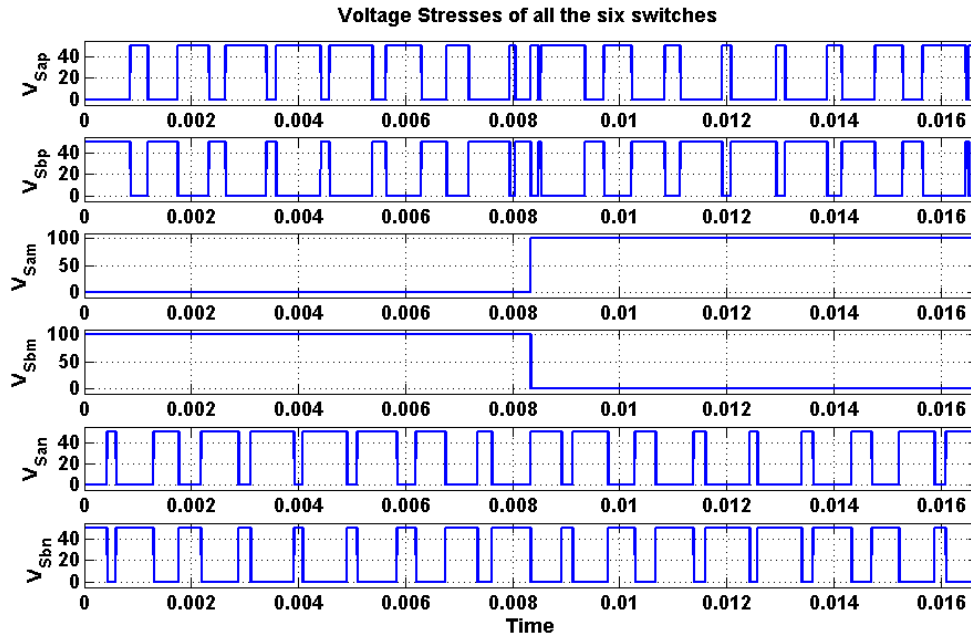


Figure 5.7 Simulation results of voltage stress of all the six switches of the converter.
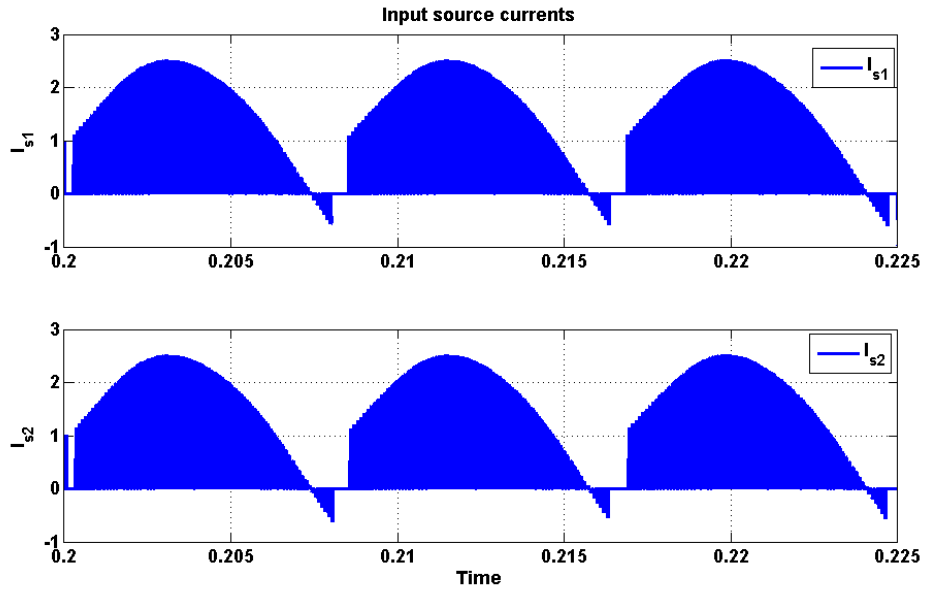
Figure 5.8 Simulation result of input source currents.
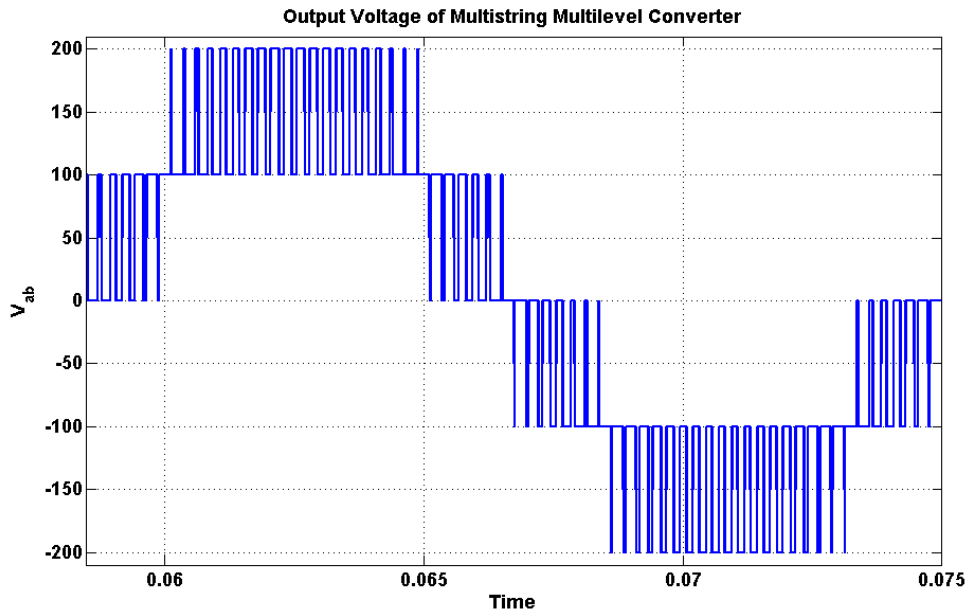


Figure 5.9 Simulation result of output phase voltage.

## 5.7 Experimental results

The experiments on multi string five-level inverter were performed on a laboratory prototype using TMS 320 F28335 eZdsp to generate the switching pulses of both the legs which are shown in Figures 5.10 and 5.11 respectively. The waveform of the output voltage can also be seen in Figure 5.12. The waveform of filtered output voltage including the output voltage was also presented and it can be seen in Figure 5.13. The experimental results and simulation results agree with each other.
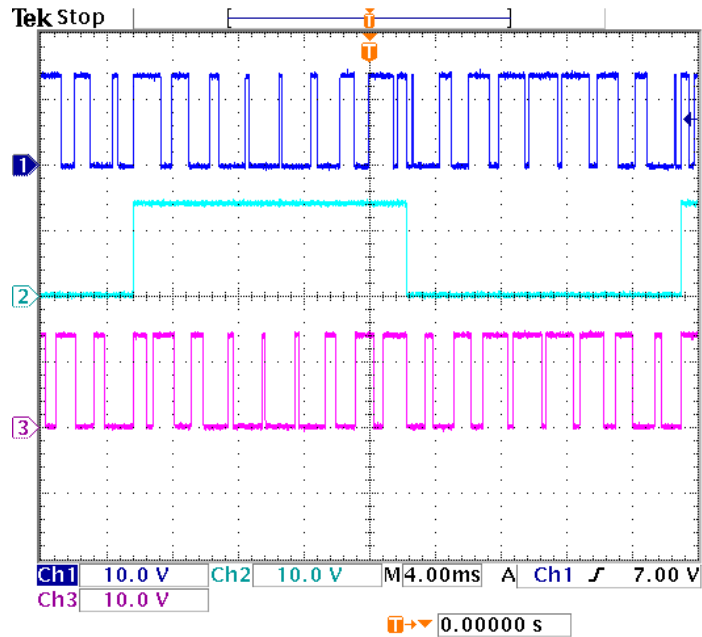


Figure 5.10 Experimental result of switching pulses of switches in first leg.
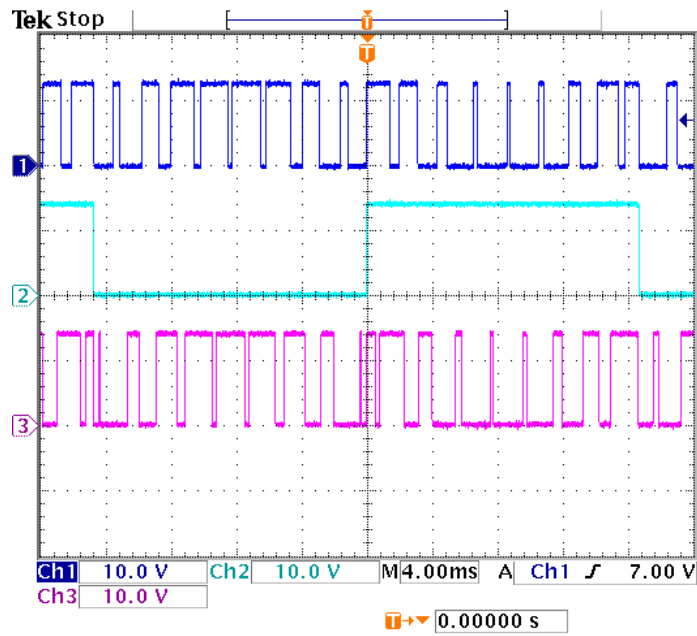
Figure 5.11 Experimental result of switching pulses of switches in second leg.
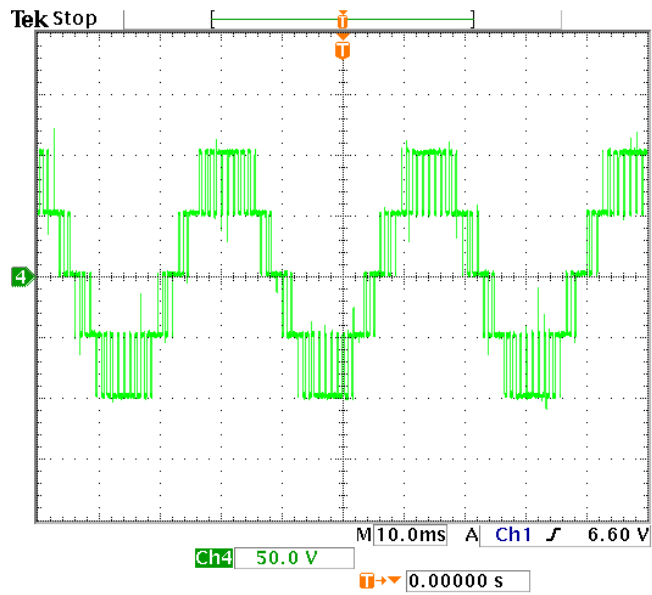


Figure 5.12 Experimental result of output phase voltage (50V/div).
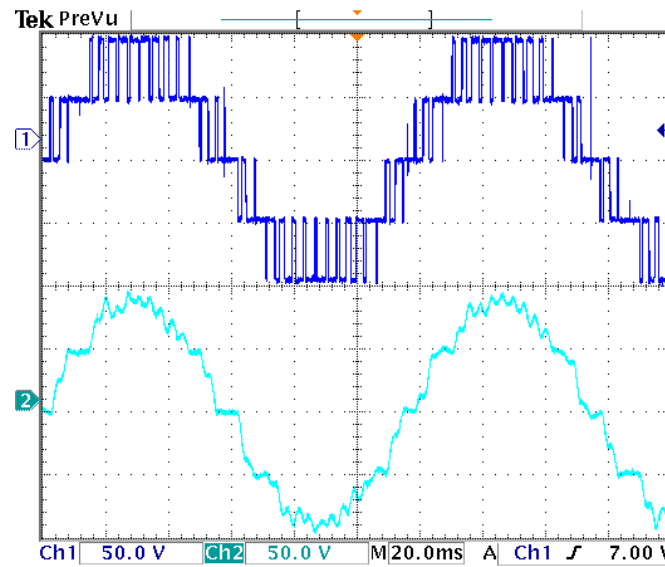
Figure 5.13 Experimental result of output phase voltage and load voltage of single phase

multi string five level inverter (50V/div).

## 5.8 Summary

This chapter presented a single-phase multistring five-level inverter topology which has less number of switches required to produce the desired multi-level output for distributed energy resources compared to cascaded H-bridge converter topology. The modes of operation of five-level inverter topology are also discussed in this chapter. The equations for output voltage and input source currents are calculated in terms of the input voltages and output current respectively using Karnaugh mapping technique. The expression of voltage stress for each switch is determined. The modulation scheme for this topology is also presented. The expression for modulation signal is determined using

Fourier series analysis by approximating switching functions. The calculation of switching loss for multi string five-level inverter is performed and the proposed topology reduces more than 50% of switching loss compared to cascaded H bridge multi-level converter. Simulation of the proposed system is carried out and waveforms of output voltage, input source currents, voltage stress are generated. Experimental results are conducted on 1kW laboratory prototype and the waveforms of switching pulses, output voltage and load voltage are presented. The experimental results and simulation results agree with each other. The only disadvantage with this type of converter when compared with cascade H bridge multi-level converter is the rating of switches. The rating of two middle switches should be twice the rating of other four switches.

# CHAPTER 6

# SINGLE PHASE MULTI STRING SEVEN LEVEL DC-AC CONVERTER

## 6.1 Introduction

This chapter presents the modeling and analysis of novel multi-string seven level DC-AC converter. This multi-level inverter is called multi-string as it is mainly designed for strings of PV cells. In this chapter, modeling and analysis has been done considering the DC sources instead of PV cells.

The topology of single phase multi string seven level inverter can be seen in figure 6.1. This topology offers strong advantages like improved output voltage waveforms, smaller filter size and low electromagnetic interference and THD [72]. This topology requires three DC sources like three cell cascaded H-bridge inverter which also gives seven level output voltage. So, this topology can be compared with the conventional cascaded H-bridge multi-level inverter.

This topology requires four less switches than three cell cascaded H-bridge inverter. And moreover, four of the switches are operated at almost line frequency. As a result, the switching losses when compared with three cell cascaded converter are considerably less. The carrier based PWM is used to generate PWM signals for the switches.
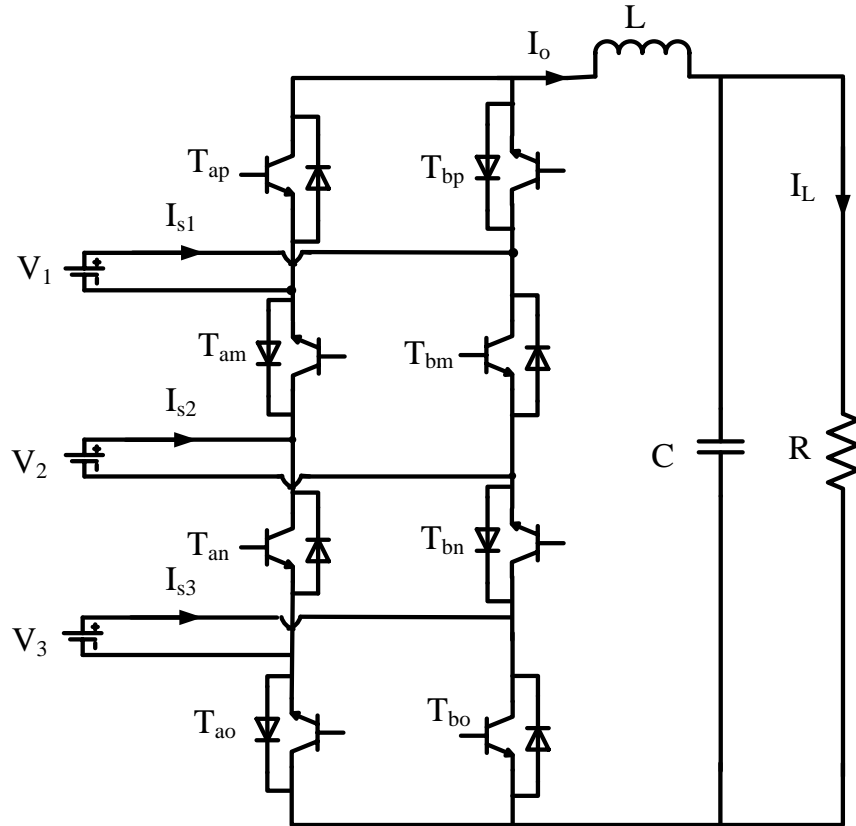
Figure 6.1 Schematic diagram of single phase multi string seven level inverter.

From the Figure 6.1, $S_{ip}, S_{im}, S_{in}, S_{io}$, are the switching functions of switches $T_{ip}, T_{im}, T_{in}, T_{io}$, $i = a,b$, respectively. $V_1, V_2, V_3$ are input DC sources, $I_{s1}, I_{s2}, I_{s3}$ are respective input currents, and $I_o$ is inverter output current.
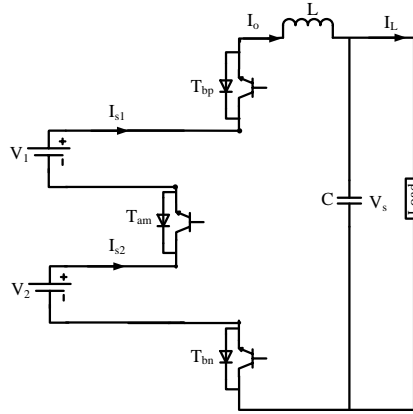
## 6.2 Modes of Operation

The different modes of operation of multi-string seven level inverter are shown in Table 6.1. Each mode shown in Table 6.1 is described in terms of output voltage.

Table 6.1 Switching modes of multi string seven level converter

| $S_{ap}$ | $S_{am}$ | $S_{an}$ | $S_{ao}$ | $S_{bp}$ | $S_{bm}$ | $S_{bn}$ | $S_{bo}$ | $V_{AB}$ | $I_{s1}$ | $I_{s2}$ | $I_{s3}$ |
|---|---|---|---|---|---|---|---|---|---|---|---|
| 0 | 1 | 0 | 1 | 1 | 0 | 1 | 0 | $V_1+V_2+V_3$ | $I_0$ | $I_0$ | $I_0$ |
| 0 | 1 | 0 | 0 | 1 | 0 | 1 | 1 | $2V_s(V_1+V_2)$ | $I_0$ | $I_0$ | 0 |
| 1 | 1 | 0 | 1 | 0 | 0 | 1 | 0 | $2V_s(V_2+V_3)$ | 0 | $I_0$ | $I_0$ |
| 0 | 0 | 0 | 1 | 1 | 1 | 1 | 0 | $V_3$ | 0 | 0 | $I_0$ |
| 1 | 1 | 0 | 0 | 0 | 0 | 1 | 1 | $V_2$ | 0 | $I_0$ | 0 |
| 0 | 1 | 1 | 1 | 1 | 0 | 0 | 0 | $V_1$ | $I_0$ | 0 | 0 |
| 1 | 1 | 1 | 1 | 0 | 0 | 0 | 0 | 0 | 0 | 0 | 0 |
| 0 | 0 | 0 | 0 | 1 | 1 | 1 | 1 | 0 | 0 | 0 | 0 |
| 1 | 0 | 0 | 1 | 0 | 1 | 1 | 0 | $V_3-V_1$ | $-I_0$ | 0 | $I_0$ |
| 0 | 1 | 1 | 0 | 1 | 0 | 0 | 1 | $V_1-V_3$ | $I_0$ | 0 | $-I_0$ |
| 1 | 1 | 1 | 0 | 0 | 0 | 0 | 1 | $-V_3$ | 0 | 0 | $-I_0$ |
| 0 | 0 | 1 | 1 | 1 | 1 | 0 | 0 | $-V_2$ | 0 | $-I_0$ | 0 |
| 1 | 0 | 0 | 0 | 0 | 1 | 1 | 1 | $-V_1$ | $-I_0$ | 0 | 0 |
| 1 | 0 | 1 | 1 | 0 | 1 | 0 | 0 | $-2V_s(-V_1-V_2)$ | $-I_0$ | $-I_0$ | 0 |
| 0 | 0 | 1 | 0 | 1 | 1 | 0 | 1 | $-2V_s(-V_2-V_3)$ | 0 | $-I_0$ | $-I_0$ |
| 1 | 0 | 1 | 0 | 0 | 1 | 0 | 1 | $-V_1-V_2-V_3$ | $-I_0$ | $-I_0$ | $-I_0$ |

This type of Multistring Converter has seven levels. So it will be having seven levels of operation. Maximum positive output voltage of $V_1 +V_2 +V_3$, positive output voltage of $V_1 +V_2$ or $V_2 +V_3$, minimum positive output voltage of $V_1$ or $V_2$ or $V_3$, zero output

voltage, minimum negative output voltage of $-V_1$, $-V_2$ or $-V_3$, negative output voltage of $-V_1$ $-V_2$ or $-V_2$ $-V_3$ and maximum negative output voltage of $-V_1$ $-V_2$ $-V_3$. There are 16 modes of operation for this eight switch multi string seven level converter.

- **Maximum Positive Output Voltage:**

When the switches $T_{bp}$, $T_{am}$, $T_{bn}$ and $T_{ao}$ are ON; the output voltage $V_{AB}$ is $V_1+V_2+V_3$. This mode of operation can be seen in Figure 6.2 (a).

- **Positive output Voltage:**

This output condition is possible for two different switching combinations. One switching combination is such that active switches $T_{bp}$, $T_{am}$, $T_{bn}$ and $T_{bo}$ are ON; the other combination is such that switches $T_{ap}$, $T_{am}$, $T_{bn}$ and $T_{ao}$ are ON. During these operating stages, output voltage $V_{AB}$ is $V_1+V_2$ and $V_2+V_3$ respectively. These modes of operation can be seen in Figure 6.2 (b) and Figure 6.2 (c) respectively.

- **Minimum Positive output Voltage:**

This output condition is possible for three different switching combinations. One switching combination is such that active switches $T_{bp}$, $T_{bm}$, $T_{bn}$ and $T_{ao}$ are ON; the second combination is such that switches $T_{ap}$, $T_{am}$, $T_{bn}$ and $T_{bo}$ are ON, the third combination is such that switches $T_{bp}$, $T_{am}$, $T_{an}$ and $T_{ao}$ are ON. During these operating stages, output voltage $V_{AB}$ is $V_3$, $V_2$ and $V_1$ respectively. These modes of operation can be seen in Figure 6.2 (d), Figure 6.2 (e) and Figure 6.2 (f) respectively.

- **Zero output voltage:**

This output condition is possible for two different switching combinations, either when whole first leg is ON or whole second leg is ON. At that instant, load will be short-circuited, and there will be no transfer of power from one side to the other side.

- **Minimum Negative Output Voltage:**

This output condition is possible for three different switching combinations. One switching combination is such that active switches $T_{ap}$, $T_{am}$, $T_{an}$ and $T_{bo}$ are ON; the second combination is such that switches $T_{bp}$, $T_{bm}$, $T_{an}$ and $T_{ao}$ are ON, the third combination is such that switches $T_{ap}$, $T_{bm}$, $T_{bn}$ and $T_{bo}$ are ON. During these operating stages, output voltage $V_{AB}$ is $-V_3$, $-V_2$ and $-V_1$ respectively. These modes of operation can be seen in Figure 6.3 (a), Figure 6.3 (b) and Figure 6.2 (c) respectively.

- **Negative output Voltage:**

This output condition is possible for two different switching combinations. One switching combination is such that active switches $T_{ap}$, $T_{bm}$, $T_{an}$ and $T_{ao}$ are ON; the other combination is such that switches $T_{bp}$, $T_{bm}$, $T_{an}$ and $T_{bo}$ are ON. During these operating stages, output voltage $V_{AB}$ is $-V_1$-$V_2$ and $-V_2$-$V_3$ respectively. These modes of operation can be seen in Figure 6.3 (d) and Figure 6.2 (e) respectively.

- **Maximum negative output Voltage:**

When the active power switches $T_{ap}$, $T_{bm}$, $T_{an}$ and $T_{bo}$ are ON; the output voltage $V_{AB}$ is $-V_1$-$V_2$-$V_3$ .This mode of operation can be seen in Figure 6.3 (f).
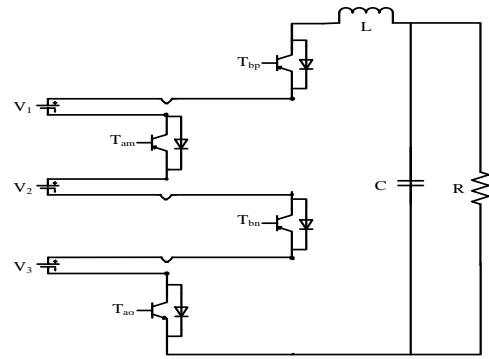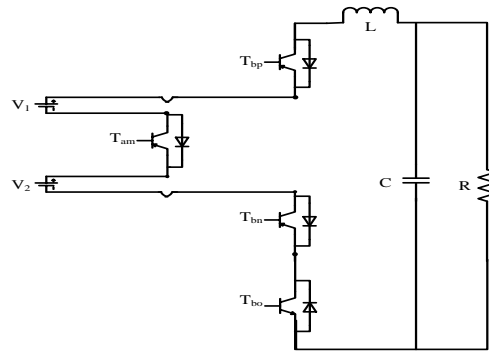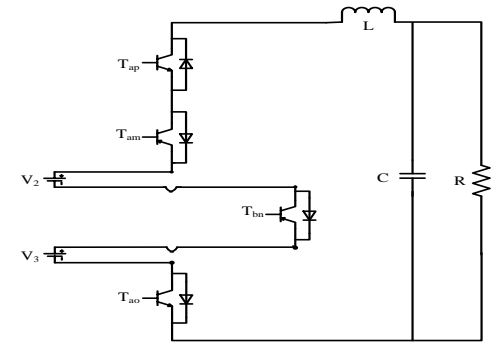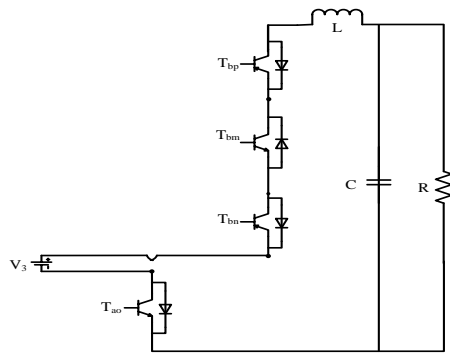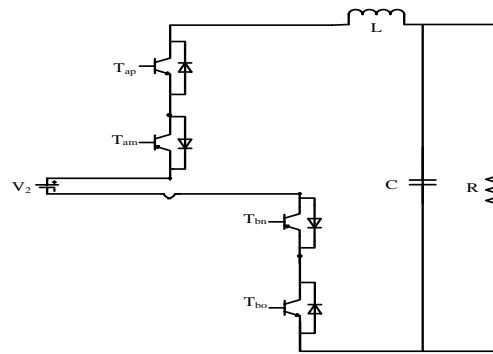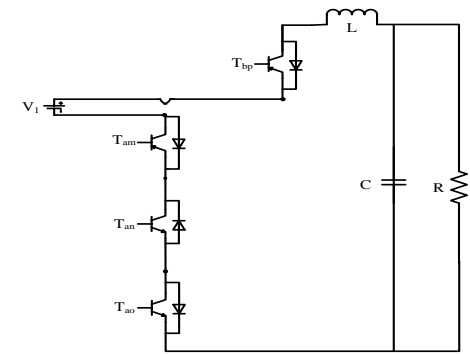
Figure 6.2 Positive modes of operation of multi string seven level inverter.

144
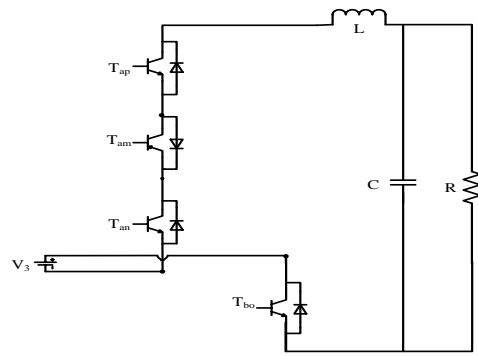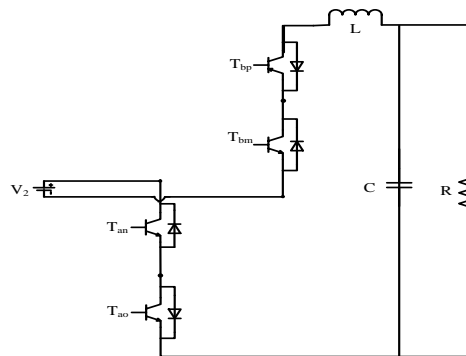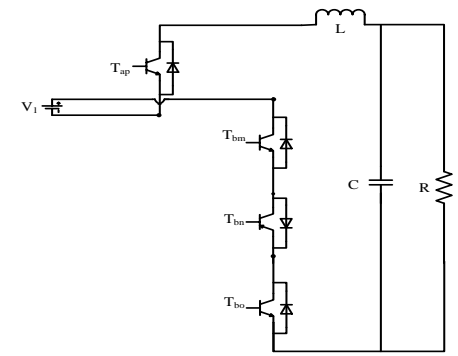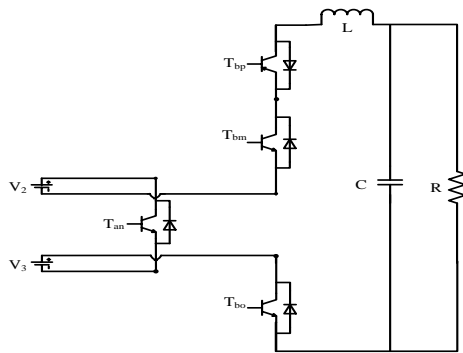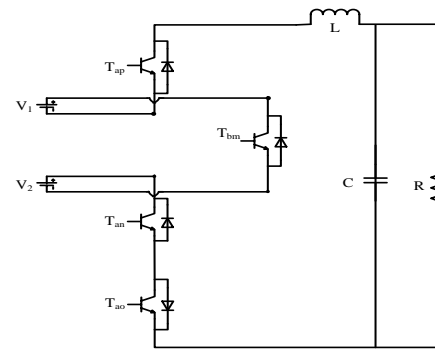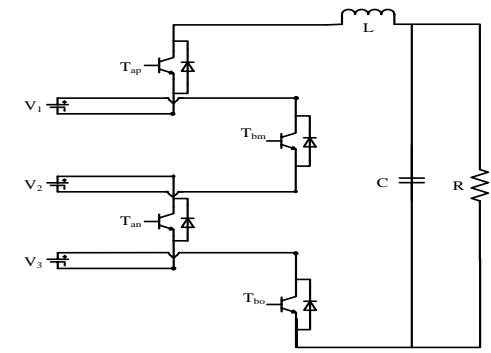
Figure 6.3 Negative modes of operation of multi string seven level inverter.

145

## 6.3 Logic Realization

According to Kirchoff's Current Law (KCL) and Kirchoff's Voltage Law (KVL),

$$S_{bj} = 1 - S_{aj}; \; j = p, m, n, o .$$ (6.1)

where $S_{aj}, S_{bj}$ are the switching functions of switches $T_{aj}, T_{bj}$ , $j = p, m, n, o$ respectively.

According to Karnaugh mapping, any output '$y$' can be written as the sum of all operating modes. From Table 6.1, the voltage equation using Karnaugh mapping is written as

$$V_{AB} = \sum (1,2,3,4,5,6,9,10,11,12,13,14,15,16), \text{ where } 1,2,3,... = \text{Operating Modes} .$$

Therefore

$$V_{AB} = \begin{cases} S_{bp}S_{am}S_{bn}S_{ao}(V_1 + V_2 + V_3) + S_{bp}S_{am}S_{bn}S_{bo}(V_1 + V_2) + S_{ap}S_{am}S_{bn}S_{ao}(V_2 + V_3) \\ + S_{bp}S_{bm}S_{bn}S_{ao}(V_3) + S_{ap}S_{am}S_{bn}S_{bo}(V_2) + S_{bp}S_{am}S_{an}S_{ao}(V_1) \\ + S_{ap}S_{bm}S_{bn}S_{ao}(V_3 - V_1) + S_{bp}S_{am}S_{an}S_{bo}(V_1 - V_3) + S_{ap}S_{am}S_{an}S_{bo}(-V_3) \\ + S_{bp}S_{bm}S_{an}S_{ao}(-V_2) + S_{ap}S_{bm}S_{bn}S_{bo}(-V_1) + S_{ap}S_{bm}S_{an}S_{ao}(-V_1 - V_2) \\ + S_{bp}S_{bm}S_{an}S_{bo}(-V_2 - V_3) + S_{ap}S_{bm}S_{an}S_{bo}(-V_1 - V_2 - V_3) \end{cases} .$$ (6.2)

$$V_{AB} = \begin{cases} V_1 \begin{pmatrix} S_{bp}S_{am}S_{bn}S_{ao} + S_{bp}S_{am}S_{bn}S_{bo} + S_{bp}S_{am}S_{an}S_{ao} - S_{ap}S_{bm}S_{bn}S_{ao} \\ + S_{bp}S_{am}S_{an}S_{bo} - S_{ap}S_{bm}S_{bn}S_{bo} - S_{ap}S_{bm}S_{an}S_{ao} - S_{ap}S_{bm}S_{an}S_{bo} \end{pmatrix} \\ + V_2 \begin{pmatrix} S_{bp}S_{am}S_{bn}S_{ao} + S_{bp}S_{am}S_{bn}S_{bo} + S_{ap}S_{am}S_{bn}S_{ao} + S_{ap}S_{am}S_{bn}S_{bo} \\ - S_{bp}S_{bm}S_{an}S_{ao} - S_{ap}S_{bm}S_{an}S_{ao} - S_{bp}S_{bm}S_{an}S_{bo} - S_{ap}S_{bm}S_{an}S_{bo} \end{pmatrix} \\ + V_3 \begin{pmatrix} S_{bp}S_{am}S_{bn}S_{ao} + S_{ap}S_{am}S_{bn}S_{bo} + S_{bp}S_{bm}S_{bn}S_{ao} + S_{ap}S_{bm}S_{bn}S_{ao} \\ - S_{bp}S_{am}S_{an}S_{bo} - S_{ap}S_{am}S_{an}S_{bo} - S_{bp}S_{bm}S_{an}S_{bo} - S_{ap}S_{bm}S_{an}S_{bo} \end{pmatrix} \end{cases} .$$

$$V_{AB} = \begin{Bmatrix} V_1 \begin{pmatrix} S_{bp}S_{am}S_{bn}(S_{ao}+S_{bo}) + S_{bp}S_{am}S_{an}(S_{ao}+S_{bo}) \\ -S_{ap}S_{bm}S_{bn}(S_{ao}+S_{bo}) - S_{ap}S_{bm}S_{an}(S_{ao}+S_{bo}) \end{pmatrix} \\ +V_2 \begin{pmatrix} S_{bp}S_{am}S_{bn}(S_{ao}+S_{bo}) + S_{ap}S_{am}S_{bn}(S_{ao}+S_{bo}) \\ -(S_{ap}+S_{bp})S_{bm}S_{an}S_{ao} - (S_{ap}+S_{bp})S_{bm}S_{an}S_{bo} \end{pmatrix} \\ +V_3 \begin{pmatrix} (S_{ap}+S_{bp})S_{am}S_{bn}S_{ao} + (S_{ap}+S_{bp})S_{bm}S_{bn}S_{ao} \\ -(S_{ap}+S_{bp})S_{am}S_{an}S_{bo} - (S_{ap}+S_{bp})S_{bm}S_{an}S_{bo} \end{pmatrix} \end{Bmatrix}.$$

$$V_{AB} = \begin{Bmatrix} V_1(S_{bp}S_{am}S_{bn} + S_{bp}S_{am}S_{an} - S_{ap}S_{bm}S_{bn} - S_{ap}S_{bm}S_{an}) \\ +V_2(S_{bp}S_{am}S_{bn} + S_{ap}S_{am}S_{bn} - S_{bm}S_{an}S_{ao} - S_{bm}S_{an}S_{bo}) \\ +V_3(S_{am}S_{bn}S_{ao} + S_{bm}S_{bn}S_{ao} - S_{am}S_{an}S_{bo} - S_{bm}S_{an}S_{bo}) \end{Bmatrix}.$$

$$V_{AB} = V_1 \begin{pmatrix} S_{bp}S_{am}(S_{an}+S_{bn}) \\ -S_{ap}S_{bm}(S_{an}+S_{bn}) \end{pmatrix} + V_2 \begin{pmatrix} (S_{ap}+S_{bp})S_{am}S_{bn} \\ -S_{bm}S_{an}(S_{ao}+S_{bo}) \end{pmatrix} + V_3 \begin{pmatrix} (S_{am}+S_{bm})S_{bn}S_{ao} \\ -(S_{am}+S_{bm})S_{an}S_{bo} \end{pmatrix}.$$

$$V_{AB} = V_1(S_{bp}S_{am} - S_{ap}S_{bm}) + V_2(S_{am}S_{bn} - S_{bm}S_{an}) + V_3(S_{bn}S_{ao} - S_{an}S_{bo}).$$

$$V_{AB} = V_1 \begin{pmatrix} (1-S_{ap})S_{am} \\ -S_{ap}(1-S_{am}) \end{pmatrix} + V_2 \begin{pmatrix} S_{am}(1-S_{an}) \\ -(1-S_{am})S_{an} \end{pmatrix} + V_3 \begin{pmatrix} (1-S_{an})S_{ao} \\ -S_{an}(1-S_{ao}) \end{pmatrix}.$$

$$V_{AB} = V_1(S_{am} - S_{ap}) + V_2(S_{am} - S_{an}) + V_3(S_{ao} - S_{an}) \tag{6.3}$$

The expression for voltage equation in terms of switching functions is given in (6.3). Similarly, the expressions for input currents $I_{s1}, I_{s2}, I_{s3}$ can also be found and are given in (6.6), (6.9) and (6.12), respectively.

For $I_{s1}$, $I_{s1} = \sum(1,2,6,9,10,13,14,16).$ \hfill (6.4)

$$I_{s1} = I_o \begin{Bmatrix} S_{bp}S_{am}S_{bn}S_{ao} + S_{bp}S_{am}S_{bn}S_{bo} + S_{bp}S_{am}S_{an}S_{ao} + S_{bp}S_{am}S_{an}S_{bo} \\ -S_{ap}S_{bm}S_{bn}S_{ao} - S_{ap}S_{bm}S_{bn}S_{bo} - S_{ap}S_{bm}S_{an}S_{ao} - S_{ap}S_{bm}S_{an}S_{bo} \end{Bmatrix}. \tag{6.5}$$

$$I_{s1} = I_o \begin{Bmatrix} S_{bp}S_{am}S_{bn}(S_{ao}+S_{bo}) + S_{bp}S_{am}S_{an}(S_{ao}+S_{bo}) \\ -S_{ap}S_{bm}S_{bn}(S_{ao}+S_{bo}) - S_{ap}S_{bm}S_{an}(S_{ao}+S_{bo}) \end{Bmatrix}.$$

$$I_{s1} = I_o \left\{ S_{bp} S_{am} S_{bn} + S_{bp} S_{am} S_{an} - S_{ap} S_{bm} S_{bn} - S_{ap} S_{bm} S_{an} \right\}.$$

$$I_{s1} = I_o \left\{ S_{bp} S_{am} \left( S_{bn} + S_{an} \right) - S_{ap} S_{bm} \left( S_{bn} + S_{an} \right) \right\}.$$

$$I_{s1} = I_o \left\{ \left( 1 - S_{ap} \right) S_{am} - S_{ap} \left( 1 - S_{am} \right) \right\}.$$

$$I_{s1} = I_o \left\{ S_{am} - S_{ap} \right\}. \tag{6.6}$$

For $I_{s2}$, $I_{s2} = \sum (1,2,3,5,12,14,15,16).$ $\tag{6.7}$

$$I_{s2} = I_o \left\{ \begin{matrix} S_{bp} S_{am} S_{bn} S_{ao} + S_{bp} S_{am} S_{bn} S_{bo} + S_{ap} S_{am} S_{bn} S_{ao} + S_{ap} S_{am} S_{bn} S_{bo} \\ - S_{bp} S_{bm} S_{an} S_{ao} - S_{ap} S_{bm} S_{an} S_{ao} - S_{bp} S_{bm} S_{an} S_{bo} - S_{ap} S_{bm} S_{an} S_{bo} \end{matrix} \right\}. \tag{6.8}$$

$$I_{s2} = I_o \left\{ S_{bp} S_{am} S_{bn} + S_{ap} S_{am} S_{bn} - S_{bm} S_{an} S_{ao} - S_{bm} S_{an} S_{bo} \right\}.$$

$$I_{s2} = I_o \left\{ S_{am} S_{bn} - S_{bm} S_{an} \right\}.$$

$$I_{s2} = I_o \left\{ S_{am} - S_{an} \right\}. \tag{6.9}$$

For $I_{s3}$, $I_{s3} = \sum (1,3,4,9,10,11,15,16).$ $\tag{6.10}$

$$I_{s3} = I_o \left\{ \begin{matrix} S_{bp} S_{am} S_{bn} S_{ao} + S_{ap} S_{am} S_{bn} S_{ao} + S_{bp} S_{bm} S_{bn} S_{ao} + S_{ap} S_{bm} S_{bn} S_{ao} \\ - S_{bp} S_{am} S_{an} S_{bo} - S_{ap} S_{am} S_{an} S_{bo} - S_{bp} S_{bm} S_{an} S_{bo} - S_{ap} S_{bm} S_{an} S_{bo} \end{matrix} \right\}. \tag{6.11}$$

$$I_{s3} = I_o \left\{ S_{am} S_{bn} S_{ao} + S_{bm} S_{bn} S_{ao} - S_{am} S_{an} S_{bo} - S_{bm} S_{an} S_{bo} \right\}.$$

$$I_{s3} = I_o \left\{ S_{bn} S_{ao} - S_{an} S_{bo} \right\}.$$

$$I_{s3} = I_o \left\{ S_{ao} - S_{an} \right\}. \tag{6.12}$$

Therefore the dynamic model equations of the system are given as

$$V_1 \left( S_{am} - S_{ap} \right) + V_2 \left( S_{am} - S_{an} \right) + V_3 \left( S_{ao} - S_{an} \right) = L_o p I_o + V_c. \tag{6.13}$$

$$Cp V_c = I_o - I_L. \tag{6.14}$$

### 6.3.1      Voltage stress calculations

Voltage stress is defined as the voltage across each switch at any time. Since the voltage across each switch is different, the voltage stresses are calculated and are given from (6.15) to (6.22).

$$V_{Sap} = S_{bp}V_1 . \tag{6.15}$$

$$V_{Sbp} = S_{ap}V_1 . \tag{6.16}$$

$$V_{Sam} = S_{bm}(V_1 + V_2) . \tag{6.17}$$

$$V_{Sbm} = S_{am}(V_1 + V_2) . \tag{6.18}$$

$$V_{San} = S_{bn}(V_2 + V_3) . \tag{6.19}$$

$$V_{Sbn} = S_{an}(V_2 + V_3) . \tag{6.20}$$

$$V_{Sao} = S_{bo}V_3 . \tag{6.21}$$

$$V_{Sbo} = S_{ao}V_3 . \tag{6.22}$$

### 6.4 Modulation Scheme

For modulation scheme, level shifted carrier based PWM is used. In level shifted PWM, the carrier waveforms are one above another with equal amplitude. If the switching pulses of switches in one leg are generated, then their complementary will be respectively the switching pulses of switches in another leg. The generation of switching pulses is as follows:

149
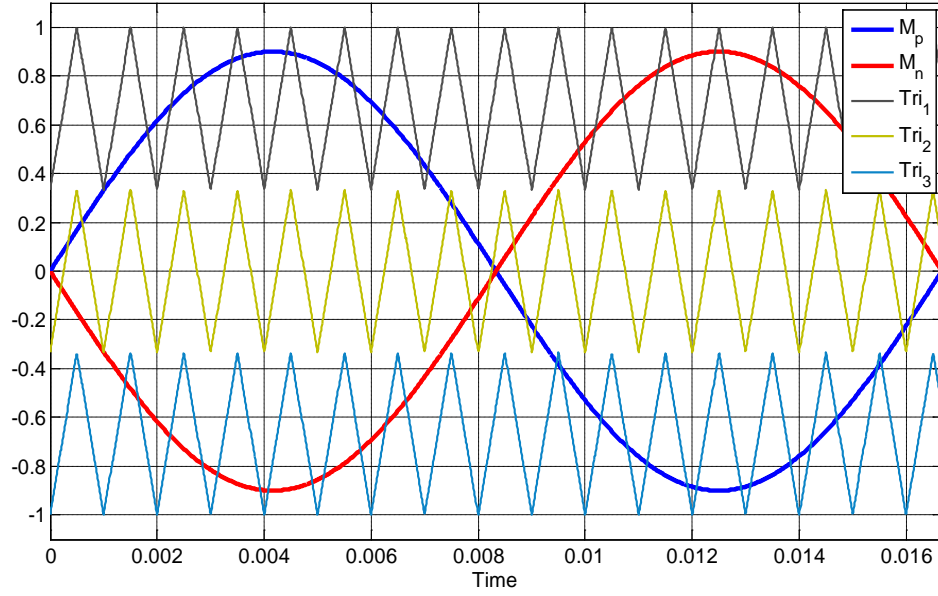
Figure 6.4 Modulation Scheme.

$$S_{ap} = \begin{bmatrix} 1 \text{ when } Tri_1 < M_p < Tri_2 \text{ for } M_p > 0, \text{and } M_p < Tri_3 \text{ for } M_p < 0 \\ 0 \text{ when } M_p > Tri_1 \text{ for } M_p > 0, \text{and } Tri_2 < M_p < Tri_3 \text{ for } M_p < 0 \end{bmatrix} \quad (6.23)$$

$$S_{am} = \begin{bmatrix} 1 \text{ when } M_p > Tri_2 \text{ for } M_p > 0 \\ 0 \text{ when } M_p < 0 \end{bmatrix} \quad (6.24)$$

$$S_{an} = \begin{bmatrix} 1 \text{ when } M_n > Tri_2 \text{ for } M_n > 0 \\ 0 \text{ when } M_n < 0 \end{bmatrix} \quad (6.25)$$

$$S_{ao} = \begin{bmatrix} 1 \text{ when } Tri_1 < M_n < Tri_2 \text{ for } M_n > 0, \text{and } M_n < Tri_3 \text{ for } M_n < 0 \\ 0 \text{ when } M_n > Tri_1 \text{ for } M_n > 0, \text{and } Tri_2 < M_n < Tri_3 \text{ for } M_n < 0 \end{bmatrix} \quad (6.26)$$

where $M_p$ and $M_n$ are the modulation signals and $Tri_1$, $Tri_2$ and $Tri_3$ are the three carrier

waveforms used to generate switching pulses by level shifted carrier based PWM. The

modulation signals and carrier waveforms can be seen in figure 6.4.

150

**6.4.1 Determination of expressions for modulation signals**

The expressions for modulation signals are determined using double Fourier series analysis. At any time, if the carrier frequency is much larger than the frequency of modulation signals, the switching functions are approximated based on the instantaneous values of modulation signal [74].

Let the two modulation waveforms used be of the form $M_p = M_1 \sin(\theta + \psi_1)$ and $M_n = M_2 \sin(\theta + \psi_2)$, where $\psi_1$ and $\psi_2$ are the initial phase angles of modulation signals respectively and $\theta = \omega t$, where $\omega$ is the frequency of the reference voltage waveform.



Figure 6.5 Approximations of switching functions in terms of instantaneous values of modulation signals.

From Figure 6.5, the switching functions are approximated by their instantaneous values of modulation signal.

$$S_{ap} = \begin{cases} 1 - M_p & \psi_1 \le \theta_1 < \pi + \psi_1 \\ -M_p & \pi + \psi_1 \le \theta_1 \le 2\pi + \psi_1 \end{cases}. \tag{6.27}$$

$$S_{am} = \begin{cases} 1 & \psi_1 \le \theta_1 < \pi + \psi_1 \\ 0 & \pi + \psi_1 \le \theta_1 \le 2\pi + \psi_1 \end{cases}. \tag{6.28}$$

$$S_{an} = \begin{cases} 0 & \psi_2 \le \theta_2 < \pi + \psi_2 \\ 1 & \pi + \psi_2 \le \theta_2 \le 2\pi + \psi_2 \end{cases}. \tag{6.29}$$

$$S_{ao} = \begin{cases} 1 - M_n & \psi_2 \le \theta_2 < \pi + \psi_2 \\ -M_n & \pi + \psi_2 \le \theta_2 \le 2\pi + \psi_2 \end{cases}. \tag{6.30}$$

The double Fourier series approximation of converter switching functions given in [4] as

$$S_{ij}(\omega_s, \omega_c) = \begin{bmatrix} \dfrac{A_{00}}{2} + \displaystyle\sum_{n=1}^{\infty}\left(A_{0n}\cos(n\omega_s t) + B_{0n}\sin(n\omega_s t)\right) \\ + \displaystyle\sum_{m=1}^{\infty}\left(A_{m0}\cos(m\omega_c t) + B_{m0}\sin(m\omega_c t)\right) \\ + \displaystyle\sum_{m=1}^{\infty}\sum_{\substack{n=-\infty \\ n\ne 0}}^{\infty}\left(A_{mn}\cos(m\omega_c t + n\omega_s t) + B_{mn}\sin(m\omega_c t + n\omega_s t)\right) \end{bmatrix}. \tag{6.31}$$

Using Fourier series analysis, the expressions for switching functions are given in (6.32-6.35). The detailed derivations are given in Appendix B.

The expressions for $S_{ap,}$ $S_{am,}$ $S_{an,}$ and $S_{ao}$ are given as

$$S_{ap} = \frac{1}{2} - 2M_p - \frac{2}{\pi}\left(\sin(\psi_1 - \theta)\right). \tag{6.32}$$

152

$$S_{am} = \frac{1}{2} - \frac{2}{\pi}\left(\sin(\psi_1 - \theta)\right).$$

(6.33)

$$S_{an} = \frac{1}{2} - \frac{2}{\pi}\left(\sin(\psi_2 - \theta)\right).$$

(6.34)

$$S_{ao} = \frac{1}{2} - 2M_n - \frac{2}{\pi}\left(\sin(\psi_2 - \theta)\right).$$

(6.35)

Substituting (6.32), (6.33), (6.34), (6.35) into (6.3), the output voltage equation becomes

$$V_{AB} = \begin{Bmatrix} V_1\left(\frac{1}{2} - \frac{2}{\pi}\left(\sin(\psi_1 - \theta)\right) - \frac{1}{2} + 2M_1\sin(\theta + \psi_1) + \frac{2}{\pi}\left(\sin(\psi_1 - \theta)\right)\right) \\ + V_2\left(\frac{1}{2} - \frac{2}{\pi}\left(\sin(\psi_1 - \theta)\right) - \frac{1}{2} + \frac{2}{\pi}\left(\sin(\psi_2 - \theta)\right)\right) \\ + V_3\left(\frac{1}{2} - 2M_2\sin(\theta + \psi_2) + \frac{2}{\pi}\left(\sin(\psi_2 - \theta)\right) - \frac{1}{2} - \frac{2}{\pi}\left(\sin(\psi_2 - \theta)\right)\right) \end{Bmatrix}.$$

(6.36)

$$V_{AB} = \left\{ V_1\left(2M_1\sin(\theta + \psi_1)\right) + V_3\left(-2M_2\sin(\theta + \psi_2)\right) \right\}.$$

(6.37)

Let $\psi_1 = \psi_2$ and $M_2 = \alpha M_1$.

$$M_1\sin(\theta + \psi_1) = M_p = \frac{V_{AB} - V_2\left(\frac{4}{\pi}\left(\sin(\theta - \psi_1)\right)\right)}{V_1 + \alpha V_3}.$$

(6.38)

$$M_2\sin(\theta + \psi_2) = M_n = \alpha \frac{V_{AB} - V_2\left(\frac{4}{\pi}\left(\sin(\theta - \psi_1)\right)\right)}{V_1 + \alpha V_3}. \text{ where } \alpha = [0,1].$$

(6.39)

## 6.5 Switching Loss Comparison with Three Cell Cascaded H-bridge inverter

The switching power loss for this proposed topology is compared with the three cascaded H bridge multilevel Inverter topology. The average switching power loss $P_s$ in the switch caused by these transitions [75] can be defined as

$$P_s = 0.5 V_S I_o f_s \left( t_{(on)} + t_{(off)} \right), \tag{6.40}$$

where $t_{(on)}$ and $t_{(off)}$ are the turn-on and turn-off times, respectively; $V_S$ is the voltage stress across the switch; and $I_o$ is the current flowing through the switch.

Let both the proposed circuit and cascaded H bridge multi-level converter be operated at the same turn-on and turn-off times and at the same load current $I_o$. Then the average switching power loss $P_s$ is proportional to $V_S$ and $f_s$. So in general

$$P_s \propto V_S f_s. \tag{6.41}$$

The voltage stresses of the twelve switches of the conventional cascaded H-bridge inverter are all equal to $V_s$. According to Figure 6.6, the switching loss of cascaded H-bridge inverter from twelve switches can be obtained as

$$P_{s,H-bridge} \propto 12 V_s f_s. \tag{6.42}$$

Similarly the switching power loss of multi string seven-level inverter shown in figure 6.1 with eight switches can also be obtained as

$$P_{s,\text{multi string}} \propto 4 V_s f_s + 4 \left( 2 V_s \right) f_m. \tag{6.43}$$

$$P_{s,\text{multi string}} \propto 4 V_s \left( f_s + 2 f_m \right). \tag{6.44}$$

where $f_m$ is the line frequency.
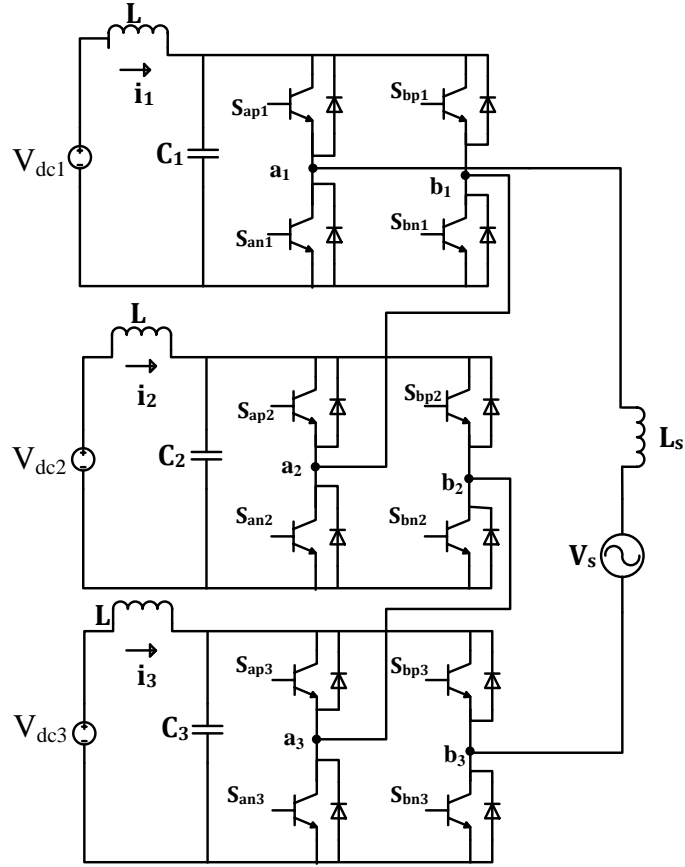
Figure 6.6 Three cell cascaded H-bridge inverter.

Because the switches $S_{am}, S_{bm}$, $S_{an}, S_{bn}$ are operated at almost line frequency and switching frequency is larger than line frequency $f_m \ll f_s$, the switching losses of the proposed circuit is approximated to

$$P_{s,\text{multi string}} \propto 4V_s f_s. \tag{6.45}$$

Comparing equations (6.42) and (6.45), switching losses in multi string seven-level converter are about 40% less than three cascaded H bridge multi-level converter in this case.

## 6.6 Simulation Results and Discussions

The simulation of multi string seven-level inverter topology is carried out using Matlab/Simulink software. The parameters used for simulation are, $V_{AB} = 140V$, $V_1 = 50V$, $V_2 = 50V$, $V_3 = 50V$ and $\alpha = -1$. $M_1, M_2$ are derived from (6.38) and (6.39) respectively. Figure 6.3 shows the modulation scheme that is used to generate switching pulses shown in Figures 6.7 and 6.8. From Figures 6.7 and 6.8, the switching pulses of the middle switches can be seen at almost line frequency. Figure 6.9 shows the voltage across each switch in the first leg, as can be seen from figure 6.9, the voltage stress of middle two switches in the first leg $T_{am}, T_{an}$ are twice that of other two switches. Figure 6.11 shows the waveforms of output phase voltage $V_{AB}$ and. Figure 6.10 shows the waveforms of three input source currents.
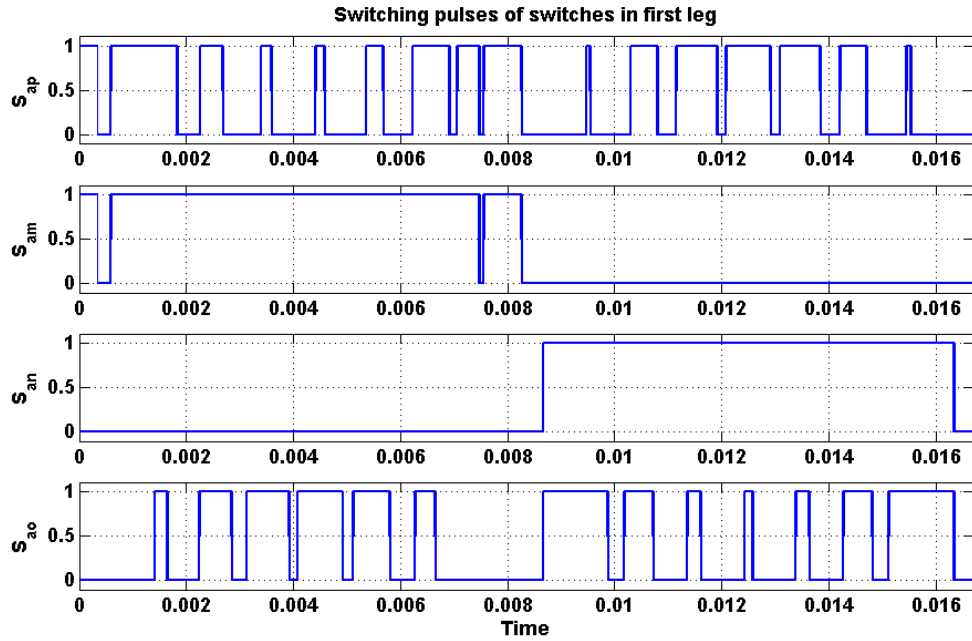
Figure 6.7 Simulation result of switching pulses of the switches in first leg.
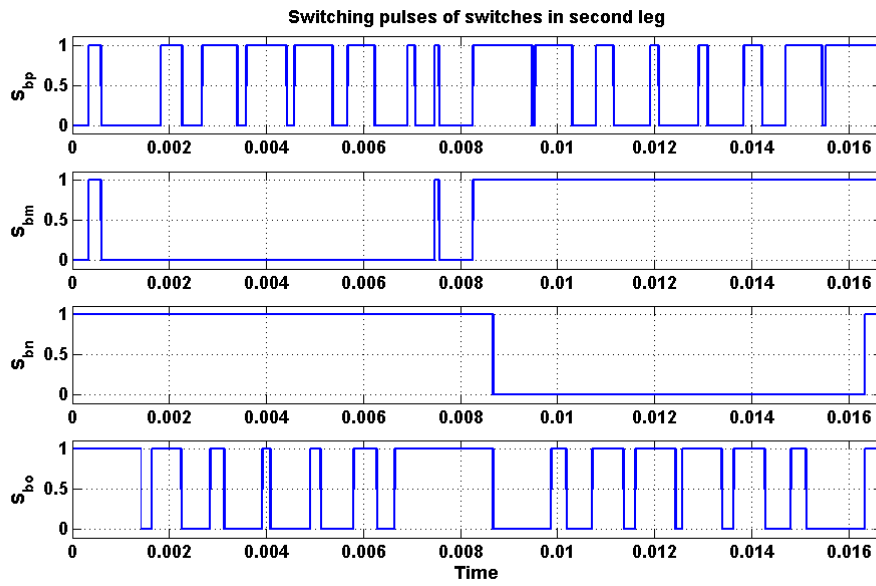


Figure 6.8 Switching result of switching pulses of the switches in second leg.
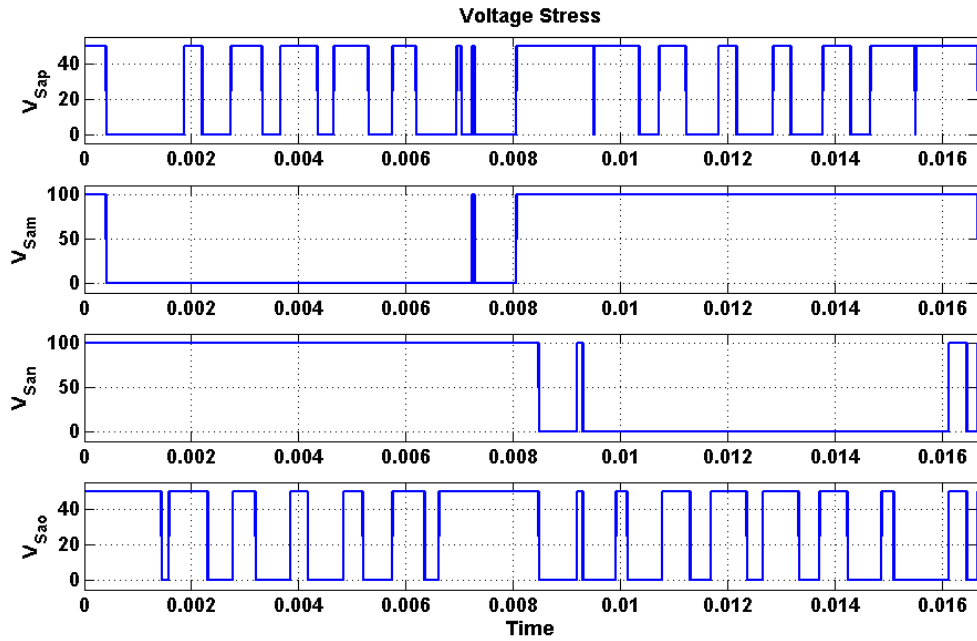
Figure 6.9 Simulation result of voltage stress of switches in first leg of the converter.
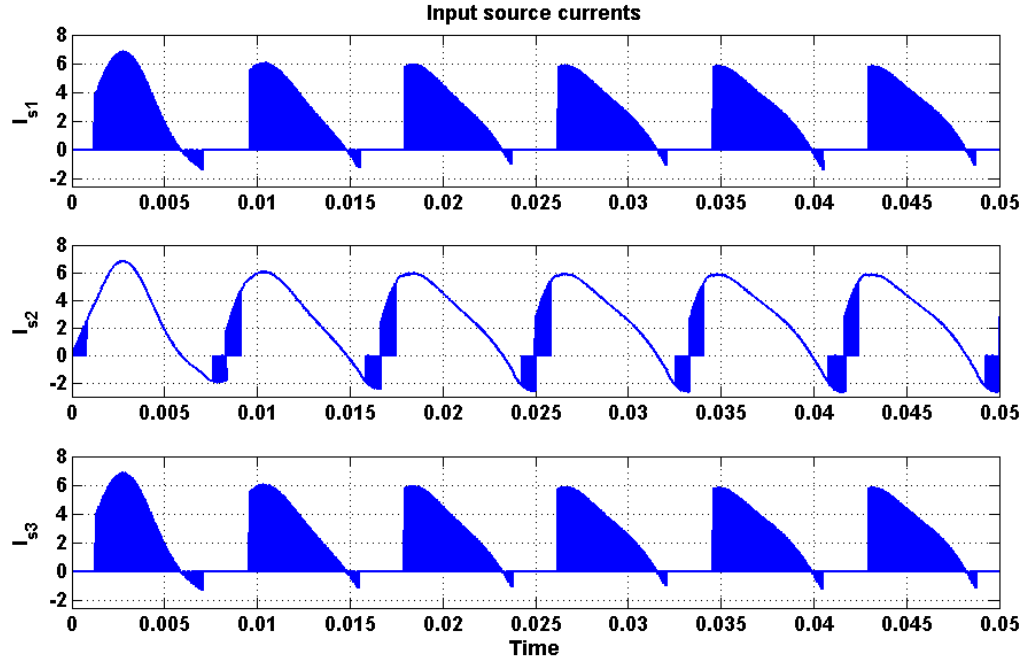


Figure 6.10 Simulation result of input source currents.

158
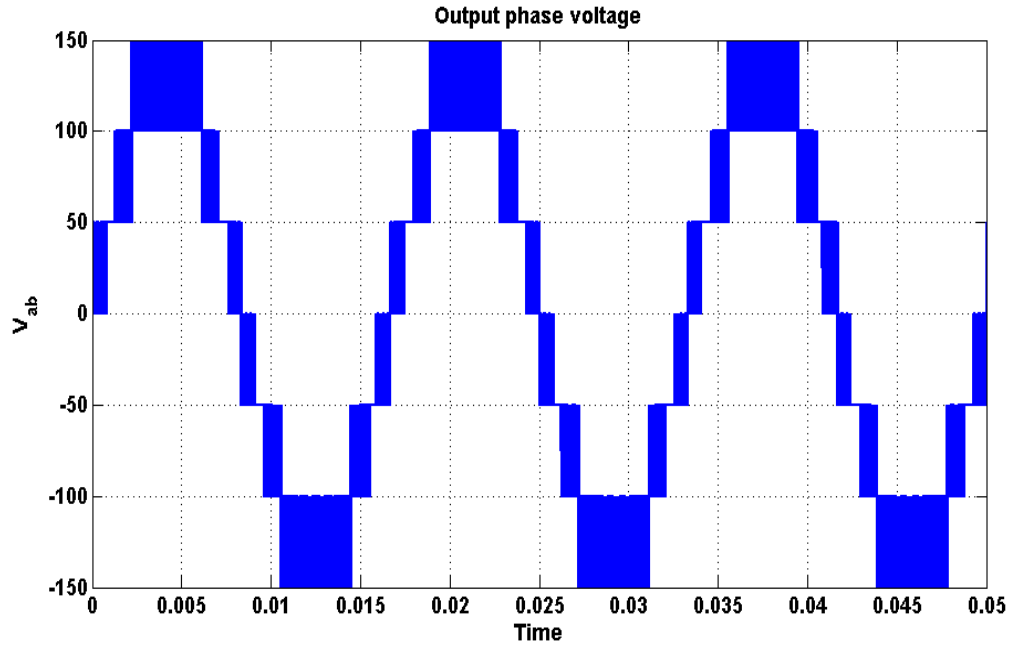
Figure 6.11 Simulation result of output phase voltage.

**6.7 Experimental results**

Experiments on multi string seven-level inverter are also performed on a laboratory prototype using TMS 320 F28335 eZdsp to generate the switching pulses of both the legs which are shown in Figures 6.12 and 6.13 respectively. The waveform of the output voltage can also be seen in Figure 6.14. The experimental results and simulation results validate each other.

159
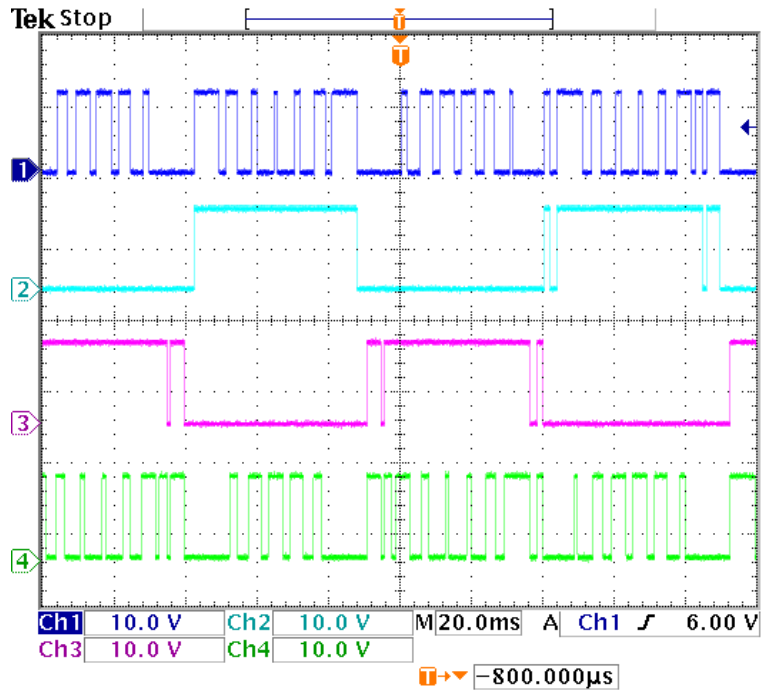
Figure 6.12 Experimental result of switching pulses of switches in first leg.
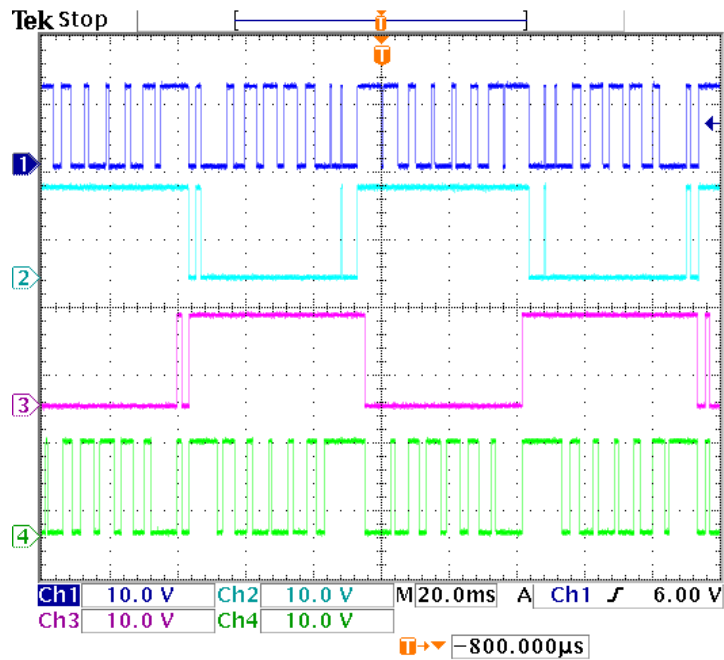


Figure 6.13 Experimental result of switching pulses of switches in second leg.
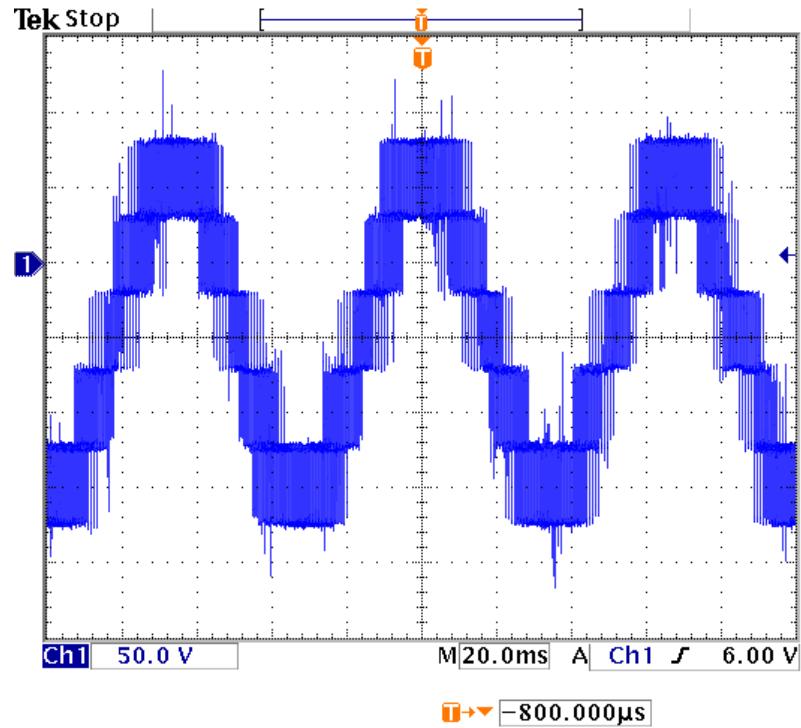
Figure 6.14 Output phase voltage (50V/div).

## 6.8 Summary

This chapter presents a single-phase multistring seven-level inverter topology which has less number of switches required to produce the desired multi-level output for distributed energy resources compared to cascaded H-bridge converter topology. The modes of operation of seven-level inverter topology are also discussed in this chapter. The equations for output voltage and input source currents are calculated in terms of the input voltages and output current respectively using Karnaugh mapping technique. The expression of voltage stress for each switch is determined. The modulation scheme for this topology is also presented. The expression for modulation signal is determined using

Fourier series analysis by approximating switching functions. The calculation of switching loss for multi string seven-level inverter is performed and the proposed topology reduces about 40% of switching loss compared to three cell cascaded H bridge multi-level converter. Simulation of the proposed system is carried out and waveforms of output voltage, input source currents, voltage stress are generated. Experimental results are conducted on 1kW laboratory prototype and the waveforms of switching pulses, and output voltage are presented. The experimental results and simulation results validate each other. The only disadvantage with this type of converter when compared with cascade H bridge multi-level converter is rating of switches. The rating of four middle switches should be twice the rating of other four switches.

# CHAPTER 7

# SINGLE PHASE MULTI STRING NINE LEVEL DC-AC CONVERTER

## 7.1 Introduction

The topology of single phase multi string nine level inverter can be seen in Figure 7.1. This topology offers strong advantages like improved output voltage waveforms, smaller filter size and low electromagnetic interference and THD [72]. This topology requires three DC sources like four cell cell cascaded H-bridge inverter which also gives nine level output voltage. So, this topology can always be compared with the conventional cascaded H-bridge multi-level inverter.

This topology requires six less switches than four cell cascaded H-bridge inverter. And moreover, two switches are operated at line frequency and four other switches are operated at almost line frequency. As a result, the switching losses when compared with four cell cascaded converter are considerably less. The carrier based PWM is used to generate PWM signals for the switches.

From the figure 7.1, $S_{ip}, S_{im}, S_{in}, S_{io}, S_{ir}$, are the switching functions of switches $T_{ip}, T_{im}, T_{in}, T_{io}, T_{io}, i = a, b$ respectively. $V_1, V_2, V_3, V_4$ are input DC sources, $I_{s1}, I_{s2}, I_{s3}, I_{s4}$ are respective input currents, and $I_o$ is output current.
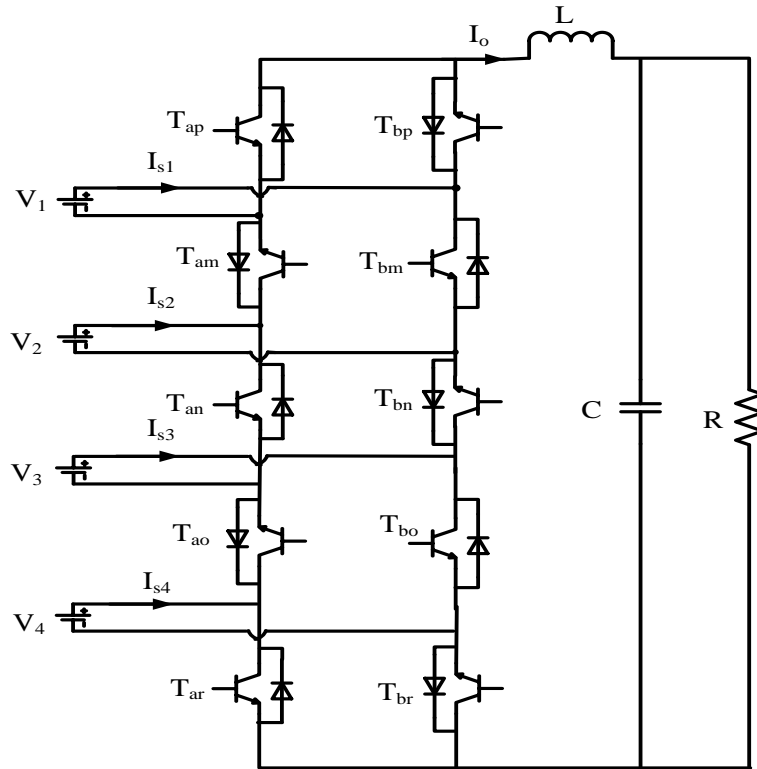
Figure 7.1 Schematic diagram of single phase multi string nine level inverter.

## 7.2 Modes of Operation

Since there are switches on each leg and each switch has two modes either ON or OFF, there will be $2^5$ different modes. Switches in the second leg are complementary with the switches in first leg. The different modes of operation of multi-string nine level inverter are shown in Table 7.1. Each mode shown in Table 7.1 is described in terms of output voltage.

Table 7.1 Switching modes of multi string nine level converter.

| S.No | $S_{ap}$ | $S_{am}$ | $S_{an}$ | $S_{ao}$ | $S_{ar}$ | $V_{AB}$ | $I_{s1}$ | $I_{s2}$ | $I_{s3}$ | $I_{s4}$ |
|------|------|------|------|------|------|---------|------|------|------|------|
| 1 | 0 | 1 | 0 | 1 | 0 | $V_1+V_2+V_3+V_4$ | $I_0$ | $I_0$ | $I_0$ | $I_0$ |
| 2 | 0 | 1 | 0 | 1 | 1 | $V_1+V_2+V_3$ | $I_0$ | $I_0$ | $I_0$ | 0 |
| 3 | 1 | 1 | 0 | 1 | 0 | $V_2+V_3+V_4$ | 0 | $I_0$ | $I_0$ | $I_0$ |
| 4 | 0 | 1 | 0 | 0 | 0 | $V_1+V_2$ | $I_0$ | $I_0$ | 0 | 0 |
| 5 | 0 | 1 | 1 | 1 | 0 | $V_1+V_4$ | $I_0$ | 0 | 0 | $I_0$ |
| 6 | 1 | 1 | 0 | 1 | 1 | $V_2+V_3$ | 0 | $I_0$ | $I_0$ | 0 |
| 7 | 0 | 0 | 0 | 1 | 0 | $V_4+V_3$ | 0 | 0 | $I_0$ | $I_0$ |
| 8 | 0 | 1 | 1 | 1 | 1 | $V_1$ | $I_0$ | 0 | 0 | 0 |
| 9 | 1 | 1 | 0 | 0 | 0 | $V_2$ | 0 | $I_0$ | 0 | 0 |
| 10 | 0 | 0 | 0 | 1 | 1 | $V_3$ | 0 | 0 | $I_0$ | 0 |
| 11 | 1 | 1 | 1 | 1 | 0 | $V_4$ | 0 | 0 | 0 | $I_0$ |
| 12 | 1 | 0 | 0 | 1 | 0 | $V_3+V_4-V_1$ | $- I_0$ | 0 | $I_0$ | $I_0$ |
| 13 | 0 | 1 | 0 | 0 | 1 | $V_1+V_2-V_4$ | $I_0$ | $I_0$ | 0 | $- I_0$ |
| 14 | 1 | 1 | 1 | 1 | 1 | 0 | 0 | 0 | 0 | 0 |
| 15 | 0 | 0 | 0 | 0 | 0 | 0 | 0 | 0 | 0 | 0 |
| 16 | 1 | 1 | 0 | 0 | 1 | $V_2-V_4$ | 0 | $I_0$ | 0 | $- I_0$ |
| 17 | 1 | 0 | 0 | 1 | 1 | $V_3-V_1$ | $- I_0$ | 0 | $I_0$ | 0 |
| 18 | 0 | 1 | 1 | 0 | 0 | $V_1-V_3$ | $I_0$ | 0 | $- I_0$ | 0 |
| 19 | 0 | 0 | 1 | 1 | 0 | $V_4-V_2$ | 0 | $- I_0$ | 0 | $I_0$ |
| 20 | 1 | 0 | 0 | 0 | 0 | $-V_1$ | $- I_0$ | 0 | 0 | 0 |

| 21 | 0 | 0 | 1 | 1 | 1 | $-V_2$ | 0 | $-I_0$ | 0 | 0 |
|----|---|---|---|---|---|--------|---|--------|---|---|
| 22 | 1 | 1 | 1 | 0 | 0 | $-V_3$ | 0 | 0 | $-I_0$ | 0 |
| 23 | 0 | 0 | 0 | 0 | 1 | $-V_4$ | 0 | 0 | 0 | $-I_0$ |
| 24 | 0 | 1 | 1 | 0 | 1 | $V_1-V_3-V_4$ | $I_0$ | 0 | $-I_0$ | $-I_0$ |
| 25 | 1 | 0 | 1 | 1 | 0 | $V_4-V_2-V_1$ | $-I_0$ | $-I_0$ | 0 | $I_0$ |
| 26 | 1 | 0 | 1 | 1 | 1 | $-V_1-V_2$ | $-I_0$ | $-I_0$ | 0 | 0 |
| 27 | 0 | 0 | 1 | 0 | 0 | $-V_2-V_3$ | 0 | $-I_0$ | $-I_0$ | 0 |
| 28 | 1 | 1 | 1 | 0 | 1 | $-V_3-V_4$ | 0 | 0 | $-I_0$ | $-I_0$ |
| 29 | 1 | 0 | 0 | 0 | 1 | $-V_1-V_4$ | $-I_0$ | 0 | 0 | $-I_0$ |
| 30 | 1 | 0 | 1 | 0 | 0 | $-V_1-V_2-V_3$ | $-I_0$ | $-I_0$ | $-I_0$ | 0 |
| 31 | 0 | 0 | 1 | 0 | 1 | $-V_2-V_3-V_4$ | 0 | $-I_0$ | $-I_0$ | $-I_0$ |
| 32 | 1 | 0 | 1 | 0 | 1 | $-V_1-V_2-V_3-V_4$ | $-I_0$ | $-I_0$ | $-I_0$ | $-I_0$ |

This type of Multistring Converter has nine levels of output voltage. So it will be having nine levels of operation Maximum positive output voltage of $V_1+V_2+V_3+V_4$, voltage level of $3V_s$ is $V_1+V_2+V_3$ or $V_2+V_3+V_4$, voltage level of $2V_s$ is $V_1+V_2$, $V_1+V_4$, $V_2+V_3$, $V_4+V_3$, minimum positive output voltage of $V_1$, $V_2$, $V_3$, $V_4$, $V_3+V_4-V_1$, $V_1+V_2-V_4$, zero output voltage, minimum negative output voltage of $-V_1$, $-V_2$ or $-V_3$, $-V_4$, $-V_3-V_4+V_1$, $-V_1-V_2+V_4$, voltage levels of $-2V_s$ are $-V_1-V_2$, $-V_1-V_4$, $-V_2-V_3$, $-V_4-V_3$, voltage levels of $-3V_s$ are $-V_1-V_2-V_3$ or $-V_2-V_3-V_4$ and maximum negative output voltage of $-V_1-V_2-V_3-V_4$. There are 32 modes of operation for this ten switch multi string nine level converter.

- **Maximum Positive Output Voltage:**

When the switches $T_{bp}$, $T_{am}$, $T_{bn}$, $T_{ao}$ and $T_{br}$ are ON; the output voltage $V_{AB}$ is $V_1+V_2+V_3+V_4$ .This mode of operation can be seen in Figure 7.2 (a).

- **Second Maximum Positive Output Voltage:**

This output condition is possible for two different switching combinations. One switching combination is such that active switches $T_{bp}$, $T_{am}$, $T_{bn}$, $T_{ao}$ and $T_{ar}$ are ON; the other combination is such that switches $T_{ap}$, $T_{am}$, $T_{bn}$, $T_{ao}$ and $T_{br}$ are ON. During these operating stages, output voltage $V_{AB}$ is $V_1+V_2+V_3$ and $V_2+V_3+V_4$ respectively. These modes of operation can be seen in Figure 7.2 (b) and Figure 7.2 (c) respectively.

- **Positive Output Voltage:**

This output condition is possible for four different switching combinations. One switching combination is such that active switches $T_{bp}$, $T_{am}$, $T_{bn}$, $T_{bo}$ and $T_{br}$ are ON; the second combination is such that switches $T_{bp}$, $T_{am}$, $T_{an}$, $T_{ao}$ and $T_{br}$ are ON, the third combination is such that switches $T_{ap}$, $T_{bm}$, $T_{an}$, $T_{ao}$ and $T_{ar}$ are ON, the fourth combination is such that switches $T_{bp}$, $T_{bm}$, $T_{bn}$, $T_{ao}$ and $T_{br}$ are ON. During these operating stages, output voltage $V_{AB}$ is $V_1+V_2$, $V_1+V_4$, $V_2+V_3$ and $V_3+V_4$ respectively. These modes of operation can be seen in Figure 7.2 (d), Figure 7.2 (e), Figure 7.2 (f) and Figure 7.2 (g) respectively.

- **Minimum Positive Output Voltage:**

This output condition is possible for six different switching combinations. One switching combination is such that active switches $T_{bp}$, $T_{am}$, $T_{an}$, $T_{ao}$ and $T_{ar}$ are ON; the

second combination is such that switches $T_{ap}$, $T_{am}$, $T_{bn}$, $T_{bo}$ and $T_{br}$ are ON, the third combination is such that switches $T_{bp}$, $T_{bm}$, $T_{bn}$, $T_{ao}$ and $T_{ar}$ are ON, the fourth combination is such that switches $T_{ap}$, $T_{am}$, $T_{an}$, $T_{ao}$ and $T_{br}$ are ON, the fifth combination is such that switches $T_{ap}$, $T_{bm}$, $T_{bn}$, $T_{ao}$ and $T_{br}$ are ON, the fourth combination is such that switches $T_{bp}$, $T_{am}$, $T_{bn}$, $T_{bo}$ and $T_{ar}$ are ON. During these operating stages, output voltage $V_{AB}$ is $V_1$, $V_2$, $V_3$, $V_4$, $V_1+V_2-V_4$ and $V_3+V_4-V_1$ respectively. These modes of operation can be seen in Figure 7.2 (h), Figure 7.2 (i), Figure 7.2 (j), Figure 7.2 (k), Figure 7.2 (l) and Figure 7.2 (m) respectively.

- **Zero Output voltage:**

This output condition is possible for four different switching combinations, either when whole first leg is ON or whole second leg is ON, the third combination is such that switches $T_{ap}$, $T_{am}$, $T_{bn}$, $T_{bo}$ and $T_{ar}$ are ON, the fourth combination is such that switches $T_{ap}$, $T_{bm}$, $T_{bn}$, $T_{ao}$ and $T_{ar}$ are ON. At that instant, load will be short-circuited, and there will be no transfer of power from one side to the other side.

- **Minimum Negative Output Voltage:**

This output condition is possible for six different switching combinations. One switching combination is such that active switches $T_{ap}$, $T_{bm}$, $T_{bn}$, $T_{bo}$ and $T_{br}$ are ON; the second combination is such that switches $T_{bp}$, $T_{bm}$, $T_{an}$, $T_{ao}$ and $T_{ar}$ are ON, the third combination is such that switches $T_{ap}$, $T_{am}$, $T_{an}$, $T_{bo}$ and $T_{br}$ are ON, the fourth combination is such that switches $T_{bp}$, $T_{bm}$, $T_{bn}$, $T_{bo}$ and $T_{ar}$ are ON, the fifth combination is such that switches $T_{bp}$, $T_{am}$, $T_{an}$, $T_{bo}$ and $T_{ar}$ are ON, the fourth combination is such that switches $T_{ap}$, $T_{bm}$, $T_{an}$, $T_{ao}$ and $T_{br}$ are ON. During these operating stages, output voltage

$V_{AB}$ is $-V_1$, $-V_2$, $-V_3$, $-V_4$, $-V_1-V_2+V_4$ and $-V_3-V_4+V_1$ respectively. These modes of operation can be seen in figure 7.3 (a), figure 7.3 (b), figure 7.3 (c), figure 7.3 (d), figure 7.3 (e) and figure 7.3 (f) respectively.

- **Negative Output Voltage:**

This output condition is possible for four different switching combinations. One switching combination is such that active switches $T_{ap}$, $T_{bm}$, $T_{an}$, $T_{ao}$ and $T_{ar}$ are ON; the second combination is such that switches $T_{ap}$, $T_{bm}$, $T_{bn}$, $T_{bo}$ and $T_{ar}$ are ON, the third combination is such that switches $T_{bp}$, $T_{am}$, $T_{bn}$, $T_{bo}$ and $T_{br}$ are ON, the fourth combination is such that switches $T_{ap}$, $T_{am}$, $T_{an}$, $T_{bo}$ and $T_{ar}$ are ON. During these operating stages, output voltage $V_{AB}$ is $-V_1-V_2$, $-V_1-V_4$, $-V_2-V_3$ and $-V_3-V_4$ respectively. These modes of operation can be seen in Figure 7.3 (g), Figure 7.3 (h), Figure 7.3 (i) and Figure 7.3 (j) respectively.

- **Second Maximum negative Output Voltage:**

This output condition is possible for two different switching combinations. One switching combination is such that active switches $T_{ap}$, $T_{bm}$, $T_{an}$, $T_{bo}$ and $T_{br}$ are ON; the other combination is such that switches $T_{bp}$, $T_{bm}$, $T_{an}$, $T_{bo}$ and $T_{ar}$ are ON. During these operating stages, output voltage $V_{AB}$ is $-V_1-V_2-V_3$ and $-V_2-V_3-V_4$ respectively. These modes of operation can be seen in Figure 7.3 (k) and Figure 7.3 (l) respectively.

- **Maximum Negative Output Voltage:**

When the switches $T_{ap}$, $T_{bm}$, $T_{an}$, $T_{bo}$ and $T_{ar}$ are ON; the output voltage $V_{AB}$ is $-V_1$ $-V_2-V_3-V_4$ .This mode of operation can be seen in Figure 7.3 (m).

(a)

(b)

(c)

(d)

(e)



(f)



(g)



(h)

171

(i)

(j)

(k)

(l)

172
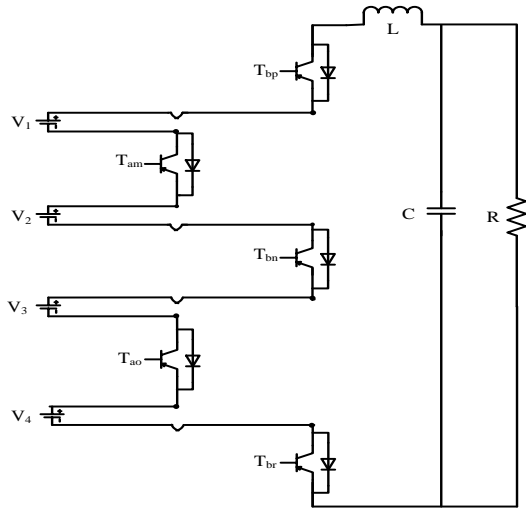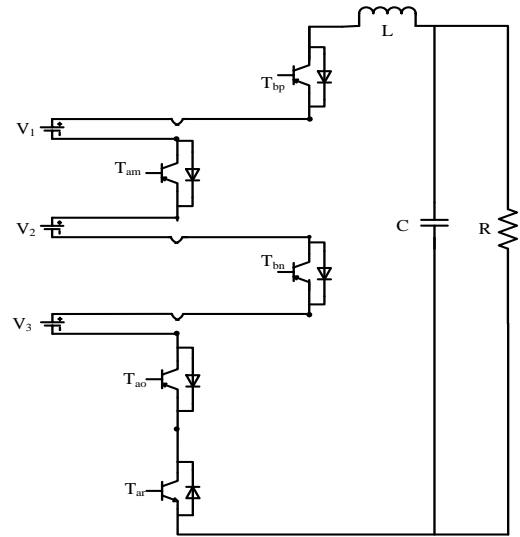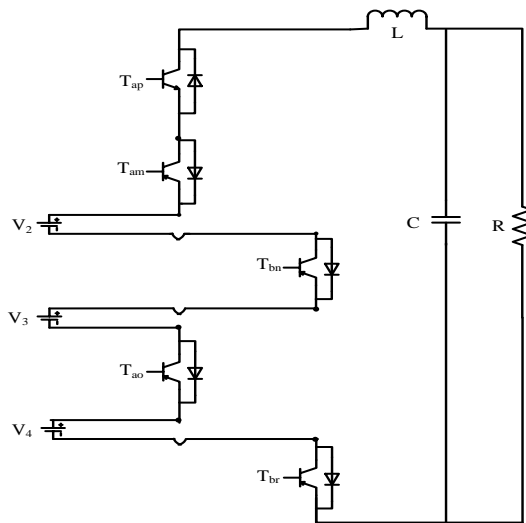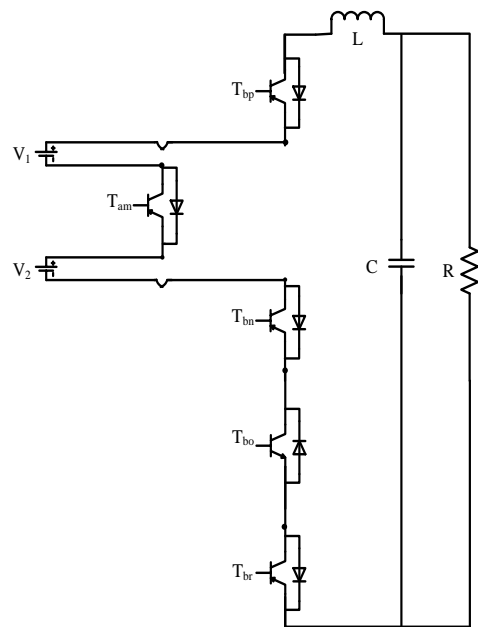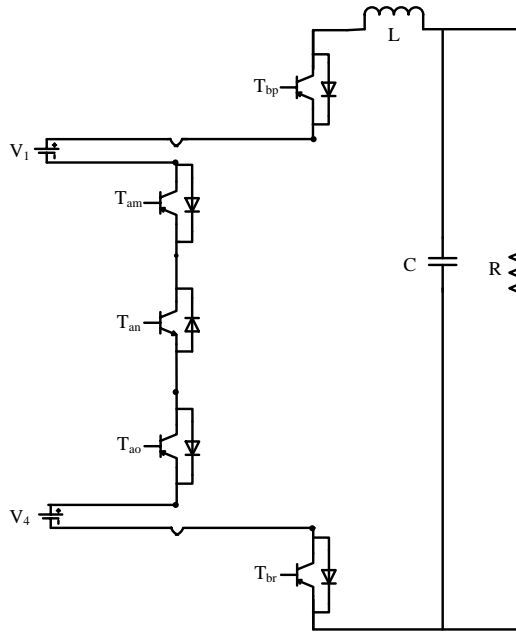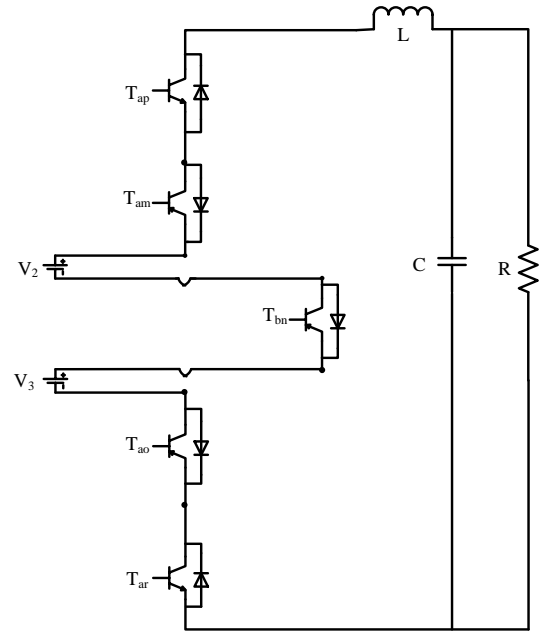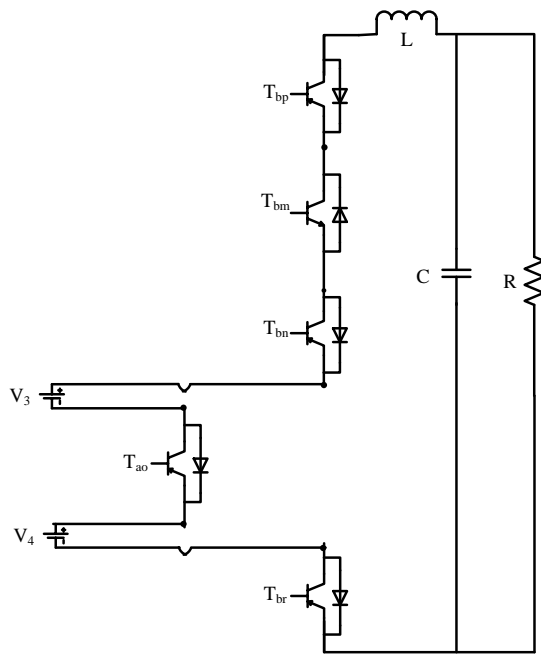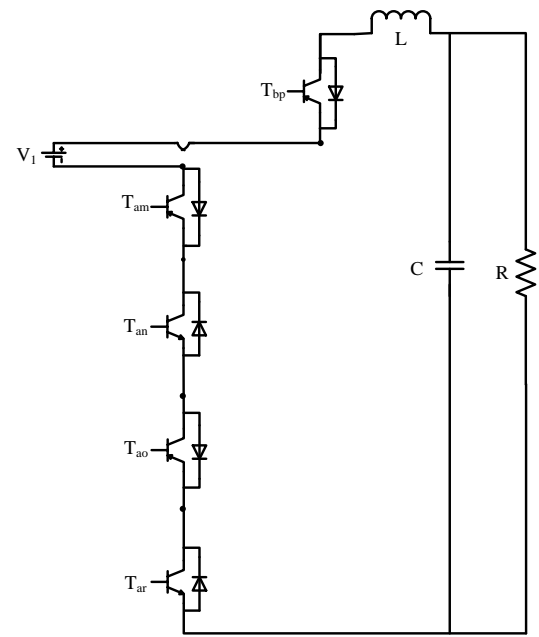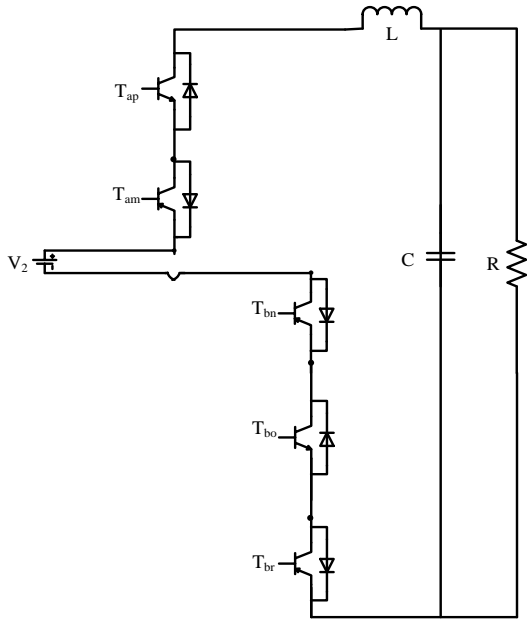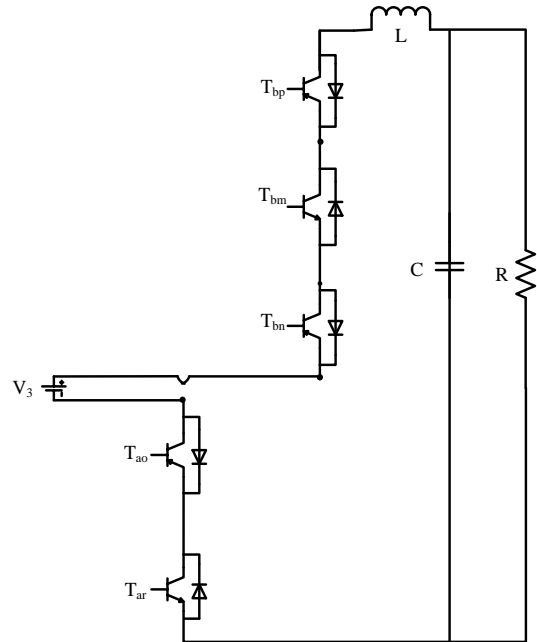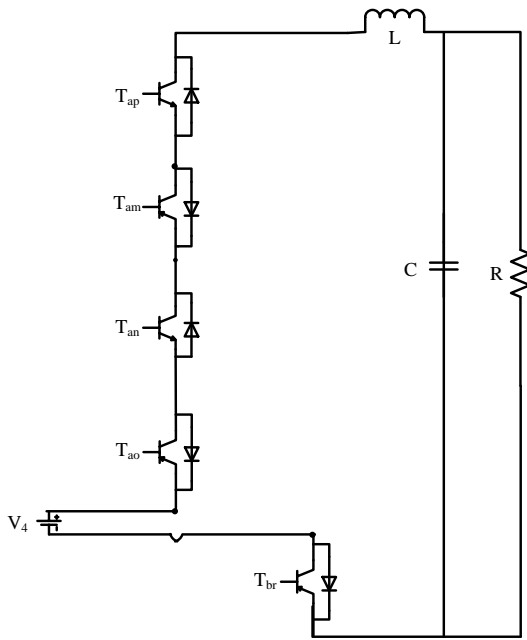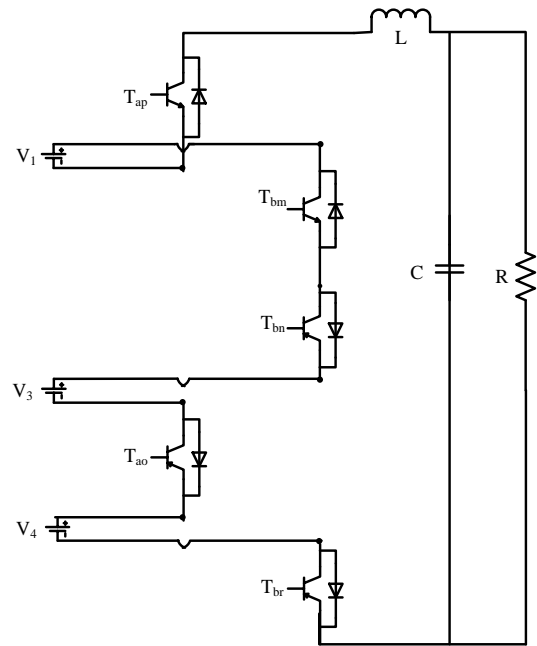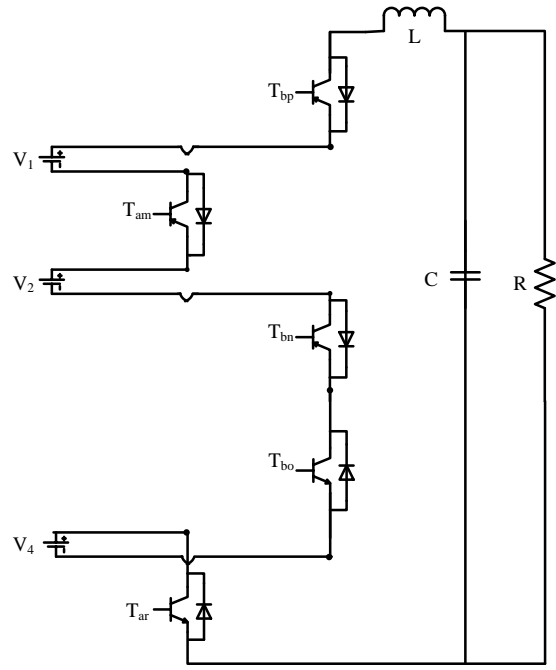
(m)

Figure 7.2 Positive modes of operation of multi string seven level inverter.



(a)

173

(b)

(c)

(d)

(e)

174

(f)

(g)

(h)

(i)

175
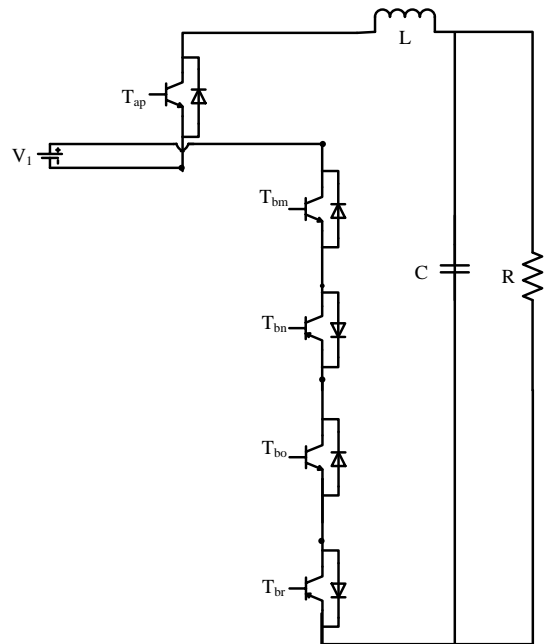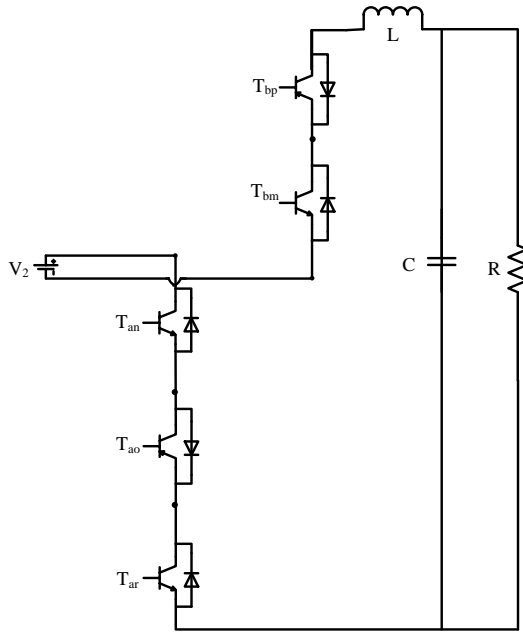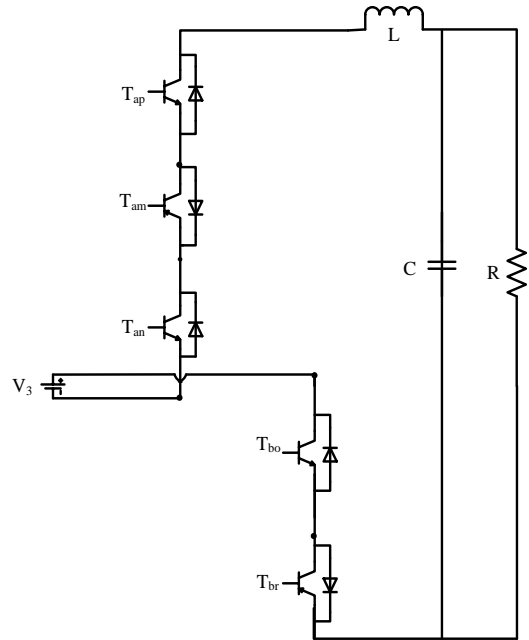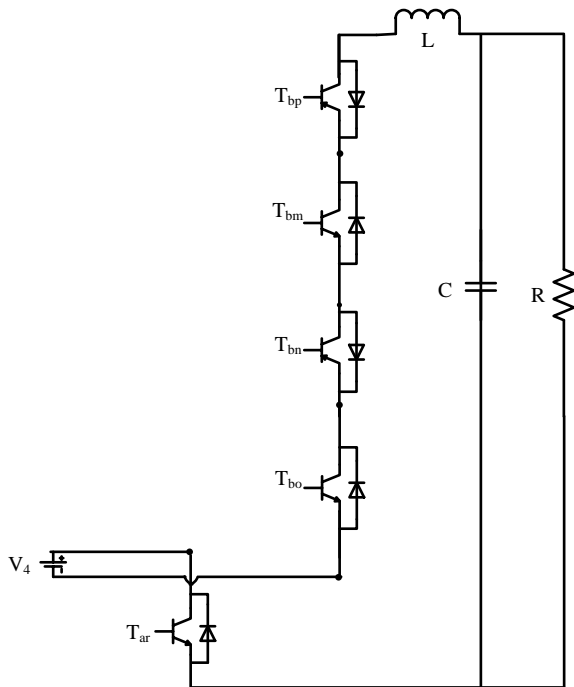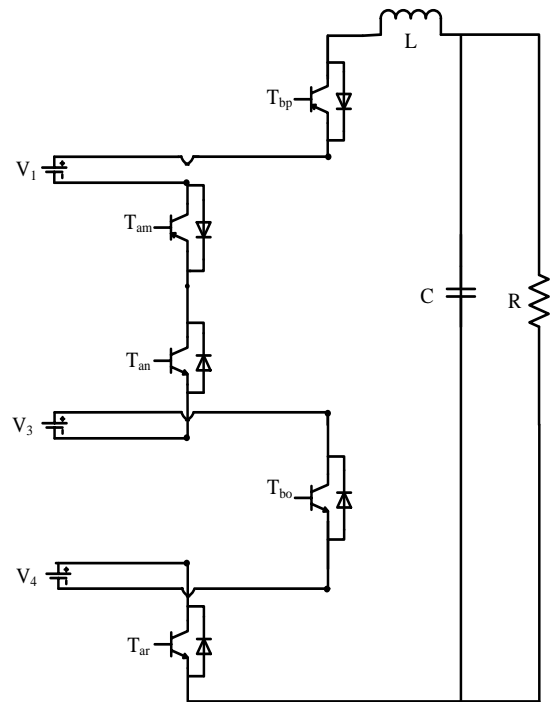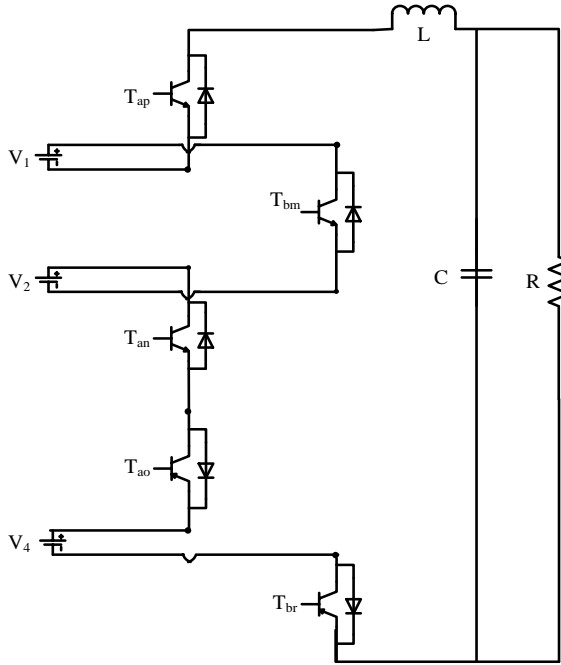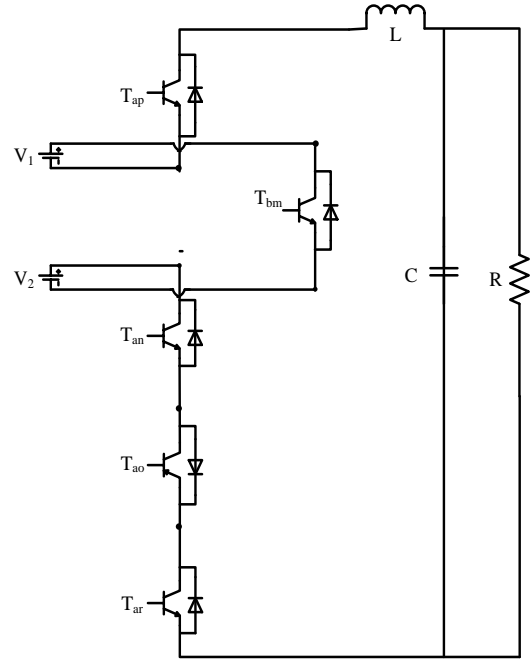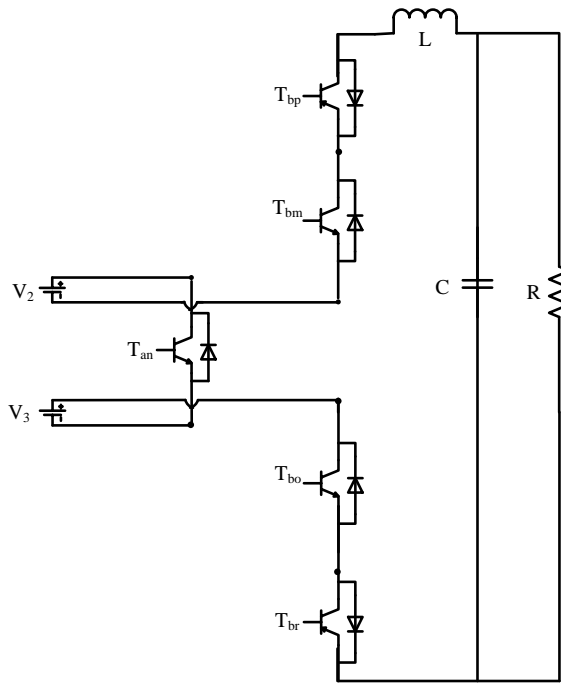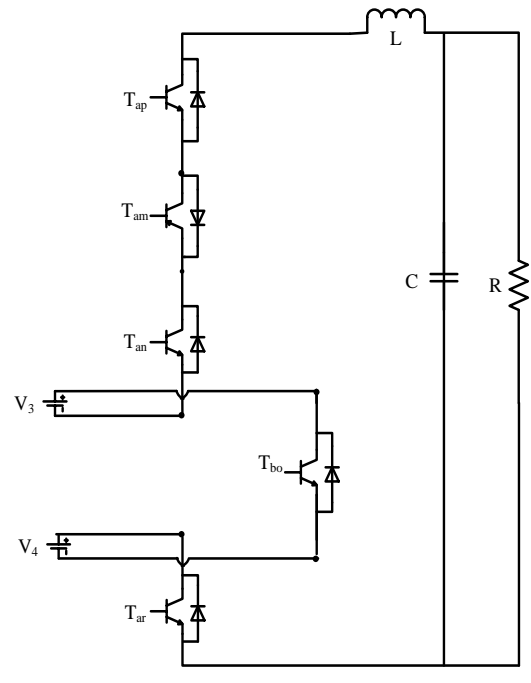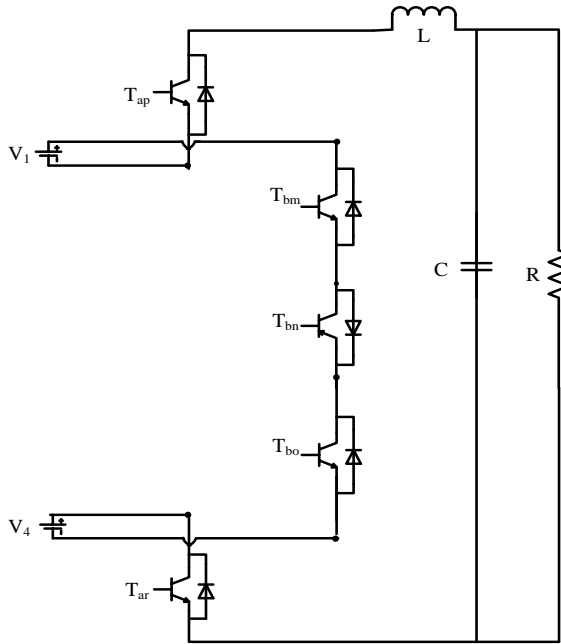
(j)
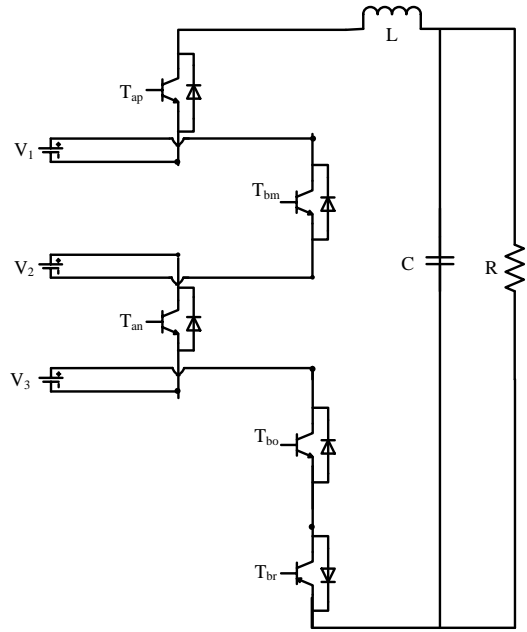
(k)
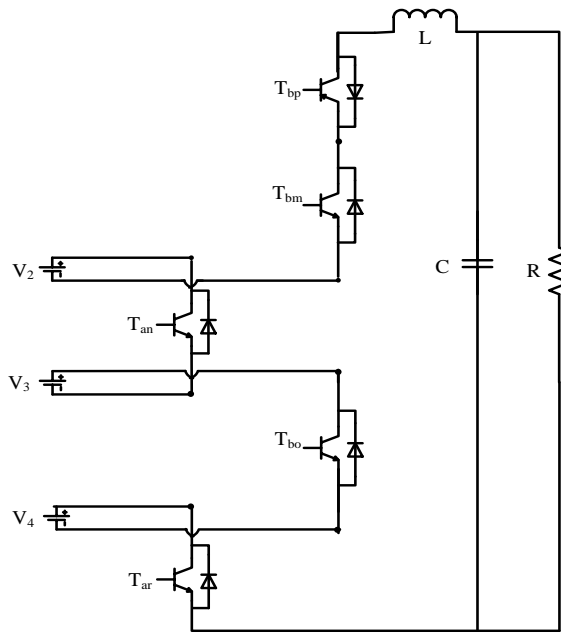
(l)
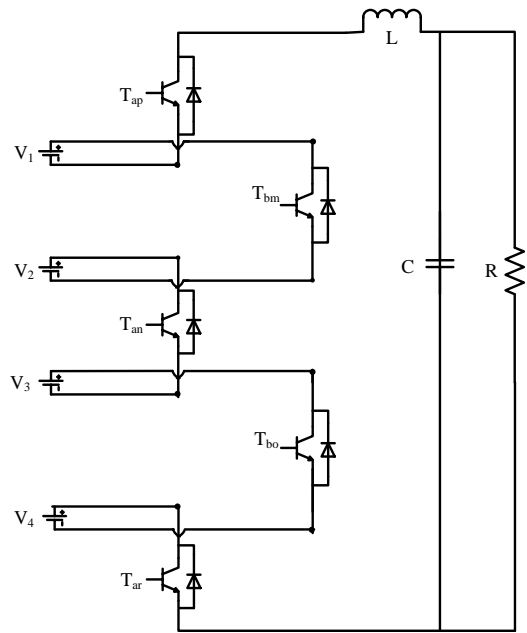
(m)

Figure 7.3 Negative modes of operation of multi string seven level inverter.

## 7.3 Logic Realization

According to Kirchoff's Current Law (KCL) and Kirchoff's Voltage Law (KVL),

$$S_{bj} = 1 - S_{aj}; j = p, m, n, o, r .$$

(7.1)

where $S_{aj}, S_{bj}$ are the switching functions of switches $T_{aj}, T_{bj}$ , $j = p, m, n, o, r$ respectively.

According to Karnaugh mapping, any output '$y$' can be written as the sum of all operating modes. From Table 7.1, the voltage equation using Karnaugh mapping is written as

$$V_{AB} = \sum (1,2,3,4,5,6,7,8,9,10,11,12,13,16,17,18,19,20,21,22,23,24,25,26,27,28,29,30,31,32).$$

where $1,2,3,...$ are Operating Modes

Therefore

$$V_{AB} = \left\{ \begin{array}{l} (V_1 + V_2 + V_3 + V_4)(S_{bp}S_{am}S_{bn}S_{ao}S_{br}) + (V_1 + V_2 + V_3)(S_{bp}S_{am}S_{bn}S_{ao}S_{ar}) \\ + (V_2 + V_3 + V_4)(S_{ap}S_{am}S_{bn}S_{ao}S_{br}) + (V_1 + V_2)(S_{bp}S_{am}S_{bn}S_{bo}S_{br}) \\ + (V_1 + V_4)(S_{bp}S_{am}S_{an}S_{ao}S_{br}) + (V_2 + V_3)(S_{ap}S_{am}S_{bn}S_{ao}S_{ar}) \\ + (V_3 + V_4)(S_{bp}S_{bm}S_{bn}S_{ao}S_{br}) + (V_1)(S_{bp}S_{am}S_{an}S_{ao}S_{ar}) \\ + (V_2)(S_{ap}S_{am}S_{bn}S_{bo}S_{br}) + (V_3)(S_{bp}S_{bm}S_{bn}S_{ao}S_{ar}) \\ + (V_4)(S_{ap}S_{am}S_{an}S_{ao}S_{br}) + (V_3 + V_4 - V_1)(S_{ap}S_{bm}S_{bn}S_{ao}S_{br}) \\ + (V_1 + V_2 - V_4)(S_{bp}S_{am}S_{bn}S_{bo}S_{ar}) + (V_2 - V_4)(S_{ap}S_{am}S_{bn}S_{bo}S_{ar}) \\ + (V_3 - V_1)(S_{ap}S_{bm}S_{bn}S_{ao}S_{ar}) + (V_1 - V_3)(S_{bp}S_{am}S_{an}S_{bo}S_{br}) \\ + (V_4 - V_2)(S_{bp}S_{bm}S_{an}S_{ao}S_{br}) + (-V_1)(S_{ap}S_{bm}S_{bn}S_{bo}S_{br}) \\ + (-V_2)(S_{bp}S_{bm}S_{an}S_{ao}S_{ar}) + (-V_3)(S_{ap}S_{am}S_{an}S_{bo}S_{br}) \\ + (-V_4)(S_{bp}S_{bm}S_{bn}S_{bo}S_{ar}) + (V_1 - V_3 - V_4)(S_{bp}S_{am}S_{an}S_{bo}S_{ar}) \\ + (V_4 - V_1 - V_2)(S_{ap}S_{bm}S_{an}S_{ao}S_{br}) + (-V_1 - V_2)(S_{ap}S_{bm}S_{an}S_{ao}S_{ar}) \\ + (-V_2 - V_3)(S_{bp}S_{bm}S_{an}S_{bo}S_{br}) + (-V_3 - V_4)(S_{ap}S_{am}S_{an}S_{bo}S_{ar}) \\ + (-V_1 - V_4)(S_{ap}S_{bm}S_{bn}S_{bo}S_{ar}) + (-V_1 - V_2 - V_3)(S_{ap}S_{bm}S_{an}S_{bo}S_{br}) \\ + (-V_2 - V_3 - V_4)(S_{bp}S_{bm}S_{an}S_{bo}S_{ar}) + (-V_1 - V_2 - V_3 - V_4)(S_{ap}S_{bm}S_{an}S_{bo}S_{ar}) \end{array} \right\}$$

(7.2)

Separating (7.2) into four different equations with each DC source

$$V_{AB} = V_{AB1} + V_{AB2} + V_{AB3} + V_{AB4}.$$

$$V_{AB1} = V_1 \left\{ \begin{array}{l} S_{bp}S_{am}S_{bn}S_{ao}S_{br} + S_{bp}S_{am}S_{bn}S_{ao}S_{ar} + S_{bp}S_{am}S_{bn}S_{bo}S_{br} \\ + S_{bp}S_{am}S_{an}S_{ao}S_{br} + S_{bp}S_{am}S_{an}S_{ao}S_{ar} - S_{ap}S_{bm}S_{bn}S_{ao}S_{br} \\ + S_{bp}S_{am}S_{bn}S_{bo}S_{ar} - S_{ap}S_{bm}S_{bn}S_{ao}S_{ar} + S_{bp}S_{am}S_{an}S_{bo}S_{br} \\ - S_{ap}S_{bm}S_{bn}S_{bo}S_{br} + S_{bp}S_{am}S_{an}S_{bo}S_{ar} - S_{ap}S_{bm}S_{an}S_{ao}S_{br} \\ - S_{ap}S_{bm}S_{an}S_{ao}S_{ar} - S_{ap}S_{bm}S_{bn}S_{bo}S_{ar} - S_{ap}S_{bm}S_{an}S_{bo}S_{br} \\ - S_{ap}S_{bm}S_{an}S_{bo}S_{ar} \end{array} \right\}.$$

$$V_{AB1} = V_1 \left\{ \begin{array}{l} S_{bp}S_{am}S_{bn}S_{ao} + S_{bp}S_{am}S_{bn}S_{bo} + S_{bp}S_{am}S_{an}S_{ao} - S_{ap}S_{bm}S_{bn}S_{ao} \\ + S_{bp}S_{am}S_{an}S_{bo} - S_{ap}S_{bm}S_{bn}S_{bo} - S_{ap}S_{bm}S_{an}S_{ao} - S_{ap}S_{bm}S_{an}S_{bo} \end{array} \right\}.$$

$$V_{AB1} = V_1 \left\{ S_{bp}S_{am}S_{bn} + S_{bp}S_{am}S_{an} - S_{ap}S_{bm}S_{bn} - S_{ap}S_{bm}S_{an} \right\}.$$

$$V_{AB1} = V_1 \left\{ S_{bp}S_{am} - S_{ap}S_{bm} \right\} = V_1 (S_{am} - S_{ap}).$$

178

$$V_{AB2} = V_2 \left\{ \begin{array}{l} S_{bp}S_{am}S_{bn}S_{ao}S_{br} + S_{bp}S_{am}S_{bn}S_{ao}S_{ar} + S_{ap}S_{am}S_{bn}S_{ao}S_{br} \\ + S_{bp}S_{am}S_{bn}S_{bo}S_{br} + S_{ap}S_{am}S_{bn}S_{ao}S_{ar} + S_{ap}S_{am}S_{bn}S_{bo}S_{br} \\ + S_{bp}S_{am}S_{bn}S_{bo}S_{ar} + S_{ap}S_{am}S_{bn}S_{bo}S_{ar} - S_{bp}S_{bm}S_{an}S_{ao}S_{br} \\ - S_{bp}S_{bm}S_{an}S_{ao}S_{ar} - S_{ap}S_{bm}S_{an}S_{ao}S_{br} - S_{ap}S_{bm}S_{an}S_{ao}S_{ar} \\ - S_{bp}S_{bm}S_{an}S_{bo}S_{br} - S_{ap}S_{bm}S_{an}S_{bo}S_{br} \\ - S_{bp}S_{bm}S_{an}S_{bo}S_{ar} - S_{ap}S_{bm}S_{an}S_{bo}S_{ar} \end{array} \right\}. \tag{7.3}$$

$$V_{AB2} = V_2 \left\{ \begin{array}{l} S_{bp}S_{am}S_{bn}S_{ao} + S_{ap}S_{am}S_{bn}S_{ao} + S_{bp}S_{am}S_{bn}S_{bo} + S_{ap}S_{am}S_{bn}S_{bo} \\ - S_{bp}S_{bm}S_{an}S_{ao} - S_{ap}S_{bm}S_{an}S_{ao} - S_{bp}S_{bm}S_{an}S_{bo} - S_{ap}S_{bm}S_{an}S_{bo} \end{array} \right\}.$$

$$V_{AB2} = V_2 \left\{ S_{bp}S_{am}S_{bn} + S_{ap}S_{am}S_{bn} - S_{bp}S_{bm}S_{an} - S_{ap}S_{bm}S_{an} \right\}.$$

$$V_{AB2} = V_2 \left\{ S_{am}S_{bn} - S_{bm}S_{an} \right\} = V_2 \left( S_{am} - S_{an} \right).$$

$$V_{AB3} = V_3 \left\{ \begin{array}{l} S_{bp}S_{am}S_{bn}S_{ao}S_{br} + S_{bp}S_{am}S_{bn}S_{ao}S_{ar} + S_{ap}S_{am}S_{bn}S_{ao}S_{br} + S_{ap}S_{am}S_{bn}S_{ao}S_{ar} \\ + S_{bp}S_{bm}S_{bn}S_{ao}S_{br} + S_{bp}S_{bm}S_{bn}S_{ao}S_{ar} + S_{ap}S_{bm}S_{bn}S_{ao}S_{br} + S_{ap}S_{bm}S_{bn}S_{ao}S_{ar} \\ - S_{bp}S_{am}S_{an}S_{bo}S_{br} - S_{ap}S_{am}S_{an}S_{bo}S_{br} - S_{bp}S_{am}S_{an}S_{bo}S_{ar} - S_{bp}S_{bm}S_{an}S_{bo}S_{br} \\ - S_{ap}S_{am}S_{an}S_{bo}S_{ar} - S_{ap}S_{bm}S_{an}S_{bo}S_{br} - S_{bp}S_{bm}S_{an}S_{bo}S_{ar} - S_{ap}S_{bm}S_{an}S_{bo}S_{ar} \end{array} \right\}. \tag{7.4}$$

$$V_{AB3} = V_3 \left\{ \begin{array}{l} S_{bp}S_{am}S_{bn}S_{ao} + S_{ap}S_{am}S_{bn}S_{ao} + S_{bp}S_{bm}S_{bn}S_{ao} + S_{ap}S_{bm}S_{bn}S_{ao} \\ - S_{bp}S_{am}S_{an}S_{bo} - S_{bp}S_{bm}S_{an}S_{bo} - S_{ap}S_{am}S_{an}S_{bo} - S_{ap}S_{bm}S_{an}S_{bo} \end{array} \right\}.$$

$$V_{AB3} = V_3 \left\{ S_{am}S_{bn}S_{ao} + S_{bm}S_{bn}S_{ao} - S_{am}S_{an}S_{bo} - S_{bm}S_{an}S_{bo} \right\}.$$

$$V_{AB3} = V_3 \left\{ S_{bn}S_{ao} - S_{an}S_{bo} \right\} = V_3 \left( S_{ao} - S_{an} \right).$$

$$V_{AB4} = V_4 \left\{ \begin{array}{l} S_{bp}S_{am}S_{bn}S_{ao}S_{br} + S_{ap}S_{am}S_{bn}S_{ao}S_{br} + S_{bp}S_{am}S_{an}S_{ao}S_{br} + S_{bp}S_{bm}S_{bn}S_{ao}S_{br} \\ + S_{ap}S_{am}S_{an}S_{ao}S_{br} + S_{ap}S_{bm}S_{bn}S_{ao}S_{br} - S_{bp}S_{am}S_{bn}S_{bo}S_{ar} - S_{ap}S_{am}S_{bn}S_{bo}S_{ar} \\ + S_{bp}S_{bm}S_{an}S_{ao}S_{br} - S_{bp}S_{bm}S_{bn}S_{bo}S_{ar} - S_{bp}S_{am}S_{an}S_{bo}S_{ar} + S_{ap}S_{bm}S_{an}S_{ao}S_{br} \\ - S_{ap}S_{am}S_{an}S_{bo}S_{ar} - S_{ap}S_{bm}S_{bn}S_{bo}S_{ar} - S_{bp}S_{bm}S_{an}S_{bo}S_{ar} - S_{ap}S_{bm}S_{an}S_{bo}S_{ar} \end{array} \right\}.$$

$$V_{AB4} = V_4 \left\{ \begin{array}{l} S_{am}S_{bn}S_{ao}S_{br} + S_{bm}S_{bn}S_{ao}S_{br} + S_{am}S_{an}S_{ao}S_{br} - S_{am}S_{bn}S_{bo}S_{ar} \\ + S_{bm}S_{an}S_{ao}S_{br} - S_{am}S_{an}S_{bo}S_{ar} - S_{bm}S_{bn}S_{bo}S_{ar} - S_{bm}S_{an}S_{bo}S_{ar} \end{array} \right\}.$$

$$V_{AB4} = V_4 \left\{ S_{bn}S_{ao}S_{br} - S_{bn}S_{bo}S_{ar} + S_{an}S_{ao}S_{br} - S_{an}S_{bo}S_{ar} \right\}.$$

$$V_{AB4} = V_4 \left\{ S_{ao}S_{br} - S_{bo}S_{ar} \right\} = V_4 \left( S_{ao} - S_{ar} \right).$$

$$V_{AB} = V_{AB1} + V_{AB2} + V_{AB3} + V_{AB4}.$$

$$V_{AB} = V_1 \left( S_{am} - S_{ap} \right) + V_2 \left( S_{am} - S_{an} \right) + V_3 \left( S_{ao} - S_{an} \right) + V_4 \left( S_{ao} - S_{ar} \right). \tag{7.5}$$

The expression for voltage equation in terms of switching functions is given in (7.5). Similarly, the expressions for input currents $I_{s1}, I_{s2}, I_{s3}, I_{s4}$ can also be found and are given in (7.8), (7.11), (7.14) and (7.17) respectively.

For $I_{s1}$

$$I_{s1} = \sum \left( 1,2,4,5,8,12,13,17,18,20,24,25,26,29,30,32 \right). \tag{7.6}$$

$$I_{s1} = I_o \left\{ \begin{array}{l} S_{bp}S_{am}S_{bn}S_{ao}S_{br} + S_{bp}S_{am}S_{bn}S_{ao}S_{ar} + S_{bp}S_{am}S_{bn}S_{bo}S_{br} + S_{bp}S_{am}S_{an}S_{ao}S_{br} \\ + S_{bp}S_{am}S_{an}S_{ao}S_{ar} - S_{ap}S_{bm}S_{bn}S_{ao}S_{br} + S_{bp}S_{am}S_{bn}S_{bo}S_{ar} - S_{ap}S_{bm}S_{bn}S_{ao}S_{ar} \\ + S_{bp}S_{am}S_{an}S_{bo}S_{br} - S_{ap}S_{bm}S_{bn}S_{bo}S_{br} + S_{bp}S_{am}S_{an}S_{bo}S_{ar} - S_{ap}S_{bm}S_{an}S_{ao}S_{br} \\ - S_{ap}S_{bm}S_{an}S_{ao}S_{ar} - S_{ap}S_{bm}S_{bn}S_{bo}S_{ar} - S_{ap}S_{bm}S_{an}S_{bo}S_{br} - S_{ap}S_{bm}S_{an}S_{bo}S_{ar} \end{array} \right\}. \tag{7.7}$$

$$I_{s1} = I_o \left\{ \begin{array}{l} S_{bp}S_{am}S_{bn}S_{ao} + S_{bp}S_{am}S_{bn}S_{bo} + S_{bp}S_{am}S_{an}S_{ao} - S_{ap}S_{bm}S_{bn}S_{ao} \\ + S_{bp}S_{am}S_{an}S_{bo} - S_{ap}S_{bm}S_{an}S_{ao} - S_{ap}S_{bm}S_{bn}S_{bo} - S_{ap}S_{bm}S_{an}S_{bo} \end{array} \right\}.$$

$$I_{s1} = I_o \left\{ S_{bp}S_{am}S_{bn} + S_{bp}S_{am}S_{an} - S_{ap}S_{bm}S_{bn} - S_{ap}S_{bm}S_{an} \right\}.$$

$$I_{s1} = I_o \left\{ S_{bp}S_{am} - S_{ap}S_{bm} \right\} = I_o \left( S_{am} - S_{ap} \right). \tag{7.8}$$

For $I_{s2}$

$$I_{s2} = \sum \left( 1,2,3,4,6,9,13,16,19,21,25,26,27,30,31,32 \right). \tag{7.9}$$

$$I_{s2} = I_o \left\{ \begin{array}{l} S_{bp}S_{am}S_{bn}S_{ao}S_{br} + S_{bp}S_{am}S_{bn}S_{ao}S_{ar} + S_{ap}S_{am}S_{bn}S_{ao}S_{br} + S_{bp}S_{am}S_{bn}S_{bo}S_{ar} \\ + S_{ap}S_{am}S_{bn}S_{ao}S_{ar} + S_{ap}S_{am}S_{bn}S_{bo}S_{br} + S_{bp}S_{am}S_{bn}S_{bo}S_{ar} + S_{ap}S_{am}S_{bn}S_{bo}S_{ar} \\ - S_{bp}S_{bm}S_{an}S_{ao}S_{br} - S_{bp}S_{bm}S_{an}S_{ao}S_{ar} - S_{ap}S_{bm}S_{an}S_{ao}S_{br} - S_{ap}S_{bm}S_{an}S_{ao}S_{ar} \\ - S_{bp}S_{bm}S_{an}S_{bo}S_{br} - S_{ap}S_{bm}S_{an}S_{bo}S_{br} - S_{bp}S_{bm}S_{an}S_{bo}S_{ar} - S_{ap}S_{bm}S_{an}S_{bo}S_{ar} \end{array} \right\}. \tag{7.10}$$

$$I_{s2} = I_o \left\{ \begin{array}{l} S_{bp}S_{am}S_{bn}S_{ao} + S_{ap}S_{am}S_{bn}S_{ao} + S_{bp}S_{am}S_{bn}S_{bo} + S_{ap}S_{am}S_{bn}S_{bo} \\ - S_{bp}S_{bm}S_{an}S_{ao} - S_{ap}S_{bm}S_{an}S_{ao} - S_{bp}S_{bm}S_{an}S_{bo} - S_{ap}S_{bm}S_{an}S_{bo} \end{array} \right\}.$$

$$I_{s2} = I_o \left\{ S_{am}S_{bn}S_{ao} + S_{am}S_{bn}S_{bo} - S_{bm}S_{an}S_{ao} - S_{bm}S_{an}S_{bo} \right\}.$$

$$I_{s2} = I_o \left\{ S_{am}S_{bn} - S_{bm}S_{an} \right\} = I_o \left( S_{am} - S_{an} \right). \tag{7.11}$$

For $I_{s3}$

$$I_{s3} = \sum \left(1,2,3,6,7,10,12,17,18,22,24,27,28,30,31,32\right). \tag{7.12}$$

$$I_{s3} = I_o \left\{ \begin{array}{l} S_{bp}S_{am}S_{bn}S_{ao}S_{br} + S_{bp}S_{am}S_{bn}S_{ao}S_{ar} + S_{ap}S_{am}S_{bn}S_{ao}S_{br} + S_{bp}S_{bm}S_{bn}S_{ao}S_{br} \\ + S_{ap}S_{am}S_{bn}S_{ao}S_{ar} + S_{bp}S_{bm}S_{bn}S_{ao}S_{ar} + S_{ap}S_{bm}S_{bn}S_{ao}S_{br} + S_{ap}S_{bm}S_{bn}S_{ao}S_{ar} \\ - S_{bp}S_{am}S_{an}S_{bo}S_{br} - S_{ap}S_{am}S_{an}S_{bo}S_{br} - S_{bp}S_{am}S_{an}S_{bo}S_{ar} - S_{bp}S_{bm}S_{an}S_{bo}S_{br} \\ - S_{ap}S_{am}S_{an}S_{bo}S_{ar} - S_{ap}S_{bm}S_{an}S_{bo}S_{br} - S_{bp}S_{bm}S_{an}S_{bo}S_{ar} - S_{ap}S_{bm}S_{an}S_{bo}S_{ar} \end{array} \right\}. \tag{7.13}$$

$$I_{s3} = I_o \left\{ \begin{array}{l} S_{bp}S_{am}S_{bn}S_{ao} + S_{ap}S_{am}S_{bn}S_{ao} + S_{bp}S_{bm}S_{bn}S_{ao} + S_{ap}S_{bm}S_{bn}S_{ao} \\ - S_{bp}S_{am}S_{an}S_{bo} - S_{ap}S_{am}S_{an}S_{bo} - S_{ap}S_{bm}S_{an}S_{bo} - S_{bp}S_{bm}S_{an}S_{bo} \end{array} \right\}.$$

$$I_{s3} = I_o \left\{ S_{am}S_{bn}S_{ao} + S_{bm}S_{bn}S_{ao} - S_{am}S_{an}S_{bo} - S_{bm}S_{an}S_{bo} \right\}.$$

$$I_{s3} = I_o \left\{ S_{bn}S_{ao} - S_{an}S_{bo} \right\} = I_o \left( S_{ao} - S_{an} \right). \tag{7.14}$$

For $I_{s4}$

$$I_{s4} = \sum \left(1,3,5,7,11,12,13,16,19,23,24,25,28,29,31,32\right). \tag{7.15}$$

181

$$I_{s4} = I_o \begin{cases} S_{bp}S_{am}S_{bn}S_{ao}S_{br} + S_{ap}S_{am}S_{bn}S_{ao}S_{br} + S_{bp}S_{am}S_{an}S_{ao}S_{br} + S_{bp}S_{bm}S_{bn}S_{ao}S_{br} \\ + S_{ap}S_{am}S_{an}S_{ao}S_{br} + S_{ap}S_{bm}S_{bn}S_{ao}S_{br} - S_{bp}S_{am}S_{bn}S_{bo}S_{ar} - S_{ap}S_{am}S_{bn}S_{bo}S_{ar} \\ + S_{bp}S_{bm}S_{an}S_{ao}S_{br} - S_{bp}S_{bm}S_{bn}S_{bo}S_{ar} - S_{bp}S_{am}S_{an}S_{bo}S_{ar} + S_{ap}S_{bm}S_{an}S_{ao}S_{br} \\ - S_{ap}S_{am}S_{an}S_{bo}S_{ar} - S_{ap}S_{bm}S_{bn}S_{bo}S_{ar} - S_{bp}S_{bm}S_{an}S_{bo}S_{ar} - S_{ap}S_{bm}S_{an}S_{bo}S_{ar} \end{cases} . \tag{7.16}$$

$$I_{s4} = I_o \begin{cases} S_{am}S_{bn}S_{ao}S_{br} + S_{am}S_{an}S_{ao}S_{br} + S_{bm}S_{bn}S_{ao}S_{br} - S_{am}S_{bn}S_{bo}S_{ar} \\ - S_{am}S_{an}S_{bo}S_{ar} + S_{bm}S_{an}S_{ao}S_{br} - S_{bm}S_{bn}S_{bo}S_{ar} - S_{bm}S_{an}S_{bo}S_{ar} \end{cases} .$$

$$I_{s4} = I_o \left\{ S_{an}S_{ao}S_{br} + S_{bn}S_{ao}S_{br} - S_{bn}S_{bo}S_{ar} - S_{an}S_{bo}S_{ar} \right\}.$$

$$I_{s4} = I_o \left\{ S_{ao}S_{br} - S_{bo}S_{ar} \right\} = I_o \left( S_{ao} - S_{ar} \right). \tag{7.17}$$

Therefore the dynamic model equations of the system are given as

$$V_1 \left( S_{am} - S_{ap} \right) + V_2 \left( S_{am} - S_{an} \right) + V_3 \left( S_{ao} - S_{an} \right) + V_4 \left( S_{ao} - S_{ar} \right) = L_o p I_o + V_c. \tag{7.18}$$

$$CpV_c = I_o - I_L. \tag{7.19}$$

### 7.3.1 Voltage stress calculations

The voltage stresses are calculated for switches in first leg and are given from (7.20) to (7.24).

$$V_{Sap} = S_{bp}V_1. \tag{7.20}$$

$$V_{Sam} = S_{bm}(V_1 + V_2). \tag{7.21}$$

$$V_{San} = S_{bn}(V_{s2} + V_{s3}). \tag{7.22}$$

$$V_{Sao} = S_{bo}(V_{s3} + V_{s4}). \tag{7.23}$$

$$V_{Sar} = S_{br}V_{s4}. \tag{7.24}$$

## 7.4 Modulation Scheme

For modulation scheme, level shifted carrier based PWM is used. In level shifted PWM, the carrier waveforms are one above another with equal amplitude.

If the switching pulses of switches in one leg are generated, then their complementary will be respectively the switching pulses of switches in another leg. The generation of switching pulses is as follows:

$$S_{ap} = \begin{bmatrix} 1 \text{ when } Tri_1 < M_p < Tri_2 \text{ for } M_p > 0, \text{and } M_p > Tri_3, M_p < Tri_4 \text{ for } M_p < 0 \\ 0 \text{ when } M_p > Tri_1, M_p < Tri_2 \text{ for } M_p > 0, \text{and } Tri_3 < M_p < Tri_4 \text{ for } M_p < 0 \end{bmatrix}. \quad (7.25)$$

$$S_{am} = \begin{bmatrix} 1 \text{ when } M_p > Tri_2 \text{ for } M_p > 0 \text{ and } M_p > Tri_3 \text{ for } M_p < 0 \\ 0 \text{ when } M_p < Tri_2 \text{ for } M_p > 0 \text{ and } M_p < Tri_3 \text{ for } M_p < 0 \end{bmatrix}. \quad (7.26)$$

$$S_{an} = \begin{bmatrix} 1 \text{ when } M_n > 0 \\ 0 \text{ when } M_n < 0 \end{bmatrix}. \quad (7.27)$$

$$S_{ao} = \begin{bmatrix} 1 \text{ when } M_n < Tri_2 \text{ for } M_n > 0 \text{ and } M_n < Tri_3 \text{ for } M_n < 0 \\ 0 \text{ when } M_n > Tri_2 \text{ for } M_n > 0 \text{ and } M_n > Tri_3 \text{ for } M_n < 0 \end{bmatrix}. \quad (7.28)$$

$$S_{ar} = \begin{bmatrix} 1 \text{ when } Tri_3 < M_n < Tri_4 \text{ for } M_n < 0, \text{and } M_n < Tri_2, M_n > Tri_1 \text{ for } M_n > 0 \\ 0 \text{ when } Tri_1 < M_n < Tri_2 \text{ for } M_n > 0, \text{and } M_n > Tri_3, M_n < Tri_4 \text{ for } M_n < 0 \end{bmatrix}. \quad (7.29)$$

where $M_p$ and $M_n$ are the modulation signals and $Tri_1$, $Tri_2$, $Tri_3$ and $Tri_4$ are the four carrier waveforms used to generate switching pulses by level shifted carrier based PWM. The modulation signals and carrier waveforms can be seen in Figure 7.4.
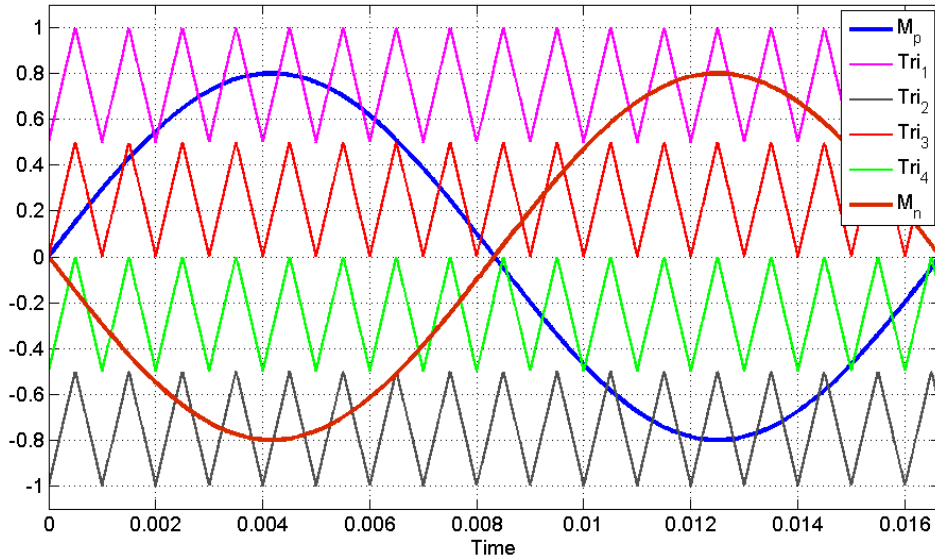
Figure 7.4 Modulation Scheme.

### 7.4.1 Determination of expressions for modulation signals

The expressions for modulation signals are determined using double Fourier series analysis. At any time, if the carrier frequency is much larger than the frequency of modulation signals, the switching functions are approximated based on the instantaneous values of modulation signal [74].

Let the two modulation waveforms used be of the form $M_p = M_1 \sin(\theta + \psi_1)$ and $M_n = M_2 \sin(\theta + \psi_2)$, where $\psi_1$ and $\psi_2$ are the initial phase angles of modulation signals respectively and $\theta = \omega t$, where $\omega$ is the frequency of the reference voltage waveform.

From figure 7.5, the switching functions are approximated by their instantaneous values of modulation signal.

184
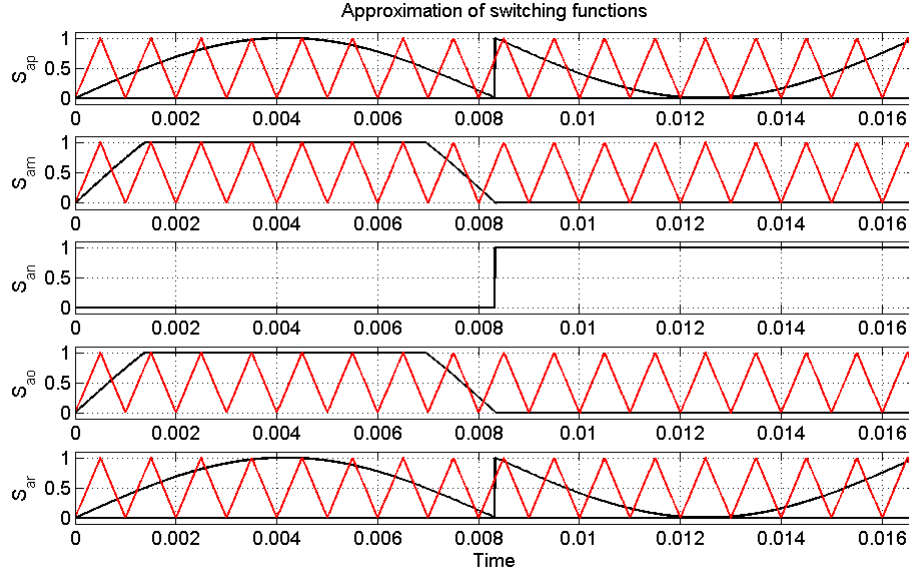
Figure 7.5 Approximations of switching functions in terms of instantaneous values of

modulation signals.

$$S_{ap} = \begin{cases} M_p & \psi_1 \leq \theta_1 < \pi + \psi_1 \\ 1 + M_p & \pi + \psi_1 \leq \theta_1 \leq 2\pi + \psi_1 \end{cases}.$$ (7.30)

$$S_{am} = \begin{cases} 2M_p & \psi_1 \leq \theta_1 < \pi + \psi_1 \\ 0 & \pi + \psi_1 \leq \theta_1 \leq 2\pi + \psi_1 \end{cases}.$$ (7.31)

$$S_{an} = \begin{cases} 0 & \psi_2 \leq \theta_2 < \pi + \psi_2 \\ 1 & \pi + \psi_2 \leq \theta_2 \leq 2\pi + \psi_2 \end{cases}.$$ (7.32)

$$S_{ao} = \begin{cases} -2M_n & \psi_2 \leq \theta_2 < \pi + \psi_2 \\ 0 & \pi + \psi_2 \leq \theta_2 \leq 2\pi + \psi_2 \end{cases}.$$ (7.33)

$$S_{ao} = \begin{cases} -M_n & \psi_2 \leq \theta_2 < \pi + \psi_2 \\ 1 - M_n & \pi + \psi_2 \leq \theta_2 \leq 2\pi + \psi_2 \end{cases}.$$ (7.34)

The double Fourier series approximation of converter switching functions given in [4] as

185

$$
S_{ij}(\omega_s,\omega_c) = \begin{bmatrix} \dfrac{A_{00}}{2} + \sum_{n=1}^{\infty}\left(A_{0n}\cos(n\omega_s t) + B_{0n}\sin(n\omega_s t)\right) \\[2mm] + \sum_{m=1}^{\infty}\left(A_{m0}\cos(m\omega_c t) + B_{m0}\sin(m\omega_c t)\right) \\[2mm] + \sum_{m=1}^{\infty}\sum_{\substack{n=-\infty \\ n\neq 0}}^{\infty}\left(A_{mn}\cos(m\omega_c t + n\omega_s t) + B_{mn}\sin(m\omega_c t + n\omega_s t)\right) \end{bmatrix}.
$$

(7.35)

According to Fourier series, the clear derivations of expression for switching functions are given in Appendix C. The expression for $S_{ap}$, $S_{am}$, $S_{an}$, $S_{ao}$, $S_{ar}$ is given as

$$
S_{ap} = \frac{1}{2} + M_1\sin(\theta+\psi_1) + \frac{2}{\pi}\left(\sin(\psi_1-\theta)\right).
$$

(7.36)

$$
S_{am} = \frac{2M_1}{\pi}\cos(2\psi_1) + \left(M_1\right)\sin(\theta+\psi_1).
$$

(7.37)

$$
S_{an} = \frac{1}{2} + \frac{2}{\pi}\left(\sin(\psi_2-\theta)\right).
$$

(7.38)

$$
S_{ao} = \frac{2M_2}{\pi}\cos(2\psi_2) + \left(M_2\right)\sin(\theta+\psi_2).
$$

(7.39)

$$
S_{ar} = \frac{1}{2} - M_2\sin(\theta+\psi_2) + \frac{2}{\pi}\left(\sin(\psi_2-\theta)\right).
$$

(7.40)

Substituting (7.36), (7.37), (7.38), (7.39), (7.40) into (7.5), and considering $V_1 = V_2 = V_3 = V_4 = V_s$, then the output voltage equation becomes

$$
V_{AB} = \left\{ \begin{array}{l} V_1\left(\left[\dfrac{2M_1}{\pi}\cos(2\psi_1)+\left(M_1\right)\sin(\theta+\psi_1)\right]-\left[\dfrac{1}{2}-M_1\sin(\theta+\psi_1)+\dfrac{2}{\pi}\left(\sin(\psi_1-\theta)\right)\right]\right) \\[3mm] +V_2\left(\left[\dfrac{2M_1}{\pi}\cos(2\psi_1)+\left(M_1\right)\sin(\theta+\psi_1)\right]-\left\{-\dfrac{1}{2}-\dfrac{2}{\pi}\left(\sin(\psi_2-\theta)\right)\right\}\right) \\[3mm] +V_3\left(\left[\dfrac{2M_2}{\pi}\cos(2\psi_2)-\left(M_2\right)\sin(\theta+\psi_2)\right]-\left\{-\dfrac{1}{2}-\dfrac{2}{\pi}\left(\sin(\psi_2-\theta)\right)\right\}\right) \\[3mm] +V_4\left(\left[\dfrac{2M_2}{\pi}\cos(2\psi_2)-\left(M_2\right)\sin(\theta+\psi_2)\right]-\left[\dfrac{1}{2}+M_2\sin(\theta+\psi_2)+\dfrac{2}{\pi}\left(\sin(\psi_2-\theta)\right)\right]\right) \end{array} \right\}.
$$

(7.41)

Let $\psi_1 = \psi_2$ .

$$M_p = M_1 \sin(\theta + \psi_1) = \frac{V_{AB} - (V_2 + V_3)\left(\frac{4}{\pi}\left(\sin(\theta - \psi_1)\right)\right)}{V_1 + \alpha V_4}.$$  (7.42)

$$M_n = M_2 \sin(\theta + \psi_2) = \alpha \frac{V_{AB} - (V_2 + V_3)\left(\frac{4}{\pi}\left(\sin(\theta - \psi_1)\right)\right)}{V_1 + \alpha V_4}.$$  (7.43)

### 7.5 Switching Loss Comparison with Four Cell Cascaded H-bridge inverter

The switching power loss for this proposed topology is compared with the three cascaded H bridge multilevel Inverter topology. The average switching power loss $P_s$ in the switch caused by these transitions [75] can be defined as

$$P_s = 0.5 V_S I_o f_s \left(t_{(on)} + t_{(off)}\right),$$  (7.44)

where $t_{(on)}$ and $t_{(off)}$ are the turn-on and turn-off times, respectively; $V_S$ is the voltage stress across the switch; and $I_o$ is the current flowing through the switch.

Let both the proposed circuit and cascaded H bridge multi-level converter be operated at the same turn-on and turn-off times and at the same load current $I_o$. Then the average switching power loss $P_s$ is proportional to $V_S$ and $f_s$. So in general

$$P_s \propto V_S f_s.$$  (7.45)

The voltage stresses of the sixteen switches of the conventional cascaded H-bridge inverter are all equal to $V_s$.
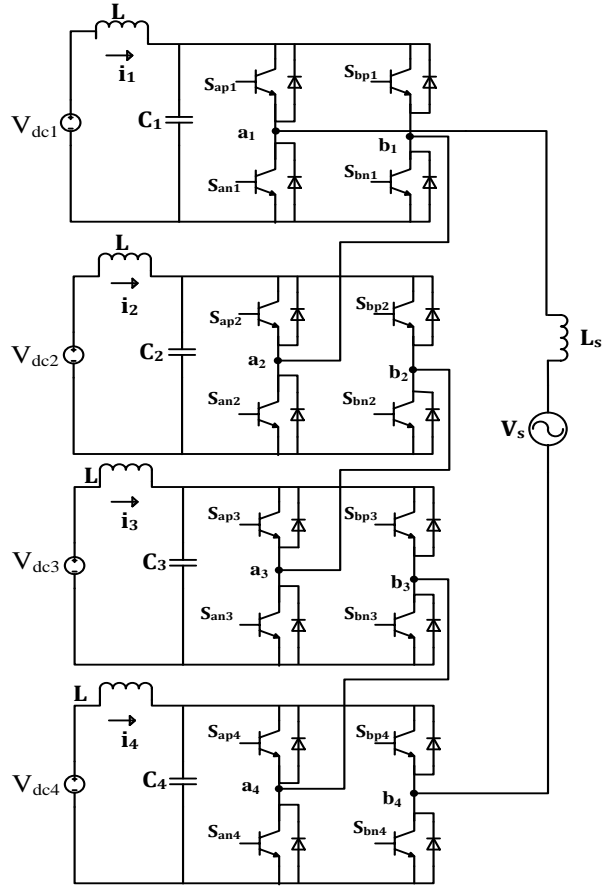
Figure 7.6 Four cell cascaded H-bridge inverter.

According to figure 7.6, the switching loss of cascaded H-bridge inverter from sixteen switches can be obtained as

$$P_{s,H-bridge} \propto 16V_s f_s. \tag{7.46}$$

Similarly the switching power loss of multi string seven-level inverter shown in figure 7.1 with ten switches can also be obtained as

$$P_{s,\text{multi string}} \propto 4V_s f_s + 6(2V_s)f_m. \tag{7.47}$$

$$P_{s,\text{multi string}} \propto 4V_s(f_s + 3f_m). \tag{7.48}$$

where $f_m$ is the line frequency.

Because the switches $S_{am}, S_{bm}, S_{an}, S_{bn}, S_{ao}, S_{bo}$ are operated at near line frequency and switching frequency is larger than line frequency $f_m \ll f_s$, the switching losses of the proposed circuit is approximated to

$$P_{s,\text{multi string}} \propto 4 V_s f_s \qquad (7.1)$$

Comparing equations (7.46) and (7.49), switching losses in multi string nine-level converter are about 30% less than four cascaded H bridge multi-level converter in this case.


## 7.6 Simulation Results and Discussions


The simulation of multi string nine-level inverter topology is carried out using Matlab/Simulink software. The parameters used for simulation are, $V_{AB} = 180V$, $V_1 = 50V$, $V_2 = 50V$, $V_3 = 50V$, $V_4 = 50V$ and $\alpha = -1$. $M_1, M_2$ are derived from (7.42) and (7.43) respectively. Figure 7.4 shows the modulation scheme that is used to generate switching pulses shown in Figures 7.7 and 7.8. From Figures 7.7 and 7.8, the switching pulses of the middle switches can be seen at almost line frequency. Figure 7.9 shows the voltage across each switch in the first leg, as can be seen from Figure 7.9, the voltage stress of middle two switches in the first leg $T_{am}, T_{an}, T_{ao}$ are twice that of other two switches. Figure 7.11 shows the waveforms of output phase voltage $V_{AB}$ and. Figure 7.10 shows the waveforms of four input source currents.
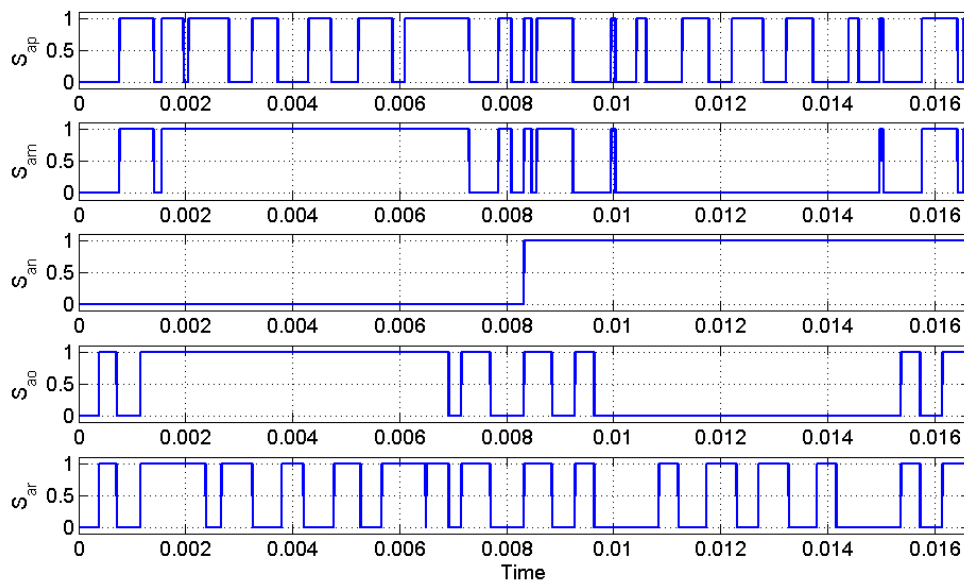
Figure 7.7 Simulation result of switching pulses of the switches in first leg.
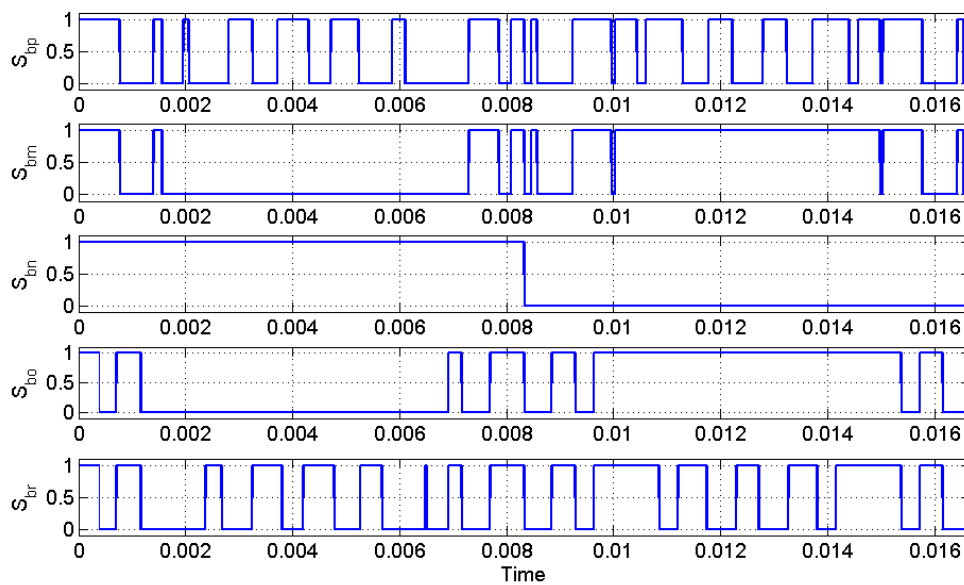


Figure 7.8 Simulation result of switching pulses of the switches in second leg.
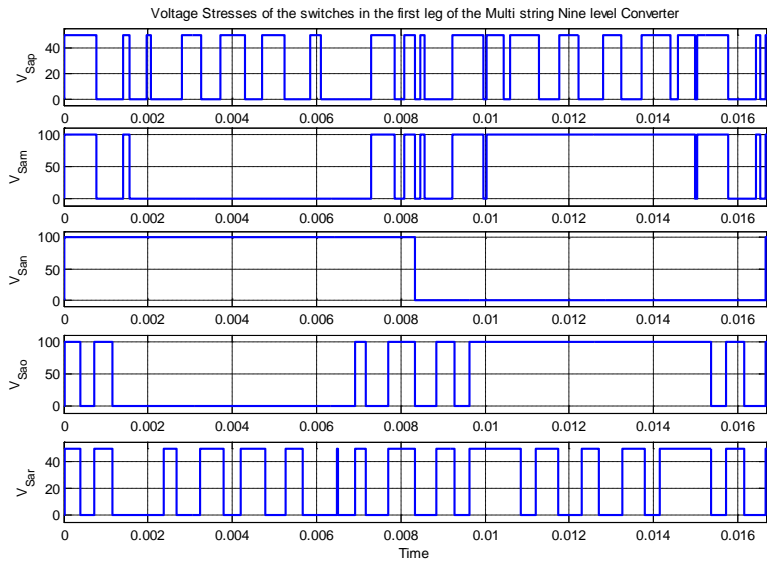
Figure 7.9 Simulation result of voltage stress of the switches in first leg of the converter.
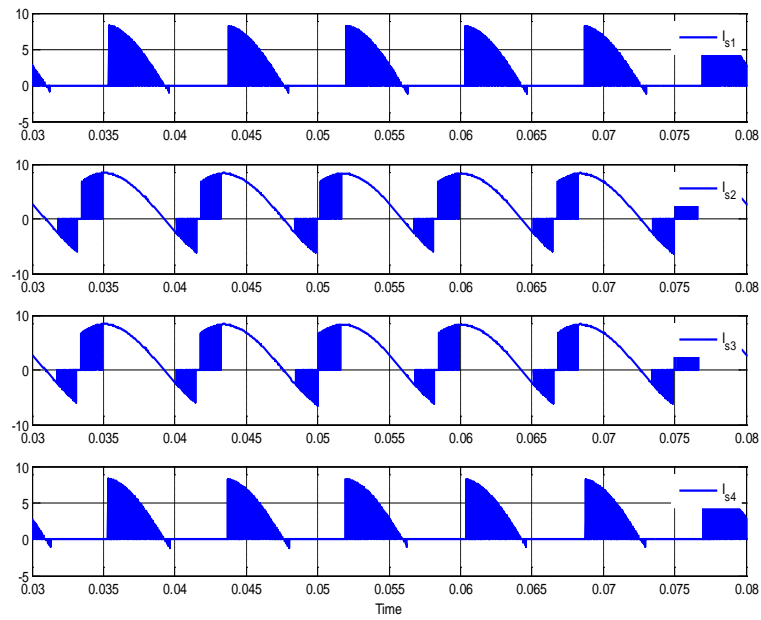


Figure 7.10 Simulation result of input source currents.
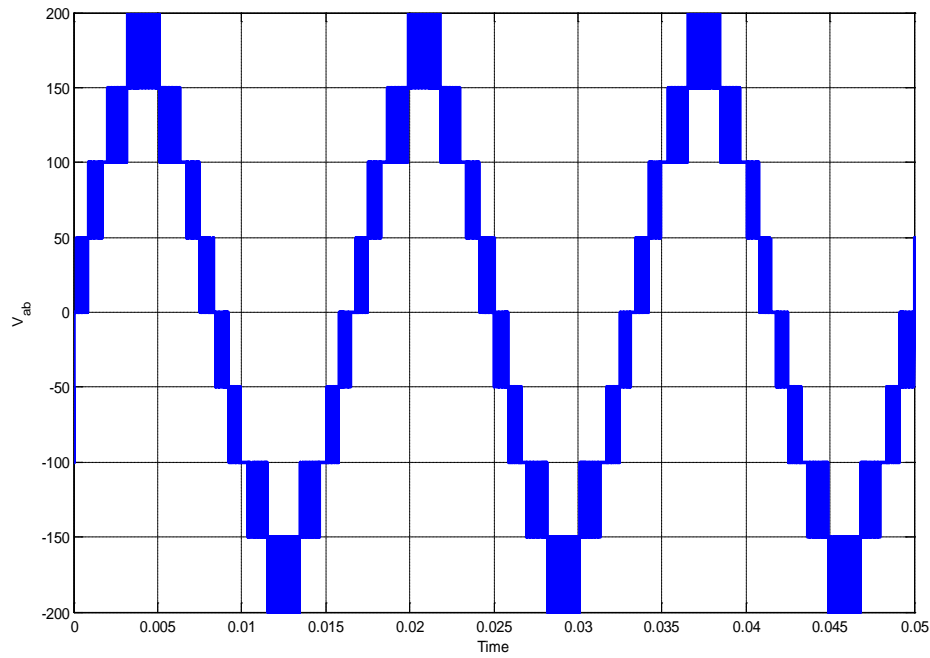
Figure 7.11 Simulation result of output phase voltage.

## 7.7 Experimental results

The experiments on multi string nine-level inverter are also performed on a laboratory prototype using TMS 320 F28335 eZdsp to generate the switching pulses of both the legs which are shown in Figures 7.12 and 7.13 respectively. The waveform of the output voltage can also be seen in Figure 7.14. The experimental results and simulation results validate each other.
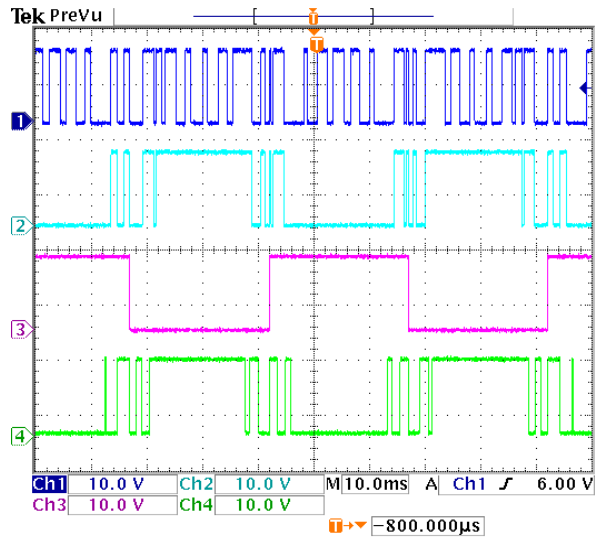
(a)
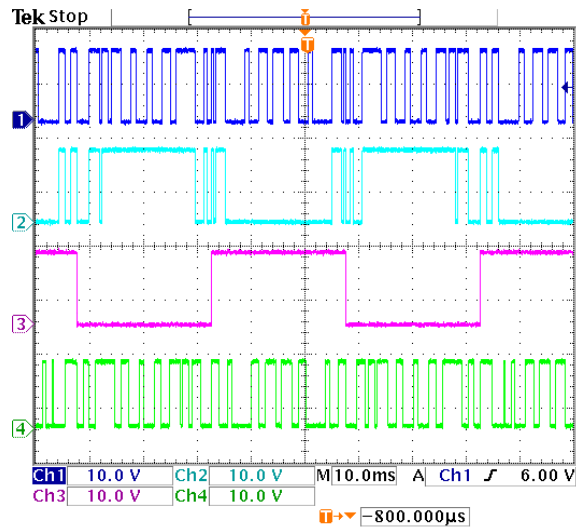


(b)

Figure 7.12 Experimental results of switching pulses of switches in first leg: (a) $S_{ap}, S_{am}, S_{an}, S_{ao}$,

(b) $S_{ap}, S_{am}, S_{an}, S_{ar}$.
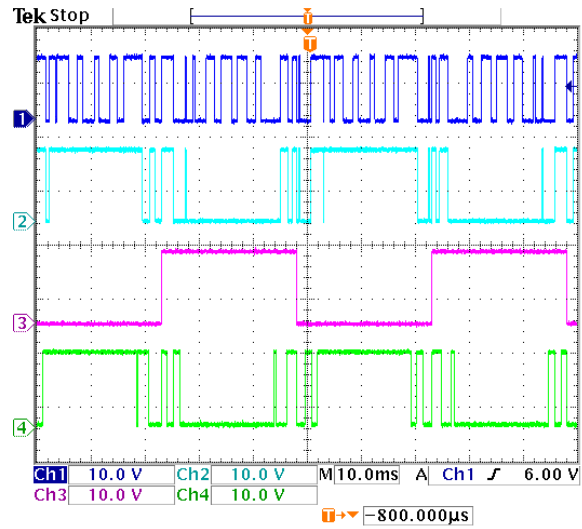
(a)
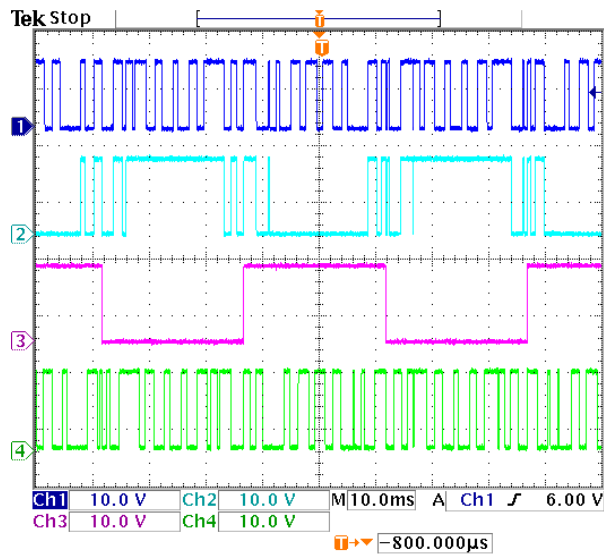


(b)

Figure 7.13 Experimental results of switching pulses of switches in second leg, (a)

$S_{bp}, S_{bm}, S_{bn}, S_{bo}$, (b) $S_{bp}, S_{bm}, S_{bn}, S_{br}$.
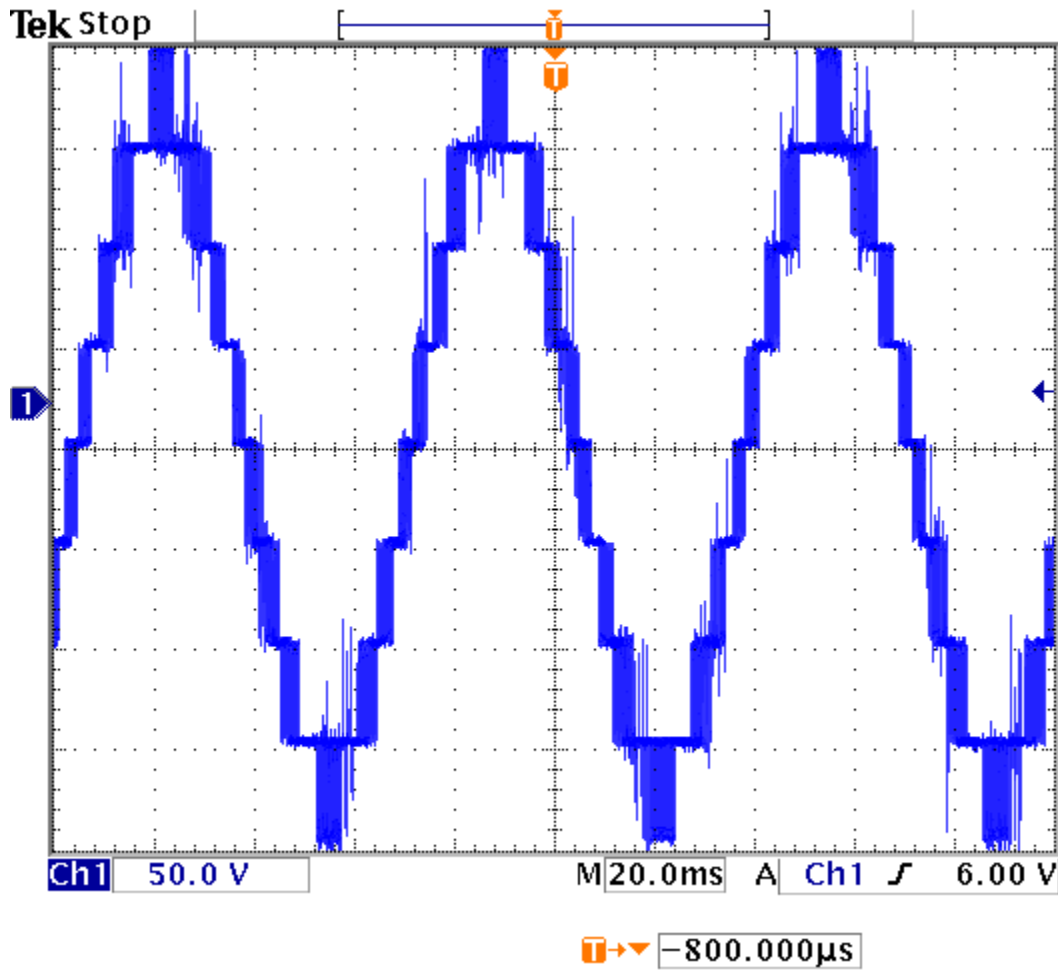
Figure 7.14 Experimental result of output phase voltage (50V/div).

**7.8 Summary**

This chapter presented a single-phase multistring nine-level inverter topology which has less number of switches required to produce the desired multi-level output for distributed energy resources compared to cascaded H-bridge converter topology. The modes of operation of nine-level inverter topology are also discussed in this chapter. The equations for output voltage and

input source currents are calculated in terms of the input voltages and output current respectively using Karnaugh mapping technique. The expression of voltage stress for the switches in first leg are determined. The modulation scheme for this topology is also presented. The expression for modulation signal is determined using Fourier series analysis by approximating switching functions using the instantaneous values of modulation signals. The calculation of switching loss for multi string seven-level inverter is performed and the proposed topology reduces about 30% of switching loss compared to four cell cascaded H bridge multi-level converter. Simulation of the proposed system is carried out and waveforms of output voltage, input source currents, voltage stress are generated. Experimental results are conducted on 1kW laboratory prototype and the waveforms of switching pulses and output voltage are presented. The experimental results and simulation results validate each other. The only disadvantage with this type of converter when compared with cascade H bridge multi-level converter is the rating of switches. The rating of six middle switches should be twice the rating of other four switches.

# CHAPTER 8

# GRID CONNECTED SINGLE PHASE MULTI STRING MULTI LEVEL INVERTER

## 8.1 Introduction

This chapter presents modelling of multi string multilevel inverter connected to the grid through an LCL filter. The LCL filter brings the advantage of providing a better decoupling between the filter and grid impedance (as it reduces the dependence of the filter on the grid parameters) and a lower ripple of the current stress across the grid inductor. The main objective regarding this topology is to control the overall active and reactive power going into the grid. The interests of distributed power system using a renewable energy have been increased. In terms of application strategies, a residential power generation concept with a capability of grid tie is rapidly being commercialized by an industry. In most cases, residential loads are supplied with a single-phase power from the grid. Therefore, the single-phase grid tie inverter with instantaneous power control scheme is deeply researched [68].

A rotating frame is widely used in a three-phase system. It has many advantages such as a time invariant control variable, a zero state error at steady state, an easy filtering and a decoupling control of active and reactive power. To use these advantages in a single-phase system, recently, a new rotating frame method for a single-phase is proposed in [64]. To implement these schemes, imaginary variables shifted by $\frac{\pi}{2}$ must be obtained instantaneously which is called as Orthogonal Signal Generation (OSG).

The control of three-phase power converters in the *qd* rotating reference frame is now a matured and well-developed research topic. However, for single-phase converters, it is not as well established as three-phase applications. The main reason behind this lies partly in its more complex structure than the conventional stationary reference frame controller and also a secondary orthogonal signal that is needed to implement a single-phase controller in the *qd* reference frame. The different orthogonal signal generation (OSG) techniques are reviewed first by several authors, and their advantages and limitations are examined [67]. Then, the most suitable OSG technique for this study is selected. The structure of the suggested *qd* reference frame control is introduced afterward. Finally, based on a mathematical analysis, the stationary reference frame equivalent of the suggested control system is derived, which significantly simplifies the stability analysis and the controller parameter design.

The modeling equations of single phase multi string multilevel converter are transformed into qd reference frame using harmonic balance technique. The modeling using harmonic balance technique is presented in this chapter and the controller design to control active and reactive power will be presented in next chapter.

## 8.2 Topology and the design of LCL filter

The topology of a single phase multi string nine level Inverter can be seen in Figure 8.1, where $S_{ip}, S_{im}, S_{in}, S_{io}$ and $S_{ir}$ are the switching functions of switches $T_{ip}, T_{im}, T_{in}, T_{io}$ and $T_{ir}$, $i = a, b$ respectively. $V_1, V_2, V_3,$ and $V_4$ are input DC sources and $I_{s1}, I_{s2}, I_{s3},$ and $I_{s4}$ are respective input currents.

Figure 8.1: Topology of single phase multi string nine level inverter connected to grid with LCL filter.

The multi-level inverter is connected to the grid through a LCL filter while controlling active and reactive power going into the grid $V_g$ with $L_1$ as the inductor on the inverter side and current $I_1$ passing through it and $L_2$ as the inductor on the grid side with current $I_2$ passing through it.

## 8.2.1    Design of LCL filter

LCL filters have been used in grid-connected inverters and pulse width-modulated (PWM) active rectifiers, because they minimize the amount of current distortion injected into the

199

utility grid. LCL filters have good performances in current ripple attenuations, but they introduce a resonance frequency in the system. Besides L-filters, LCL-filters are used for the grid connection. LCL-filters give advantages in costs and dynamic as smaller inductors can be used compared to L-filters in order to achieve the necessary damping of the switching harmonics. As a drawback the filters tend to oscillations with the filter resonance frequency. The several methods for the design of LCL filters are presented in [76], [77], [78], [79], [80], and [81].

***Procedure (Limits on the filter parameters):***

- The value of the capacitance is limited by the decrease of the power factor, that has to be less than 5% at the rated power;

- The total value of the filter inductance has to be less than 0.1 p.u. for low power filters. However, for high power levels, the main aim is to avoid the saturation of the inductors;

- The resonance frequency of the filter should be higher than 10 times the grid frequency and half of the switching frequency.

***Calculation of the filter values:***

A step by step procedure to obtain the parameters of LCL filter design under the conditions given in table 8.1 [79].

Base impedance $Z_b = \dfrac{V_g^{\,2}}{P} = 8.066\Omega$

Upper limit base capacitance $C_b = 5\% \dfrac{P_{rated}}{V_g^{\,2}\omega_s} = 16.44\,\mu F$

1. The capacitor value 'C' is limited to decrease the capacitive reactive power at rated load to less than 5%. The percentage that is chosen randomly as 1.69%.

Therefore

$$C = 1.69\% \frac{P_{rated}}{V_g^2 \omega_s} = 5.55\mu F$$

The reference peak current can be found out as $I_{ref} = \frac{P_{rated}}{V} = 19.28A$

1. Choose a tolerable current ripple on the inverter side:

$$15\% \leq \frac{\Delta I_1}{I_{ref}} = \frac{V_{dc}}{4L_1 f_s I_{ref}} \leq 40\%$$

where $\Delta I_1$ is the inverter side current ripple.

Current ripple is chosen as 16.91%. Calculating $L_1$ based on the above equation.

$$L_1 = 2.3mH$$

2. The resonant frequency $f_r$ or $\omega_r$ should be in a range between ten times the line frequency and one half of the switching frequency in order to not create resonance problems in the lower and higher parts of the harmonic spectrum.

Table 8.1 Parameters for the calculation of filter values

| Switching frequency | $f_{sw} = 5kHz$ |
|---|---|
| Rated Power | $P_{rated} = 1500W$ |
| Input DC voltage | $V_{dc} = 150V$ |
| Grid voltage | $V_g = 110V$ |
| Frequency of the grid voltage | 60Hz |
| Resonant frequency | $f_r = 2kHz$ |

201

Table 8.2 Derived filter parameters

| Inverter side Inductance | $L_1 = 2.3mH$ |
|---|---|
| Capacitance | $C = 5.55\mu F$ |
| Grid side Inductance | $L_2 = 2.3mH$ |

So the resonant frequency should be between $600 < f_r < 2.5kHz$.

The resonant frequency is chosen as 2kHz in order to find $L_2$.

The expression for resonant frequency can be found using the impedances of $L_1$, $L_2$ and $C_f$. The resonance frequency is the frequency for which $Z_1 \, // \, Z_C \, // \, Z_2$ is purely real, i.e., set the imaginary part of $Z_1 \, // \, Z_C \, // \, Z_2$ equal to zero and solve for the frequency.

$$f_r = \frac{1}{2\pi} \sqrt{\frac{L_1 + L_2}{L_1 L_2 C_f}}$$

$L_2 = 2.3mH$ .

The final parameters of the filter are given in table 8.2.

### 8.2.2 Determination of Transfer Function

The transfer function of LCL filter is determined to plot the bode plot and to check the resonant frequency.

$$V_{ab} = L_1 p I_1 + V_c \tag{8.1}$$

$$\Rightarrow V_{ab}(s) = L_1 s I_1(s) + V_c(s) \qquad (8.2)$$

Similarly $CpV_c = I_1 - I_2$ $\qquad (8.3)$

$$\Rightarrow CsV_c(s) = I_1(s) - I_2(s) \qquad (8.4)$$

And $V_c = L_2 pI_2 + V_g$ $\qquad (8.5)$

$$\Rightarrow V_c(s) = L_2 s I_2(s) + V_g(s) \qquad (8.6)$$

$$\Rightarrow L_2 s I_2(s) = V_c(s) - V_g(s)$$

$$\Rightarrow I_2(s) = \frac{V_c(s) - V_g(s)}{L_2 s}$$

From (8.4),

$$CsV_c(s) = I_1(s) - \frac{V_c(s) - V_g(s)}{L_2 s}$$

$$\Rightarrow CsV_c(s) = I_1(s) - \frac{V_c(s)}{L_2 s} + \frac{V_g(s)}{L_2 s}$$

$$\Rightarrow \left( Cs + \frac{1}{L_2 s} \right) V_c(s) = I_1(s) + \frac{V_g(s)}{L_2 s}$$

$$\Rightarrow V_c(s) = \frac{I_1(s) + \dfrac{V_g(s)}{L_2 s}}{Cs + \dfrac{1}{L_2 s}} \qquad (8.7)$$

From (8.2),

$$V_{ab}(s) = L_1 s I_1(s) + \frac{I_1(s) + \dfrac{V_g(s)}{L_2 s}}{Cs + \dfrac{1}{L_2 s}}$$

$$\Rightarrow V_{ab}(s) = L_1 s I_1(s) + \frac{s L_2 I_1(s) + V_g(s)}{L_2 C s^2 + 1}$$

$$\Rightarrow V_{ab}(s) = \frac{(L_2 C s^2 + 1) L_1 s I_1(s) + s L_2 I_1(s)}{L_2 C s^2 + 1} + \frac{V_g(s)}{L_2 C s^2 + 1}$$

$$\Rightarrow V_{ab}(s) = \frac{(L_1 s L_2 C s^2 + L_1 s) + s L_2}{L_2 C s^2 + 1} I_1(s) + \frac{V_g(s)}{L_2 C s^2 + 1}$$

$$\Rightarrow V_{ab}(s) = \frac{L_1 L_2 C s^3 + (L_1 + L_2) s}{L_2 C s^2 + 1} I_1(s) + \frac{V_g(s)}{L_2 C s^2 + 1}$$

The transfer function $\dfrac{I_1(s)}{V_{ab}(s)} = \dfrac{L_2 C s^2 + 1}{L_1 L_2 C s^3 + (L_1 + L_2) s}, \dfrac{I_s(s)}{V_g(s)} = \dfrac{1}{L_1 L_2 C s^3 + (L_1 + L_2) s}$ (8.8)

The design of filter parameters can follow the basic guideline of attenuating the switching current harmonics through two inductors. The Bode plot of the LCL filter without damping is shown in Figure 8.2. From the Figure 8.2, the current is easily resonated at the natural resonance frequency. The insertion of a series resistance with the capacitor eliminates the gain spike, smoothes the overall response. It is possible to observe in this Bode diagram that the closed loop bandwidth must be within 2000 Hz when the phase shift is around -90°. At the resonant frequency of 2 kHz, the magnitude of the output current will be decreasing at a higher slope than before and the phase difference will be changed from -90° to +90°.
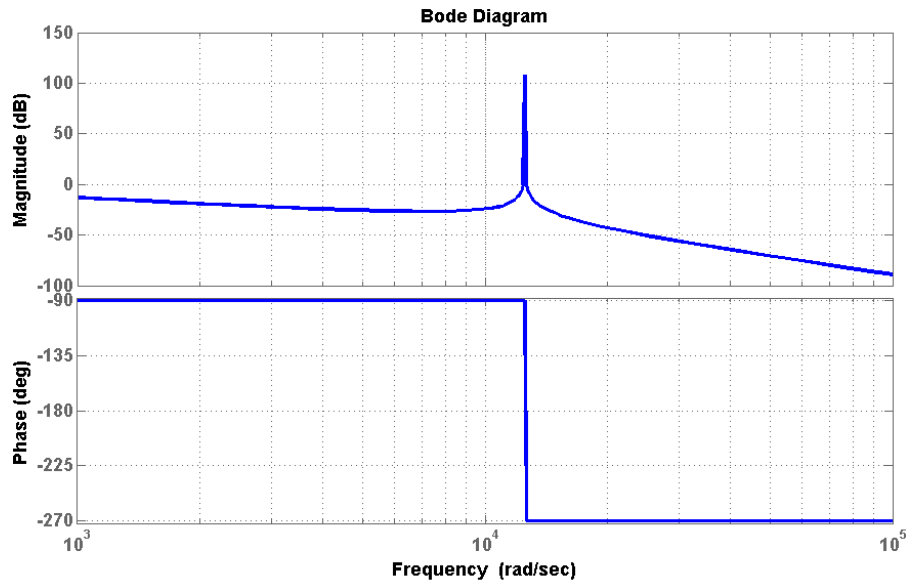
(a)

Figure 8.2 Bode plot for transfer function of $\frac{I_S(s)}{V_g(s)}$

## 8.3 Harmonic Balance Technique

The definition and application of HBT was presented in the early 1937 named by the Ukrainian scientists Kryloff and Bogoliuboff [82]. J.C. Lindenlaub presented a new approach of using HBT to acquire the sinusoidal steady state response of nonlinear system [83]. A more advanced and improved HBT was introduced by M. S. Nakhla and J. Vlach [84], [85].

HBT is a technique for the numerical solution of nonlinear analog circuits operating in the periodic regime. It is an efficient method for the simulation of the steady state response. HBT (also called the describing function method) is critical for the application of frequency response

of nonlinear system. The method uses frequency domain (Fourier series) techniques to decompose the system into two separate subsystems, a linear and a non-linear part.

### 8.3.1 Dynamic Equations

The dynamic equations of the system are given below.

$$V_{ab} = V_1(S_{am} - S_{ap}) + V_2(S_{am} - S_{an}) + V_3(S_{ao} - S_{an}) + V_4(S_{ao} - S_{ar}) \tag{8.9}$$

$$V_1(S_{am} - S_{ap}) + V_2(S_{am} - S_{an}) + V_3(S_{ao} - S_{an}) + V_4(S_{ao} - S_{ar}) = R_1 I_1 + L_1 p I_1 + V_c \tag{8.10}$$

$$Cp V_c = I_1 - I_2 \tag{8.11}$$

$$V_c = R_2 I_2 + L_2 p I_2 + V_g \tag{8.12}$$

By using Harmonic Balance Technique in equations (8.9-8.12), the state variables and switching functions are assumed to have average components and ripple quantities individually as below. The Fourier series analysis to find the average and ripple quantities are derived in Appendix E.

$$V_g = \mathrm{Re}(V_{gg} e^{j\theta_e})$$

$$V_c = \mathrm{Re}(V_{cc} e^{j\theta_e})$$

$$I_1 = \mathrm{Re}(I_{11} e^{j\theta_e})$$

$$I_2 = \mathrm{Re}(I_{22} e^{j\theta_e})$$

$$V_1 = \mathrm{Re}(V_{d1} + V_{11} e^{j2\theta_e})$$

$$V_2 = \mathrm{Re}(V_{d2} + V_{22} e^{j2\theta_e})$$

$$V_3 = \mathrm{Re}(V_{d3} + V_{33} e^{j2\theta_e})$$

$$V_4 = \text{Re}\left(V_{d4} + V_{44}e^{j2\theta_e}\right)$$

$$D_1 = \text{Re}\left(M_1e^{j\theta_e}\right)$$

$$D_2 = \text{Re}\left(M_2e^{j\theta_e}\right)$$

The main expression that will be used in the derivations of fundamental and ripple components in harmonic balance technique of the rectifier is given as

$$\text{Re}(Z_1).\text{Re}(Z_2) = \frac{1}{2}\text{Re}(Z_1.Z_2) + \frac{1}{2}\text{Re}\left(Z_1.Z_2^*\right) \tag{8.13}$$

Equation (8.9) implies

$$L_1 \text{Re}\left(pI_{11} + j\omega_e I_{11}\right)e^{j\theta_e} = \left\{ \begin{matrix} (V_{d1})\text{Re}\left(M_1e^{j\theta_e}\right) + (V_{d4})\text{Re}\left(M_2e^{j\theta_e}\right) - R_1\,\text{Re}\left(I_{11}e^{j\theta_e}\right) \\ \frac{1}{2}\text{Re}\left((V_{11})M_1e^{j3\theta_e}\right) + \frac{1}{2}\text{Re}\left((V_{11})M_1^*e^{j\theta_e}\right) \\ + \frac{1}{2}\text{Re}\left((V_{44})M_2e^{j3\theta_e}\right) + \frac{1}{2}\text{Re}\left((V_{44})M_2^*e^{j\theta_e}\right) \end{matrix} \right\} - \text{Re}\left(V_{cc}e^{j\theta_e}\right)$$

Comparing left hand side and right hand side of equations

$$L_1\left(pI_{11} + j\omega_e I_{11}\right) = \begin{bmatrix} (V_{d1})M_1 + (V_{d4})M_2 + \frac{1}{2}(V_{11} + V_{22})M_1^* \\ + \frac{1}{2}(V_{33} + V_{44})M_2^* - R_1I_{11} - V_{cc} \end{bmatrix} \tag{8.14}$$

$$\frac{1}{2}(V_{11})M_1 + \frac{1}{2}(V_{44})M_2 = 0 \tag{8.15}$$

Equation (8.10) implies

$$CpV_c = I_1 - I_2$$

$$Cp\,\text{Re}\left(V_{cc}e^{j\theta_e}\right) = \text{Re}\left(I_{11}e^{j\theta_e}\right) - \text{Re}\left(I_{22}e^{j\theta_e}\right)$$

$$C\,\text{Re}\left(pV_{cc} + j\omega_e V_{cc}\right)e^{j\theta_e} = \text{Re}\left(I_{11}e^{j\theta_e}\right) - \text{Re}\left(I_{22}e^{j\theta_e}\right)$$

$$C(pV_{cc} + j\omega_e V_{cc}) = I_{11} - I_{22} \tag{8.16}$$

Equation (8.11) implies

$$L_2 pI_2 = V_c - R_2 I_2 - V_g$$

$$L_2 p \operatorname{Re}\!\left(I_{22} e^{j\theta_e}\right) = \operatorname{Re}\!\left(V_{cc} e^{j\theta_e}\right) - R_2 \operatorname{Re}\!\left(I_{22} e^{j\theta_e}\right) - \operatorname{Re}\!\left(V_{gg} e^{j\theta_e}\right)$$

$$L_2 \operatorname{Re}\!\left(pI_{22} + j\omega_e I_{22}\right) e^{j\theta_e} = \operatorname{Re}\!\left(V_{cc} e^{j\theta_e}\right) - R_2 \operatorname{Re}\!\left(I_{22} e^{j\theta_e}\right) - \operatorname{Re}\!\left(V_{gg} e^{j\theta_e}\right)$$

$$L_2 \left(pI_{22} + j\omega_e I_{22}\right) = V_{cc} - R_2 I_{22} - V_{gg} \tag{8.17}$$

The dynamic equations after doing the harmonic balance technique are

$$L_1\left(pI_{11} + j\omega_e I_{11}\right) = \begin{bmatrix} \left(V_{d1}\right)M_1 + \left(V_{d4}\right)M_2 + \dfrac{1}{2}\left(V_{11} + V_{22}\right)M_1{}^* \\[2mm] + \dfrac{1}{2}\left(V_{33} + V_{44}\right)M_2{}^* - R_1 I_{11} - V_{cc} \end{bmatrix} \tag{8.18}$$

$$\frac{1}{2}\left(V_{11}\right)M_1 + \frac{1}{2}\left(V_{44}\right)M_2 = 0 \tag{8.19}$$

$$C\left(pV_{cc} + j\omega_e V_{cc}\right) = I_{11} - I_{22} \tag{8.20}$$

$$L_2\left(pI_{22} + j\omega_e I_{22}\right) = V_{cc} - R_2 I_{22} - V_{gg} \tag{8.21}$$

### 8.3.2 Steady State Analysis

In the steady state, the state variables remain constant. Hence, the rate of change of each state variable with respect to time is zero, which means the derivative terms are equal to zero.

Let $M_1 = M_{q1} + jM_{d1}$, $M_2 = M_{q2} + jM_{d2}$, $I_{11} = I_{q1} + jI_{d1}$, $I_{22} = I_{q2} + jI_{d2}$, $V_{cc} = V_{qc} + jV_{dc}$,

$V_{gg} = V_{qg} + jV_{dg}$

Equating the derivative terms to zero, the steady state equations are

$$j\omega_e L_1 I_{11} == \begin{bmatrix} (V_{d1})M_1 + (V_{d4})M_2 + \dfrac{1}{2}(V_{11}+V_{22})M_1^* \\ + \dfrac{1}{2}(V_{33}+V_{44})M_2^* - R_1 I_{11} - V_{cc} \end{bmatrix} \qquad (8.22)$$

$$\frac{1}{2}(V_{11})M_1 + \frac{1}{2}(V_{44})M_2 = 0 \qquad (8.23)$$

$$jC\omega_e V_{cc} = I_{11} - I_{22} \qquad (8.24)$$

$$jL_2\omega_e I_{22} = V_{cc} - R_2 I_{22} - V_{gg} \qquad (8.25)$$

$$V_{dg}I_{q2} - V_{qg}I_{d2} = Q_g \qquad (8.26)$$

Equation (8.22) implies

$$j\omega_e L_1 I_{11} = \begin{bmatrix} (V_{d1})M_1 + (V_{d4})M_2 + \dfrac{1}{2}(V_{11}+V_{22})M_1^* \\ + \dfrac{1}{2}(V_{33}+V_{44})M_2^* - R_1 I_{11} - V_{cc} \end{bmatrix}$$

$$\begin{bmatrix} j\omega_e L_1 I_{q1} \\ -\omega_e L_1 I_{d1} \end{bmatrix} = \begin{bmatrix} M_{q1}(V_{d1}+V_{d2}) + jM_{d1}(V_{d1}+V_{d2}) + (V_{d3}+V_{d4})M_{q2} + jM_{d2}(V_{d3}+V_{d4}) - R_1 I_{q1} - jR_1 I_{d1} \\ + \dfrac{M_{q1}}{2}(V_{11}+V_{22}) - j\dfrac{M_{d1}}{2}(V_{11}+V_{22}) + \dfrac{M_{q2}}{2}(V_{33}+V_{44}) - j\dfrac{M_{d2}}{2}(V_{33}+V_{44}) - (V_{qc}+jV_{dc}) \end{bmatrix}$$

Comparing real and imaginary parts

$$\omega_e L_1 I_{d1} + M_{q1}(V_{d1}+V_{d2}) + (V_{d3}+V_{d4})M_{q2} + \frac{M_{q1}}{2}(V_{11}+V_{22}) + \frac{M_{q2}}{2}(V_{33}+V_{44}) - R_1 I_{q1} - V_{qc} = 0 \qquad (8.27)$$

$$\omega_e L_1 I_{q1} - M_{d1}(V_{d1}+V_{d2}) - M_{d2}(V_{d3}+V_{d4}) + \frac{M_{d1}}{2}(V_{11}+V_{22}) + \frac{M_{d2}}{2}(V_{33}+V_{44}) + R_1 I_{q1} + V_{dc} = 0 \qquad (8.28)$$

Equation (8.23) implies

$$\frac{1}{2}(V_{11}+V_{22})M_1 + \frac{1}{2}(V_{33}+V_{44})M_2 = 0$$

$$\frac{1}{2}(V_{11}+V_{22})(M_{q1}+jM_{d1}) + \frac{1}{2}(V_{33}+V_{44})(M_{q2}+jM_{d2}) = 0$$

$$\frac{M_{q1}}{2}(V_{11} + V_{22}) + j\frac{M_{d1}}{2}(V_{11} + V_{22}) + \frac{M_{q2}}{2}(V_{33} + V_{44}) + j\frac{M_{d2}}{2}(V_{33} + V_{44}) = 0$$

Comparing real and imaginary parts

$$\frac{M_{q1}}{2}(V_{11} + V_{22}) + \frac{M_{q2}}{2}(V_{33} + V_{44}) = 0 \tag{8.29}$$

$$\frac{M_{d1}}{2}(V_{11} + V_{22}) + \frac{M_{d2}}{2}(V_{33} + V_{44}) = 0 \tag{8.30}$$

Equation (8.24) implies

$$jC\omega_e V_{cc} = I_{11} - I_{22}$$

$$jC\omega_e(V_{qc} + jV_{dc}) = I_{q1} + jI_{d1} - (I_{q2} + jI_{d2})$$

$$jC\omega_e V_{qc} - C\omega_e V_{dc} = I_{q1} + jI_{d1} - I_{q2} - jI_{d2}$$

Comparing real and imaginary parts

$$I_{q1} - I_{q2} + C\omega_e V_{dc} = 0 \tag{8.31}$$

$$C\omega_e V_{qc} - I_{d1} + I_{d2} = 0 \tag{8.32}$$

Equation (8.25) implies

$$jL_2\omega_e I_{22} = V_{cc} - R_2 I_{22} - V_{gg}$$

$$jL_2\omega_e(I_{q2} + jI_{d2}) = (V_{qc} + jV_{dc}) - R_2(I_{q2} + jI_{d2}) - (V_{qg} + jV_{dg})$$

$$jL_2\omega_e I_{q2} - L_2\omega_e I_{d2} = V_{qc} + jV_{dc} - R_2 I_{q2} - jR_2 I_{d2} - V_{qg} - jV_{dg}$$

Comparing real and imaginary parts

$$V_{qc} - R_2 I_{q2} - V_{qg} + L_2\omega_e I_{d2} = 0 \tag{8.33}$$

$$L_2\omega_e I_{q2} - V_{dc} + R_2 I_{d2} + V_{dg} = 0 \tag{8.34}$$

Equation (8.26) implies

$$V_{dg}I_{q2} - V_{qg}I_{d2} = Q_g \qquad (8.35)$$

Equations (8.27-8.35) are the 9 steady state equations with 10 unknowns $M_{q1}, M_{d1}, M_{q2}, M_{d2}, I_{q1}, I_{d1}, I_{q2}, I_{d2}, V_{qc}, V_{dc}$. A constraint to make the phase angle between two modulation signals to be $180^\circ$ is added.

$$\tan^{-1}\left(\frac{M_{d1}}{M_{q1}}\right) = \pi + \tan^{-1}\left(\frac{M_{d2}}{M_{q2}}\right)$$

$$\left(\frac{M_{d1}}{M_{q1}}\right) = \tan\left(\pi + \tan^{-1}\left(\frac{M_{d2}}{M_{q2}}\right)\right)$$

$$\left(\frac{M_{d1}}{M_{q1}}\right) = \tan\left(\tan^{-1}\left(\frac{M_{d2}}{M_{q2}}\right)\right)$$

Therefore.

$$\frac{M_{d1}}{M_{q1}} = \frac{M_{d2}}{M_{q2}} \qquad (8.36)$$

$$\mathrm{sgn}(M_{d1}) = -\mathrm{sgn}(M_{d2}) \qquad (8.37)$$

The unknown steady state variables are plotted for different power factors when the active power is varied from 0 to 1kW. The parameters and the conditions that are used for plotting these steady state variables are given in table 8.3. The unknown parameters that are plotted are

$$M_1 = \sqrt{M_{q1}^2 + M_{d1}^2}, M_2 = \sqrt{M_{q2}^2 + M_{d2}^2}, I_1 = \sqrt{I_{q1}^2 + I_{d1}^2}, I_2 = \sqrt{I_{q2}^2 + I_{d2}^2}, V_c = \sqrt{V_{qc}^2 + V_{dc}^2}$$

Table 8.3 Parameters used to plot unknown steady state variables.

| | |
|---|---|
| Frequency of the grid | 60Hz |
| Magnitude of grid voltage | 1000V |

| | |
|---|---|
| Input DC voltages | 600V,600V,100V,100V |
| Active power | 0-1kW |
| Power factor | 0.4, 0.6, 0.8, 1.0 |
| Inverter side Inductor | $L_1 = 2.3mH$ |
| Capacitor capacitance | $C = 5.55\mu F$ |
| Grid side inductor | $L_2 = 2.3mH$ |
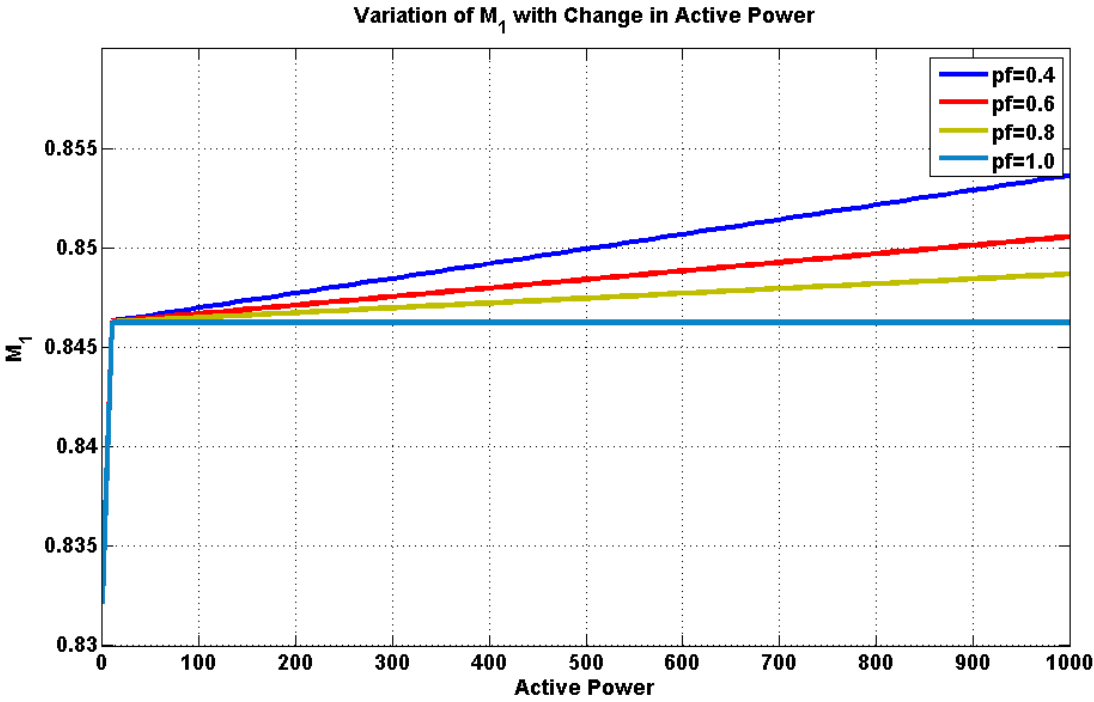


Figure 8.3 Variation of $M_1$ with the change in active power.
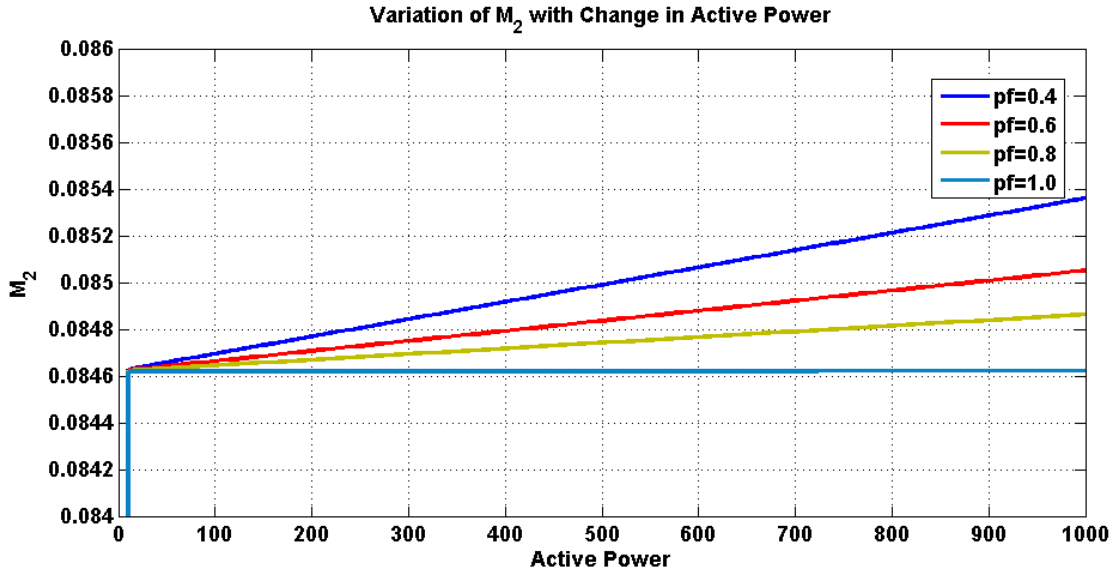
Figure 8.4 Variation of $M_2$ with the change in active power.
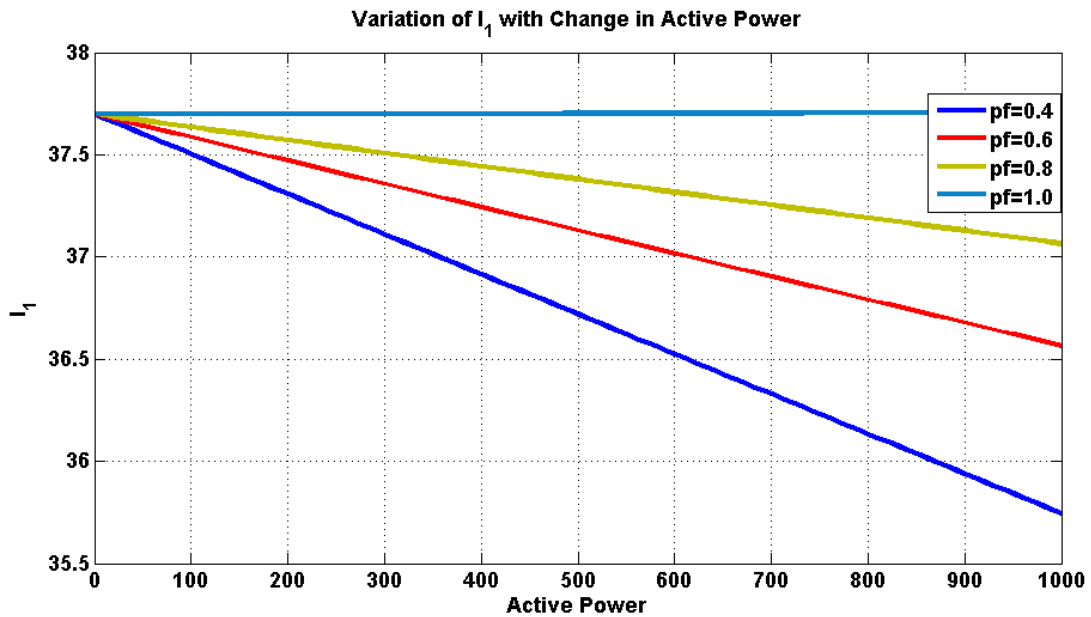


Figure 8.5 Variation of $I_1$ with the change in active power.

213
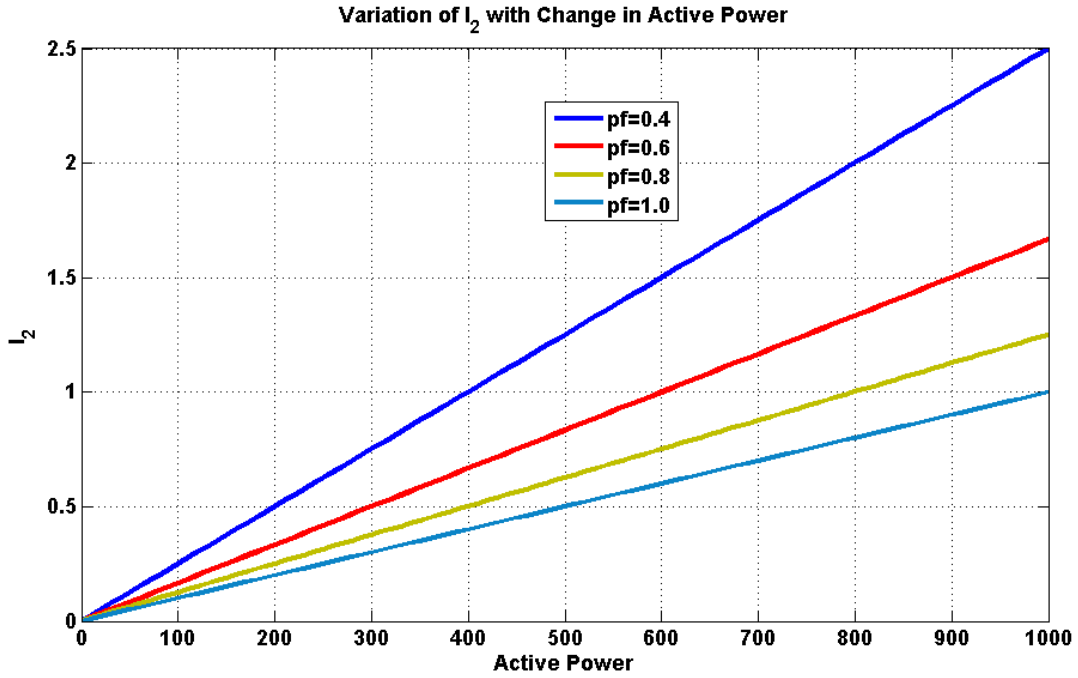
Figure 8.6 Variation of I₂ with the change in active power.
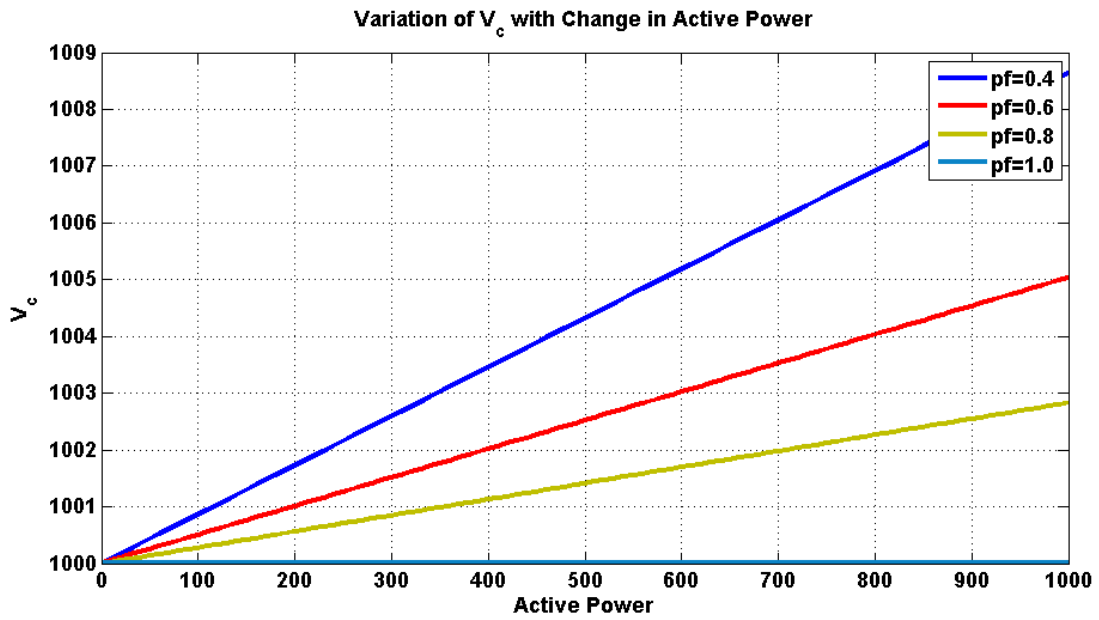


Figure 8.7 Variation of capacitor voltage with the change in active power.

214

## 8.4 Summary

The topology of single phase multi string nine-level inverter with an LCL filter connected to the grid is presented in this chapter. The LCL filter is designed and Bode plot of transfer function is plotted. The Harmonic Balance Technique to transfer the single phase system to qd synchronous reference frame is presented. The steady state analysis of the system is also performed. The unknown variables in the steady state analysis are plotted for different power factors with the change in active power.

# CHAPTER 9

## CONTROLLER DESIGN FOR MULTI STRING NINE LEVEL INVERTER CONNECTED TO THE GRID

### 9.1 Introduction

This chapter presents the controller designs of both the 'L' and 'LCL' filters of multistring nine-level inverter connected to the grid. The control schemes are designed in qd synchronous reference frame. As in every other grid connected control systems, this system also needs phase locked loop (PLL) control to synchronize the grid voltage and frequency to the filtered output voltage and frequency. A single phase PLL common to both the filters is set forth. The simulation results of both the filter types verify the proposed control schemes.
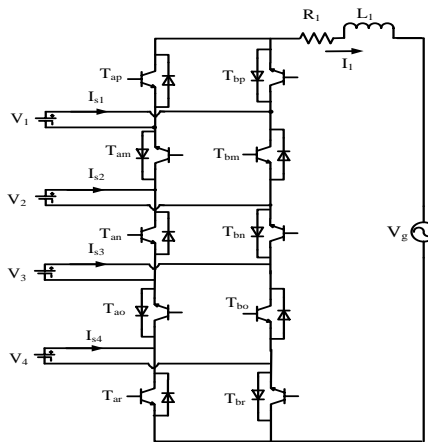


Figure 9.1 Topology of single phase multi string nine level inverter connected to grid with L filter
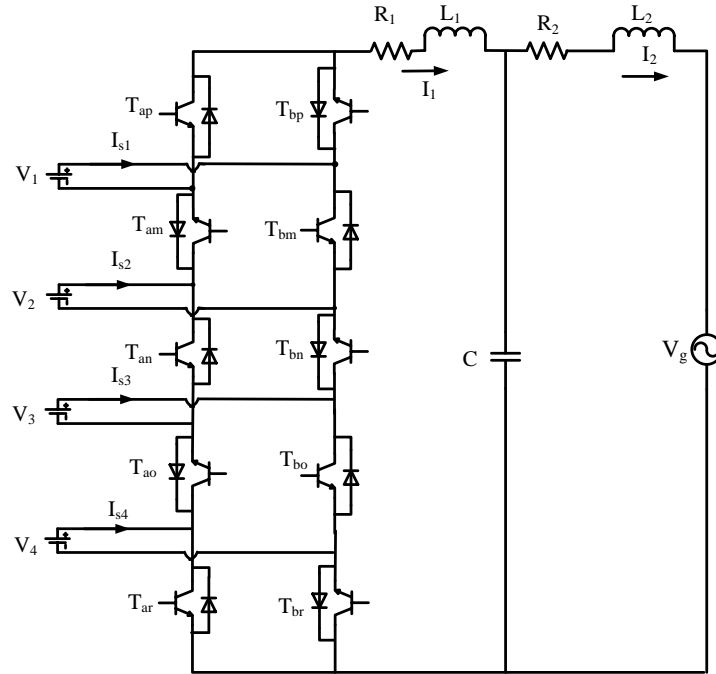
Figure 9.2: Topology of single phase multi string nine level inverter connected to grid with LCL

filter

The topologies of a single phase multi string nine level Inverter can be seen in Figure 9.1 and Figure 9.2, where $S_{ip}, S_{im}, S_{in}, S_{io}$ and $S_{ir}$ are the switching functions of switches $T_{ip}, T_{im}, T_{in}, T_{io}$ and $T_{ir}$, $i = a, b$ respectively. $V_1, V_2, V_3$, and $V_4$ are input DC sources and $I_{s1}, I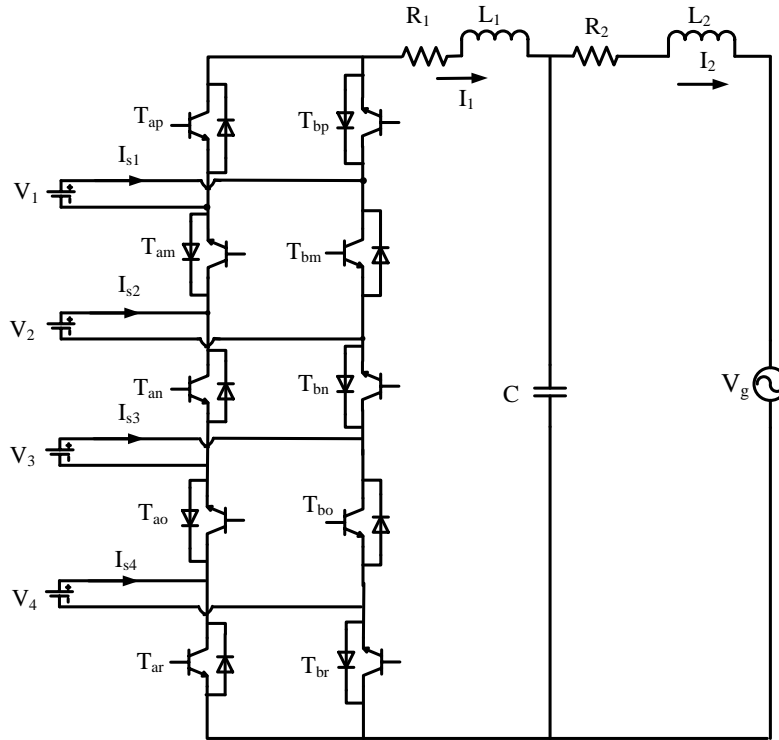_{s2}, I_{s3}$, and $I_{s4}$ are respective input currents. The multi-level inverter is connected to the grid through both L and LCL filters for controlling active and reactive power going into the grid $V_g$ with $L_1$ as the inductor on the inverter side and current $I_1$ passing through it and $L_2$ as the inductor on the grid side with current $I_2$ passing through it.

## 9.2 Single Phase PLL
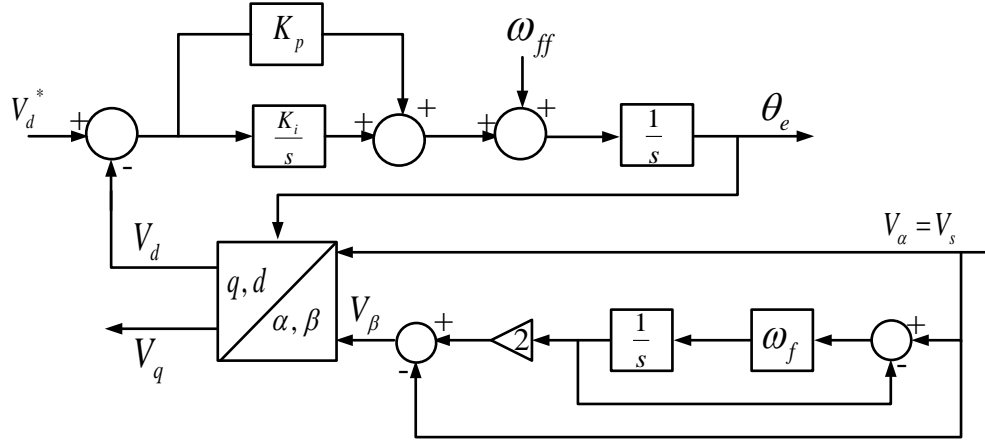


Figure 9.3 Single phase PLL control scheme.

As in every other grid connected controlled system, this system also need phase locked loop (PLL) control to synchronize the grid voltage and frequency to the filtered output voltage and frequency. The active and reactive power control schemes of single phase multi string multi-level converter with LCL filter connected to the grid are designed in *qd* synchronous reference frame. The transformation to *qd* synchronous reference frame from single phase is not well established as the Park's transformation requires a minimum of two orthogonal signals to transform. Hence, a fictitious orthogonal signal is generated using the APF (all pass filter) method to transfer the two signals into *qd* reference frame. Using the APF, a three phase *qd* phase locked loop (PLL) control scheme is applied to single phase.

The transfer function for all pass filter (APF) is given as

$$\frac{V_\beta}{V_\alpha} = \frac{\omega_f - p}{\omega_f + p} \tag{9.1}$$

218

$$\frac{V_\beta}{V_\alpha} = \frac{\omega_f + p - 2p}{\omega_f + p}$$

$$\frac{V_\beta}{V_\alpha} = 1 - \frac{2p}{\omega_f + p}$$

$$V_\beta(\omega_f + p) = V_\alpha(\omega_f + p) - 2pV_\alpha$$

$$V_\beta\omega_f + V_\beta p = \omega_f V_\alpha + pV_\alpha - 2pV_\alpha$$

$$(V_\alpha + V_\beta)p = \omega_f(V_\alpha - V_\beta) \tag{9.2}$$

If

$$\begin{bmatrix} V_q \\ V_d \end{bmatrix} = \begin{bmatrix} \cos\theta_e & \sin\theta_e \\ -\sin\theta_e & \cos\theta_e \end{bmatrix} \begin{bmatrix} V_\alpha \\ V_\beta \end{bmatrix} \tag{9.3}$$

$$\Rightarrow \begin{bmatrix} V_\alpha \\ V_\beta \end{bmatrix} = \begin{bmatrix} \cos\theta_e & -\sin\theta_e \\ \sin\theta_e & \cos\theta_e \end{bmatrix} \begin{bmatrix} V_q \\ V_d \end{bmatrix} \tag{9.4}$$

Therefore,

$$V_\alpha = V_q \cos\theta_e - V_d \sin\theta_e \tag{9.5}$$

$$V_\beta = V_q \sin\theta_e + V_d \cos\theta_e \tag{9.6}$$

Substituting (9.5) and (9.6) in (9.2)

$$(V_q \cos\theta_e - V_d \sin\theta_e + V_q \sin\theta_e + V_d \cos\theta_e)p = \omega_f(V_q \cos\theta_e - V_d \sin\theta_e - V_q \sin\theta_e - V_d \cos\theta_e) \tag{9.7}$$

$$(V_q(\cos\theta_e + \sin\theta_e) - V_d(\sin\theta_e - \cos\theta_e))p = \omega_f(V_q(\cos\theta_e - \sin\theta_e) - V_d(\sin\theta_e + \cos\theta_e))$$

$$(V_q(\cos\theta_e + \sin\theta_e) - V_d(\sin\theta_e - \cos\theta_e))p = \omega_f(V_q(\cos\theta_e - \sin\theta_e) - V_d(\sin\theta_e + \cos\theta_e))$$

$$(V_q(-\sin\theta_e + \cos\theta_e) - V_d(\cos\theta_e + \sin\theta_e))p\theta_e = \omega_f(V_q(\cos\theta_e - \sin\theta_e) - V_d(\sin\theta_e + \cos\theta_e))$$

$$(V_q(-\sin\theta_e + \cos\theta_e) - V_d(\sin\theta_e + \cos\theta_e))p\theta_e = \omega_f(V_q(\cos\theta_e - \sin\theta_e) - V_d(\sin\theta_e + \cos\theta_e))$$

$$p\theta_e\left(V_q\left(\cos\theta_e - \sin\theta_e\right) - V_d\left(\sin\theta_e + \cos\theta_e\right)\right) = \omega_f\left(V_q\left(\cos\theta_e - \sin\theta_e\right) - V_d\left(\sin\theta_e + \cos\theta_e\right)\right)$$

$$p\theta_e = \omega_f \tag{9.8}$$

Let $V_s = V_\alpha$ be the grid voltage. Therefore,

$$V_s = V_\alpha = V_m \cos(\omega_g t) \tag{9.9}$$

$$V_\beta = V_m \sin(\omega_g t) \tag{9.10}$$

Using $\alpha\beta$ to qd transformation

$$\begin{bmatrix} V_q \\ V_d \end{bmatrix} = \begin{bmatrix} \cos\theta_e & \sin\theta_e \\ -\sin\theta_e & \cos\theta_e \end{bmatrix} \begin{bmatrix} V_\alpha \\ V_\beta \end{bmatrix} \tag{9.11}$$

$$V_q = V_\alpha \cos\theta_e + V_\beta \sin\theta_e \tag{9.12}$$

$$V_d = -V_\alpha \sin\theta_e + V_\beta \cos\theta_e \tag{9.13}$$

Substituting for $V_\alpha, V_\beta$ in (9.11).

$$V_d = -V_m \cos(\omega_g t)\sin\theta_e + V_m \sin(\omega_g t)\cos\theta_e \tag{9.14}$$

$$V_d = V_m \sin(\omega_g t - \theta_e) \tag{9.15}$$

If $V_d = 0 \Rightarrow V_m \sin(\theta_e - \omega_g t) = 0 \tag{9.16}$

$$\sin(\theta_e - \omega_g t) = 0 \Rightarrow \theta_e = \omega_g t \tag{9.17}$$

Based on the block diagram of single phase PLL, the transfer function is given as

$$\left(\left[K_p + \frac{K_i}{p}\right]e + \omega_{ff}\right)\frac{1}{p} = \theta_g \tag{9.18}$$

$$\left(\left[K_p + \frac{K_i}{p}\right](0 - V_d) + \omega_{ff}\right)\frac{1}{p} = \theta_g \tag{9.19}$$

$$\left[K_p + \frac{K_i}{p}\right]\left(0 - V_m \sin(\omega_g t - \theta_e) + \omega_{ff}\right)\frac{1}{p} = \theta_g \tag{9.20}$$

$$\left[K_p + \frac{K_i}{p}\right]\left(0 - V_m \sin(\theta_g - \theta_e) + \omega_{ff}\right)\frac{1}{p} = \theta_g \tag{9.21}$$

If $\theta_g - \theta_e$ is small, then $\sin(\theta_g - \theta_e) = \theta_g - \theta_e$

$$\left[K_p + \frac{K_i}{p}\right]\left(-V_m(\theta_g - \theta_e) + \omega_{ff}\right)\frac{1}{p} = \theta_g \tag{9.22}$$

$$\left(-V_m(\theta_g - \theta_e) + \omega_{ff}\right)\frac{K_F}{p} = \theta_g$$

$$\left(-V_m\theta_g + V_m\theta_e + \omega_{ff}\right)K_F = p\theta_g$$

$$V_m\theta_e K_F = (p + K_F V_m)\theta_g - \omega_{ff}K_F$$

The transfer function $\dfrac{\theta_g}{\theta_e} = \dfrac{V_m K_F}{p + K_F V_m}$ \hfill (9.23)

$$\frac{\theta_g}{\theta_e} = \frac{V_m\left[K_P + \dfrac{K_I}{p}\right]}{p + \left[K_P + \dfrac{K_I}{p}\right]V_m}$$

$$\frac{\theta_g}{\theta_e} = \frac{V_m\left[pK_P + K_I\right]}{p^2 + \left[pK_P + K_I\right]V_m}$$

$$\frac{\theta_g}{\theta_e} = \frac{pK_P V_m + K_I V_m}{p^2 + pK_P V_m + K_I V_m} = \frac{2\xi\omega_{n1}p + \omega_{n1}^2}{p^2 + 2\xi\omega_{n1}p + \omega_{n1}^2} \tag{9.24}$$

$$K_P = \frac{2\xi\omega_{n1}}{V_m}; K_I = \frac{\omega_{n1}^2}{V_m} \tag{9.25}$$

where $\xi$ is the damping factor and is usually chosen as critical damping factor which is 0.707

$\omega_{n1}$ is the natural frequency and it is chosen as 377($rad/s$).
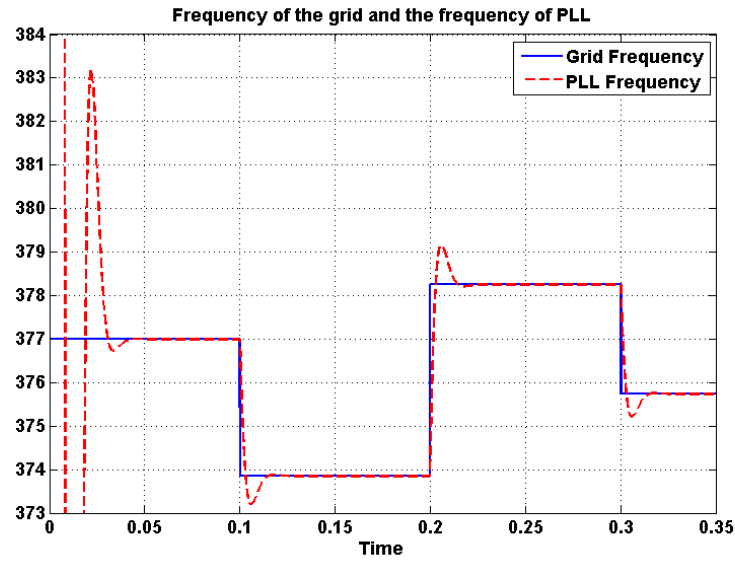


Figure 9.4 Simulation result of PLL frequency and grid frequency.
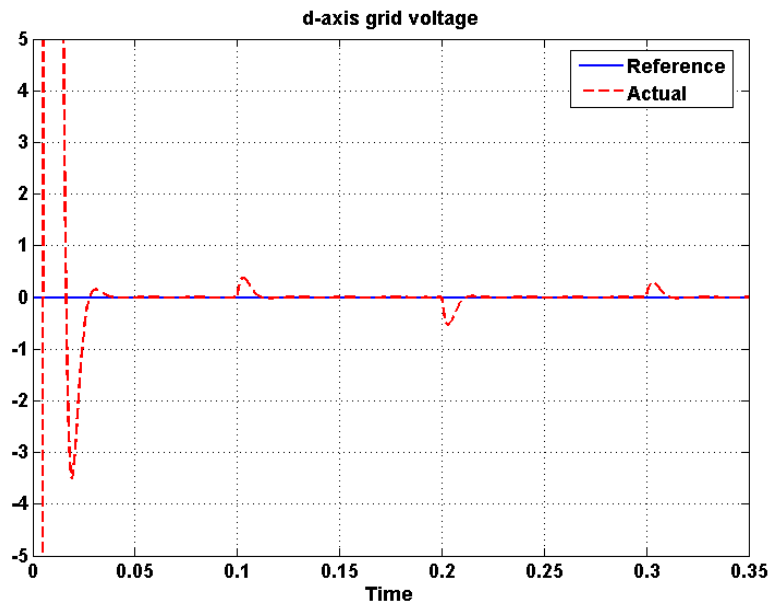


Figure 9.5 Simulation result of d-axis grid voltage
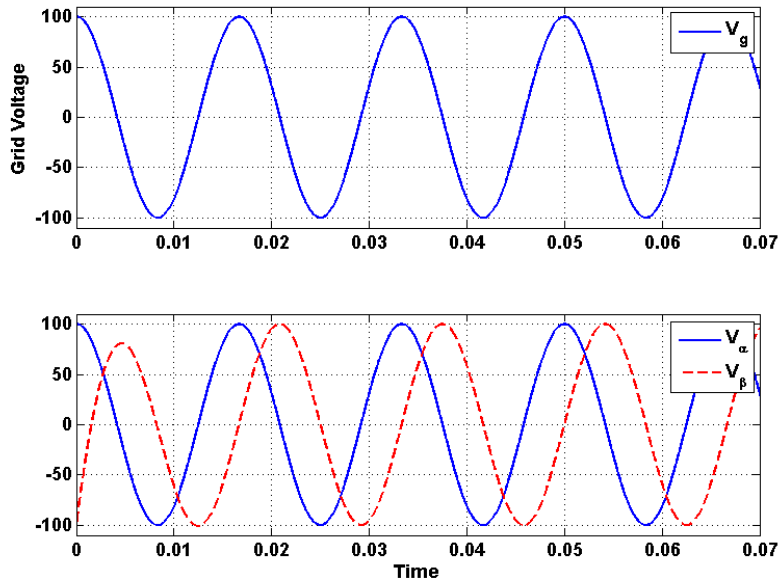
Figure 9.6 Simulation result of orthogonal signal generation using APF.
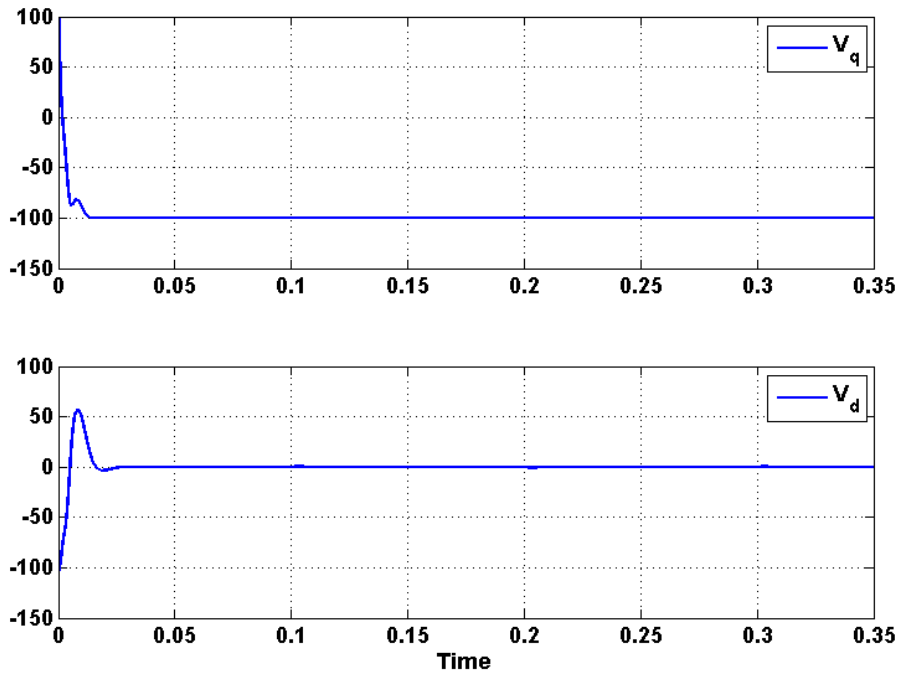


Figure 9.7 Simulation result of q and d axis grid voltages.
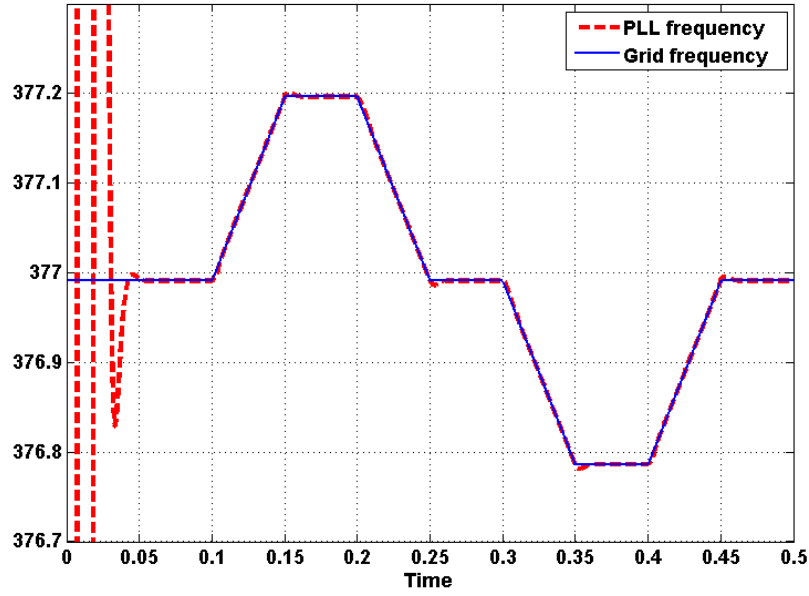
Figure 9.8 Simulation of PLL frequency and grid frequency plots for ramp reference.

## 9.3 Controller Design for Multi string Nine level Inverter connected to the grid through 'L' filter

The dynamic equations after doing the harmonic balance technique are

$$L_1 pI_{q1} - L_1 \omega_e I_{d1} = M_{q1} V_{d1} + M_{q2} V_{d4} + \frac{4}{\pi} (\sin(\theta - \psi_1))(V_{d2} + V_{d3}) - V_{qg} \tag{9.26}$$

$$L_1 pI_{d1} + L_1 \omega_e I_{q1} = M_{d1} V_{d1} + M_{d2} V_{d4} + \frac{4}{\pi} (\sin(\theta - \psi_1))(V_{d2} + V_{d3}) - V_{dg} \tag{9.27}$$

The expressions for active and reactive powers are given below.

$$P_g = V_{qg} I_{q1} + V_{dg} I_{d1} \tag{9.28}$$

$$Q_g = V_{dg} I_{q1} - V_{qg} I_{d1} \tag{9.29}$$

From the equations of active and reactive power,

$$I_{q1} = \frac{P_g V_{qg} + Q_g V_{dg}}{V_{qg}^2 + V_{dg}^2} \tag{9.30}$$

$$I_{d1} = \frac{P_g V_{dg} - Q_g V_{qg}}{V_{qg}^2 + V_{dg}^2} \tag{9.31}$$

### 9.3.1 Current controller design:

The dynamic equation for controller design in qd reference frame is given as

$$M_{qd1}V_{d1} + M_{qd2}V_{d4} + \frac{4}{\pi}\left(\sin(\theta - \psi_1)\right)(V_{d2} + V_{d3}) = R_1 I_{qd1} + L_1 p I_{qd1} + j L_1 \omega_e I_{qd1} + V_{qdg} \tag{9.32}$$

### 9.3.1.1 q-axis current control:

$$M_{q1}V_{d1} + M_{q2}V_{d4} + \frac{4}{\pi}\left(\sin(\theta - \psi_1)\right)(V_{d2} + V_{d3}) = L_1 p I_{q1} - \omega_e L_1 I_{d1} + V_{qg} \tag{9.33}$$

$$M_{q1}V_{d1} + M_{q2}V_{d4} + \frac{4}{\pi}\left(\sin(\theta - \psi_1)\right)(V_{d2} + V_{d3}) + \omega_e L_1 I_{d1} - V_{qg} = L_1 p I_{q1}$$

$$M_{q1}V_{d1} + M_{q2}V_{d4} + \frac{4}{\pi}\left(\sin(\theta - \psi_1)\right)(V_{d2} + V_{d3}) + \omega_e L_1 I_{d1} - V_{qg} = L_1 p I_{q1} = \sigma_{1q} = K_{1q}\left(I_{q1}^* - I_{q1}\right) \tag{9.34}$$

$$\frac{I_{q1}}{I_{q1}^*} = \frac{K_{1q}}{L_1 p + K_{1q}} \tag{9.35}$$

$$K_{1q} = K_{P1q} + \frac{K_{I1q}}{p} \tag{9.36}$$

$$\frac{I_{q1}}{I_{q1}^{*}} = \frac{K_{P1q} + \dfrac{K_{I1q}}{p}}{L_1 p + K_{P1q} + \dfrac{K_{I1q}}{p}}$$

$$\frac{I_{q1}}{I_{q1}^{*}} = \frac{p K_{P1q} + K_{I1q}}{L_1 p^2 + K_{P1q} p + K_{I1q}}$$

$$\frac{I_{q1}}{I_{q1}^{*}} = \frac{p K_{P1q} + K_{I1q}}{L_1 p^2 + K_{P1q} p + K_{I1q}} = \frac{2\xi\omega_{n1} p + \omega_{n1}^2}{p^2 + 2\xi\omega_{n1} p + \omega_{n1}^2} \tag{9.37}$$

$$K_{P1q} = 2\xi\omega_{n1} \, ; K_{I1q} = \omega_{n1}^2 \tag{9.38}$$

where $\xi$ is the damping factor and is usually chosen as critical damping factor which is 0.707

$\omega_{n1}$ is the natural frequency

### 9.3.1.2 d-axis current control:

$$M_{d1}V_{d1} + M_{d2}V_{d4} + \frac{4}{\pi}\big(\sin(\theta - \psi_1)\big)(V_{d2} + V_{d3}) = L_1 p I_{d1} + \omega_e L_1 I_{q1} + V_{dg} \tag{9.39}$$

$$M_{d1}V_{d1} + M_{d2}V_{d4} + \frac{4}{\pi}\big(\sin(\theta - \psi_1)\big)(V_{d2} + V_{d3}) - \omega_e L_1 I_{q1} - V_{dg} = L_1 p I_{d1}$$

$$M_{d1}V_{d1} + M_{d2}V_{d4} + \frac{4}{\pi}\big(\sin(\theta - \psi_1)\big)(V_{d2} + V_{d3}) - \omega_e L_1 I_{q1} - V_{dg} = L_1 p I_{d1} = \sigma_{1d} = K_{1d}\big(I_{d1}^{*} - I_{d1}\big) \tag{9.40}$$

$$\frac{I_{d1}}{I_{d1}^{*}} = \frac{K_{1d}}{L_1 p + K_{1d}} \tag{9.41}$$

$$K_{1d} = K_{P1d} + \frac{K_{I1d}}{p} \tag{9.42}$$

$$\frac{I_{d1}}{I_{d1}^{*}} = \frac{K_{P1d} + \dfrac{K_{I1d}}{p}}{L_1 s + K_{P1d} + \dfrac{K_{I1d}}{p}}$$

$$\frac{I_{d1}}{I_{d1}^{*}} = \frac{p K_{P1d} + K_{I1d}}{L_1 p^2 + K_{P1d} p + K_{I1d}}$$

$$\frac{I_{d1}}{I_{d1}^{*}} = \frac{p K_{P1d} + K_{I1d}}{L_1 p^2 + K_{P1d} p + K_{I1d}} = \frac{2\xi\omega_{n1} p + \omega_{n1}^2}{p^2 + 2\xi\omega_{n1} p + \omega_{n1}^2} \tag{9.43}$$

$$K_{P1d} = 2\xi\omega_{n1}; K_{I1d} = \omega_{n1}^2 \tag{9.44}$$

Where $\xi$ is the damping factor and is usually chosen as critical damping factor which is 0.707

$\omega_{n1}$ is the natural frequency

Therefore,

$$M_{q1}V_{d1} + M_{q2}V_{d4} + \frac{4}{\pi}\left(\sin(\theta - \psi_1)\right)(V_{d2} + V_{d3}) = \sigma_{1q} + V_{qg} - L_1\omega_e I_{d1} \tag{9.45}$$

$$M_{d1}V_{d1} + M_{d2}V_{d4} + \frac{4}{\pi}\left(\sin(\theta - \psi_1)\right)(V_{d2} + V_{d3}) = \sigma_{1d} + V_{dg} + L_1\omega_e I_{q1} \tag{9.46}$$

Therefore the final equations used for controlling active and reactive power going into the grid for multi string nine level inverter with 'L' filter are

$$I_{q1}^{*} = \frac{P_g^{*}V_{qg} + Q_g^{*}V_{dg}}{V_{qg}^2 + V_{dg}^2} \tag{9.47}$$

$$I_{d1}^{*} = \frac{P_g^{*}V_{dg} - Q_g^{*}V_{qg}}{V_{qg}^2 + V_{dg}^2} \tag{9.48}$$

$$M_{q1}V_{d1} + M_{q2}V_{d4} + \frac{4}{\pi}\left(\sin(\theta - \psi_1)\right)(V_{d2} + V_{d3}) = \sigma_{1q} + V_{qg} - L_1\omega_e I_{d1} \tag{9.49}$$

$$M_{d1}V_{d1} + M_{d2}V_{d4} + \frac{4}{\pi}\left(\sin(\theta - \psi_1)\right)\left(V_{d2} + V_{d3}\right) = \sigma_{1d} + V_{dg} + L_1\omega_e I_{q1} \tag{9.50}$$

$$M_{d1}{}^* M_{q2}{}^* = M_{d2}{}^* M_{q1}{}^* \tag{9.51}$$

The three equations that will be used to find the expressions for modulation indices are (9.49), (9.50) and (9.51). Since there are only three equations to find four unknowns, an equation is used to limit the modulation indices. The fourth equation is given in (9.52).

$$M_{d1} = \alpha M_{d2} \tag{9.52}$$
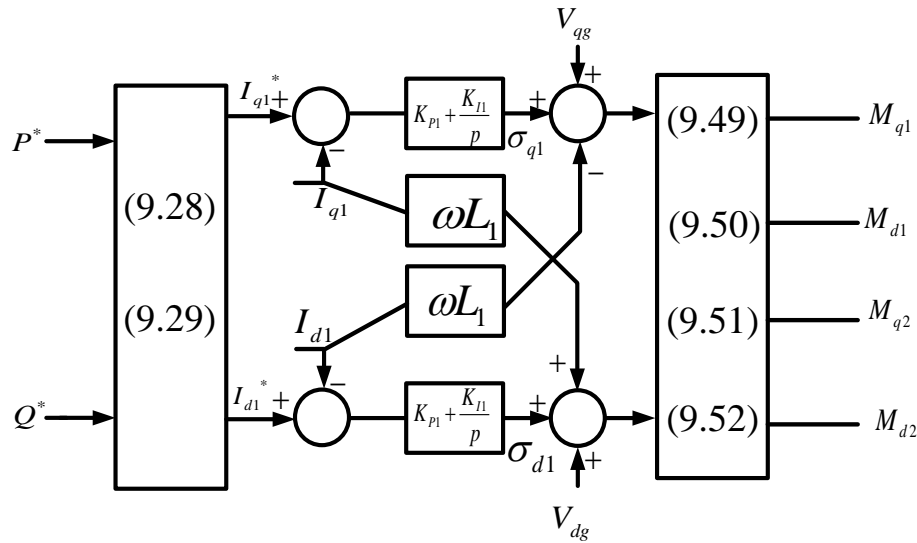


Figure 9.9 Control scheme of multi string nine level inverter connected to the grid through 'L' filter.
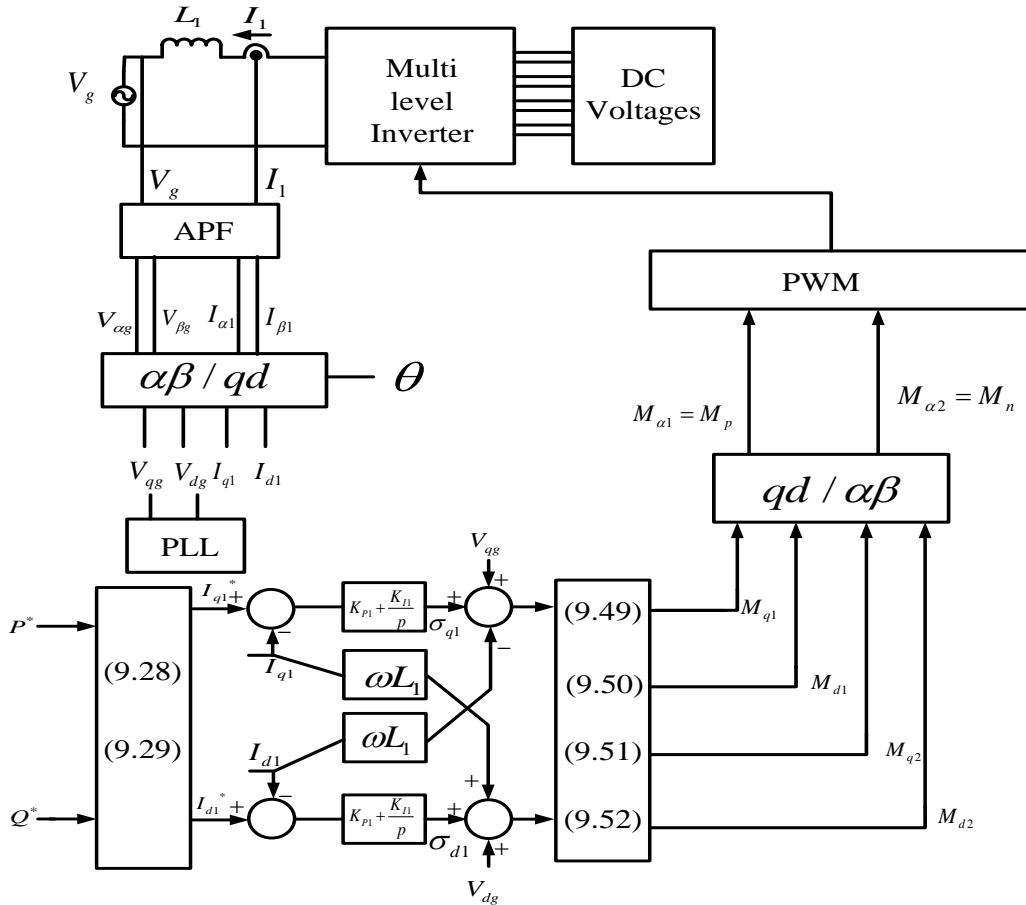
Figure 9.10 Overall control scheme.

## 9.4 Simulation Results with 'L' filter

The active and reactive powers are maintained at 1000W and 0Var for 0.2seconds. The reactive

power is changed from 0Var to 600Var at 0.2 seconds. Similarly, the active power is changed

from 1kW to 2kW at 0.4seconds. The main objective of changing the active and reactive powers

in a step response is to verify the control scheme. From the figure 9.11, the tracking of the

control scheme tracks the reference waves perfectly, which verifies the proposed control scheme.
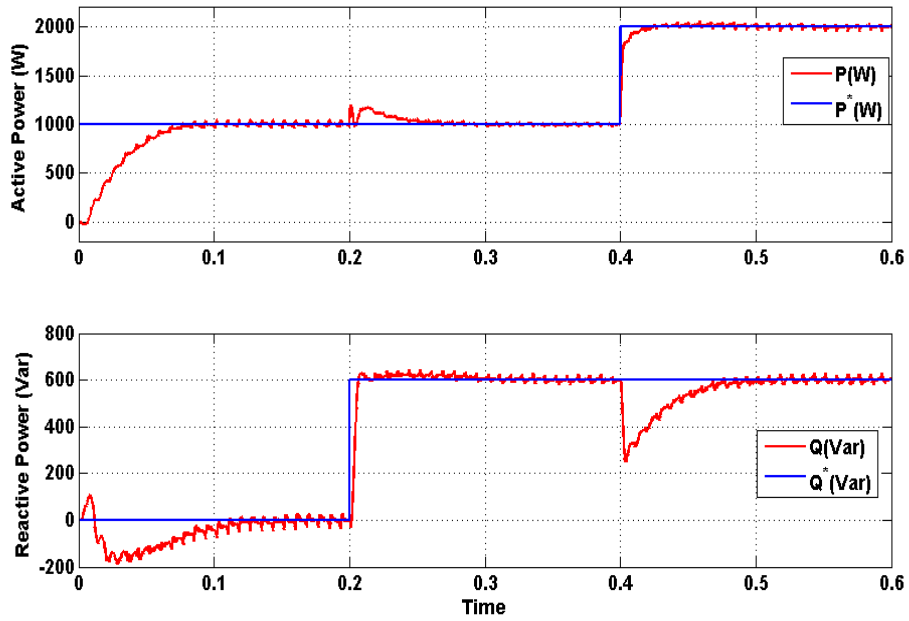
Figure 9.11 Simulation results of reference and actual waveforms of Active and Reactive

powers.
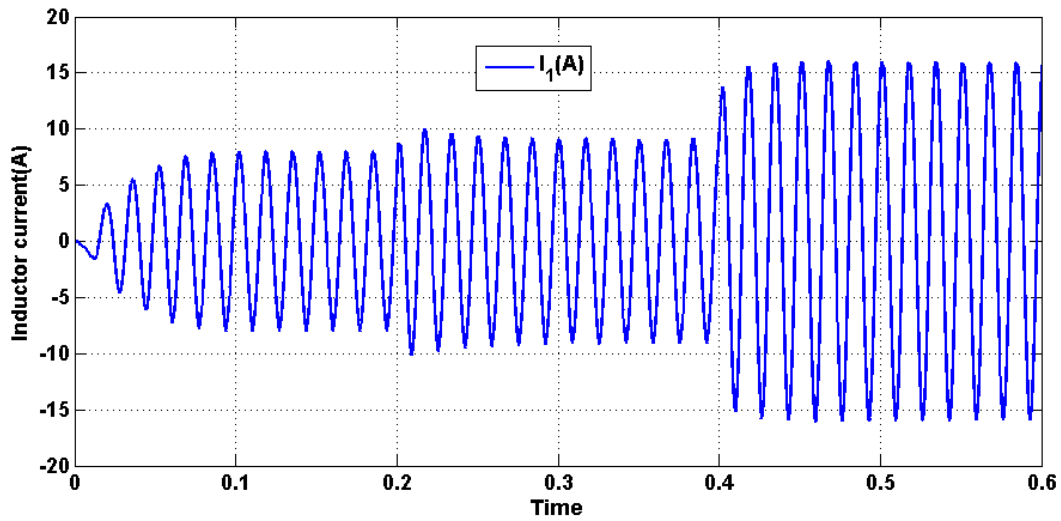


Figure 9.12 Simulation result of output current of Inverter
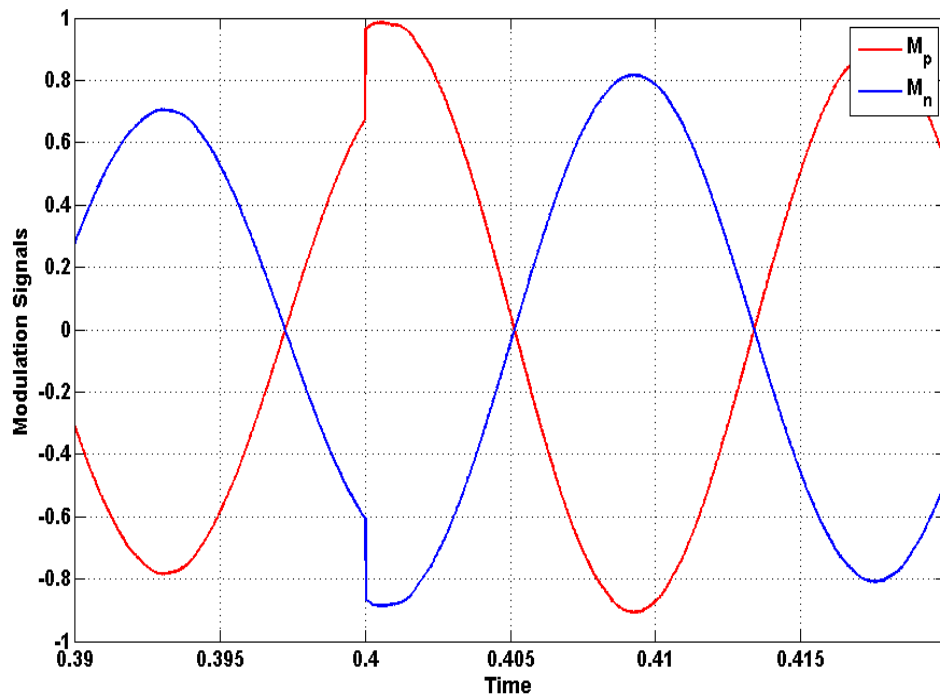
Figure 9.13 Simulation result of calculated Modulation signals
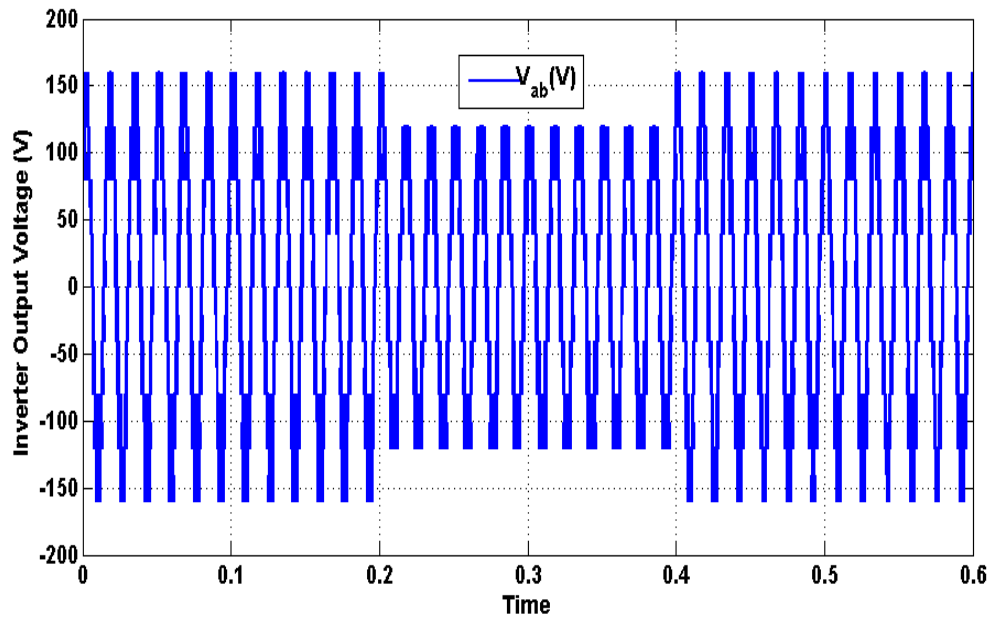


Figure 9.14 Simulation of output voltage of inverter

## 9.5 Controller Design for Multi string Nine level Inverter connected to the grid through 'LCL' filter

The dynamic equations after writing them in standard form are

$$pI_{q1} = \omega_e I_{d1} + \frac{M_{q1}}{L_1}V_{d1} + \frac{M_{q2}}{L_1}V_{d4} + \frac{4}{\pi L_1}\left(\sin(\theta - \psi_1)\right)\left(V_{d2} + V_{d3}\right) - \frac{V_{qc}}{L_1}$$  (9.53)

$$pI_{d1} = \frac{M_{d1}}{L_1}V_{d1} + \frac{M_{d2}}{L_1}V_{d4} + \frac{4}{\pi L_1}\left(\sin(\theta - \psi_1)\right)\left(V_{d2} + V_{d3}\right) - \omega_e I_{q1} - \frac{V_{dc}}{L_1}$$  (9.54)

$$pI_{q2} = \omega_e I_{d2} + \frac{V_{qc}}{L_2} - \frac{V_{qg}}{L_2}$$  (9.55)

$$pI_{d2} = \frac{V_{dc}}{L_2} - \frac{V_{dg}}{L_2} - \omega_e I_{q2}$$  (9.56)

$$pV_{qc} = \omega_e V_{dc} + \frac{I_{q1}}{C} - \frac{I_{q2}}{C}$$  (9.57)

$$pV_{dc} = \frac{I_{d1}}{C} - \frac{I_{d2}}{C} - \omega_e V_{qc}$$  (9.58)

Writing them in matrix form

$$pX = AX + BU + FX_d$$

$$\text{where } X = \begin{bmatrix} I_{q1} \\ I_{d1} \\ I_{q2} \\ I_{d2} \\ V_{qc} \\ V_{dc} \end{bmatrix}, \ U = \begin{bmatrix} M_{q1} \\ M_{d1} \\ M_{q2} \\ M_{d2} \end{bmatrix}, \ X_d = \begin{bmatrix} V_{qg} \\ V_{dg} \end{bmatrix}$$

232

Where $A = \begin{bmatrix} 0 & \omega_e & 0 & 0 & -\dfrac{1}{L_1} & 0 \\ -\omega_e & 0 & 0 & 0 & 0 & -\dfrac{1}{L_1} \\ 0 & 0 & 0 & \omega_e & \dfrac{1}{L_2} & 0 \\ 0 & 0 & -\omega_e & 0 & 0 & \dfrac{1}{L_2} \\ \dfrac{1}{C} & 0 & -\dfrac{1}{C} & 0 & 0 & \omega_e \\ 0 & \dfrac{1}{C} & 0 & -\dfrac{1}{C} & -\omega_e & 0 \end{bmatrix}$, $B = \begin{bmatrix} \dfrac{V_{d1}}{L_1} & 0 & \dfrac{V_{d4}}{L_1} & 0 \\ 0 & \dfrac{V_{d1}}{L_1} & 0 & \dfrac{V_{d4}}{L_1} \\ 0 & 0 & 0 & 0 \\ 0 & 0 & 0 & 0 \\ 0 & 0 & 0 & 0 \\ 0 & 0 & 0 & 0 \end{bmatrix}$, $F = \begin{bmatrix} 0 & 0 \\ 0 & 0 \\ -\dfrac{1}{L_2} & 0 \\ 0 & -\dfrac{1}{L_2} \\ 0 & 0 \\ 0 & 0 \end{bmatrix}$

$$\begin{bmatrix} pI_{q1} \\ pI_{d1} \\ pI_{q2} \\ pI_{d2} \\ pV_{qc} \\ pV_{dc} \end{bmatrix} = \begin{bmatrix} 0 & \omega_e & 0 & 0 & -\dfrac{1}{L_1} & 0 \\ -\omega_e & 0 & 0 & 0 & 0 & -\dfrac{1}{L_1} \\ 0 & 0 & 0 & \omega_e & \dfrac{1}{L_2} & 0 \\ 0 & 0 & -\omega_e & 0 & 0 & \dfrac{1}{L_2} \\ \dfrac{1}{C} & 0 & -\dfrac{1}{C} & 0 & 0 & \omega_e \\ 0 & \dfrac{1}{C} & 0 & -\dfrac{1}{C} & -\omega_e & 0 \end{bmatrix} \begin{bmatrix} I_{q1} \\ I_{d1} \\ I_{q2} \\ I_{d2} \\ V_{qc} \\ V_{dc} \end{bmatrix} + \begin{bmatrix} \dfrac{V_{d1}}{L_1} & 0 & \dfrac{V_{d4}}{L_1} & 0 \\ 0 & \dfrac{V_{d1}}{L_1} & 0 & \dfrac{V_{d4}}{L_1} \\ 0 & 0 & 0 & 0 \\ 0 & 0 & 0 & 0 \\ 0 & 0 & 0 & 0 \\ 0 & 0 & 0 & 0 \end{bmatrix} \begin{bmatrix} M_{q1} \\ M_{d1} \\ M_{q2} \\ M_{d2} \end{bmatrix} + \begin{bmatrix} 0 & 0 \\ 0 & 0 \\ -\dfrac{1}{L_2} & 0 \\ 0 & -\dfrac{1}{L_2} \\ 0 & 0 \\ 0 & 0 \end{bmatrix} \begin{bmatrix} V_{qg} \\ V_{dg} \end{bmatrix}$$

233

The expressions for active and reactive powers are given in

$$P_g = V_{qg} I_{q2} + V_{dg} I_{d2} \qquad (9.59)$$

$$Q_g = V_{dg} I_{q2} - V_{qg} I_{d2}. \qquad (9.60)$$

Based on the references for active and reactive powers, the references for the grid side current can be found.

$$I_{q2}^* = \frac{P_g^* V_{qg} + Q_g^* V_{dg}}{V_{qg}^2 + V_{dg}^2} \qquad (9.61)$$

$$I_{d2}^* = \frac{P_g^* V_{dg} - Q_g^* V_{qg}}{V_{qg}^2 + V_{dg}^2} \qquad (9.62)$$

The three controllers are needed in this control scheme. They are called as

1.  Grid side current controller.

2.  Capacitor voltage controller.

3.  Inverter side current controller.

### 9.5.2 Grid Side Current Controller I$_{qd2}$:

The dynamic equation for the grid side loop is given here.

$$V_{qdc} = L_2 p I_{qd2} + j L_2 \omega_e I_{qd2} + V_{qdg} \qquad (9.63)$$

**q - axis grid side current controller:**

$$V_{qc} = L_2 p I_{q2} - L_2 \omega_e I_{d2} + V_{qg} \qquad (9.64)$$

$$V_{qc} - V_{qg} + L_2 \omega_e I_{d2} = (L_2 p) I_{q2}$$

$$V_{qc} - V_{qg} + L_2\omega_e I_{d2} = (L_2 p)I_{q2} = \sigma_{3q} = K_{3q}\left(I_{q2}^{*} - I_{q2}\right) \quad (9.65)$$

$$\frac{I_{q2}}{I_{q2}^{*}} = \frac{K_{3q}}{L_2 p + K_{3q}} \quad (9.66)$$

$$K_{3q} = K_{P3q} + \frac{K_{I3q}}{p}$$

$$\frac{I_{q2}}{I_{q2}^{*}} = \frac{K_{P3q} + \dfrac{K_{I3q}}{p}}{L_2 s + K_{P3q} + \dfrac{K_{I3q}}{p}}$$

$$\frac{I_{q2}}{I_{q2}^{*}} = \frac{pK_{P3q} + K_{I3q}}{L_2 p^2 + K_{P3q} p + K_{I3q}}$$

$$\frac{I_{q2}}{I_{q2}^{*}} = \frac{pK_{P3q} + K_{I3q}}{L_2 p^2 + pK_{P3q} + K_{I3q}} = \frac{2\xi\omega_{n3} p + \omega_{n3}^2}{p^2 + 2\xi\omega_{n3} p + \omega_{n3}^2} \quad (9.67)$$

$$K_{P3q} = 2\xi\omega_{n3}; K_{I3q} = \omega_{n3}^2 \quad (9.68)$$

where $\xi$ is the damping factor and is usually chosen as critical damping factor which is 0.707

$\omega_{n3}$ is the natural frequency.

*d - axis grid side current controller:*

$$V_{dc} = L_2 pI_{d2} + L_2\omega_e I_{q2} + V_{dg} \quad (9.69)$$

$$V_{dc} - V_{dg} - L_2\omega_e I_{q2} = (L_2 p)I_{d2}$$

$$V_{dc} - V_{dg} - L_2\omega_e I_{q2} = (L_2 p)I_{d2} = \sigma_{3d} = K_{3d}\left(I_{d2}^{*} - I_{d2}\right) \quad (9.70)$$

$$\frac{I_{d2}}{I_{d2}^{*}} = \frac{K_{3d}}{L_2 p + K_{3d}} \quad (9.71)$$

$$K_{3d} = K_{P3d} + \frac{K_{I3d}}{p}$$

$$\frac{I_{d2}}{I_{d2}{}^*} = \frac{K_{P3d} + \dfrac{K_{I3d}}{p}}{L_2 p + K_{P3d} + \dfrac{K_{I3d}}{p}}$$

$$\frac{I_{d2}}{I_{d2}{}^*} = \frac{pK_{P3d} + K_{I3d}}{L_2 p^2 + K_{P3d} p + K_{I3d}}$$

$$\frac{I_{d2}}{I_{d2}{}^*} = \frac{pK_{P3d} + K_{I3d}}{L_2 p^2 + pK_{P3d} + K_{I3d}} = \frac{2\xi\omega_{n3} p + \omega_{n3}{}^2}{p^2 + 2\xi\omega_{n3} p + \omega_{n3}{}^2} \qquad (9.72)$$

$$K_{P3d} = 2\xi\omega_{n3} ; K_{I3d} = \omega_{n3}{}^2 \qquad (9.73)$$

where $\xi$ is the damping factor and is usually chosen as critical damping factor which is 0.707

$\omega_{n1}$ is the natural frequency.

### 9.5.3    Capacitor Voltage controller $V_{qdc}$:

*q - axis capacitor voltage controller:*

$$I_{q1} = CpV_{qc} - \omega_e CV_{dc} + I_{q2} \qquad (9.74)$$

$$I_{q1}{}^* - I_{q2}{}^* + \omega_e CV_{dc}{}^* = CpV_{qc}{}^* $$

$$(Cs)V_{qc} = \sigma_{2q} = K_{2q}\left(V_{qc}{}^* - V_{qc}\right) \qquad (9.75)$$

$$\frac{V_{qc}}{V_{qc}{}^*} = \frac{K_{2q}}{Cp + K_{2q}} \qquad (9.76)$$

$$K_{2q} = K_{P2q} + \frac{K_{I2q}}{p}$$

$$\frac{V_{qc}}{V_{qc}{}^*} = \frac{K_{P2q} + \dfrac{K_{I2q}}{p}}{Cp + K_{P2q} + \dfrac{K_{I2q}}{p}}$$

$$\frac{V_{qc}}{V_{qc}{}^*} = \frac{pK_{P2q} + K_{I2q}}{Cp^2 + pK_{P2q} + K_{I2q}}$$

$$\frac{V_{qc}}{V_{qc}{}^*} = \frac{pK_{P2q} + K_{I2q}}{Cp^2 + pK_{P2q} + K_{I2q}} = \frac{2\xi\omega_{n2}p + \omega_{n2}{}^2}{p^2 + 2\xi\omega_{n2}p + \omega_{n2}{}^2} \tag{9.77}$$

$$K_{P2q} = 2\xi\omega_{n2}C \; ; K_{I2q} = \omega_{n2}{}^2C \tag{9.78}$$

where $\xi$ is the damping factor and is usually chosen as critical damping factor which is 0.707

$\omega_{n2}$ is the natural frequency.

### d - axis capacitor voltage controller:

$$I_{d1} = CpV_{dc} + \omega_e CV_{qc} + I_{d2} \tag{9.79}$$

$$I_{d1} - I_{d2} - \omega_e CV_{qc} = CpV_{dc}$$

$$(C)pV_{dc} = \sigma_{2d} = K_{2d}\left(V_{dc}{}^* - V_{dc}\right) \tag{9.80}$$

$$\frac{V_{dc}}{V_{dc}{}^*} = \frac{K_{2d}}{Cp + K_{2d}} \tag{9.81}$$

$$K_{2d} = K_{P2d} + \frac{K_{I2d}}{p}$$

$$\frac{V_{dc}}{V_{dc}^{*}} = \frac{K_{P2d} + \dfrac{K_{I2d}}{p}}{Cp + K_{P2d} + \dfrac{K_{I2d}}{p}}$$

$$\frac{V_{dc}}{V_{dc}^{*}} = \frac{pK_{P2d} + K_{I2d}}{Cp^{2} + pK_{P2d} + K_{I2d}}$$

$$\frac{V_{dc}}{V_{dc}^{*}} = \frac{pK_{P2d} + K_{I2d}}{Cp^{2} + pK_{P2d} + K_{I2d}} = \frac{2\xi\omega_{n2}p + \omega_{n2}^{2}}{p^{2} + 2\xi\omega_{n2}p + \omega_{n2}^{2}} \tag{9.82}$$

$$K_{P2d} = 2\xi\omega_{n2};\, K_{I2d} = \omega_{n2}^{2} \tag{9.83}$$

where $\xi$ is the damping factor and is usually chosen as critical damping factor which is 0.707

$\omega_{n2}$ is the natural frequency.

### 9.5.4    Inverter side current controller $I_{qd1}$:

$$M_{qd1}V_{d1} + M_{qd2}V_{d4} + \frac{4}{\pi}\left(\sin(\theta - \psi_{1})\right)(V_{d2} + V_{d3}) = R_{1}I_{qd1} + L_{1}pI_{qd1} + jL_{1}\omega_{e}I_{qd1} + V_{qdc}$$

*q - axis inverter side current controller:*

$$M_{q1}V_{d1} + M_{q2}V_{d4} + \frac{4}{\pi}\left(\sin(\theta - \psi_{1})\right)(V_{d2} + V_{d3}) = L_{1}pI_{q1} - \omega_{e}L_{1}I_{d1} + V_{qc} \tag{9.84}$$

$$M_{q1}V_{d1} + M_{q2}V_{d4} + \frac{4}{\pi}\left(\sin(\theta - \psi_{1})\right)(V_{d2} + V_{d3}) + \omega_{e}L_{1}I_{d1} - V_{qc} = L_{1}pI_{q1}$$

$$M_{q1}V_{d1} + M_{q2}V_{d4} + \frac{4}{\pi}\left(\sin(\theta - \psi_{1})\right)(V_{d2} + V_{d3}) + \omega_{e}L_{1}I_{d1} - V_{qc} = L_{1}pI_{q1} = \sigma_{1q} = K_{1q}\left(I_{q1}^{*} - I_{q1}\right) \tag{9.85}$$

$$\frac{I_{q1}}{I_{q1}^{*}} = \frac{K_{1q}}{L_{1}p + K_{1q}}$$

$$K_{1q} = K_{P1q} + \frac{K_{I1q}}{p}$$

$$\frac{I_{q1}}{I_{q1}^{*}} = \frac{K_{P1q} + \dfrac{K_{I1q}}{p}}{L_1 p + K_{P1q} + \dfrac{K_{I1q}}{p}}$$

$$\frac{I_{q1}}{I_{q1}^{*}} = \frac{pK_{P1q} + K_{I1q}}{L_1 p^2 + K_{P1q} p + K_{I1q}}$$

$$\frac{I_{q1}}{I_{q1}^{*}} = \frac{pK_{P1q} + K_{I1q}}{L_1 p^2 + K_{P1q} p + K_{I1q}} = \frac{2\xi\omega_{n1} p + \omega_{n1}^{2}}{p^2 + 2\xi\omega_{n1} p + \omega_{n1}^{2}} \tag{9.86}$$

$$K_{P1q} = 2\xi\omega_{n1}; K_{I1q} = \omega_{n1}^{2} \tag{9.87}$$

where $\xi$ is the damping factor and is usually chosen as critical damping factor which is 0.707

$\omega_{n1}$ is the natural frequency.

### d - axis inverter side current controller:

$$M_{d1}V_{d1} + M_{d2}V_{d4} + \frac{4}{\pi}\left(\sin(\theta - \psi_1)\right)(V_{d2} + V_{d3}) = L_1 pI_{d1} + \omega_e L_1 I_{q1} + V_{dc} \tag{9.88}$$

$$M_{d1}V_{d1} + M_{d2}V_{d4} + \frac{4}{\pi}\left(\sin(\theta - \psi_1)\right)(V_{d2} + V_{d3}) - \omega_e L_1 I_{q1} - V_{dc} = L_1 pI_{d1}$$

$$M_{d1}V_{d1} + M_{d2}V_{d4} + \frac{4}{\pi}\left(\sin(\theta - \psi_1)\right)(V_{d2} + V_{d3}) - \omega_e L_1 I_{q1} - V_{dc} = L_1 pI_{d1} = \sigma_{1d} = K_{1d}\left(I_{d1}^{*} - I_{d1}\right) \tag{9.89}$$

$$\frac{I_{d1}}{I_{d1}^{*}} = \frac{K_{1d}}{L_1 p + K_{1d}}$$

$$K_{1d} = K_{P1d} + \frac{K_{I1d}}{p}$$

$$\frac{I_{d1}}{I_{d1}^{*}} = \frac{K_{P1d} + \dfrac{K_{I1d}}{p}}{L_{1}p + K_{P1d} + \dfrac{K_{I1d}}{p}}$$

$$\frac{I_{d1}}{I_{d1}^{*}} = \frac{pK_{P1d} + K_{I1d}}{L_{1}p^{2} + K_{P1d}\,p + K_{I1d}}$$

$$\frac{I_{d1}}{I_{d1}^{*}} = \frac{pK_{P1d} + K_{I1d}}{L_{1}p^{2} + K_{P1d}\,p + K_{I1d}} = \frac{2\xi\omega_{n1}p + \omega_{n1}^{2}}{p^{2} + 2\xi\omega_{n1}p + \omega_{n1}^{2}} \tag{9.90}$$

$$K_{P1d} = 2\xi\omega_{n1}; K_{I1d} = \omega_{n1}^{2}$$

where $\xi$ is the damping factor and is usually chosen as critical damping factor which is 0.707

$\omega_{n1}$ is the natural frequency.

Therefore, the final control equations are

$$M_{q1}V_{d1} + M_{q2}V_{d4} + \frac{4}{\pi}\left(\sin(\theta - \psi_{1})\right)\left(V_{d2} + V_{d3}\right) = \sigma_{1q} + V_{qc} - L_{1}\omega_{e}I_{d1} \tag{9.91}$$

$$M_{d1}V_{d1} + M_{d2}V_{d4} + \frac{4}{\pi}\left(\sin(\theta - \psi_{1})\right)\left(V_{d2} + V_{d3}\right) = \sigma_{1d} + V_{dc} + L_{1}\omega_{e}I_{q1} \tag{9.92}$$

$$M_{d1}^{*}M_{q2}^{*} = M_{d2}^{*}M_{q1}^{*} \tag{9.93}$$

The three equations that will be used to find the expressions for modulation indices are (9.97), (9.98) and (9.99). Since there are only three equations to find four unknowns, an equation is used to limit the modulation indices. The fourth equation is given in (9.100).

$$M_{d1} = \alpha M_{d2} \tag{9.94}$$
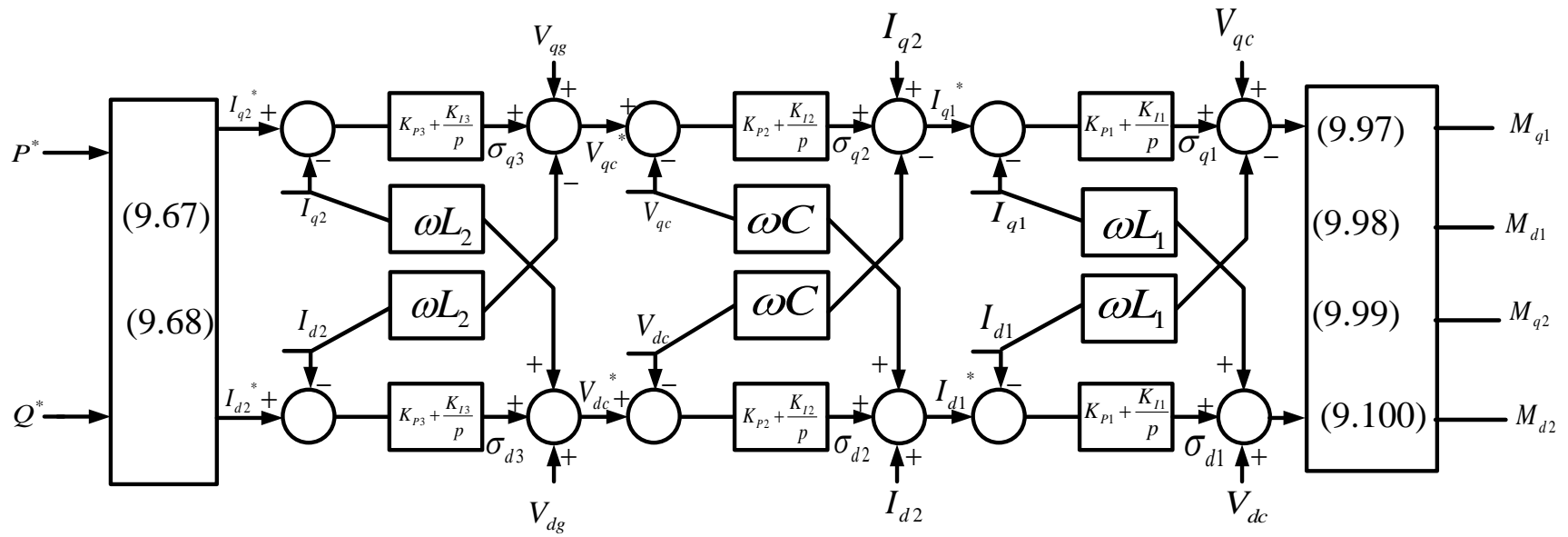
Figure 9.15 Control diagram of all the three controllers

Figure 9.16 Overall control block diagram of the system

242
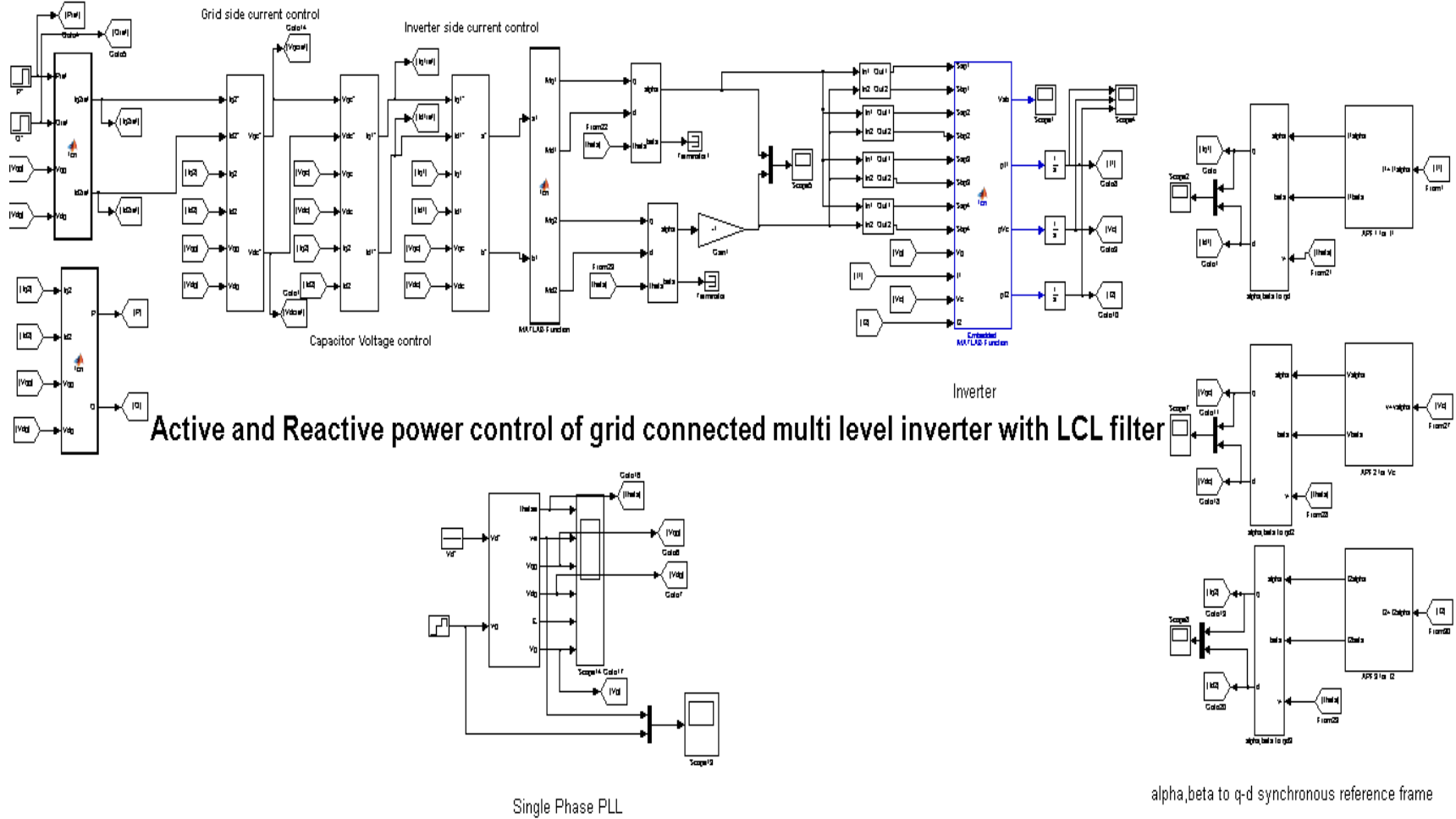
Figure 9.17 Closed loop control system in SIMULINK

## 9.6 Simulation Results with 'LCL' filter
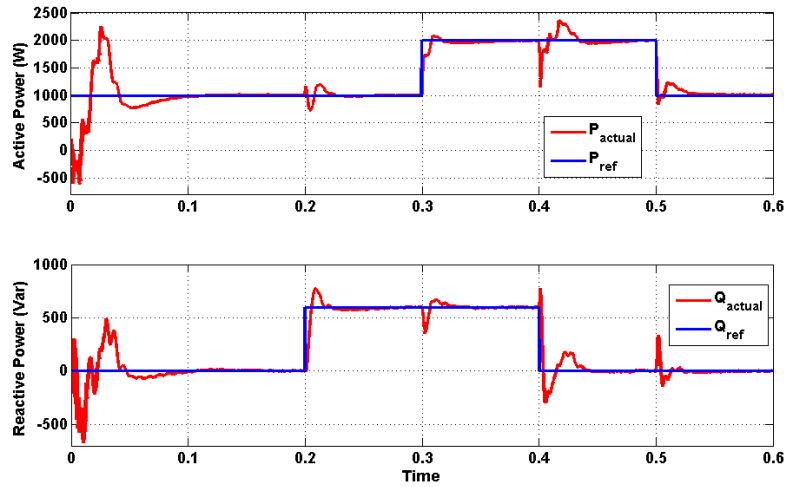


Figure 9.18 Simulation result of reference and actual waveforms of Active and reactive

powers
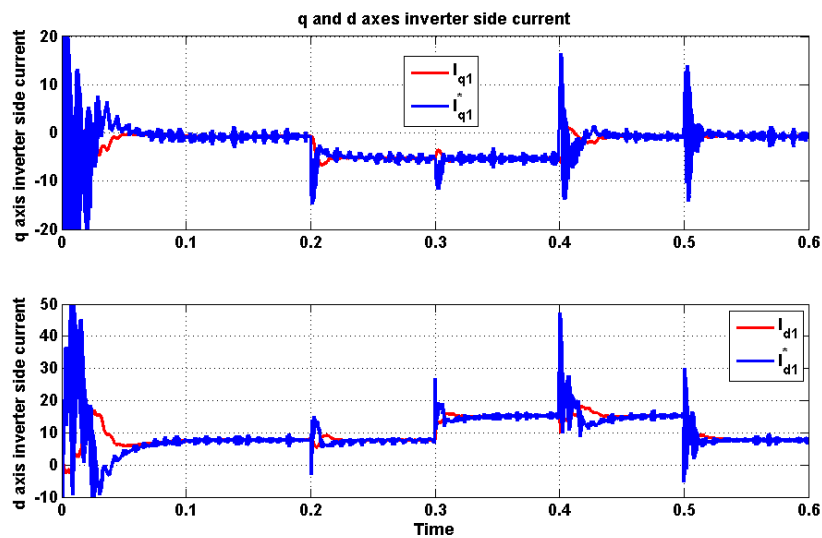


Figure 9.19 Simulation result of q and d axis inverter side currents
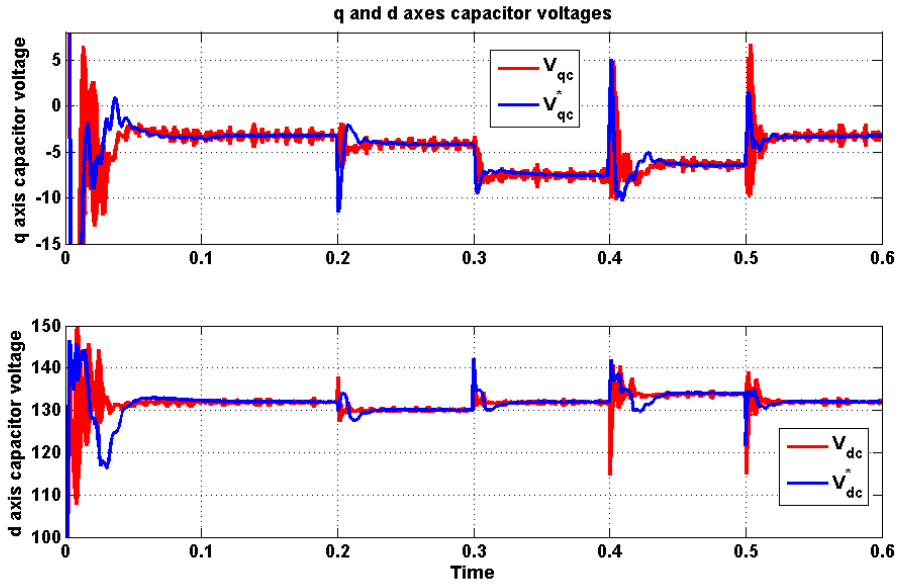
Figure 9.20 Simulation result of reference and actual waveforms of q and d axes

capacitor voltages
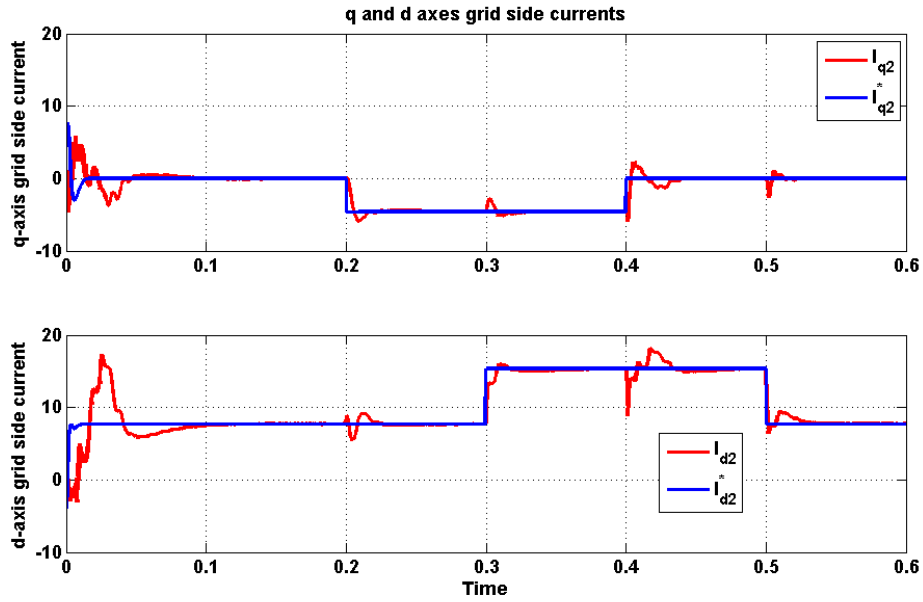


Figure 9.21 Simulation result of reference and actual waveforms of q and d axes grid side

currents

245
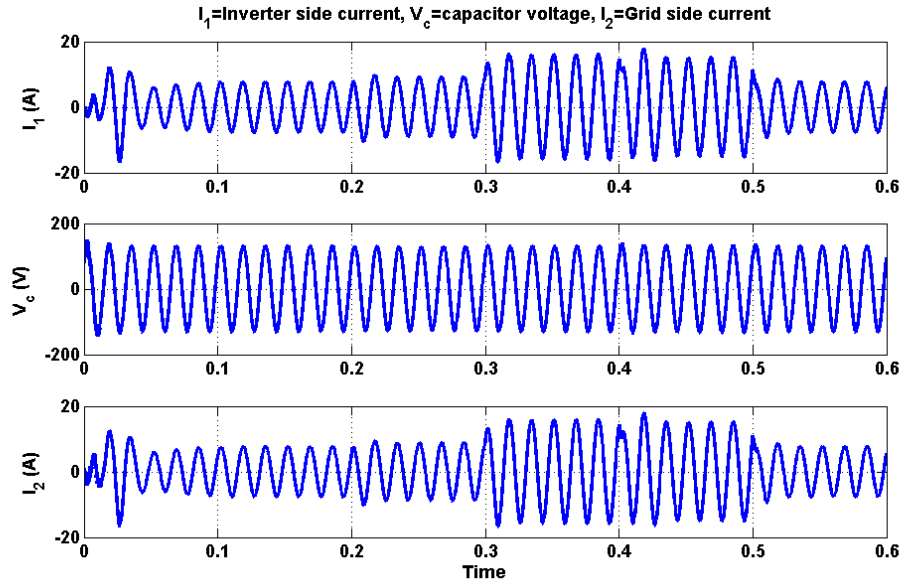
Figure 9.22 Simulation result of State variables inverter side current, capacitor voltages

and grid side current
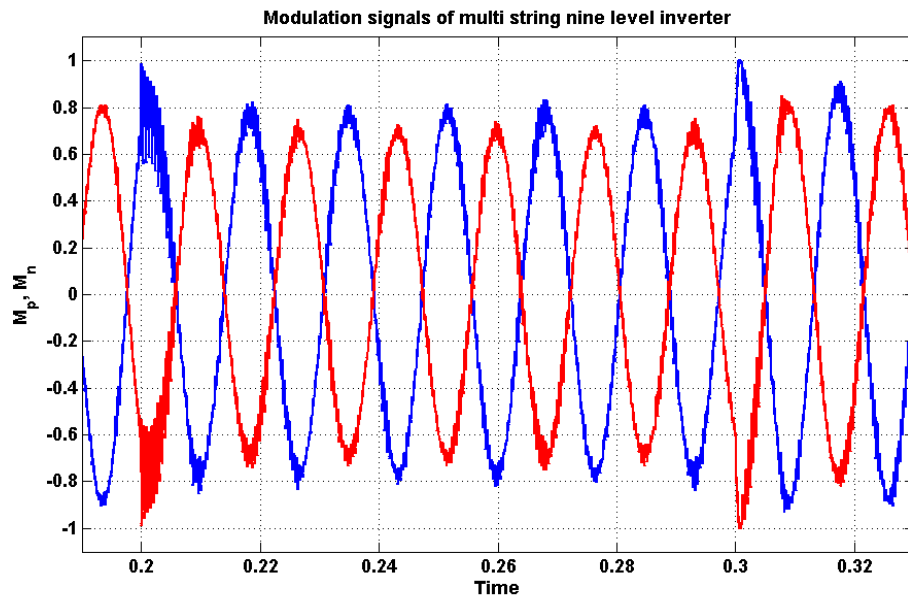


Figure 9.23 Simulation result of closed loop modulation signals
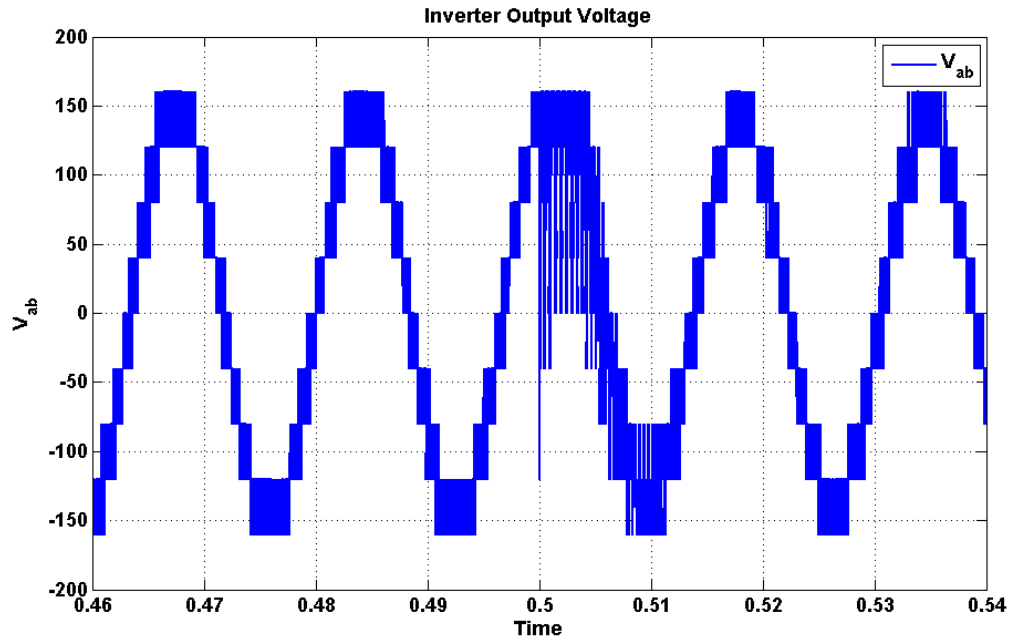
Figure 9.24 Simulation result of inverter output voltage
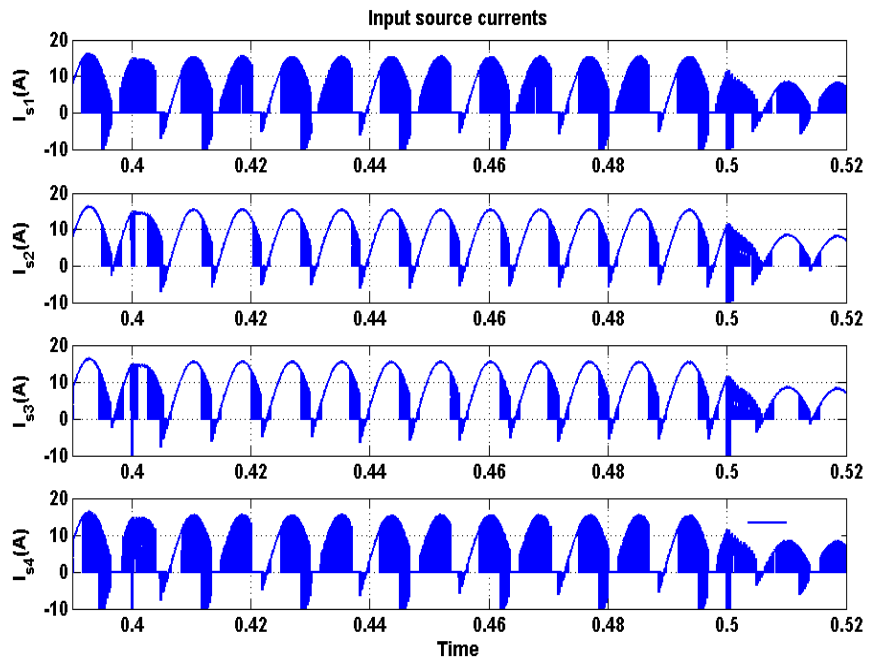


Figure 9.25 Simulation result of input source currents

## 9.7 Summary

The active and reactive power control schemes of single phase multi string multi-level converter with L and LCL filters connected to the grid are designed in qd synchronous reference frame. The transformation to qd synchronous reference frame from single phase is not well established as the Park's transformation requires a minimum of two orthogonal signals to transform. Hence, a fictitious orthogonal signal is generated using the APF (all pass filter) method to transfer the two signals into qd reference frame. Using the APF, the grid voltage is transformed into q and d axes voltages and a three phase qd phase locked loop (PLL) control scheme is applied. The control scheme to control active and reactive powers going into the grid is set forth. Computer simulation results obtained using a MATLAB/Simulink platform compared with experiment results for multi string seven-level inverter verifies the proposed control scheme.

# CHAPTER 10  CONCLUSIONS AND FUTURE SUGGESTION

## 10.1      Conclusions

This thesis presents a method for the determination of the modulation signals for the multilevel cascaded single phase inverters which eliminate the dominant harmonics in the desired output voltage for both the linear and over-modulation operating regions. This method is applicable to the cases when the DC input voltages are either equal or unequal. The proposed method can also be extended to higher multilevel cascaded single-phase converters for the determination of the modulation signals. Computer simulation results, contour plot and experimental results are provided to demonstrate the utility of the proposed approach. This thesis therefore provides a transparent analytical method to determine the modulation signals required for unipolar PWM modulation of cascaded multi-level single-phase DC-AC converters.

This thesis also presents a single-phase multistring multi-level inverter topology which has less number of switches required to produce the desired multi-level output for distributed energy resources compared to cascaded H-bridge converter topology. The modes of operation of multi string multi-level inverter topology are also discussed. The proposed method of Karnaugh mapping technique which was rarely used in power electronics converters is used to determine the expression for output voltage and input source currents in terms of the input voltages and output current respectively. The expression of voltage stress for the switches are also determined. The modulation scheme

for topologies are also presented which was never presented before. The expression for modulation signal is determined using Fourier series analysis by approximating switching functions using the instantaneous values of modulation signals. The calculation of switching loss for multi string seven-level inverter is performed and the topology reduces switching loss compared to cascaded H bridge multi-level converter. Simulation of the proposed system is carried out and waveforms of output voltage, input source currents, voltage stress are generated. Experimental results are conducted on 1kW laboratory prototype and the waveforms of switching pulses and output voltage are presented. The experimental results and simulation results validate each other. The only disadvantage with this type of converter when compared with cascade H bridge multi-level converter is rating of switches. The rating of all the middle switches should be twice the rating of other four switches.

The experiment results are obtained using the Texas Instruments DSP F28335. The switching signals of bidirectional switches are generated using carrier based modulation technique. The results show that the generated switching pulses give a balanced set of output voltages with the desired magnitude and frequency.

The topology of single phase multi string nine-level inverter with an LCL filter connected to the grid is also presented in this thesis. The LCL filter is designed and bode plot of transfer function is plotted. The Harmonic Balance Technique to transfer the single phase system to qd synchronous reference frame is presented. The active and reactive power control schemes of single phase multi string multi-level converter with L and LCL filters connected to the grid are designed in qd synchronous reference frame.

The transformation to qd synchronous reference frame from single phase is not well established as the Park's transformation requires a minimum of two orthogonal signals to transform. Hence, a fictitious orthogonal signal is generated using the APF (all pass filter) method to transfer the two signals into qd reference frame. Using the APF, the grid voltage is transformed into q and d axes voltages and a three phase qd reference frame phase locked loop (PLL) control scheme is applied. The control scheme to control active and reactive powers going into the grid is set forth. Computer simulation results obtained using a MATLAB/Simulink platform for multi string nine-level inverter verifies the proposed control scheme.

## 10.2     List of Contributions

The main contributions of the thesis are listed below

- This thesis presents a method for the determination of the modulation signals for the multilevel cascaded single phase inverters which eliminate the dominant harmonics in the desired output voltage for both the linear and over-modulation operating regions.

- The thesis also extends the multi-string five-level inverter topology to multi-string seven and nine-level inverter topologies. This thesis also presents the modeling and analysis of multi string five, seven and nine-level inverter topologies which was never presented before.

251

- As a part of modeling this thesis clearly presents the proposed method of Karnaugh mapping technique which was rarely used in power electronics converters. The Karnaugh mapping technique is used to determine the expression for output voltage and input source currents in terms of the input voltages and output current respectively.

- As a part of analysis this thesis presents the double Fourier series analysis to determine the expression for modulation signals. The expressions for modulation signals are determined by approximating switching functions using the instantaneous values of modulation signals.

- The simulation and experimental results of both the cascaded H-bridge multi-level converter and multi-string multi-level converter are also presented. TMS 320 F28335 eZdsp was used to generate the switching pulses of both the converters in the experimental setup.

- The Harmonic Balance Technique to transfer the single phase system to qd synchronous reference frame is presented. The active and reactive power control schemes of single phase multi string multi-level converter with L and LCL filters connected to the grid are designed in qd synchronous reference frame. A control scheme to control active and reactive powers going into the grid is set forth.

## 10.3　　　Recommendations for Future Work

This thesis assumes that there is a constant DC voltage at the input side of the converter. But for the future work, PV with maximum power point (MPPT) or batteries or fuel cells can also be considered as the inputs.

Controlling the DC voltages of AC-DC multi-level converters can also be an incentive option to do the future work. The converter can also use the batteries from hybrid electric vehicles (HEV) and invert the DC voltage and supply the single phase AC voltage to the grid when needed. This thesis describes only about single phase multi-level inverters, but it can also be extended to three phase and multi-phase converters.

The block diagram of the experimental system of cascaded H-bridge multi-level converter consisting of the power circuit, driver circuit, digital signal processor TMS 320 F28335 eZdsp is given in Figure 10.1. The laboratory prototype is shown in Figure 10.2. The power stage of the converter is realized with sixteen bidirectional switches. The power circuit as well as the gate driver board are done on PCB. External connectors are used to interface the gate driver with the IGBTs.
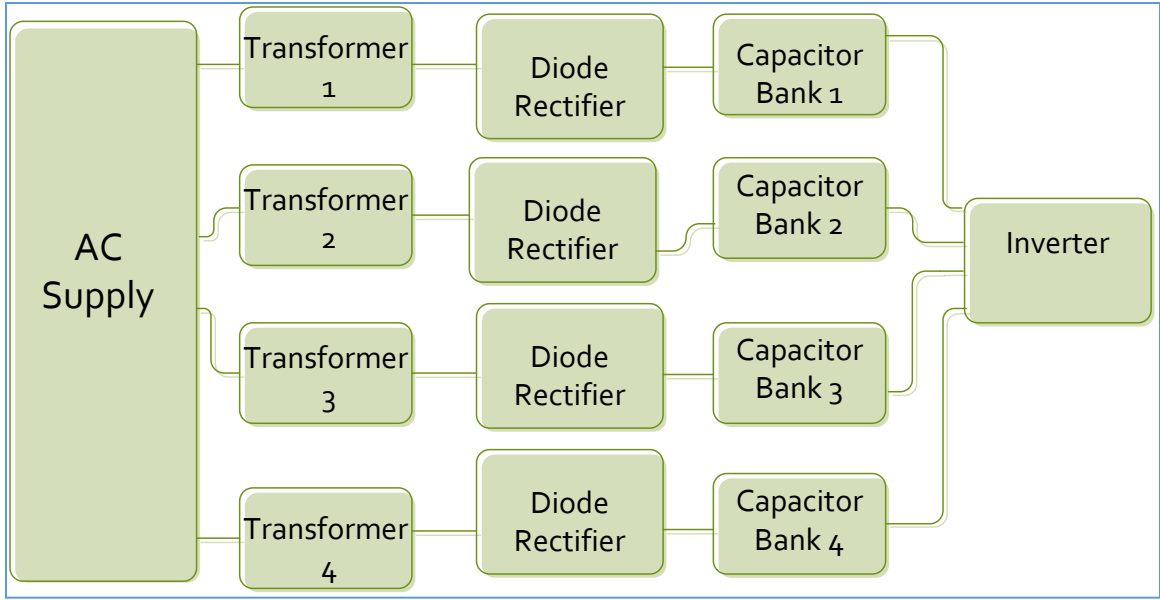
Figure 10.1 Block diagram for the experimental set up.
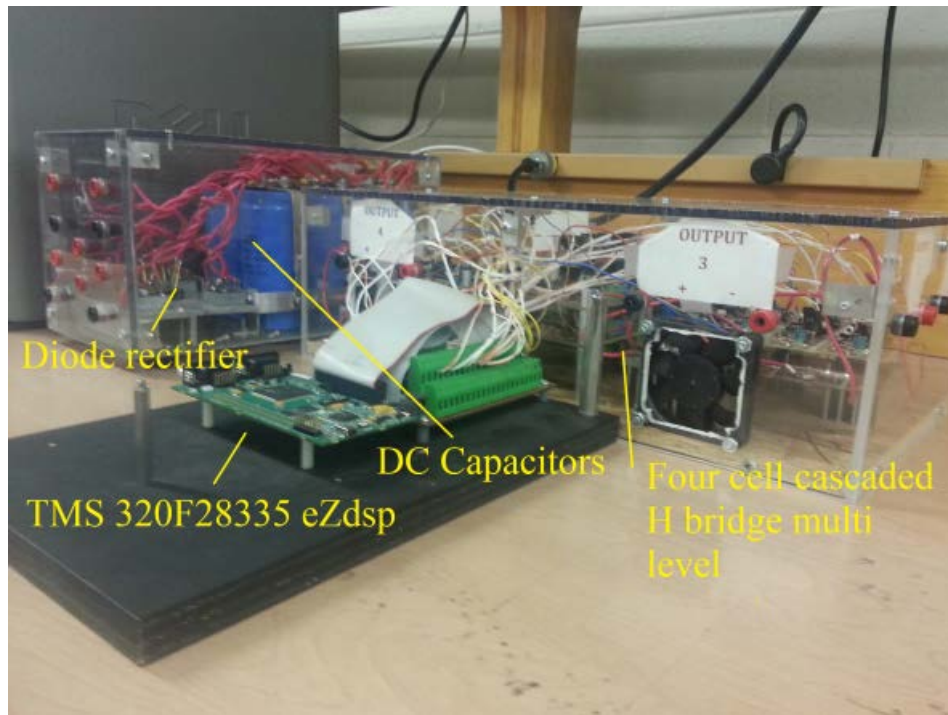


Figure 10.2 Laboratory prototype cascaded converter.

# REFERENCES

[1]     A. Keyhani, *Design of smart power grid renewable energy systems*: Wiley-IEEE Press, 2011.

[2]     M. Malinowski, K. Gopakumar, J. Rodriguez, and M. A. Perez, "A Survey on Cascaded Multilevel Inverters," *IEEE Transactions on Industrial Electronics,* vol. 57, no. 7, pp. 2197-2206, 2010.

[3]     H. Sepahvand, J. Liao, M. Ferdowsi, and K. Corzine, "Capacitor Voltage Regulation in Single-DC-Source Cascaded H-bridge Multilevel Converters Using Phase-Shift Modulation," *IEEE Transactions on Industrial Electronics*, vol. 60, no. 9, pp. 3619-3626, September 2013.

[4]     D. G. Holmes and T. A. Lipo, *Pulse width modulation for power converters: principles and practice* vol. 18: Wiley-IEEE Press, 2003.

[5]     A. Lesnicar and R. Marquardt, "An innovative modular multilevel converter topology suitable for a wide power range," in Proc. *2003 IEEE Bologna Power Tech Conference Proceedings*, p. 6 pp. Vol.3, 2003.

[6]     H. Akagi, "Classification, Terminology, and Application of the Modular Multilevel Cascade Converter (MMCC)," *IEEE Transactions on Power Electronics,* vol. 26, no. 11, pp. 3119-3130, 2011.

[7]     M. A. Perez, J. Rodriguez, E. J. Fuentes, and F. Kammerer, "Predictive Control of AC-AC Modular Multilevel Converters," *IEEE Transactions on Industrial Electronics,* vol. 59, no. 7, pp. 2832-2839, 2012.

[8]     S. Gum Tae, L. Hee-Jin, N. Tae Sik, C. Yong-Ho, L. Uk-Hwa, B. Seung-Taek, H. Kyeon, and P. Jung-Wook, "Design and Control of a Modular Multilevel HVDC Converter With Redundant Power Modules for Noninterruptible Energy Transfer," *IEEE Transactions on Power Delivery,* vol. 27, no. 3, pp. 1611-1619, 2012.

[9]     L. G. Franquelo, J. Rodriguez, J. I. Leon, S. Kouro, R. Portillo, and M. A. M. Prats, "The age of multilevel converters arrives," *IEEE Industrial Electronics Magazine,* vol. 2, no. 2, pp. 28-39, 2008.

[10]    K. A. Corzine and J. R. Baker, "Multilevel voltage-source duty-cycle modulation: analysis and implementation," *IEEE Transactions on Industrial Electronics,* vol. 49, no. 5, pp. 1009-1016, 2002.

[11]    J. Rodriguez, L. Jih-Sheng, and P. Fang Zheng, "Multilevel inverters: a survey of topologies, controls, and applications," *IEEE Transactions on Industrial Electronics,* vol. 49, no. 4, pp. 724-738, 2002.

[12] S. Kouro, M. Malinowski, K. Gopakumar, J. Pou, L. G. Franquelo, W. Bin, J. Rodriguez, M. A. Perez, and J. I. Leon, "Recent Advances and Industrial Applications of Multilevel Converters," *IEEE Transactions on Industrial Electronics,* vol. 57, no. 8, pp. 2553-2580, 2010.

[13] T. A. Meynard, H. Foch, P. Thomas, J. Courault, R. Jakob, and M. Nahrstaedt, "Multicell converters: basic concepts and industry applications," *IEEE Transactions on Industrial Electronics,* vol. 49, no. 5, pp. 955-964, 2002.

[14] C.-L. Chen, W. Yubin, L. Jih-Sheng, L. Yuang-Shung, and D. Martin, "Design of Parallel Inverters for Smooth Mode Transfer Microgrid Applications," *IEEE Transactions on Power Electronics,* vol. 25, no. 1, pp. 6-15, 2010.

[15] S. Daher, J. Schmid, and F. L. M. Antunes, "Multilevel Inverter Topologies for Stand-Alone PV Systems," *IEEE Transactions on Industrial Electronics,* vol. 55, no. 7, pp. 2703-2712, 2008.

[16] C. K. Lee, S. S. Y. R. Hui, and H. S. H. Chung, "A 31-level cascade inverter for power applications," *IEEE Transactions on Industrial Electronics,* vol. 49, no. 3, pp. 613-617, 2002.

[17] A. Nami, F. Zare, A. Ghosh, and F. Blaabjerg, "A Hybrid Cascade Converter Topology With Series-Connected Symmetrical and Asymmetrical Diode-Clamped H-Bridge Cells," *IEEE Transactions on Power Electronics,* vol. 26, no. 1, pp. 51-65, 2011.

[18] S. Gui-Jia, "Multilevel DC-link inverter," *IEEE Transactions on Industry Applications,* vol. 41, no. 3, pp. 848-854, 2005.

[19] K. Corzine and Y. Familiant, "A new cascaded multilevel H-bridge drive," *IEEE Transactions on Power Electronics,* vol. 17, no. 1, pp. 125-131, 2002.

[20] C. Rech and J. R. Pinheiro, "Hybrid Multilevel Converters: Unified Analysis and Design Considerations," *IEEE Transactions on Industrial Electronics,* vol. 54, no. 2, pp. 1092-1104, 2007.

[21] G. Ceglia, V. Guzman, C. Sanchez, F. Ibanez, J. Walter, and M. I. Gimenez, "A New Simplified Multilevel Inverter Topology for DC-AC Conversion," *IEEE Transactions on Power Electronics,* vol. 21, no. 5, pp. 1311-1319, 2006.

[22] B. Gultekin and M. Ermis, "Cascaded Multilevel Converter Based Transmission STATCOM: System Design Methodology and Development of a 12 kV±12MVAr Power-Stage," *IEEE Transactions on Power Electronics,* vol. 28, no. 11, pp. 4930-4950, 2013.

[23] P. Lezana, J. Rodríguez, and D. A. Oyarzún, "Cascaded multilevel inverter with regeneration capability and reduced number of switches," *IEEE Transactions on Industrial Electronics,* vol. 55, no. 3, pp. 1059-1066, 2008.

[24] D. Zhong, B. Ozpineci, L. M. Tolbert, and J. N. Chiasson, "DC-AC Cascaded H-Bridge Multilevel Boost Inverter With No Inductors for Electric/Hybrid Electric Vehicle Applications," *IEEE Transactions on Industry Applications,* vol. 45, no. 3, pp. 963-970, 2009.

[25] T. Zhao, *Design and Control of a Cascaded H-Bridge Converter based Solid State Transformer (SST),* A Ph.D Dissertation presented to the Faculty of Graduate School, North Carolina State University, 2010.

[26] J. Pereda and J. Dixon, "High-frequency link: a solution for using only one DC source in asymmetric cascaded multilevel inverters," *IEEE Transactions on Industrial Electronics,* vol. 58, no. 9, pp. 3884-3892, 2011.

[27] L. M. Tolbert, P. Fang Zheng, and T. G. Habetler, "Multilevel PWM methods at low modulation indices," *IEEE Transactions on Power Electronics,* vol. 15, no. 4, pp. 719-725, 2000.

[28] S. Kouro, P. Lezana, M. Angulo, and J. Rodriguez, "Multicarrier PWM With DC-Link Ripple Feedforward Compensation for Multilevel Inverters," *IEEE Transactions on Power Electronics,* vol. 23, no. 1, pp. 52-59, 2008.

[29] J. Chavarria, D. Biel, F. Guinjoan, C. Meza, and J. J. Negroni, "Energy-Balance Control of PV Cascaded Multilevel Grid-Connected Inverters Under Level-Shifted and Phase-Shifted PWMs," *IEEE Transactions on Industrial Electronics,* vol. 60, no. 1, pp. 98-111, 2013.

[30] K. Xiaomin, K. A. Corzine, and M. W. Wielebski, "Overdistention operation of cascaded multilevel inverters," *IEEE Transactions on Industry Applications,* vol. 42, no. 3, pp. 817-824, 2006.

[31] K. Dae-Wook, L. Yo-Han, S. Bum-Seok, C. Chang-Ho, and H. Dong-Seok, "An improved carrier-based SVPWM method using leg voltage redundancies in generalized cascaded multilevel inverter topology," *IEEE Transactions on Power Electronics,* vol. 18, no. 1, pp. 180-187, 2003.

[32] W. Jun and K. M. Smedley, "Synthesis of Multilevel Converters Based on Single-and/or Three-Phase Converter Building Blocks," *IEEE Transactions on Power Electronics,* vol. 23, no. 3, pp. 1247-1256, 2008.

[33] P. Flores, J. Dixon, M. Ortuzar, R. Carmi, P. Barriuso, and L. Moran, "Static Var Compensator and Active Power Filter With Power Injection Capability, Using 27-

Level Inverters and Photovoltaic Cells," *IEEE Transactions on Industrial Electronics,* vol. 56, no. 1, pp. 130-138, 2009.

[34]   M. Hagiwara and H. Akagi, "Control and Experiment of Pulsewidth-Modulated Modular Multilevel Converters," *IEEE Transactions on Power Electronics,* vol. 24, no. 7,  pp. 1737-1746, 2009.

[35]   A. J. Watson, P. W. Wheeler, and J. C. Clare, "A Complete Harmonic Elimination Approach to DC Link Voltage Balancing for a Cascaded Multilevel Rectifier," *IEEE Transactions on Industrial Electronics,* vol. 54, no. 6, pp. 2946-2953, 2007.

[36]   D. Zhong, L. M. Tolbert, and J. N. Chiasson, "Active harmonic elimination for multilevel converters," *IEEE Transactions on Power Electronics,* vol. 21, no. 2, pp. 459-469, 2006.

[37]   M. Mihret, C. Odeh, B. N. V. Angirekula, and O. Ojo, "Optimal synthesis of output voltage waveforms for multilevel cascaded single phase DC-AC converters," in Proc. *Twenty-Eighth Annual IEEE Applied Power Electronics Conference and Exposition (APEC),* pp. 2690-2697, 2013.

[38]   V. G. Agelidis, A. I. Balouktsis, and M. S. A. Dahidah, "A Five-Level Symmetrically Defined Selective Harmonic Elimination PWM Strategy: Analysis and Experimental Validation," *IEEE Transactions on Power Electronics,* vol. 23, no. 1, pp. 19-26, 2008.

[39]   D. Zhong, L. M. Tolbert, B. Ozpineci, and J. N. Chiasson, "Fundamental Frequency Switching Strategies of a Seven-Level Hybrid Cascaded H-Bridge Multilevel Inverter," *IEEE Transactions on Power Electronics,* vol. 24, no. 1, pp. 25-33, 2009.

[40]   M. S. Ortmann, S. A. Mussa, and M. L. Heldwein, "Generalized Analysis of a Multistate Switching Cells-Based Single-Phase Multilevel PFC Rectifier," *IEEE Transactions on Power Electronics,* vol. 27, no. 1, pp. 46-56, 2012.

[41]   B. Diong, H. Sepahvand, and K. Corzine, "Harmonic Distortion Optimization of Cascaded H-Bridge Inverters Considering Device Voltage Drops and Non-Integer DC Voltage Ratios," *IEEE Transactions on Industrial Electronics,* vol. 60, no. 8, pp. 3106-3114, 2013.

[42]   H. Taghizadeh and M. T. Hagh, "Harmonic elimination of cascade multilevel inverters with nonequal DC sources using particle swarm optimization," *IEEE Transactions on Industrial Electronics,* vol. 57, no. 11, pp. 3678-3684, 2010.

[43]  J. R. Wells, G. Xin, P. L. Chapman, P. T. Krein, and B. M. Nee, "Modulation-Based Harmonic Elimination," *IEEE Transactions on Power Electronics,* vol. 22, no. 1, pp. 336-340, 2007.

[44]  D. G. Holmes and B. P. McGrath, "Opportunities for harmonic cancellation with carrier-based PWM for a two-level and multilevel cascaded inverters," *IEEE Transactions on Industry Applications,* vol. 37, no. 2, pp. 574-582, 2001.

[45]  D. Zhong, L. M. Tolbert, J. N. Chiasson, and B. Ozpineci, "Reduced Switching-Frequency Active Harmonic Elimination for Multilevel Converters," *IEEE Transactions on Industrial Electronics,* vol. 55, no. 3, pp. 1761-1770, 2008.

[46]  R. Gupta, A. Ghosh, and A. Joshi, "Switching Characterization of Cascaded Multilevel-Inverter-Controlled Systems," *IEEE Transactions on Industrial Electronics,* vol. 55, no. 3, pp. 1047-1058, 2008.

[47]  R. Teodorescu, M. Liserre, and P. Rodriguez, *Grid converters for photovoltaic and wind power systems* vol. 29: John Wiley & Sons, 2011.

[48]  H. Iman-Eini, J.-L. Schanen, S. Farhangi, and J. Roudet, "A modular strategy for control and voltage balancing of cascaded H-bridge rectifiers," *IEEE Transactions on Power Electronics,* vol. 23, no. 5, pp. 2428-2442, 2008.

[49]  S. Vazquez, J. I. Leon, L. G. Franquelo, J. J. Padilla, and J. M. Carrasco, "DC-voltage-ratio control strategy for multilevel cascaded converters fed with a single DC source," *IEEE Transactions on Industrial Electronics,* vol. 56, no. 7, pp. 2513-2521, 2009.

[50]  T. Zhao, G. Wang, S. Bhattacharya, and A. Huang, "Voltage and Power Balance Control for a Cascaded H-Bridge Converter based Solid State Transformer," *IEEE Transactions on Power Electronics,* vol. 28, no. 4, pp. 1523-1532, 2013.

[51]  A. Dell'Aquila, M. Liserre, V. G. Monopoli, and P. Rotondo, "Overview of PI-based solutions for the control of DC buses of a single-phase H-bridge multilevel active rectifier," *IEEE Transactions on Industry Applications,* vol. 44, pp. 857-866, 2008.

[52]  H. Sepahvand, L. Jingsheng, M. Ferdowsi, and K. A. Corzine, "Capacitor Voltage Regulation in Single-DC-Source Cascaded H-Bridge Multilevel Converters Using Phase-Shift Modulation," *IEEE Transactions on Industrial Electronics,* vol. 60, no. 9, pp. 3619-3626, 2013.

[53]  J. Rodriguez, L. Moran, J. Pontt, P. Correa, and C. Silva, "A high-performance vector control of an 11-level inverter," *IEEE Transactions on Industrial Electronics,* vol. 50, no. 1, pp. 80-85, 2003.

[54]    S. Lu and K. A. Corzine, "Advanced Control and Analysis of Cascaded Multilevel Converters Based on P-Q Compensation," *IEEE Transactions on Power Electronics,* vol. 22, no. 4, pp. 1242-1252, 2007.

[55]    L. M. Tolbert, P. Fang Zheng, T. Cunnyngham, and J. N. Chiasson, "Charge balance control schemes for cascade multilevel converter in hybrid electric vehicles," *IEEE Transactions on Industrial Electronics,* vol. 49, no. 5, pp. 1058-1064, 2002.

[56]    M. Veenstra and A. Rufer, "Control of a hybrid asymmetric multilevel inverter for competitive medium-voltage industrial drives," *IEEE Transactions on Industry Applications,* vol. 41, no. 2, pp. 655-664, 2005.

[57]    K. A. Corzine, M. W. Wielebski, F. Z. Peng, and W. Jin, "Control of cascaded multilevel inverters," *IEEE Transactions on Power Electronics,* vol. 19, no. 3, pp. 732-738, 2004.

[58]    J. I. Leon, S. Vazquez, A. J. Watson, L. G. Franquelo, P. W. Wheeler, and J. M. Carrasco, "Feed-forward space vector modulation for single-phase multilevel cascaded converters with any DC voltage ratio," *IEEE Transactions on Industrial Electronics,* vol. 56, no. 2, pp. 315-325, 2009.

[59]    A. Abrishamifar, A. A. Ahmad, and M. Mohamadian, "Fixed switching frequency sliding mode control for single-phase unipolar inverters," *IEEE Transactions on Power Electronics,* vol. 27, no. 5, pp. 2507-2514, 2012.

[60]    R. Gupta, A. Ghosh, and A. Joshi, "Multiband Hysteresis Modulation and Switching Characterization for Sliding-Mode-Controlled Cascaded Multilevel Inverter," *IEEE Transactions on Industrial Electronics,* vol. 57, no. 7, pp. 2344-2353, 2010.

[61]    N. A. Rahim and J. Selvaraj, "Multistring Five-Level Inverter With Novel PWM Control Scheme for PV Application," *IEEE Transactions on Industrial Electronics,* vol. 57, no. 6, pp. 2111-2123, 2010.

[62]    C. R. Baier, J. I. Guzman, J. R. Espinoza, M. A. Perez, and J. R. Rodriguez, "Performance Evaluation of a Multicell Topology Implemented With Single-Phase Nonregenerative Cells Under Unbalanced Supply Voltages," *IEEE Transactions on Industrial Electronics,* vol. 54, no. 6, pp. 2969-2978, 2007.

[63]    P. Zanchetta, D. B. Gerry, V. G. Monopoli, J. C. Clare, and P. W. Wheeler, "Predictive Current Control for Multilevel Active Rectifiers With Reduced Switching Frequency," *IEEE Transactions on Industrial Electronics,* vol. 55, no. 1, pp. 163-172, 2008.

[64]     P. Lezana, C. A. Silva, J. Rodriguez, and M. A. Perez, "Zero-Steady-State-Error Input-Current Controller for Regenerative Multilevel Converters Based on Single-Phase Cells," *IEEE Transactions on Industrial Electronics,* vol. 54, no. 2, pp. 733-740, 2007.

[65]     M. Monfared, S. Golestan, and J. M. Guerrero, "Analysis, Design, and Experimental Verification of a Synchronous Reference Frame Voltage Control for Single-Phase Inverters," *IEEE Transactions on Industrial Electronics,* vol. 61, no. 1, pp. 258-269, 2014.

[66]     H. Seon-Hwan, L. Liming, L. Hui, and K. Jang-Mok, "DC Offset Error Compensation for Synchronous Reference Frame PLL in Single-Phase Grid-Connected Converters," *IEEE Transactions on Power Electronics,* vol. 27, no. 8, pp. 3467-3471, 2012.

[67]     B. Bahrani, A. Rufer, S. Kenzelmann, and L. A. C. Lopes, "Vector Control of Single-Phase Voltage-Source Converters Based on Fictive-Axis Emulation," *IEEE Transactions on Industry Applications,* vol. 47, no. 2, pp. 831-840, 2011.

[68]     K. Rae-Young, C. See-Young, and S. In-Young, "Instantaneous control of average power for grid tie inverter using single phase D-Q rotating frame with all pass filter," in Proc. *30th Annual Conference of IEEE*, 2004 *Industrial Electronics Society, IECON 2004.*, pp. 274-279 Vol. 1, *2004*.

[69]     S. A. Khajehoddin, M. Karimi-Ghartemani, A. Bakhshai, and P. Jain, "A Power Control Method With Simple Structure and Fast Dynamic Response for Single-Phase Grid-Connected DG Systems," *IEEE Transactions on Power Electronics,* vol. 28, no. 1, pp. 221-233, 2013.

[70]     M. Karimi-Ghartemani, "A Unifying Approach to Single-Phase Synchronous Reference Frame PLLs," *IEEE Transactions on Power Electronics,* vol. 28, no. 10, pp. 4550-4556, 2013.

[71]     P. Wood, "Switching power converters," *New York: Van Nostrand Reinhold,/ c1981,* vol. 1, 1981.

[72]     L. Yi-Hung and L. Ching-Ming, "Newly-Constructed Simplified Single-Phase Multistring Multilevel Inverter Topology for Distributed Energy Resources," *IEEE Transactions on Power Electronics,* vol. 26, no. 9, pp. 2386-2392, 2011.

[73]     J. F. Wakerly, *Digital design: principles and practices*: Prentice-Hall, Inc., 2000.

[74]     M. Saeedifard, R. Iravani, and J. Pou, "Analysis and Control of DC-Capacitor-Voltage-Drift Phenomenon of a Passive Front-End Five-Level Converter," *IEEE Transactions on Industrial Electronics,* vol. 54, no. 6, pp. 3255-3266, 2007.

[75]     D. W. Hart, *Power electronics*: Tata McGraw-Hill Education, 2011.

[76] B. Bolsens, K. De Brabandere, J. van den Keybus, J. Driesen, and R. Belmans, "Model-based generation of low distortion currents in grid-coupled PWM-inverters using an LCL output filter," *IEEE Transactions on Power Electronics,* vol. 21, no. 4, pp. 1032-1040, 2006.

[77] J. Dannehl, M. Liserre, and F. W. Fuchs, "Filter-Based Active Damping of Voltage Source Converters With LCL Filter," *IEEE Transactions on Industrial Electronics,* vol. 58, no. 8, pp. 3623-3633, 2011.

[78] J. Dannehl, F. W. Fuchs, and P. B. Thogersen, "PI State Space Current Control of Grid-Connected PWM Converters With LCL Filters," *IEEE Transactions on Power Electronics,* vol. 25, no. 9, pp. 2320-2330, 2010.

[79] M. Liserre, F. Blaabjerg, and S. Hansen, "Design and control of an LCL-filter-based three-phase active rectifier," *IEEE Transactions on Industry Applications,* vol. 41, no. 5, pp. 1281-1291, 2005.

[80] W. Weimin, H. Yuanbin, T. Tianhao, and F. Blaabjerg, "A New Design Method for the Passive Damped LCL and LLCL Filter-Based Single-Phase Grid-Tied Inverter," *IEEE Transactions on Industrial Electronics,* vol. 60, no. 10, pp. 4339-4350, 2013.

[81] W. Weimin, H. Yuanbin, and F. Blaabjerg, "An LLCL Power Filter for Single-Phase Grid-Tied Inverter," *IEEE Transactions on Power Electronics,* vol. 27, no. 2, pp. 782-789, 2012.

[82] N. M. Krylov and N. N. Bogoliubov, *Introduction to non-linear mechanics*: Princeton University Press, 1947.

[83] J. C. Lindenlaub, "An approach for finding the sinusoidal steady state response of nonlinear systems," in *Proc. 7th Ann. Allerton Conf. Circuit and System Theory*, 1969.

[84] M. Nakhla and J. Vlach, "A piecewise harmonic balance technique for determination of periodic response of nonlinear systems," *IEEE Transactions on Circuits and Systems,* vol. 23, no. 2, pp. 85-91, 1976.

[85] J. Fu, *Multiport High Frequency Transformer Coupled Bidirectional DC-DC Converters for Hybrid Renewable Energy System*, A Ph.D Dissertation Presented to the Faculty of the Graduate School, Tennessee Technological University, Tennessee Technological University, 2012.

**APPENDICES**

# APPENDIX A

# COMPLETE DERIVATION OF FOURIER SERIES ANALYSIS OF MULTI-STRING FIVE LEVEL INVERTER

The double Fourier series approximation of converter switching functions given in [4] as

$$
S_{ij}(\omega_s, \omega_c) = \begin{bmatrix} \dfrac{A_{00}}{2} + \sum_{n=1}^{\infty} \left(A_{0n}\cos(n\omega_s t) + B_{0n}\sin(n\omega_s t)\right) \\ + \sum_{m=1}^{\infty} \left(A_{m0}\cos(m\omega_c t) + B_{m0}\sin(m\omega_c t)\right) \\ + \sum_{\substack{m=1 \\ }}^{\infty} \sum_{\substack{n=-\infty \\ n\neq 0}}^{\infty} \left(A_{mn}\cos(m\omega_c t + n\omega_s t) + B_{mn}\sin(m\omega_c t + n\omega_s t)\right) \end{bmatrix}
$$

(A.1)

Solving for each switching function over a period, considering the average and fundamental components only

## Solving for $S_{ap}$:

The average component of $S_{ap}$ is derived as

$$
a_{o\,S_{ap}} = \frac{1}{2\pi}\left(\int_{\psi_1}^{\pi+\psi_1}(1-M_1\sin(\theta+\psi_1))d\theta + \int_{\pi+\psi_1}^{2\pi+\psi_1}(-M_1\sin(\theta+\psi_1))d\theta\right)
$$

(A.2)

$$
a_{oS_{ap}} = \frac{1}{2\pi}\left(\begin{array}{l}\pi + M_1\left[\cos(\pi+\psi_1+\psi_1)-\cos(\psi_1+\psi_1)\right] \\ + M_1\left[\cos(2\pi+\psi_1+\psi_1)-\cos(\pi+\psi_1+\psi_1)\right]\end{array}\right)
$$

$$
a_{oS_{ap}} = \frac{1}{2\pi}\left(\begin{array}{l}\pi + M_1\left[\cos(\pi+2\psi_1)-\cos(2\psi_1)\right] \\ + M_1\left[\cos(2\pi+2\psi_1)-\cos(\pi+2\psi_1)\right]\end{array}\right)
$$

$$
a_{oS_{ap}} = \frac{1}{2\pi}\left(\pi + M_1\left[-\cos(2\psi_1)-\cos(2\psi_1)\right] + M_1\left[\cos(2\psi_1)+\cos(2\psi_1)\right]\right)
$$

$$a_{oS_{ap}} = \frac{1}{2\pi}\left(\pi - 2M_1[\cos(2\psi_1)] + 2M_1[\cos(2\psi_1)]\right)$$

$$a_{oS_{ap}} = \frac{1}{2\pi}(\pi)$$

$$a_{oS_{ap}} = \frac{1}{2} \tag{A.3}$$

The fundamental component ($n=1$) for S$_{ap}$ is derived as:

$$a_{1S_{ap}} = \frac{1}{\pi}\left( \begin{array}{l} \int\limits_{\psi_1}^{\pi+\psi_1}(1 - M_1\sin(\theta+\psi_1))\cos(\theta+\psi_1)d\theta \\[4mm] + \int\limits_{\pi+\psi_1}^{2\pi+\psi_1}(-M_1\sin(\theta+\psi_1))\cos(\theta+\psi_1)d\theta \end{array} \right) \tag{A.4}$$

$$a_{1S_{ap}} = \frac{1}{\pi}\left( \begin{array}{l} \int\limits_{\psi_1}^{\pi+\psi_1}\cos(\theta+\psi_1) - M_1\sin(\theta+\psi_1)\cos(\theta+\psi_1)d\theta \\[4mm] - \int\limits_{\pi+\psi_1}^{2\pi+\psi_1}M_1\sin(\theta+\psi_1)\cos(\theta+\psi_1)d\theta \end{array} \right)$$

$$a_{1S_{ap}} = \frac{1}{\pi}\left( \begin{array}{l} \sin(\pi+\psi_1+\psi_1) - \sin(\psi_1+\psi_1) - \dfrac{M_1}{2}\int\limits_{\psi_1}^{\pi+\psi_1}2\sin(\theta+\psi_1)\cos(\theta+\psi_1)d\theta \\[4mm] - \dfrac{M_1}{2}\int\limits_{\pi+\psi_1}^{2\pi+\psi_1}2\sin(\theta+\psi_1)\cos(\theta+\psi_1)d\theta \end{array} \right)$$

$$= \frac{1}{\pi}\left( -2\sin(2\psi_1) - \frac{M_1}{2}\int\limits_{\psi_1}^{\pi+\psi_1}\sin(2\theta+2\psi_1)d\theta - \frac{M_1}{2}\int\limits_{\pi+\psi_1}^{2\pi+\psi_1}\sin(2\theta+2\psi_1)d\theta \right)$$

$$a_{1S_{ap}} = \frac{1}{\pi}\left( \begin{array}{l} -2\sin(2\psi_1) - \dfrac{M_1}{4}\left(\cos(2\pi+2\psi_1+2\psi_1) - \cos(2\psi_1+2\psi_1)\right) \\[4mm] - \dfrac{M_1}{4}\left(\cos(4\pi+2\psi_1+2\psi_1) - \cos(2\pi+2\psi_1+2\psi_1)\right) \end{array} \right)$$

266

$$a_{1S_{ap}} = \frac{1}{\pi}\left( \begin{array}{l} -2\sin(2\psi_1) - \dfrac{M_1}{4}\left(\cos(4\psi_1) - \cos(4\psi_1)\right) \\[3mm] -\dfrac{M_1}{4}\left(\cos(4\psi_1) - \cos(4\psi_1)\right) \end{array} \right)$$

$$a_{1S_{ap}} = \frac{1}{\pi}\left(-2\sin(2\psi_1)\right)$$

$$a_{1S_{ap}} = -\frac{2}{\pi}\sin(2\psi_1)$$ 

<div align="right">(A.5)</div>

$$b_{1S_{ap}} = \frac{1}{\pi}\left( \begin{array}{l} \displaystyle\int_{\psi_1}^{\pi+\psi_1}\left(\sin(\theta+\psi_1) - M_1\sin(\theta+\psi_1)\sin(\theta+\psi_1)\right)d\theta \\[5mm] \displaystyle+ \int_{\pi+\psi_1}^{2\pi+\psi_1}\left(-M_1\sin(\theta+\psi_1)\right)\sin(\theta+\psi_1)d\theta \end{array} \right)$$

$$b_{1S_{ap}} = \frac{1}{\pi}\left( \begin{array}{l} -\left(\cos(\pi+\psi_1+\psi_1) - \cos(\psi_1+\psi_1)\right) - \dfrac{M_1}{2}\displaystyle\int_{\psi_1}^{\pi+\psi_1}\left(2\sin(\theta+\psi_1)\right)\sin(\theta+\psi_1)d\theta \\[5mm] -\dfrac{M_1}{2}\displaystyle\int_{\pi+\psi_1}^{2\pi+\psi_1}\left(2\sin(\theta+\psi_1)\right)\sin(\theta+\psi_1)d\theta \end{array} \right)$$

$$b_{1S_{ap}} = \frac{1}{\pi}\left( \begin{array}{l} -\left(-\cos(2\psi_1) - \cos(2\psi_1)\right) \\[3mm] -\dfrac{M_1}{2}\displaystyle\int_{\psi_1}^{\pi+\psi_1}\left(1 - \cos(2\theta+2\psi_1)\right)d\theta - \dfrac{M_1}{4}\displaystyle\int_{\pi+\psi_1}^{2\pi+\psi_1}\left(1 - \cos(2\theta+2\psi_1)\right)d\theta \end{array} \right)$$

$$b_{1S_{ap}} = \frac{1}{\pi}\left( \begin{array}{l} 2\cos(2\psi_1) - \dfrac{M_1}{2}(\pi+\psi_1-\psi_1) - \dfrac{M_1}{2}(2\pi+\psi_1-\pi-\psi_1) \\[3mm] +\dfrac{M_1}{4}\left(\sin(2\pi+2\psi_1+2\psi_1) - \sin(2\psi_1+2\psi_1)\right) \\[3mm] +\dfrac{M_1}{4}\left(\sin(4\pi+2\psi_1+2\psi_1) - \sin(2\pi+2\psi_1+2\psi_1)\right) \end{array} \right)$$

$$b_{1S_{ap}} = \frac{1}{\pi} \left( \begin{array}{l} 2\cos(2\psi_1) - \dfrac{M_1}{2}(\pi) + \dfrac{M_1}{4}\left(\sin(4\psi_1) - \sin(4\psi_1)\right) \\[2mm] -\dfrac{M_1}{2}(\pi) + \dfrac{M_1}{4}\left(\sin(4\psi_1) - \sin(4\psi_1)\right) \end{array} \right)$$

$$b_{1S_{ap}} = \frac{2}{\pi}\cos(2\psi_1) - M_1 \tag{A.6}$$

According to Fourier series, the expression for $S_{ap}$ is given as

$$S_{ap} = \frac{1}{2} - \frac{2}{\pi}\sin(2\psi_1)\cos(\theta + \psi_1) + \left(\frac{2}{\pi}\cos(2\psi_1) - M_1\right)\sin(\theta + \psi_1) \tag{A.7}$$

$$S_{ap} = \frac{1}{2} - M_p - \frac{2}{\pi}\left(\sin(\psi_1 - \theta)\right) \tag{A.8}$$

**Solving for $S_{am}$:**

The average component of $S_{am}$ is derived as

$$a_{oS_{am}} = \frac{1}{2\pi}\left( \int_{\psi_1}^{\pi+\psi_1} 1.d\theta \right) \tag{A.9}$$

$$a_{oS_{am}} = \frac{1}{2\pi}\left(\pi + \psi_1 - \psi_1\right)$$

$$a_{oS_{am}} = \frac{1}{2\pi}\left(\pi\right)$$

$$a_{oS_{am}} = \frac{1}{2} \tag{A.10}$$

The fundamental component ($n=1$) for $S_{am}$ is derived as:

$$a_{1S_{am}} = \frac{1}{\pi}\left( \int_{\psi_1}^{\pi+\psi_{1(}} 1.\cos(\theta + \psi_1)d\theta \right) \tag{A.11}$$

$$a_{1S_{am}} = \frac{1}{\pi}\left(\sin(\pi + \psi_1 + \psi_1) - \sin(\psi_1 + \psi_1)\right)$$

$$a_{1S_{am}} = \frac{1}{\pi}\left(-\sin(2\psi_1) - \sin(2\psi_1)\right)$$

$$a_{1S_{am}} = -\frac{2}{\pi}\sin(2\psi_1) \tag{A.12}$$

$$b_{1S_{am}} = \frac{1}{\pi}\left(\int_{\psi_1}^{\pi+\psi_1(} 1.\sin(\theta+\psi_1)d\theta\right) \tag{A.13}$$

$$b_{1S_{am}} = \frac{-1}{\pi}\left(\cos(\pi+\psi_1+\psi_1) - \cos(\psi_1+\psi_1)\right)$$

$$b_{1S_{am}} = \frac{-1}{\pi}\left(-\cos(2\psi_1) - \cos(2\psi_1)\right)$$

$$b_{1S_{am}} = \frac{2}{\pi}\cos(2\psi_1) \tag{A.14}$$

According to Fourier series, the expression for $S_{am}$ is given as

$$S_{am} = \frac{1}{2} - \frac{2}{\pi}\sin(2\psi_1)\cos(\theta+\psi_1) + \left(\frac{2}{\pi}\cos(2\psi_1)\right)\sin(\theta+\psi_1) \tag{A.15}$$

$$S_{am} = \frac{1}{2} - \frac{2}{\pi}\left(\sin(\psi_1-\theta)\right) \tag{A.16}$$

**Solving for $S_{an}$:**

The average component of $S_{an}$ is derived as

$$a_{oS_{an}} = \frac{1}{2\pi}\left(\int_{\psi_2}^{\pi+\psi_2}(1-M_2\sin(\theta+\psi_2))d\theta + \int_{\pi+\psi_2}^{2\pi+\psi_2} -(M_2\sin(\theta+\psi_2))d\theta\right) \tag{A.17}$$

$$a_{oS_{an}} = \frac{1}{2\pi}\left(\begin{array}{l}\pi+\psi_2-\psi_2+M_2[\cos(\pi+\psi_2+\psi_2)-\cos(\psi_2+\psi_2)]\\+M_2[\cos(2\pi+\psi_2+\psi_2)-\cos(\pi+\psi_2+\psi_2)]\end{array}\right)$$

$$a_{o\,S_{an}} = \frac{1}{2\pi}\left(\begin{array}{l}\pi + M_2\left[\cos(\pi + 2\psi_2) - \cos(2\psi_2)\right] \\ + M_2\left[\cos(2\pi + 2\psi_2) - \cos(\pi + 2\psi_2)\right]\end{array}\right)$$

$$a_{o\,S_{an}} = \frac{1}{2\pi}\left(\pi + M_2\left[-\cos(2\psi_2) - \cos(2\psi_2)\right] + M_2\left[\cos(2\psi_2) + \cos(2\psi_2)\right]\right)$$

$$a_{o\,S_{an}} = \frac{1}{2\pi}\left(\pi - 2M_2\left[\cos(2\psi_2)\right] + 2M_2\left[\cos(2\psi_2)\right]\right)$$

$$a_{o\,S_{an}} = \frac{1}{2\pi}(\pi)$$

$$a_{o\,S_{an}} = \frac{1}{2} \tag{A.18}$$

The fundamental component ($n=1$) for $S_{an}$ is derived as:

$$\tag{A.19}$$

$$a_{1\,S_{an}} = \frac{1}{\pi}\left(\begin{array}{l}\displaystyle\int_{\psi_1}^{\pi+\psi_1}\left(1 - M_2\sin(\theta+\psi_2)\right)\cos(\theta+\psi_2)d\theta \\ \displaystyle + \int_{\pi+\psi_1}^{2\pi+\psi_1}-\left(M_2\sin(\theta+\psi_2)\cos(\theta+\psi_2)\right)d\theta\end{array}\right)$$

$$a_{1\,S_{an}} = \frac{1}{\pi}\left(\begin{array}{l}\displaystyle\int_{\psi_2}^{\pi+\psi_2}\cos(\theta+\psi_2) - M_2\sin(\theta+\psi_2)\cos(\theta+\psi_2)d\theta \\ \displaystyle - \int_{\pi+\psi_2}^{2\pi+\psi_2}M_2\sin(\theta+\psi_2)\cos(\theta+\psi_2)d\theta\end{array}\right)$$

$$a_{1\,S_{an}} = \frac{1}{\pi}\left(\begin{array}{l}\displaystyle\sin(\pi+\psi_2+\psi_2) - \sin(\psi_2+\psi_2) - \frac{M_2}{2}\int_{\psi_2}^{\pi+\psi_2}2\sin(\theta+\psi_2)\cos(\theta+\psi_2)d\theta \\ \displaystyle - \frac{M_2}{2}\int_{\pi+\psi_2}^{2\pi+\psi_2}2\sin(\theta+\psi_2)\cos(\theta+\psi_2)d\theta\end{array}\right)$$

$$a_{1\,S_{an}} = \frac{1}{\pi}\left(-2\sin(2\psi_2) - \frac{M_2}{2}\int_{\psi_2}^{\pi+\psi_2}\sin(2\theta+2\psi_2)d\theta - \frac{M_2}{2}\int_{\pi+\psi_2}^{2\pi+\psi_2}\sin(2\theta+2\psi_2)d\theta\right)$$

$$a_{1S_{an}} = \frac{1}{\pi} \left( \begin{array}{l} -2\sin(2\psi_2) - \dfrac{M_2}{4}\left(\cos(2\pi + 2\psi_2 + 2\psi_2) - \cos(2\psi_2 + 2\psi_2)\right) \\[3mm] -\dfrac{M_2}{4}\left(\cos(4\pi + 2\psi_2 + 2\psi_2) - \cos(2\pi + 2\psi_2 + 2\psi_2)\right) \end{array} \right)$$

$$a_{1S_{an}} = \frac{1}{\pi}\left(-2\sin(2\psi_2) - \frac{M_2}{4}\left(\cos(4\psi_2) - \cos(4\psi_2)\right) - \frac{M_2}{4}\left(\cos(4\psi_2) - \cos(4\psi_2)\right)\right)$$

$$a_{1S_{an}} = \frac{1}{\pi}\left(-2\sin(2\psi_2)\right)$$

$$a_{1S_{an}} = -\frac{2}{\pi}\sin(2\psi_2) \tag{A.20}$$

$$\tag{A.21}$$

$$b_{1S_{an}} = \frac{1}{\pi}\left( \begin{array}{l} \displaystyle\int_{\psi 2}^{\pi + \psi 2} \left(1 - M_2 \sin(\theta + \psi_2)\right)\sin(\theta + \psi_2)\,d\theta \\[4mm] + \displaystyle\int_{\pi + \psi 2}^{2\pi + \psi 2} -\left(M_2 \sin(\theta + \psi_2)\sin(\theta + \psi_2)\right)d\theta \end{array} \right)$$

$$b_{1S_{an}} = \frac{1}{\pi}\left( \begin{array}{l} \displaystyle\int_{\psi 2}^{\pi + \psi 2} \left(\sin(\theta + \psi_2) - M_2 \sin(\theta + \psi_2)\sin(\theta + \psi_2)\right)d\theta \\[4mm] + \displaystyle\int_{\pi + \psi 2}^{2\pi + \psi 2} -\left(M_2 \sin(\theta + \psi_2)\sin(\theta + \psi_2)\right)d\theta \end{array} \right)$$

$$b_{1S_{an}} = \frac{1}{\pi}\left( \begin{array}{l} -\left(\cos(\pi + \psi_2 + \psi_2) - \cos(\psi_2 + \psi_2)\right) \\[3mm] -\dfrac{M_2}{2}\displaystyle\int_{\psi 1}^{\pi + \psi 1} \left(2\sin(\theta + \psi_2)\sin(\theta + \psi_2)\right)d\theta \\[4mm] -\dfrac{M_2}{2}\displaystyle\int_{\pi + \psi 1}^{2\pi + \psi 1} \left(2\sin(\theta + \psi_2)\sin(\theta + \psi_2)\right)d\theta \end{array} \right)$$

$$b_{1S_{an}} = \frac{1}{\pi} \left( \begin{array}{l} -(-\cos(2\psi_2) - \cos(2\psi_2)) - \dfrac{M_2}{2} \displaystyle\int_{\psi_2}^{\pi+\psi_2} (1 - \cos(2\theta + 2\psi_2)) d\theta \\ \\ -\dfrac{M_2}{2} \displaystyle\int_{\pi+\psi_1}^{2\pi+\psi_1} (1 - \cos(2\theta + 2\psi_2)) d\theta \end{array} \right)$$

$$b_{1S_{an}} = \frac{1}{\pi} \left( \begin{array}{l} (2\cos(2\psi_2)) - \dfrac{M_2}{2}(\pi + \psi_2 - \psi_2) - \dfrac{M_2}{2}(2\pi + \psi_1 - (\pi + \psi_1)) \\ \\ +\dfrac{M_2}{4}(\sin(2\pi + 2\psi_2 + 2\psi_2) - \sin(2\psi_2 + 2\psi_2)) \\ \\ +\dfrac{M_2}{4}(\sin(4\pi + 2\psi_2 + 2\psi_2) - \sin(2\pi + 2\psi_2 + 2\psi_2)) \end{array} \right)$$

$$b_{1S_{an}} = \frac{1}{\pi} \left( \begin{array}{l} (2\cos(2\psi_2)) - \dfrac{M_2}{2}(\pi) + \dfrac{M_2}{4}(\sin(4\psi_2) - \sin(4\psi_2)) \\ \\ -\dfrac{M_2}{2}(\pi) + \dfrac{M_2}{4}(\sin(4\psi_2) - \sin(4\psi_2)) \end{array} \right)$$

$$b_{1S_{an}} = \frac{1}{\pi} \left( (2\cos(2\psi_2)) - 2\frac{M_2}{2}(\pi) \right)$$

$$b_{1S_{an}} = \frac{2}{\pi}\cos(2\psi_2) - M_2 \tag{A.22}$$

According to Fourier series, the expression for $S_{an}$ is given as

$$S_{an} = \frac{1}{2} - \frac{2}{\pi}\sin(2\psi_2)\cos(\theta + \psi_2) + \left( \frac{2}{\pi}\cos(2\psi_2) - M_2 \right)\sin(\theta + \psi_2) \tag{A.23}$$

$$S_{an} = \frac{1}{2} - M_n - \frac{2}{\pi}(\sin(\psi_2 - \theta)) \tag{A.24}$$

**Solving for $S_{bp}$:**

The average component of $S_{bp}$ is derived as

$$a_{oS_{bp}} = \frac{1}{2\pi} \left( \int_{\psi_1}^{\pi+\psi_1} M_1 \sin(\theta + \psi_1) d\theta + \int_{\pi+\psi_1}^{2\pi+\psi_1} (1 + M_1 \sin(\theta + \psi_1)) d\theta \right) \tag{A.25}$$

$$a_{oS_{bp}} = \frac{1}{2\pi} \left( \begin{array}{l} -M_1 (\cos(\pi + \psi_1 + \psi_1) - \cos(\psi_1 + \psi_1)) + 2\pi + \psi_1 - (\pi + \psi_1) - \\ M_1 (\cos(2\pi + \psi_1 + \psi_1) - \cos(\pi + \psi_1 + \psi_1)) \end{array} \right)$$

$$a_{oS_{bp}} = \frac{1}{2\pi} \left( -M_1 (\cos(\pi + 2\psi_1) - \cos(2\psi_1)) + \pi - M_1 (\cos(2\pi + 2\psi_1) - \cos(\pi + 2\psi_1)) \right)$$

$$a_{oS_{bp}} = \frac{1}{2\pi} \left( -M_1 (-\cos(2\psi_1) - \cos(2\psi_1)) + \pi - M_1 (\cos(2\psi_1) + \cos(2\psi_1)) \right)$$

$$a_{oS_{bp}} = \frac{1}{2\pi} \left( -M_1 (-2\cos(2\psi_1)) + \pi - M_1 (2\cos(2\psi_1)) \right)$$

$$a_{oS_{bp}} = \frac{1}{2\pi} \left( M_1 (2\cos(2\psi_1)) + \pi - M_1 (2\cos(2\psi_1)) \right)$$

$$a_{oS_{bp}} = \frac{1}{2\pi} (\pi)$$

$$a_{oS_{bp}} = \frac{1}{2} \tag{A.26}$$

The fundamental component ($n=1$) for $S_{bp}$ is derived as:

$$a_{1S_{bp}} = \frac{1}{\pi} \left( \begin{array}{l} \int_{\psi_1}^{\pi+\psi_1} M_1 \sin(\theta + \psi_1) \cos(\theta + \psi_1) d\theta \\ + \int_{\pi+\psi_1}^{2\pi+\psi_1} (\cos(\theta + \psi_1) + M_1 \sin(\theta + \psi_1) \cos(\theta + \psi_1)) d\theta \end{array} \right) \tag{A.27}$$

$$a_{1S_{bp}} = \frac{1}{\pi} \left( \begin{array}{l} \frac{M_1}{2} \int_{\psi_1}^{\pi+\psi_1} 2\sin(\theta + \psi_1) \cos(\theta + \psi_1) d\theta + \sin(2\pi + \psi_1 + \psi_1) \\ + \frac{M_1}{2} \int_{\pi+\psi_1}^{2\pi+\psi_1} (2\sin(\theta + \psi_1) \cos(\theta + \psi_1)) d\theta - \sin(\pi + \psi_1 + \psi_1) \end{array} \right)$$

$$a_{1S_{bp}} = \frac{1}{\pi} \left( \begin{array}{l} \dfrac{M_1}{2} \displaystyle\int_{\psi_1}^{\pi+\psi_1} \sin(2\theta + 2\psi_1)d\theta + \sin(2\psi_1) + \sin(2\psi_1) \\[4mm] + \dfrac{M_1}{2} \displaystyle\int_{\pi+\psi_1}^{2\pi+\psi_1} \big(\sin(2\theta + 2\psi_1)\big)d\theta \end{array} \right)$$

$$a_{1S_{bp}} = \frac{1}{\pi} \left( \begin{array}{l} 2\sin(2\psi_1) - \dfrac{M_1}{4}\big(\cos(2\pi + 2\psi_1 + 2\psi_1) - \cos(2\psi_1 + 2\psi_1)\big) \\[4mm] + \dfrac{M_1}{4}\big(\cos(4\pi + 2\psi_1 + 2\psi_1) - \cos(2\pi + 2\psi_1 + 2\psi_1)\big) \end{array} \right)$$

$$a_{1S_{bp}} = \frac{1}{\pi} \left( 2\sin(2\psi_1) - \frac{M_1}{4}\big(\cos(4\psi_1) - \cos(4\psi_1)\big) + \frac{M_1}{4}\big(\cos(4\psi_1) - \cos(4\psi_1)\big) \right)$$

$$a_{1S_{bp}} = \frac{1}{\pi}\big(2\sin(2\psi_1)\big)$$

$$a_{1S_{bp}} = \frac{2}{\pi}\sin(2\psi_1) \tag{A.28}$$

$$b_{1S_{bp}} = \frac{1}{\pi} \left( \begin{array}{l} \displaystyle\int_{\psi_1}^{\pi+\psi_1} M_1 \sin(\theta + \psi_1)\sin(\theta + \psi_1)d\theta \\[4mm] + \displaystyle\int_{\pi+\psi_1}^{2\pi+\psi_1} \big(\sin(\theta + \psi_1) + M_1 \sin(\theta + \psi_1)\sin(\theta + \psi_1)\big)d\theta \end{array} \right) \tag{A.29}$$

$$b_{1S_{bp}} = \frac{1}{\pi} \left( \begin{array}{l} \dfrac{M_1}{2} \displaystyle\int_{\psi_1}^{\pi+\psi_1} 1 - \cos(2\theta + 2\psi_1)d\theta \\[4mm] + \displaystyle\int_{\pi+\psi_1}^{2\pi+\psi_1} \left( \sin(\theta + \psi_1) + \dfrac{M_1}{2}(1 - \cos(2\theta + 2\psi_1)) \right)d\theta \end{array} \right)$$

$$b_{1S_{bp}} = \frac{1}{\pi} \begin{pmatrix} \frac{M_1}{2}(\pi + \psi_1 - \psi_1) - \frac{M_1}{4}(\sin(2\pi + 2\psi_1 + 2\psi_1) - \sin(2\psi_1 + 2\psi_1)) \\ -(\cos(2\pi + \psi_1 + \psi_1) - \cos(\pi + \psi_1 + \psi_1)) + \frac{M_1}{2}(2\pi + \psi_1 - (\pi + \psi_1)) \\ -\frac{M_1}{4}(\sin(4\pi + 2\psi_1 + 2\psi_1) - \sin(2\pi + 2\psi_1 + 2\psi_1)) \end{pmatrix}$$

$$b_{1S_{bp}} = \frac{1}{\pi} \begin{pmatrix} \frac{M_1}{2}(\pi) - \frac{M_1}{4}(\sin(4\psi_1) - \sin(4\psi_1)) - (\cos(2\psi_1) + \cos(2\psi_1)) + \frac{M_1}{2}(\pi) \\ -\frac{M_1}{4}(\sin(4\psi_1) - \sin(4\psi_1)) \end{pmatrix}$$

$$b_{1S_{bp}} = \frac{1}{\pi} \left( \frac{M_1}{2}(\pi) - (\cos(2\psi_1) + \cos(2\psi_1)) + \frac{M_1}{2}(\pi) \right)$$

$$b_{1S_{bp}} = M_1 - \frac{2}{\pi} \cos(2\psi_1) \qquad (A.30)$$

According to Fourier series, the expression for S$_{bp}$ is given as

$$S_{bp} = \frac{1}{2} + \frac{2}{\pi} \sin(2\psi_1) \cos(\theta + \psi_1) + \left( M_1 - \frac{2}{\pi} \cos(2\psi_1) \right) \sin(\theta + \psi_1) \qquad (A.31)$$

$$S_{bp} = \frac{1}{2} + M_p + \frac{2}{\pi} \left( \sin(\psi_1 - \theta) \right) \qquad (A.32)$$

**Solving for S$_{bm}$:**

The average component of S$_{bm}$ is derived as

$$a_{oS_{bm}} = \frac{1}{2\pi} \left( \int_{\pi + \psi_1}^{2\pi + \psi_1} 1.d\theta \right) \qquad (A.33)$$

$$a_{oS_{bm}} = \frac{1}{2\pi} \left( 2\pi + \psi_1 - (\pi + \psi_1) \right)$$

$$a_{o\,S_{bm}} = \frac{1}{2\pi}(\pi)$$

$$a_{o\,S_{bm}} = \frac{1}{2} \tag{A.34}$$

The fundamental component ($n=1$) for $S_{bm}$ is derived as:

$$a_{1S_{bm}} = \frac{1}{\pi}\left(\int_{\pi+\psi_1}^{2\pi+\psi_1} 1.\cos(\theta+\psi_1)d\theta\right) \tag{A.35}$$

$$a_{1S_{bm}} = \frac{1}{\pi}\left(\sin(2\pi+\psi_1+\psi_1)-\sin(\pi+\psi_1+\psi_1)\right)$$

$$a_{1S_{bm}} = \frac{1}{\pi}\left(\sin(2\psi_1)+\sin(2\psi_1)\right)$$

$$a_{1S_{bm}} = \frac{2}{\pi}\sin(2\psi_1) \tag{A.36}$$

$$b_{1S_{bm}} = \frac{1}{\pi}\left(\int_{\pi+\psi_1}^{2\pi+\psi_1} 1.\sin(\theta+\psi_1)d\theta\right) \tag{A.37}$$

$$b_{1S_{bm}} = \frac{1}{\pi}\left(-\left(\cos(2\pi+\psi_1+\psi_1)-\cos(\pi+\psi_1+\psi_1)\right)\right)$$

$$b_{1S_{bm}} = \frac{1}{\pi}\left(-\left(\cos(2\psi_1)+\cos(2\psi_1)\right)\right)$$

$$b_{1S_{bm}} = -\frac{2}{\pi}\cos(2\psi_1) \tag{A.38}$$

According to Fourier series, the expression for $S_{bm}$ is given as

$$S_{bm} = \frac{1}{2}+\frac{2}{\pi}\sin(2\psi_1)\cos(\theta+\psi_1)-\left(\frac{2}{\pi}\cos(2\psi_1)\right)\sin(\theta+\psi_1) \tag{A.39}$$

$$S_{bm} = \frac{1}{2} + \frac{2}{\pi}\left(\sin(\psi_1 - \theta)\right)$$

## Solving for $S_{bn}$:

The average component of $S_{bn}$ is derived as

$$a_{o\,S_{bn}} = \frac{1}{2\pi}\left(\int_{\psi_2}^{\pi+\psi_2} M_2 \sin(\theta + \psi_2)d\theta + \int_{\pi+\psi_2}^{2\pi+\psi_2}(1 + M_2 \sin(\theta + \psi_2))d\theta\right)$$

$$a_{o\,S_{bn}} = \frac{1}{2\pi}\left(\begin{array}{l} -M_2\left(\cos(\pi + \psi_2 + \psi_2) - \cos(\psi_2 + \psi_2)\right) + \\ \left(2\pi + \psi_2 - (\pi + \psi_2) - M_2\left(\cos(2\pi + \psi_2 + \psi_2) - \cos(\pi + \psi_2 + \psi_2)\right)\right) \end{array}\right)$$

$$a_{o\,S_{bn}} = \frac{1}{2\pi}\left(\begin{array}{l} -M_2\left(\cos(\pi + 2\psi_2) - \cos(2\psi_2)\right) \\ +\left(\pi - M_2\left(\cos(2\pi + 2\psi_2) - \cos(\pi + 2\psi_2)\right)\right) \end{array}\right)$$

$$a_{o\,S_{bn}} = \frac{1}{2\pi}\left(-M_2\left(-\cos(2\psi_2) - \cos(2\psi_2)\right) + \left(\pi - M_2\left(\cos(2\psi_2) + \cos(2\psi_2)\right)\right)\right)$$

$$a_{o\,S_{bn}} = \frac{1}{2\pi}\left(2M_2\left(\cos(2\psi_2)\right) + \pi - M_2\left(2\cos(2\psi_2)\right)\right)$$

$$a_{o\,S_{bn}} = \frac{1}{2\pi}\left(\pi\right)$$

$$a_{o\,S_{bn}} = \frac{1}{2}$$

The fundamental component ($n=1$) for $S_{bn}$ is derived as:

$$a_{1\,S_{bn}} = \frac{1}{\pi}\left(\begin{array}{l} \int_{\psi_2}^{\pi+\psi_2} M_2 \sin(\theta + \psi_2)\cos(\theta + \psi_2)d\theta \\ + \int_{\pi+\psi_2}^{2\pi+\psi_2}(1 + M_2 \sin(\theta + \psi_2))\cos(\theta + \psi_2)d\theta \end{array}\right)$$

$$a_{1S_{bn}} = \frac{1}{\pi}\left( \begin{array}{l} \dfrac{M_2}{2}\displaystyle\int_{\psi_2}^{\pi+\psi_2} 2\sin(\theta+\psi_2)\cos(\theta+\psi_2)d\theta + \sin(2\pi+\psi_2+\psi_2) \\[3ex] + \dfrac{M_2}{2}\displaystyle\int_{\pi+\psi_2}^{2\pi+\psi_2}\big(2\sin(\theta+\psi_2)\cos(\theta+\psi_2)\big)d\theta - \sin(\pi+\psi_2+\psi_2) \end{array}\right)$$

$$a_{1S_{bn}} = \frac{1}{\pi}\left( \begin{array}{l} \dfrac{M_2}{2}\displaystyle\int_{\psi_2}^{\pi+\psi_2}\sin(2\theta+2\psi_2)d\theta + \sin(2\psi_2) + \sin(2\psi_2) \\[3ex] + \dfrac{M_2}{2}\displaystyle\int_{\pi+\psi_2}^{2\pi+\psi_2}\big(\sin(2\theta+2\psi_2)\big)d\theta \end{array}\right)$$

$$a_{1S_{bn}} = \frac{1}{\pi}\left( \begin{array}{l} 2\sin(2\psi_2) - \dfrac{M_2}{4}\big(\cos(2\pi+2\psi_2+2\psi_2) - \cos(2\psi_2+2\psi_2)\big) \\[3ex] + \dfrac{M_2}{4}\big(\cos(4\pi+2\psi_2+2\psi_2) - \cos(2\pi+2\psi_2+2\psi_2)\big) \end{array}\right)$$

$$a_{1S_{bn}} = \frac{1}{\pi}\left( 2\sin(2\psi_2) - \frac{M_2}{4}\big(\cos(4\psi_2) - \cos(4\psi_2)\big) + \frac{M_2}{4}\big(\cos(4\psi_2) - \cos(4\psi_2)\big)\right)$$

$$a_{1S_{bn}} = \frac{2}{\pi}\sin(2\psi_2)$$

(A.44)

$$b_{1S_{bn}} = \frac{1}{\pi}\left( \begin{array}{l} \displaystyle\int_{\psi_2}^{\pi+\psi_2} M_2\sin(\theta+\psi_2)\sin(\theta+\psi_2)d\theta \\[3ex] + \displaystyle\int_{\pi+\psi_2}^{2\pi+\psi_2}\big(1+M_2\sin(\theta+\psi_2)\big)\sin(\theta+\psi_2)d\theta \end{array}\right)$$

(A.45)

$$b_{1S_{bn}} = \frac{1}{\pi}\left( \begin{array}{l} \dfrac{M_2}{2}\displaystyle\int_{\psi_2}^{\pi+\psi_2} 1 - \cos(2\theta+2\psi_2)d\theta \\[3ex] + \displaystyle\int_{\pi+\psi_2}^{2\pi+\psi_2}\left(\sin(\theta+\psi_2) + \dfrac{M_2}{2}(1-\cos(2\theta+2\psi_2))\right)d\theta \end{array}\right)$$

$$
b_{1S_{bn}} = \frac{1}{\pi} \left( \begin{array}{l} \dfrac{M_2}{2}(\pi + \psi_2 - \psi_2) - \dfrac{M_2}{4}(\sin(2\pi + 2\psi_2 + 2\psi_2) - \sin(2\psi_2 + 2\psi_2)) \\[2mm] -\left(\cos(2\pi + \psi_2 + \psi_2) - \cos(\pi + \psi_2 + \psi_2)\right) + \dfrac{M_2}{2}(2\pi + \psi_2 - (\pi + \psi_2)) \\[2mm] -\dfrac{M_2}{4}(\sin(4\pi + 2\psi_2 + 2\psi_2) - \sin(2\pi + 2\psi_2 + 2\psi_2)) \end{array} \right)
$$

$$
b_{1S_{bn}} = \frac{1}{\pi} \left( \begin{array}{l} \dfrac{M_2}{2}(\pi) - \dfrac{M_2}{4}(\sin(4\psi_2) - \sin(4\psi_2)) - \left(\cos(2\psi_2) + \cos(2\psi_2)\right) + \dfrac{M_2}{2}(\pi) \\[2mm] -\dfrac{M_2}{4}(\sin(4\psi_2) - \sin(4\psi_2)) \end{array} \right)
$$

$$
b_{1S_{bn}} = \frac{1}{\pi} \left( \frac{M_2}{2}(\pi) - \left(\cos(2\psi_2) + \cos(2\psi_2)\right) + \frac{M_2}{2}(\pi) \right)
$$

$$
b_{1S_{bn}} = \frac{1}{\pi} \left( M_2 \pi - 2\cos(2\psi_2) \right)
$$

$$
b_{1S_{bn}} = M_2 - \frac{2}{\pi} \cos(2\psi_2) \tag{A.46}
$$

According to Fourier series, the expression for $S_{bn}$ is given as

$$
S_{bn} = \frac{1}{2} + \frac{2}{\pi}\sin(2\psi_2)\cos(\theta + \psi_2) + \left( -\frac{2}{\pi}\cos(2\psi_2) + M_2 \right)\sin(\theta + \psi_2) \tag{A.47}
$$

$$
S_{bn} = \frac{1}{2} + M_n + \frac{2}{\pi}\left(\sin(\psi_2 - \theta)\right) \tag{A.48}
$$

# APPENDIX B

# COMPLETE DERIVATION OF FOURIER SERIES ANALYSIS OF MULTI-STRING SEVEN LEVEL INVERTER

The double Fourier series approximation of converter switching functions given in [4] as

$$
S_{ij}(\omega_s, \omega_c) = \begin{bmatrix} \dfrac{A_{00}}{2} + \sum_{n=1}^{\infty}\left(A_{0n}\cos(n\omega_s t) + B_{0n}\sin(n\omega_s t)\right) \\ + \sum_{m=1}^{\infty}\left(A_{m0}\cos(m\omega_c t) + B_{m0}\sin(m\omega_c t)\right) \\ + \sum_{m=1}^{\infty}\sum_{\substack{n=-\infty \\ n\neq 0}}^{\infty}\left(A_{mn}\cos(m\omega_c t + n\omega_s t) + B_{mn}\sin(m\omega_c t + n\omega_s t)\right) \end{bmatrix}
\tag{B.1}
$$

Solving for each switching function over a period, considering the average and fundamental components only

## Solving for $S_{ap}$:

The average component of $S_{ap}$ is derived as

$$
a_{oS_{ap}} = \frac{1}{2\pi}\left( \int_{\psi_1}^{\pi+\psi_1}\left(1 - M_1\sin(\theta+\psi_1)\right)d\theta + \int_{\pi+\psi_1}^{2\pi+\psi_1}\left(-M_1\sin(\theta+\psi_1)\right)d\theta \right)
\tag{B.2}
$$

$$
a_{oS_{ap}} = \frac{1}{2\pi}\left(\pi + M_1\left[\cos(\pi+\psi_1+\psi_1) - \cos(\psi_1+\psi_1)\right] + M_1\left[\cos(2\pi+\psi_1+\psi_1) - \cos(\pi+\psi_1+\psi_1)\right]\right)
$$

$$
a_{oS_{ap}} = \frac{1}{2\pi}\left(\pi + M_1\left[\cos(\pi+2\psi_1) - \cos(2\psi_1)\right] + M_1\left[\cos(2\pi+2\psi_1) - \cos(\pi+2\psi_1)\right]\right)
$$

$$
a_{oS_{ap}} = \frac{1}{2\pi}\left(\pi + M_1\left[-\cos(2\psi_1) - \cos(2\psi_1)\right] + M_1\left[\cos(2\psi_1) + \cos(2\psi_1)\right]\right)
$$

$$a_{oS_{ap}} = \frac{1}{2\pi}\left(\pi - 2M_1[\cos(2\psi_1)] + 2M_1[\cos(2\psi_1)]\right)$$

$$a_{oS_{ap}} = \frac{1}{2\pi}(\pi)$$

$$a_{oS_{ap}} = \frac{1}{2} \tag{B.3}$$

The fundamental component ($n=1$) for $S_{ap}$ is derived as:

$$a_{1S_{ap}} = \frac{1}{\pi}\left( \begin{array}{c} \displaystyle\int_{\psi_1}^{\pi+\psi_1}(1 - M_1\sin(\theta+\psi_1))\cos(\theta+\psi_1)d\theta \\ \displaystyle + \int_{\pi+\psi_1}^{2\pi+\psi_1}(-M_1\sin(\theta+\psi_1))\cos(\theta+\psi_1)d\theta \end{array} \right) \tag{B.4}$$

$$a_{1S_{ap}} = \frac{1}{\pi}\left( \begin{array}{c} \displaystyle\int_{\psi_1}^{\pi+\psi_1}\cos(\theta+\psi_1) - M_1\sin(\theta+\psi_1)\cos(\theta+\psi_1)d\theta \\ \displaystyle - \int_{\pi+\psi_1}^{2\pi+\psi_1}M_1\sin(\theta+\psi_1)\cos(\theta+\psi_1)d\theta \end{array} \right)$$

$$a_{1S_{ap}} = \frac{1}{\pi}\left( \begin{array}{c} \displaystyle\sin(\pi+\psi_1+\psi_1) - \sin(\psi_1+\psi_1) - \frac{M_1}{2}\int_{\psi_1}^{\pi+\psi_1}2\sin(\theta+\psi_1)\cos(\theta+\psi_1)d\theta \\ \displaystyle - \frac{M_1}{2}\int_{\pi+\psi_1}^{2\pi+\psi_1}2\sin(\theta+\psi_1)\cos(\theta+\psi_1)d\theta \end{array} \right)$$

$$a_{1S_{ap}} = \frac{1}{\pi}\left( -\sin(2\psi_1) - \sin(2\psi_1) - \frac{M_1}{2}\int_{\psi_1}^{\pi+\psi_1}\sin(2\theta+2\psi_1)d\theta - \frac{M_1}{2}\int_{\pi+\psi_1}^{2\pi+\psi_1}\sin(2\theta+2\psi_1)d\theta \right)$$

$$a_{1S_{ap}} = \frac{1}{\pi}\left( \begin{array}{c} \displaystyle -2\sin(2\psi_1) + \frac{M_1}{4}(\cos(2\pi+2\psi_1+2\psi_1) - \cos(2\psi_1+2\psi_1)) \\ \displaystyle + \frac{M_1}{4}(\cos(4\pi+2\psi_1+2\psi_1) - \cos(2\pi+2\psi_1+2\psi_1)) \end{array} \right)$$

$$a_{1S_{ap}} = \frac{1}{\pi}\left( -2\sin(2\psi_1) + \frac{M_1}{4}(\cos(4\psi_1) - \cos(4\psi_1)) + \frac{M_1}{4}(\cos(4\psi_1) - \cos(4\psi_1)) \right)$$

$$a_{1S_{ap}} = \frac{1}{\pi}\left(-2\sin(2\psi_1)\right)$$

$$a_{1S_{ap}} = -\frac{2}{\pi}\sin(2\psi_1) \tag{B.5}$$

$$b_{1S_{ap}} = \frac{1}{\pi}\left(\int_{\psi_1}^{\pi+\psi_1}\left(\sin(\theta+\psi_1)-M_1\sin(\theta+\psi_1)\sin(\theta+\psi_1)\right)d\theta + \int_{\pi+\psi_1}^{2\pi+\psi_1}\left(-M_1\sin(\theta+\psi_1)\right)\sin(\theta+\psi_1)d\theta\right) \tag{B.6}$$

$$b_{1S_{ap}} = \frac{1}{\pi}\left(\begin{array}{c} -\left(\cos(\pi+\psi_1+\psi_1)-\cos(\psi_1+\psi_1)\right)-\dfrac{M_1}{2}\displaystyle\int_{\psi_1}^{\pi+\psi_1}\left(2\sin(\theta+\psi_1)\right)\sin(\theta+\psi_1)d\theta \\[4mm] -\dfrac{M_1}{2}\displaystyle\int_{\pi+\psi_1}^{2\pi+\psi_1}\left(2\sin(\theta+\psi_1)\right)\sin(\theta+\psi_1)d\theta \end{array}\right)$$

$$b_{1S_{ap}} = \frac{1}{\pi}\left(-\left(-\cos(2\psi_1)-\cos(2\psi_1)\right)-\frac{M_1}{2}\int_{\psi_1}^{\pi+\psi_1}\left(1-\cos(2\theta+2\psi_1)\right)d\theta - \frac{M_1}{2}\int_{\pi+\psi_1}^{2\pi+\psi_1}\left(1-\cos(2\theta+2\psi_1)\right)d\theta\right)$$

$$b_{1S_{ap}} = \frac{1}{\pi}\left(\begin{array}{c} 2\cos(2\psi_1)-\dfrac{M_1}{2}(\pi+\psi_1-\psi_1)+\dfrac{M_1}{4}\left(\sin(2\pi+2\psi_1+2\psi_1)-\sin(2\psi_1+2\psi_1)\right) \\[4mm] -\dfrac{M_1}{2}(2\pi+\psi_1-\pi-\psi_1)+\dfrac{M_1}{4}\left(\sin(4\pi+2\psi_1+2\psi_1)-\sin(2\pi+2\psi_1+2\psi_1)\right) \end{array}\right)$$

$$b_{1S_{ap}} = \frac{1}{\pi}\left(2\cos(2\psi_1)-M_1(\pi)+\frac{M_1}{4}\left(\sin(4\psi_1)-\sin(4\psi_1)\right)-M_1(\pi)+\frac{M_1}{4}\left(\sin(4\psi_1)-\sin(4\psi_1)\right)\right)$$

$$b_{1S_{ap}} = \frac{2}{\pi}\cos(2\psi_1)-2M_1 \tag{B.7}$$

According to Fourier series, the expression for $S_{ap}$ is given as

$$S_{ap} = \frac{1}{2}-\frac{2}{\pi}\sin(2\psi_1)\cos(\theta+\psi_1)+\left(\frac{2}{\pi}\cos(2\psi_1)-2M_1\right)\sin(\theta+\psi_1) \tag{B.8}$$

$$S_{ap} = \frac{1}{2} - 2M_p - \frac{2}{\pi}\left(\sin(\psi_1 - \theta)\right)$$

(B.9)

**Solving for S$_{am}$:**

The average component of S$_{am}$ is derived as

$$a_{oS_{am}} = \frac{1}{2\pi}\left(\int_{\psi_1}^{\pi+\psi_1} 1.d\theta\right)$$

(B.10)

$$a_{oS_{am}} = \frac{1}{2\pi}\left(\pi + \psi_1 - \psi_1\right)$$

$$a_{oS_{am}} = \frac{1}{2\pi}\left(\pi\right)$$

$$a_{oS_{am}} = \frac{1}{2}$$

(B.11)

The fundamental component ($n=1$) for S$_{am}$ is derived as:

$$a_{1S_{am}} = \frac{1}{\pi}\left(\int_{\psi_1}^{\pi+\psi_{1(}} 1.\cos(\theta + \psi_1)d\theta\right)$$

(B.12)

$$a_{1S_{am}} = \frac{1}{\pi}\left(\sin(\pi + \psi_1 + \psi_1) - \sin(\psi_1 + \psi_1)\right)$$

$$a_{1S_{am}} = \frac{1}{\pi}\left(-\sin(2\psi_1) - \sin(2\psi_1)\right)$$

$$a_{1S_{am}} = -\frac{2}{\pi}\sin(2\psi_1)$$

(B.13)

$$b_{1S_{am}} = \frac{1}{\pi}\left(\int_{\psi_1}^{\pi+\psi_{1(}} 1.\sin(\theta + \psi_1)d\theta\right)$$

(B.14)

283

$$b_{1S_{am}} = \frac{-1}{\pi}\left(\cos(\pi + \psi_1 + \psi_1) - \cos(\psi_1 + \psi_1)\right)$$

$$b_{1S_{am}} = \frac{-1}{\pi}\left(-\cos(2\psi_1) - \cos(2\psi_1)\right)$$

$$b_{1S_{am}} = \frac{2}{\pi}\cos(2\psi_1) \tag{B.15}$$

According to Fourier series, the expression for $S_{am}$ is given as

$$S_{am} = \frac{1}{2} - \frac{2}{\pi}\sin(2\psi_1)\cos(\theta + \psi_1) + \left(\frac{2}{\pi}\cos(2\psi_1)\right)\sin(\theta + \psi_1) \tag{B.16}$$

$$S_{am} = \frac{1}{2} - \frac{2}{\pi}\left(\sin(\psi_1 - \theta)\right) \tag{B.17}$$

**Solving for $S_{an}$:**

The average component of $S_{an}$ is derived as

$$a_{oS_{an}} = \frac{1}{2\pi}\left(\int_{\pi+\psi_2}^{2\pi+\psi_2} 1.d\theta\right) \tag{B.18}$$

$$a_{oS_{an}} = \frac{1}{2\pi}\left(2\pi + \psi_2 - (\pi + \psi_2)\right)$$

$$a_{oS_{an}} = \frac{1}{2\pi}\left(\pi\right)$$

$$a_{oSan} = \frac{1}{2} \tag{B.19}$$

The fundamental component ($n=1$) for $S_{an}$ is derived as:

$$a_{1S_{an}} = \frac{1}{\pi}\left(\int_{\pi+\psi_2}^{2\pi+\psi_2} 1.\cos(\theta + \psi_2)d\theta\right) \tag{B.20}$$

$$a_{1S_{an}} = \frac{1}{\pi}\left(-\left(\sin(2\pi + \psi_2 + \psi_2) - \sin(\pi + \psi_2 + \psi_2)\right)\right)$$

$$a_{1S_{an}} = -\frac{1}{\pi}\left(\sin(2\psi_2) + \sin(2\psi_2)\right)$$

$$a_{1S_{an}} = -\frac{2}{\pi}\sin(2\psi_2) \tag{B.21}$$

$$b_{1S_{an}} = \frac{1}{\pi}\left(\int_{\pi+\psi_1}^{2\pi+\psi_1} 1.\sin(\theta + \psi_1)d\theta\right) \tag{B.22}$$

$$b_{1S_{an}} = \frac{1}{\pi}\left(\left(\cos(2\pi + \psi_1 + \psi_1) - \cos(\pi + \psi_1 + \psi_1)\right)\right)$$

$$b_{1S_{an}} = \frac{1}{\pi}\left(\left(\cos(2\psi_1) + \cos(2\psi_1)\right)\right)$$

$$b_{1S_{an}} = \frac{2}{\pi}\cos(2\psi_1) \tag{B.23}$$

According to Fourier series, the expression for $S_{an}$ is given as

$$S_{an} = \frac{1}{2} - \frac{2}{\pi}\sin(2\psi_2)\cos(\theta + \psi_2) + \left(\frac{2}{\pi}\cos(2\psi_2)\right)\sin(\theta + \psi_2) \tag{B.24}$$

$$S_{an} = \frac{1}{2} - \frac{2}{\pi}\left(\sin(\psi_2 - \theta)\right) \tag{B.25}$$

**Solving for $S_{ao}$:**

The average component of $S_{ao}$ is derived as

$$a_{oS_{ao}} = \frac{1}{2\pi}\left(\int_{\psi_2}^{\pi+\psi_2}(1 - M_2\sin(\theta + \psi_2))d\theta + \int_{\pi+\psi_2}^{2\pi+\psi_2}(-M_2\sin(\theta + \psi_2))d\theta\right) \tag{B.26}$$

$$a_{oS_{ao}} = \frac{1}{2\pi}\left(\begin{array}{l}\pi + M_2\left[\cos(\pi + \psi_2 + \psi_2) - \cos(\psi_2 + \psi_2)\right] \\ + M_2\left[\cos(2\pi + \psi_2 + \psi_2) - \cos(\pi + \psi_2 + \psi_2)\right]\end{array}\right)$$

$$a_{oS_{ao}} = \frac{1}{2\pi}\left(\pi + M_2\left[\cos(\pi + 2\psi_2) - \cos(2\psi_2)\right] + M_2\left[\cos(2\pi + 2\psi_2) - \cos(\pi + 2\psi_2)\right]\right)$$

$$a_{oS_{ao}} = \frac{1}{2\pi}\left(\pi + M_2\left[-\cos(2\psi_2) - \cos(2\psi_2)\right] + M_2\left[\cos(2\psi_2) + \cos(2\psi_2)\right]\right)$$

$$a_{oS_{ao}} = \frac{1}{2\pi}\left(\pi - 2M_2\left[\cos(2\psi_2)\right] + 2M_2\left[\cos(2\psi_2)\right]\right)$$

$$a_{oS_{ao}} = \frac{1}{2\pi}\left(\pi\right)$$

$$a_{o\,S_{ao}} = \frac{1}{2} \tag{B.27}$$

The fundamental component ($n=1$) for $S_{ao}$ is derived as:

$$\tag{B.28}$$

$$a_{1S_{ao}} = \frac{1}{\pi}\left(\begin{array}{l}\int\limits_{\psi 2}^{\pi+\psi 2}\left(1 - M_2\sin(\theta + \psi_2)\right)\cos(\theta + \psi_2)d\theta \\ + \int\limits_{\pi+\psi 2}^{2\pi+\psi 2}\left(-M_2\sin(\theta + \psi_2)\right)\cos(\theta + \psi_2)d\theta\end{array}\right)$$

$$a_{1S_{ao}} = \frac{1}{\pi}\left(\begin{array}{l}\int\limits_{\psi 2}^{\pi+\psi 2}\cos(\theta + \psi_2) - M_2\sin(\theta + \psi_2)\cos(\theta + \psi_2)d\theta \\ - \int\limits_{\pi+\psi 2}^{2\pi+\psi 2}M_2\sin(\theta + \psi_2)\cos(\theta + \psi_2)d\theta\end{array}\right)$$

$$a_{1S_{ao}} = \frac{1}{\pi}\left(\begin{array}{l}\sin(\pi + \psi_2 + \psi_2) - \sin(\psi_2 + \psi_2) - \dfrac{M_2}{2}\int\limits_{\psi 2}^{\pi+\psi 2}2\sin(\theta + \psi_2)\cos(\theta + \psi_2)d\theta \\ - \dfrac{M_2}{2}\int\limits_{\pi+\psi 2}^{2\pi+\psi 2}2\sin(\theta + \psi_2)\cos(\theta + \psi_2)d\theta\end{array}\right)$$

$$a_{1S_{ao}} = \frac{1}{\pi}\left(-\sin(2\psi_2) - \sin(2\psi_2) - \frac{M_2}{2}\int_{\psi_2}^{\pi+\psi_2}\sin(2\theta+2\psi_2)d\theta - \frac{M_2}{2}\int_{\pi+\psi_2}^{2\pi+\psi_2}\sin(2\theta+2\psi_2)d\theta\right)$$

$$a_{1S_{ao}} = \frac{1}{\pi}\left(\begin{array}{l} -2\sin(2\psi_2) + \frac{M_2}{4}\left(\cos(2\pi+2\psi_2+2\psi_2) - \cos(2\psi_2+2\psi_2)\right) \\ + \frac{M_2}{4}\left(\cos(4\pi+2\psi_2+2\psi_2) - \cos(2\pi+2\psi_2+2\psi_2)\right) \end{array}\right)$$

$$a_{1S_{ao}} = \frac{1}{\pi}\left(-2\sin(2\psi_2) + \frac{M_2}{4}\left(\cos(4\psi_2) - \cos(4\psi_2)\right) + \frac{M_2}{4}\left(\cos(4\psi_2) - \cos(4\psi_2)\right)\right)$$

$$a_{1S_{ao}} = \frac{1}{\pi}\left(-2\sin(2\psi_2)\right) \tag{B.29}$$

$$\tag{B.30}$$

$$b_{1S_{ao}} = \frac{1}{\pi}\left(\begin{array}{l} \int_{\psi_2}^{\pi+\psi_2}\left(\sin(\theta+\psi_2) - M_2\sin(\theta+\psi_2)\sin(\theta+\psi_2)\right)d\theta \\ + \int_{\pi+\psi_2}^{2\pi+\psi_2}\left(-M_2\sin(\theta+\psi_2)\right)\sin(\theta+\psi_2)d\theta \end{array}\right)$$

$$b_{1S_{ao}} = \frac{1}{\pi}\left(\begin{array}{l} -\left(\cos(\pi+2\psi_2) - \cos(\psi_2+\psi_2)\right) - \frac{M_2}{2}\int_{\psi_2}^{\pi+\psi_2}\left(2\sin(\theta+\psi_2)\right)\sin(\theta+\psi_2)d\theta \\ - \frac{M_2}{2}\int_{\pi+\psi_2}^{2\pi+\psi_2}\left(2\sin(\theta+\psi_2)\right)\sin(\theta+\psi_2)d\theta \end{array}\right)$$

$$b_{1S_{ao}} = \frac{1}{\pi}\left(\begin{array}{l} -\left(-\cos(2\psi_2) - \cos(2\psi_2)\right) - \\ \frac{M_2}{2}\int_{\psi_1}^{\pi+\psi_1}\left(1-\cos(2\theta+2\psi_2)\right)d\theta - \frac{M_2}{4}\int_{\pi+\psi_2}^{2\pi+\psi_2}\left(1-\cos(2\theta+2\psi_2)\right)d\theta \end{array}\right)$$

$$b_{1S_{ao}} = \frac{1}{\pi}\left(\begin{array}{l} 2\cos(2\psi_2) - \frac{M_2}{2}(\pi+\psi_2-\psi_2) + \frac{M_2}{4}\left(\sin(2\pi+2\psi_2+2\psi_2) - \sin(2\psi_2+2\psi_2)\right) \\ -\frac{M_2}{2}(2\pi+\psi_2-\pi-\psi_2) + \frac{M_2}{4}\left(\sin(4\pi+2\psi_2+2\psi_2) - \sin(2\pi+2\psi_2+2\psi_2)\right) \end{array}\right)$$

$$b_{1S_{ao}} = \frac{1}{\pi} \begin{pmatrix} 2\cos(2\psi_2) - M_2(\pi) + \frac{M_2}{4}(\sin(4\psi_2) - \sin(4\psi_2)) \\ -M_2(\pi) + \frac{M_2}{4}(\sin(4\psi_2) - \sin(4\psi_2)) - M_2(\pi) \end{pmatrix}$$

$$b_{1S_{ao}} = \frac{2}{\pi}\cos(2\psi_2) - 2M_2 \qquad (B.31)$$

According to Fourier series, the expression for $S_{ao}$ is given as

$$S_{ao} = \frac{1}{2} - \frac{2}{\pi}\sin(2\psi_2)\cos(\theta + \psi_2) + \left(\frac{2}{\pi}\cos(2\psi_2) - M_2\right)\sin(\theta + \psi_2) \qquad (B.32)$$

$$S_{ao} = \frac{1}{2} - M_2\sin(\theta + \psi_2) - \frac{2}{\pi}(\sin(\psi_2 - \theta)) \qquad (B.33)$$

# APPENDIX C

## COMPLETE DERIVATION OF FOURIER SERIES ANALYSIS OF

## MULTI-STRING NINE LEVEL INVERTER

The double Fourier series approximation of converter switching functions given in [4]

as

$$
S_{ij}(\omega_s, \omega_c) = \begin{bmatrix} \dfrac{A_{00}}{2} + \sum_{n=1}^{\infty}(A_{0n}\cos(n\omega_s t) + B_{0n}\sin(n\omega_s t)) \\[2mm] + \sum_{m=1}^{\infty}(A_{m0}\cos(m\omega_c t) + B_{m0}\sin(m\omega_c t)) \\[2mm] + \sum_{\substack{m=1 \\ }}^{\infty}\sum_{\substack{n=-\infty \\ n\neq 0}}^{\infty}(A_{mn}\cos(m\omega_c t + n\omega_s t) + B_{mn}\sin(m\omega_c t + n\omega_s t)) \end{bmatrix} \tag{C.1}
$$

Solving for each switching function over a period, considering the average and

fundamental components only

### Solving for $S_{ap}$:

The average component of $S_{ap}$ is derived as

$$
a_{oS_{ap}} = \frac{1}{2\pi}\left(\int_{\psi_1}^{\pi+\psi_1}(M_1\sin(\theta+\psi_1))d\theta + \int_{\pi+\psi_1}^{2\pi+\psi_1}(1+M_1\sin(\theta+\psi_1))d\theta\right) \tag{C.2}
$$

$$
a_{oS_{ap}} = \frac{1}{2\pi}\left(\begin{array}{l} -M_1[\cos(\pi+\psi_1+\psi_1)-\cos(\psi_1+\psi_1)]+\pi \\ -M_1[\cos(2\pi+\psi_1+\psi_1)-\cos(\pi+\psi_1+\psi_1)] \end{array}\right)
$$

$$
a_{oS_{ap}} = \frac{1}{2\pi}\left(\pi - M_1[\cos(\pi+2\psi_1)-\cos(2\psi_1)] - M_1[\cos(2\pi+2\psi_1)-\cos(\pi+2\psi_1)]\right)
$$

$$
a_{oS_{ap}} = \frac{1}{2\pi}\left(\pi - M_1[-\cos(2\psi_1)-\cos(2\psi_1)] - M_1[\cos(2\psi_1)+\cos(2\psi_1)]\right)
$$

289

$$a_{oS_{ap}} = \frac{1}{2\pi}\left(\pi + 2M_1[\cos(2\psi_1)] - 2M_1[\cos(2\psi_1)]\right)$$

$$a_{oS_{ap}} = \frac{1}{2}$$

The fundamental component (*n*=1) for $S_{ap}$ is derived as:

$$a_{1S_{ap}} = \frac{1}{\pi}\left(\int_{\psi_1}^{\pi+\psi_1}(M_1\sin(\theta+\psi_1))\cos(\theta+\psi_1)d\theta + \int_{\pi+\psi_1}^{2\pi+\psi_1}(1+M_1\sin(\theta+\psi_1))\cos(\theta+\psi_1)d\theta\right)$$

$$a_{1S_{ap}} = \frac{1}{\pi}\left(\int_{\psi_1}^{\pi+\psi_1}M_1\sin(\theta+\psi_1)\cos(\theta+\psi_1)d\theta + \int_{\pi+\psi_1}^{2\pi+\psi_1}M_1\sin(\theta+\psi_1)\cos(\theta+\psi_1)d\theta + \int_{\pi+\psi_1}^{2\pi+\psi_1}\cos(\theta+\psi_1)d\theta\right)$$

$$a_{1S_{ap}} = \frac{1}{\pi}\left(\begin{array}{c}\sin(2\pi+\psi_1+\psi_1)-\sin(\pi+\psi_1+\psi_1)-\dfrac{M_1}{2}\int_{\psi_1}^{\pi+\psi_1}2\sin(\theta+\psi_1)\cos(\theta+\psi_1)d\theta \\[4mm] -\dfrac{M_1}{2}\int_{\pi+\psi_1}^{2\pi+\psi_1}2\sin(\theta+\psi_1)\cos(\theta+\psi_1)d\theta\end{array}\right)$$

$$a_{1S_{ap}} = \frac{1}{\pi}\left(\sin(2\psi_1)+\sin(2\psi_1)-\frac{M_1}{2}\int_{\psi_1}^{\pi+\psi_1}\sin(2\theta+2\psi_1)d\theta - \frac{M_1}{2}\int_{\pi+\psi_1}^{2\pi+\psi_1}\sin(2\theta+2\psi_1)d\theta\right)$$

$$a_{1S_{ap}} = \frac{1}{\pi}\left(\begin{array}{c}2\sin(2\psi_1)-\dfrac{M_1}{4}\left(\cos(2\pi+2\psi_1+2\psi_1)-\cos(2\psi_1+2\psi_1)\right) \\[4mm] -\dfrac{M_1}{4}\left(\cos(4\pi+2\psi_1+2\psi_1)-\cos(2\pi+2\psi_1+2\psi_1)\right)\end{array}\right)$$

$$a_{1S_{ap}} = \frac{1}{\pi}\left(2\sin(2\psi_1)-\frac{M_1}{4}\left(\cos(4\psi_1)-\cos(4\psi_1)\right)-\frac{M_1}{4}\left(\cos(4\psi_1)-\cos(4\psi_1)\right)\right)$$

$$a_{1S_{ap}} = \frac{2}{\pi}\sin(2\psi_1)$$

$$b_{1S_{ap}} = \frac{1}{\pi}\left(\int_{\psi_1}^{\pi+\psi_1}(M_1\sin(\theta+\psi_1)\sin(\theta+\psi_1))d\theta + \int_{\pi+\psi_1}^{2\pi+\psi_1}(1+M_1\sin(\theta+\psi_1))\sin(\theta+\psi_1)d\theta\right)$$

(C.6)

$$b_{1S_{ap}} = \frac{1}{\pi}\left(\begin{array}{c}(\cos(\pi+\psi_1+\psi_1)-\cos(\psi_1+\psi_1))-\dfrac{M_1}{2}\int_{\psi_1}^{\pi+\psi_1}(2\sin(\theta+\psi_1))\sin(\theta+\psi_1)d\theta \\[2mm] -\dfrac{M_1}{2}\int_{\pi+\psi_1}^{2\pi+\psi_1}(2\sin(\theta+\psi_1))\sin(\theta+\psi_1)d\theta\end{array}\right)$$

$$b_{1S_{ap}} = \frac{1}{\pi}\left((-\cos(2\psi_1)-\cos(2\psi_1))+\frac{M_1}{2}\int_{\psi_1}^{\pi+\psi_1}(1-\cos(2\theta+2\psi_1))d\theta - \frac{M_1}{2}\int_{\pi+\psi_1}^{2\pi+\psi_1}(1-\cos(2\theta+2\psi_1))d\theta\right)$$

$$b_{1S_{ap}} = \frac{1}{\pi}\left(\begin{array}{c}-2\cos(2\psi_1)+\dfrac{M_1}{2}(\pi+\psi_1-\psi_1)+\dfrac{M_1}{2}(\sin(2\pi+2\psi_1+2\psi_1)-\sin(2\psi_1+2\psi_1)) \\[2mm] +\dfrac{M_1}{2}(2\pi+\psi_1-\pi-\psi_1)+\dfrac{M_1}{2}(\sin(4\pi+2\psi_1+2\psi_1)-\sin(2\pi+2\psi_1+2\psi_1))\end{array}\right)$$

$$b_{1S_{ap}} = \frac{1}{\pi}\left(-2\cos(2\psi_1)+M_1(\pi)+\frac{M_1}{4}(\sin(4\psi_1)-\sin(4\psi_1))+M_1(\pi)+\frac{M_1}{4}(\sin(4\psi_1)-\sin(4\psi_1))-M_1(\pi)\right)$$

$$b_{1S_{ap}} = M_1 - \frac{2}{\pi}\cos(2\psi_1)$$

(C.7)

According to Fourier series, the expression for $S_{ap}$ is given as

$$S_{ap} = \frac{1}{2} + \frac{2}{\pi}\sin(2\psi_1)\cos(\theta+\psi_1) + \left(-\frac{2}{\pi}\cos(2\psi_1)+M_1\right)\sin(\theta+\psi_1)$$

(C.8)

$$S_{ap} = \frac{1}{2} + M_1\sin(\theta+\psi_1) + \frac{2}{\pi}(\sin(\psi_1-\theta))$$

(C.9)

**Solving for $S_{am}$:**

The average component of $S_{am}$ is derived as

$$a_{oS_{am}} = \frac{1}{2\pi} \int\limits_{\psi_1}^{\pi+\psi_1} 2M_1 \sin(\theta+\psi_1)d\theta \qquad \text{(C.10)}$$

$$a_{oS_{am}} = \frac{-M_1}{\pi}\left[-2\cos(2\psi_1)\right]$$

$$a_{oS_{am}} = \frac{2M_1 \cos(2\psi_1)}{\pi} \qquad \text{(C.11)}$$

The fundamental component ($n=1$) for $S_{am}$ is derived as:

$$a_{1S_{am}} = \frac{1}{\pi}\left( \int\limits_{\psi_1}^{\pi+\psi_{1(}} 2M_1 \sin(\theta+\psi_1)\cos(\theta+\psi_1)d\theta - \int\limits_{\pi+\psi_{1(}}^{2\pi+\psi_{1(}} 0.\cos(\theta+\psi_1)d\theta \right) \qquad \text{(C.12)}$$

$$a_{1S_{am}} = \frac{-M_1}{2\pi}\left(\cos(2\pi+2\psi_1+2\psi_1) - \cos(2\psi_1+2\psi_1)\right)$$

$$a_{1S_{am}} = \frac{-M_1}{\pi}(0)$$

$$a_{1S_{am}} = 0 \qquad \text{(C.13)}$$

$$b_{1S_{am}} = \frac{1}{\pi}\left( \int\limits_{\psi_1}^{\pi+\psi_{1(}} 2M_1 \sin^2(\theta+\psi_1)d\theta - \int\limits_{\pi+\psi_{(}}^{2\pi+\psi_{(}} 0.\sin(\theta+\psi_1)d\theta \right) \qquad \text{(C.14)}$$

$$b_{1S_{am}} = \frac{M_1}{\pi}\left( \pi+\psi_1-\psi_1 - \frac{1}{2}\left(\sin(2\pi+2\psi_1+2\psi_1) - \sin(2\psi_1+2\psi_1)\right)\right)$$

$$b_{1S_{am}} = \frac{M_1}{\pi}(\pi)$$

$$b_{1S_{am}} = M_1 \qquad \text{(C.15)}$$

According to Fourier series, the expression for $S_{am}$ is given as

$$S_{am} = \frac{2M_1}{\pi}\cos(2\psi_1) + (M_1)\sin(\theta + \psi_1)$$  (C.16)

**Solving for S$_{an}$:**

The average component of S$_{an}$ is derived as

$$a_{oS_{an}} = \frac{1}{2\pi}\left(\int_{\pi+\psi_2}^{2\pi+\psi_2} 1.d\theta\right)$$  (C.17)

$$a_{oS_{an}} = \frac{1}{2\pi}\left(2\pi + \psi_2 - (\pi + \psi_2)\right)$$

$$a_{oS_{an}} = \frac{1}{2\pi}(\pi)$$

$$a_{oS_{an}} = \frac{1}{2}$$  (C.18)

The fundamental component ($n=1$) for S$_{an}$ is derived as:

$$a_{1S_{an}} = \frac{1}{\pi}\left(\int_{\pi+\psi_2}^{2\pi+\psi_2} 1.\cos(\theta + \psi_2)d\theta\right)$$  (C.19)

$$a_{1S_{an}} = \frac{1}{\pi}\left(\sin(2\pi + \psi_2 + \psi_2) - \sin(\pi + \psi_2 + \psi_2)\right)$$

$$a_{1S_{an}} = \frac{1}{\pi}\left(\sin(2\psi_2) + \sin(2\psi_2)\right)$$

$$a_{1S_{an}} = \frac{2}{\pi}\sin(2\psi_2)$$  (C.20)

$$b_{1S_{an}} = \frac{1}{\pi}\left(\int_{\pi+\psi_1}^{2\pi+\psi_1} 1.\sin(\theta + \psi_1)d\theta\right)$$  (C.21)

$$b_{1S_{an}} = \frac{1}{\pi}\left(-\left(\cos(2\pi + \psi_1 + \psi_1) - \cos(\pi + \psi_1 + \psi_1)\right)\right)$$

$$b_{1S_{an}} = \frac{1}{\pi}\left(-\left(\cos(2\psi_1) + \cos(2\psi_1)\right)\right)$$

$$b_{1S_{an}} = -\frac{2}{\pi}\cos(2\psi_1) \tag{C.22}$$

According to Fourier series, the expression for $S_{an}$ is given as

$$S_{an} = \frac{1}{2} + \frac{2}{\pi}\sin(2\psi_2)\cos(\theta + \psi_2) - \left(\frac{2}{\pi}\cos(2\psi_2)\right)\sin(\theta + \psi_2) \tag{C.23}$$

$$S_{an} = \frac{1}{2} + \frac{2}{\pi}\left(\sin(\psi_2 - \theta)\right) \tag{C.24}$$

**Solving for $S_{ao}$:**

The average component of $S_{ao}$ is derived as

$$a_{oS_{ao}} = \frac{1}{2\pi}\int_{\pi+\psi_1}^{2\pi+\psi_1} -2M_2\sin(\theta + \psi_2)d\theta \tag{C.25}$$

$$a_{oS_{ao}} = \frac{M_2}{\pi}\left[2\cos(2\psi_2)\right]$$

$$a_{oS_{ao}} = \frac{2M_2\cos(2\psi_2)}{\pi} \tag{C.26}$$

The fundamental component ($n=1$) for $S_{ao}$ is derived as:

$$a_{1S_{ao}} = \frac{1}{\pi}\left(\int_{\psi_2}^{\pi+\psi_2} -2M_2\sin(\theta+\psi_2)\cos(\theta+\psi_2)d\theta - \int_{\pi+\psi_2}^{2\pi+\psi_2} 0.\cos(\theta+\psi_2)d\theta\right) \tag{C.27}$$

$$a_{1S_{ao}} = \frac{M_2}{2\pi}\left(\cos(2\pi + 2\psi_2 + 2\psi_2) - \cos(2\psi_2 + 2\psi_2)\right)$$

$$a_{1S_{ao}} = \frac{-M_2}{\pi}(0)$$

$$a_{1S_{ao}} = 0 \tag{C.28}$$

$$b_{1S_{ao}} = \frac{1}{\pi}\left(\int_{\psi_2}^{\pi+\psi_2} -2M_2\sin^2(\theta+\psi_2)d\theta - \int_{\pi+\psi_2}^{2\pi+\psi_2} 0.\sin(\theta+\psi_2)d\theta\right) \tag{C.29}$$

$$b_{1S_{ao}} = \frac{-M_2}{\pi}\left(\pi+\psi_1-\psi_1-\frac{1}{2}(\sin(2\pi+2\psi_1+2\psi_1)-\sin(2\psi_1+2\psi_1))\right)$$

$$b_{1S_{ao}} = \frac{-M_2}{\pi}(\pi)$$

$$b_{1S_{ao}} = -M_2 \tag{C.30}$$

According to Fourier series, the expression for $S_{ao}$ is given as

$$S_{ao} = \frac{2M_2}{\pi}\cos(2\psi_2)+(M_2)\sin(\theta+\psi_2) \tag{C.31}$$

**Solving for $S_{ar}$:**

The average component of $S_{ar}$ is derived as

$$a_{oS_{ar}} = \frac{1}{2\pi}\left(\int_{\psi2}^{\pi+\psi2}(-M_2\sin(\theta+\psi_2))d\theta + \int_{\pi+\psi2}^{2\pi+\psi2}(1-M_2\sin(\theta+\psi_2))d\theta\right) \tag{C.32}$$

$$a_{oS_{ar}} = \frac{1}{2\pi}\left(\begin{array}{l}\pi+M_2[\cos(\pi+\psi_2+\psi_2)-\cos(\psi_2+\psi_2)] \\ +M_2[\cos(2\pi+\psi_2+\psi_2)-\cos(\pi+\psi_2+\psi_2)]\end{array}\right)$$

$$a_{oS_{ar}} = \frac{1}{2\pi}(\pi+M_2[\cos(\pi+2\psi_2)-\cos(2\psi_2)]+M_2[\cos(2\pi+2\psi_2)-\cos(\pi+2\psi_2)])$$

$$a_{oS_{ar}} = \frac{1}{2\pi}(\pi+M_2[-\cos(2\psi_2)-\cos(2\psi_2)]+M_2[\cos(2\psi_2)+\cos(2\psi_2)])$$

$$a_{oS_{ar}} = \frac{1}{2\pi}\left(\pi - 2M_2\left[\cos(2\psi_2)\right] + 2M_2\left[\cos(2\psi_2)\right]\right)$$

$$a_{oS_{ar}} = \frac{1}{2\pi}\left(\pi\right)$$

$$a_{oS_{ar}} = \frac{1}{2} \tag{C.33}$$

The fundamental component ($n=1$) for $S_{ar}$ is derived as:

$$a_{1S_{ar}} = \frac{1}{\pi}\left( \begin{array}{l} \int\limits_{\psi_2}^{\pi+\psi_2}\left(-M_2\sin(\theta+\psi_2)\right)\cos(\theta+\psi_2)d\theta \\ + \int\limits_{\pi+\psi_2}^{2\pi+\psi_2}\left(1-M_2\sin(\theta+\psi_2)\right)\cos(\theta+\psi_2)d\theta \end{array} \right) \tag{C.34}$$

$$a_{1S_{ar}} = \frac{1}{\pi}\left( \begin{array}{l} \int\limits_{\psi_2}^{\pi+\psi_2}\cos(\theta+\psi_2) - M_2\sin(\theta+\psi_2)\cos(\theta+\psi_2)d\theta \\ - \int\limits_{\pi+\psi_2}^{2\pi+\psi_2}M_2\sin(\theta+\psi_2)\cos(\theta+\psi_2)d\theta \end{array} \right)$$

$$a_{1S_{ar}} = \frac{1}{\pi}\left( \begin{array}{l} \sin(\pi+\psi_2+\psi_2) - \sin(\psi_2+\psi_2) - \frac{M_2}{2}\int\limits_{\psi_2}^{\pi+\psi_2}2\sin(\theta+\psi_2)\cos(\theta+\psi_2)d\theta \\ - \frac{M_2}{2}\int\limits_{\pi+\psi_2}^{2\pi+\psi_2}2\sin(\theta+\psi_2)\cos(\theta+\psi_2)d\theta \end{array} \right)$$

$$a_{1S_{ar}} = \frac{1}{\pi}\left(-\sin(2\psi_2) - \sin(2\psi_2) - \frac{M_2}{2}\int\limits_{\psi_2}^{\pi+\psi_2}\sin(2\theta+2\psi_2)d\theta - \frac{M_2}{2}\int\limits_{\pi+\psi_2}^{2\pi+\psi_2}\sin(2\theta+2\psi_2)d\theta\right)$$

$$a_{1S_{ar}} = \frac{1}{\pi}\left( \begin{array}{l} -2\sin(2\psi_2) - \frac{M_2}{4}\left(\cos(2\pi+2\psi_2+2\psi_2) - \cos(2\psi_2+2\psi_2)\right) \\ - \frac{M_2}{4}\left(\cos(4\pi+2\psi_2+2\psi_2) - \cos(2\pi+2\psi_2+2\psi_2)\right) \end{array} \right)$$

$$a_{1S_{ar}} = \frac{1}{\pi}\left(\begin{array}{l} -2\sin(2\psi_2) - \dfrac{M_2}{4}\left(\cos(4\psi_2) - \cos(4\psi_2)\right) \\ -\dfrac{M_2}{4}\left(\cos(4\psi_2) - \cos(4\psi_2)\right) \end{array}\right)$$

$$a_{1S_{ar}} = \frac{1}{\pi}\left(-2\sin(2\psi_2)\right)$$

$$a_{1S_{ar}} = \frac{-2}{\pi}\sin(2\psi_2)$$

(C.35)

(C.36)

$$b_{1S_{ar}} = \frac{1}{\pi}\left(\int_{\psi_2}^{\pi+\psi_2}\left(-M_2\sin(\theta+\psi_2)\sin(\theta+\psi_2)\right)d\theta + \int_{\pi+\psi_2}^{2\pi+\psi_2}\left(1-M_2\sin(\theta+\psi_2)\right)\sin(\theta+\psi_2)d\theta\right)$$

$$b_{1S_{ar}} = \frac{1}{\pi}\left(\begin{array}{l} -\left(\cos(2\pi+\psi_2+\psi_2) - \cos(\pi+\psi_2+\psi_2)\right) - \dfrac{M_2}{2}\int_{\psi_2}^{\pi+\psi_2}\left(2\sin(\theta+\psi_2)\right)\sin(\theta+\psi_2)d\theta \\ -\dfrac{M_2}{2}\int_{\pi+\psi_2}^{2\pi+\psi_2}\left(2\sin(\theta+\psi_2)\right)\sin(\theta+\psi_2)d\theta \end{array}\right)$$

$$b_{1S_{ar}} = \frac{1}{\pi}\left(\begin{array}{l} -\left(\cos(2\psi_2) + \cos(2\psi_2)\right) - \dfrac{M_2}{2}\int_{\psi_1}^{\pi+\psi_1}\left(1-\cos(2\theta+2\psi_2)\right)d\theta \\ -\dfrac{M_2}{2}\int_{\pi+\psi_2}^{2\pi+\psi_2}\left(1-\cos(2\theta+2\psi_2)\right)d\theta \end{array}\right)$$

$$b_{1S_{ar}} = \frac{1}{\pi}\left(\begin{array}{l} +\dfrac{M_2}{2}\left(\sin(2\pi+4\psi_2) - \sin(4\psi_2)\right) - 2\cos(2\psi_2) - \dfrac{M_2}{2}(\pi) \\ -\dfrac{M_2}{2}\left(2\pi+\psi_2 - \pi - \psi_2\right) + \dfrac{M_2}{2}\left(\sin(4\pi+4\psi_2) - \sin(2\pi+4\psi_2)\right) \end{array}\right)$$

$$b_{1S_{ar}} = \frac{1}{\pi}\left(\begin{array}{l} -2\cos(2\psi_2) - \dfrac{M_2}{2}(\pi) + \dfrac{M_2}{2}\left(\sin(4\psi_2) - \sin(4\psi_2)\right) \\ -\dfrac{M_2}{2}(\pi) + \dfrac{M_2}{2}\left(\sin(4\psi_2) - \sin(4\psi_2)\right) - M_2(\pi) \end{array}\right)$$

$$b_{1S_{ar}} = -\frac{2}{\pi}\cos(2\psi_2) - M_2 \tag{C.37}$$

According to Fourier series, the expression for $S_{ar}$ is given as

$$S_{ar} = \frac{1}{2} + \frac{2}{\pi}\sin(2\psi_2)\cos(\theta + \psi_2) + \left(-\frac{2}{\pi}\cos(2\psi_2) - M_2\right)\sin(\theta + \psi_2) \tag{C.38}$$

$$S_{ar} = \frac{1}{2} - M_2\sin(\theta + \psi_2) + \frac{2}{\pi}\left(\sin(\psi_2 - \theta)\right) \tag{C.39}$$

## APPENDIX D

## GENERATION OF SWITCHING PULSES USING DSP F28335 FOR FOUR CELL CASCADED H-BRIDGE INVERTER

The code that was written to generate the switching pulses of switches in four cell cascaded H-bridge multi-level converter is given below.

```
#include "DSP2833x_Device.h"

#include "IQmathLib.h"

#pragma DATA_SECTION(sine_table,"IQmathTables");

_iq30 sine_table[512];

// external function prototypes

extern void InitSysCtrl(void);

extern void InitPieCtrl(void);

extern void InitPieVectTable(void);

extern void InitCpuTimers(void);

extern void ConfigCpuTimer(struct CPUTIMER_VARS *, float, float);

// Prototype statements for functions found within this file.

void Gpio_select(void);

void Setup_ePWM(void);

//interrupt void ePWM1A_compare_isr(void);

interrupt void cpu_timer0_isr(void);
```

```
//#############################################################################
#####
//                                      main code

//#############################################################################
#####
void main(void)

{

InitSysCtrl();  // Basic Core Init from DSP2833x_SysCtrl.c

EALLOW;

SysCtrlRegs.WDCR= 0x00AF;        // Re-enable the watchdog

EDIS;                  // 0x00AF  to NOT disable the Watchdog, Prescaler = 64

DINT;                      // Disable all interrupts

Gpio_select();          // GPIO9, GPIO11, GPIO34 and GPIO49 as output

                                // to 4 LEDs at Peripheral Explorer Board

Setup_ePWM();               // init of ePWM

InitPieCtrl();          // basic setup of PIE table; from DSP2833x_PieCtrl.c

InitPieVectTable();     // default ISR's in PIE

EALLOW;

PieVectTable.TINT0 = &cpu_timer0_isr;

//PieVectTable.TINT0 = &cpu_timer0_isr;

EDIS;

InitCpuTimers();        // basic setup CPU Timer0, 1 and 2
```

300

```c
ConfigCpuTimer(&CpuTimer0,150,33);

// Enable EPWM INT in the PIE: Group 3 interrupt 1

 PieCtrlRegs.PIEIER1.bit.INTx7 = 1;

IER |=1;        // enable INT3 for ePWM1

EINT;

ERTM;

CpuTimer0Regs.TCR.bit.TSS = 0;    // start timer0

while(1)

{

while(CpuTimer0.InterruptCount == 0);

CpuTimer0.InterruptCount = 0;

EALLOW;

SysCtrlRegs.WDKEY = 0x55;        // service WD #1

EDIS;

}

}

void Gpio_select(void)

{

EALLOW;

GpioCtrlRegs.GPAMUX1.all = 0;            // GPIO15 ... GPIO0 = General Puropse I/O

GpioCtrlRegs.GPAMUX1.bit.GPIO0 = 1;    // ePWM1A active

GpioCtrlRegs.GPAMUX1.bit.GPIO1 = 1;    // ePWM1B active

GpioCtrlRegs.GPAMUX1.bit.GPIO2 = 1;    // ePWM2A active
```

```c
GpioCtrlRegs.GPAMUX1.bit.GPIO3 = 1;    // ePWM2B active

GpioCtrlRegs.GPAMUX1.bit.GPIO4 = 1;    // ePWM3A active

GpioCtrlRegs.GPAMUX1.bit.GPIO5 = 1;    // ePWM3B active

GpioCtrlRegs.GPAMUX1.bit.GPIO6 = 1;    // ePWM4A active

GpioCtrlRegs.GPAMUX1.bit.GPIO7 = 1;    // ePWM4B active

GpioCtrlRegs.GPAMUX1.bit.GPIO8 = 1;    // ePWM5A active

GpioCtrlRegs.GPAMUX1.bit.GPIO9 = 1;    // ePWM5B active

GpioCtrlRegs.GPAMUX1.bit.GPIO10 = 1;// ePWM6A active

GpioCtrlRegs.GPAMUX1.bit.GPIO11 = 1;// ePWM6B activ

GpioCtrlRegs.GPAMUX2.all = 0;     // GPIO31 ... GPIO16 = General Purpose I/O

GpioCtrlRegs.GPBMUX1.all = 0;     // GPIO47 ... GPIO32 = General Purpose I/O

GpioCtrlRegs.GPBMUX2.all = 0;     // GPIO63 ... GPIO48 = General Purpose I/O

GpioCtrlRegs.GPCMUX1.all = 0;     // GPIO79 ... GPIO64 = General Purpose I/O

GpioCtrlRegs.GPCMUX2.all = 0;     // GPIO87 ... GPIO80 = General Purpose I/O

GpioCtrlRegs.GPADIR.all = 0;

GpioCtrlRegs.GPBDIR.all = 0;              // GPIO63-32 as inputs

GpioCtrlRegs.GPCDIR.all = 0;              // GPIO87-64 as inputs

EDIS;

}

void Setup_ePWM(void)

{

EPwm1Regs.TBCTL.bit.CLKDIV =  0;      // CLKDIV = 1

EPwm1Regs.TBCTL.bit.HSPCLKDIV = 1; // HSPCLKDIV = 1
```

```
EPwm1Regs.TBCTL.bit.CTRMODE = 2;    // up - down mode

EPwm1Regs.AQCTLA.all = 0x0060;                   // set ePWM1A on CMPA up

EPwm1Regs.AQCTLB.all = 0x0090;

EPwm1Regs.TBPRD = 37500;               // timer period for 500 KHz

                            // TBPRD = 1/2 ( 150 MHz / 500 kHz)

EPwm1Regs.CMPA.half.CMPA = EPwm1Regs.TBPRD / 2;        // 50% duty cycle first

EPwm1Regs.DBRED = 750;                          // 10 microseconds delay

 EPwm1Regs.DBFED = 750;                          // for rising and falling edge

 EPwm1Regs.DBCTL.bit.OUT_MODE = 3; // ePWM1A = RED

 EPwm1Regs.DBCTL.bit.POLSEL = 1;               // S3=1 inverted signal at ePWM1B

 EPwm1Regs.DBCTL.bit.IN_MODE = 0;    // ePWM1A = source for RED & FED


 EPwm2Regs.TBCTL.bit.CLKDIV =  0;      // CLKDIV = 1

 EPwm2Regs.TBCTL.bit.HSPCLKDIV = 1; // HSPCLKDIV = 1

 EPwm2Regs.TBCTL.bit.CTRMODE = 2;   // up - down mode

 EPwm2Regs.AQCTLA.all = 0x0060;                   // set ePWM2A on CMPA up

 EPwm2Regs.AQCTLB.all = 0x0090;

 EPwm2Regs.TBPRD = 37500;               // timer period for 500 KHz

                            // TBPRD = 1/2 ( 150 MHz / 500 kHz)

 EPwm2Regs.CMPA.half.CMPA = EPwm2Regs.TBPRD / 2;        // 50% duty cycle first

 EPwm2Regs.DBRED = 750;                             // 10 microseconds delay        */

EPwm2Regs.DBFED = 750;                             // for rising and falling edge    */

EPwm2Regs.DBCTL.bit.OUT_MODE = 3; // ePWM2A = RED                    */
```

303

```
EPwm2Regs.DBCTL.bit.POLSEL = 1;        // S3=1 inverted signal at ePWM1B */

 EPwm2Regs.DBCTL.bit.IN_MODE = 0;     // ePWM1A = source for RED & FED  */

EPwm3Regs.TBCTL.bit.CLKDIV =  0;       // CLKDIV = 1

EPwm3Regs.TBCTL.bit.HSPCLKDIV = 1; // HSPCLKDIV = 1

EPwm3Regs.TBCTL.bit.CTRMODE = 2;     // up - down mode

EPwm3Regs.AQCTLA.all = 0x0060;                    // set ePWM3A on CMPA up

EPwm3Regs.AQCTLB.all = 0x0600;

EPwm3Regs.TBPRD = 37500;                              // timer period for 500 KHz

                                 // TBPRD = 1/2 ( 150 MHz / 500 kHz)

EPwm3Regs.CMPA.half.CMPA = EPwm3Regs.TBPRD / 2;        // 50% duty cycle first

EPwm3Regs.CMPB = EPwm3Regs.TBPRD ;          // 50% duty cycle first

EPwm4Regs.TBCTL.bit.CLKDIV =  0;       // CLKDIV = 1

EPwm4Regs.TBCTL.bit.HSPCLKDIV = 1; // HSPCLKDIV = 1

EPwm4Regs.TBCTL.bit.CTRMODE = 2;     // up - down mode

EPwm4Regs.AQCTLA.all = 0x0060;                    // set ePWM4A on CMPA up

EPwm4Regs.AQCTLB.all = 0x0600;

EPwm4Regs.TBPRD = 37500;                   // timer period for 500 KHz

                                 // TBPRD = 1/2 ( 150 MHz / 500 kHz)

EPwm4Regs.CMPA.half.CMPA = EPwm4Regs.TBPRD / 2;        // 50% duty cycle first

EPwm4Regs.CMPB = EPwm4Regs.TBPRD ;          // 50% duty cycle first

 EPwm5Regs.TBCTL.bit.CLKDIV =  0;       // CLKDIV = 1                           */

 EPwm5Regs.TBCTL.bit.HSPCLKDIV = 1; // HSPCLKDIV = 1               */

 EPwm5Regs.TBCTL.bit.CTRMODE = 2;   // up - down mode             */
```

```
EPwm5Regs.AQCTLA.all = 0x0060;                    // set ePWM5A on CMPA up

EPwm5Regs.AQCTLB.all = 0x0090;

EPwm5Regs.TBPRD = 37500;                   // timer period for 500 KHz        */

                                           // TBPRD = 1/2 ( 150 MHz / 500 kHz)    */

EPwm5Regs.CMPA.half.CMPA = EPwm5Regs.TBPRD / 2;// 50% duty cycle first    */

EPwm5Regs.DBRED = 750;                              // 10 microseconds delay

EPwm5Regs.DBFED = 750;                              // for rising and falling edge

EPwm5Regs.DBCTL.bit.OUT_MODE = 3; // ePWM5A = RED

EPwm5Regs.DBCTL.bit.POLSEL = 1;                 // S3=1 inverted signal at ePWM1B

EPwm5Regs.DBCTL.bit.IN_MODE = 0;     // ePWM1A = source for RED & FED

EPwm6Regs.TBCTL.bit.CLKDIV =  0;      // CLKDIV = 1                              */

EPwm6Regs.TBCTL.bit.HSPCLKDIV = 1; // HSPCLKDIV = 1                    */

EPwm6Regs.TBCTL.bit.CTRMODE = 2;   // up - down mode                 */

EPwm6Regs.AQCTLA.all = 0x0060;          // set ePWM6A on CMPA up             */

EPwm6Regs.AQCTLB.all = 0x0090;

EPwm6Regs.TBPRD = 37500;                   // timer period for 500 KHz        */

                                           // TBPRD = 1/2 ( 150 MHz / 500 kHz)    */

EPwm6Regs.CMPA.half.CMPA = EPwm6Regs.TBPRD / 2; // 50% duty cycle first*/

EPwm6Regs.DBRED = 750;                              // 10 microseconds delay

EPwm6Regs.DBFED = 750;                              // for rising and falling edge

EPwm6Regs.DBCTL.bit.OUT_MODE = 3; // ePWM6A = RED

EPwm6Regs.DBCTL.bit.POLSEL = 1;                 // S3=1 inverted signal at ePWM1B

EPwm6Regs.DBCTL.bit.IN_MODE = 0;     // ePWM1A = source for RED & FED
```

```
EPwm1Regs.ETSEL.all = 0;

EPwm1Regs.ETSEL.bit.INTEN = 1;          // interrupt enable for ePWM1

EPwm1Regs.ETSEL.bit.INTSEL = 5;              // interrupt on CMPA down match

EPwm1Regs.ETPS.bit.INTPRD = 1;          // interrupt on first event

EPwm2Regs.ETSEL.all = 0;

EPwm2Regs.ETSEL.bit.INTEN = 1;          // interrupt enable for ePWM2

EPwm2Regs.ETSEL.bit.INTSEL = 5;              // interrupt on CMPA down match

EPwm2Regs.ETPS.bit.INTPRD = 1;          // interrupt on first event

EPwm3Regs.ETSEL.all = 0;

EPwm3Regs.ETSEL.bit.INTEN = 1;          // interrupt enable for ePWM3

EPwm3Regs.ETSEL.bit.INTSEL = 5;              // interrupt on CMPA down match

EPwm3Regs.ETPS.bit.INTPRD = 1;          // interrupt on first event

EPwm4Regs.ETSEL.all = 0;

EPwm4Regs.ETSEL.bit.INTEN = 1;          // interrupt enable for ePWM4

EPwm4Regs.ETSEL.bit.INTSEL = 5;              // interrupt on CMPA down match

EPwm4Regs.ETPS.bit.INTPRD = 1;          // interrupt on first even

 EPwm5Regs.ETSEL.all = 0;

EPwm5Regs.ETSEL.bit.INTEN = 1;          // interrupt enable for ePWM5   */

 EPwm5Regs.ETSEL.bit.INTSEL = 5;              // interrupt on CMPA down match */

 EPwm5Regs.ETPS.bit.INTPRD = 1;               // interrupt on first event     */


 EPwm6Regs.ETSEL.all = 0;

 EPwm6Regs.ETSEL.bit.INTEN = 1;                  // interrupt enable for ePWM6   */
```

```
EPwm6Regs.ETSEL.bit.INTSEL = 5;                    // interrupt on CMPA down match */

EPwm6Regs.ETPS.bit.INTPRD = 1;                     // interrupt on first event         */

}

interrupt void cpu_timer0_isr(void)

// ISR runs every 2000 ns (PWM-frequency = 500 KHz)

// and is triggered by ePWM1 compare event

// run - time of ISR is 630 ns

{

static unsigned int index=0;

static int up_down = 1;

CpuTimer0.InterruptCount++;

// Service watchdog every interrupt

 EALLOW;

SysCtrlRegs.WDKEY = 0xAA;              // Service watchdog #2

EDIS;

EPwm1Regs.CMPA.half.CMPA=EPwm1Regs.TBPRD-

_IQsat(_IQ30mpy(((0.8*sine_table[index+128])+_IQ30(0.9999))/2,EPwm1Regs.TBPRD

),EPwm1Regs.TBPRD,0);

 EPwm2Regs.CMPA.half.CMPA=EPwm2Regs.TBPRD-

_IQsat(_IQ30mpy(((0.8*sine_table[index+384])+_IQ30(0.9999))/2,EPwm2Regs.TBPRD

),EPwm2Regs.TBPRD,0);
```

```c
EPwm3Regs.CMPA.half.CMPA=EPwm3Regs.TBPRD-

_IQsat(_IQ30mpy(((0.8*sine_table[index])+_IQ30(0.9999))/2,EPwm3Regs.TBPRD),EP

wm3Regs.TBPRD,0);

EPwm3Regs.CMPB=EPwm3Regs.TBPRD-

_IQsat(_IQ30mpy(((0.8*sine_table[index+256])+_IQ30(0.9999))/2,EPwm3Regs.TBPRD

),EPwm3Regs.TBPRD,0);

EPwm4Regs.CMPA.half.CMPA=EPwm4Regs.TBPRD-

_IQsat(_IQ30mpy(((0.8*sine_table[index+64])+_IQ30(0.9999))/2,EPwm4Regs.TBPRD)

,EPwm4Regs.TBPRD,0);

EPwm4Regs.CMPB=EPwm4Regs.TBPRD-

_IQsat(_IQ30mpy(((0.8*sine_table[index+320])+_IQ30(0.9999))/2,EPwm4Regs.TBPRD

),EPwm4Regs.TBPRD,0);

 EPwm5Regs.CMPA.half.CMPA=EPwm5Regs.TBPRD-

_IQsat(_IQ30mpy(((0.8*sine_table[index+192])+_IQ30(0.9999))/2,EPwm5Regs.TBPRD

),EPwm5Regs.TBPRD,0);

EPwm6Regs.CMPA.half.CMPA=EPwm6Regs.TBPRD-

_IQsat(_IQ30mpy(((0.8*sine_table[index])+_IQ30(0.9999))/2,EPwm6Regs.TBPRD),EP

wm6Regs.TBPRD,0);

    index +=1;        // use next element out of lookup table

   if (index >511) index = 0;

EPwm1Regs.ETCLR.bit.INT = 1;            // Clear ePWM1 Interrupt flag

EPwm2Regs.ETCLR.bit.INT = 1;            // Clear ePWM2 Interrupt flag

EPwm3Regs.ETCLR.bit.INT = 1;             // Clear ePWM3 Interrupt flag
```

```c
EPwm4Regs.ETCLR.bit.INT = 1;          // Clear ePWM4 Interrupt flag

EPwm5Regs.ETCLR.bit.INT = 1;          // Clear ePWM5 Interrupt flag

EPwm6Regs.ETCLR.bit.INT = 1;          // Clear ePWM6 Interrupt flag

// Acknowledge this interrupt to receive more interrupts from group 3

  if(up_down)

{

if(EPwm1Regs.CMPA.half.CMPA          <          EPwm1Regs.TBPRD)

EPwm1Regs.CMPA.half.CMPA++;

else up_down = 0;

}

else

{

if(EPwm1Regs.CMPA.half.CMPA > 0) EPwm1Regs.CMPA.half.CMPA--;

else up_down = 1;

}

if(up_down)

{

if(EPwm2Regs.CMPA.half.CMPA          <          EPwm2Regs.TBPRD)

EPwm2Regs.CMPA.half.CMPA++;

else up_down = 0;

}

else

{
```

```c
if(EPwm2Regs.CMPA.half.CMPA > 0) EPwm2Regs.CMPA.half.CMPA--;

else up_down = 1;

}

if(up_down)

{

if(EPwm5Regs.CMPA.half.CMPA                <                EPwm5Regs.TBPRD)

EPwm5Regs.CMPA.half.CMPA++;

else up_down = 0;

}

else

{

if(EPwm5Regs.CMPA.half.CMPA > 0) EPwm5Regs.CMPA.half.CMPA--;

else up_down = 1;

}

if(up_down)

{

if(EPwm6Regs.CMPA.half.CMPA                <                EPwm6Regs.TBPRD)

EPwm6Regs.CMPA.half.CMPA++;

else up_down = 0;

}

else

{

if(EPwm6Regs.CMPA.half.CMPA > 0) EPwm6Regs.CMPA.half.CMPA--;
```

```
        else up_down = 1;

    }

    PieCtrlRegs.PIEACK.all = PIEACK_GROUP1;

}
```

//==================================================================

=============

// End of SourceCode.

//==================================================================

=============

# APPENDIX E

## HARMONIC BALANCE TECHNIQUE AVERAGE AND RIPPLE

## COMPONENTS DERIVATION

In general, a repetitive non sinusoidal waveform f(t) repeating with an constant frequency ω can be expressed as

$$f(t) = F_o + \sum_{h=1}^{\infty} f_h(t) = \frac{1}{2}a_o + \sum_{h=1}^{\infty}\{a_h\cos(h\omega t) + b_h\sin(h\omega t)\}$$

(E.1)

where $F_o = \frac{1}{2}a_o$ is the average value,

$$a_h = \frac{1}{\pi}\int_0^{2\pi} f(t)\cos(h\omega t)d(\omega t) \qquad h = 0,...,\infty$$

(E.2)

$$b_h = \frac{1}{\pi}\int_0^{2\pi} f(t)\sin(h\omega t)d(\omega t) \qquad h = 0,...,\infty$$

(E.3)

where the RMS magnitude

$$F_h = \frac{\sqrt{a_h^2 + b_h^2}}{\sqrt{2}}$$

(E.4)

and phase $\phi_h$ is given by

$$\tan(\phi_h) = \frac{b_h}{a_h}$$

(E.5)

The Fourier analysis for switching function is shown as below:

for $a_h$

$$a_h = \frac{1}{\pi h}\left[\sin\left(\frac{1}{2}h(-2\phi - \pi + D\pi)\right) + \sin\left(\frac{1}{2}h(2\phi + \pi + D\pi)\right) - \sin\left(\frac{1}{2}h(-2\phi - 3\pi + D\pi)\right) - \sin\left(\frac{1}{2}h(2\phi + 3\pi + D\pi)\right)\right]$$

(E.6)

when h is odd:

$$a_h = \frac{1}{\pi h}\left[\sin\left(-\frac{h\pi}{2}\right)\cos\left(\frac{1}{2}h(D\pi - 2\phi)\right) + \sin\left(\frac{h\pi}{2}\right)\cos\left(\frac{1}{2}h(2\phi + D\pi)\right) - \sin\left(-\frac{3h\pi}{2}\right)\cos\left(\frac{1}{2}h(D\pi - 2\phi)\right) - \sin\left(\frac{3h\pi}{2}\right)\cos\left(\frac{1}{2}h(2\phi + D\pi)\right)\right] \quad (E.7)$$

when h is even:

$$a_h = \frac{1}{\pi h}\left[\cos\left(-\frac{h\pi}{2}\right)\sin\left(\frac{1}{2}h(D\pi - 2\phi)\right) + \cos\left(\frac{h\pi}{2}\right)\sin\left(\frac{1}{2}h(2\phi + D\pi)\right) - \cos\left(-\frac{3h\pi}{2}\right)\sin\left(\frac{1}{2}h(D\pi - 2\phi)\right) - \cos\left(\frac{3h\pi}{2}\right)\sin\left(\frac{1}{2}h(2\phi + D\pi)\right)\right] \quad (E.8)$$

Further we can get

When h is odd:

$$a_h = \frac{2}{\pi h}\left(-\sin\frac{h\pi}{2} - \sin\frac{h\pi}{2}\right)\sin\frac{hD\pi}{2}\sin h\phi \quad (E.9)$$

When h is even:

$$a_h = \frac{2}{\pi h}\left(\cos\frac{h\pi}{2} - \cos\frac{h\pi}{2}\right)\sin\frac{hD\pi}{2}\cosh\phi \quad (E.10)$$

Therefore,

$$a_h = \begin{cases} -\frac{4}{\pi h}\sin\frac{h\pi}{2}\sin\frac{hD\pi}{2}\sin h\phi, & for \ h = 1, 3, 5, 7, \cdots \\ 0, & for \ h = 2, 4, 6, 8, \cdots \end{cases} \quad (E.11)$$

Similarly, we can get the expression of $b_h$

$$b_h = \frac{1}{\pi h}\left[\cos\left(\frac{1}{2}h(-2\phi - \pi + D\pi)\right) - \cos\left(\frac{1}{2}h(2\phi + \pi + D\pi)\right) - \cos\left(\frac{1}{2}h(-2\phi - 3\pi + D\pi)\right) + \cos\left(\frac{1}{2}h(2\phi + 3\pi + D\pi)\right)\right] \quad (E.12)$$

when h is even:

$$b_h = \frac{1}{\pi h}\left[\left(\cos\left(\frac{h\pi}{2}\right) - \cos\left(\frac{3h\pi}{2}\right)\right)\left(\cos\left(\frac{1}{2}h(D\pi - 2\phi)\right) - \cos\left(\frac{1}{2}h(2\phi + D\pi)\right)\right)\right] \quad (E.13)$$

when h is odd:

$$b_h = \frac{1}{\pi h}\left[\left(\sin\frac{h\pi}{2} - \sin\frac{3h\pi}{2}\right)\left(\sin\left(\frac{1}{2}h(D\pi - 2\phi)\right) + \sin\left(\frac{1}{2}h(2\phi + D\pi)\right)\right)\right] \quad (E.14)$$

when h is odd:

$$b_h = \frac{4}{\pi h}\sin\frac{h\pi}{2}\sin\frac{1}{2}hD\pi\cos h\phi \tag{E.15}$$

when h is even:

$$b_h = 0 \tag{E.16}$$

Therefore,

$$b_h = \begin{cases} \dfrac{4}{\pi h}\sin\dfrac{h\pi}{2}\sin\dfrac{1}{2}hD\pi\cos h\phi, & h = 1,3,5,7,\cdots \\ 0, & h = 2,4,6,8,\cdots \end{cases} \tag{E.17}$$

Thus the components of the Fourier analysis are expressed as below:

$$b_h = \frac{4}{\pi h}\sin\frac{h\pi}{2}\sin\frac{1}{2}hD\pi\cos h\phi \tag{E.18}$$

$$a_0 = 0 \tag{E.19}$$

$$a_h = \begin{cases} -\dfrac{4}{\pi h}\sin\dfrac{h\pi}{2}\sin\dfrac{hD\pi}{2}\sin h\phi, & for\ h = 1,3,5,7,\cdots \\ 0, & for\ h = 2,4,6,8,\cdots \end{cases} \tag{E.20}$$

$$b_h = \begin{cases} \dfrac{4}{\pi h}\sin\dfrac{h\pi}{2}\sin\dfrac{1}{2}hD\pi\cos h\phi, & h = 1,3,5,7,\cdots \\ 0, & h = 2,4,6,8,\cdots \end{cases} \tag{E.21}$$

Therefore the general expression can be written by

$$c_h = \frac{4}{\pi}\sum_{h=1}^{n}\left[\frac{1}{h}\sin\left(\frac{h\pi}{2}\right)\sin\left(\frac{1}{2}hD\pi\right)\cos(h\phi)\sin(h\theta) - \sin\left(\frac{h\pi}{2}\right)\sin\left(\frac{hD\pi}{2}\right)\sin(h\phi)\cos(h\theta)\right] \tag{E.22}$$
$$h = 1,3,5,7,\cdots$$

Where the RMS magnitude is

$$\overline{F_h} = \frac{\sqrt{a_1^2 + b_1^2}}{\sqrt{2}} = \frac{1}{\sqrt{2}}\frac{4}{\pi h}\sin\frac{hD\pi}{2} \tag{E.23}$$

and phase $\phi_h$ is given by

314

$$\tan(\phi_h) = c \tan(\frac{\pi}{2} - h\phi)$$ (E.24)

$$\phi_h = \frac{\pi}{2} - h\phi$$

For the first fundamental component, it can be represented as,

$$F_1 = a_1 \cosh\theta + b_1 \sinh\theta$$ (E.25)

$$a_1 = \frac{4}{\pi}\sin\left(\frac{\pi}{2}\right)\sin\left(\frac{1}{2}D\pi\right)\cos(\phi)$$

$$b_1 = \frac{4}{\pi}\sin\left(\frac{\pi}{2}\right)\sin\left(\frac{D\pi}{2}\right)\sin(\phi)$$

Hence the complex form is shown as below:

$$F_1 = F_f e^{j\phi_f}$$ (E.26)

**PCB SCHEMATICS AND DESIGNS**

*DRIVER CIRCUIT:*

Every bidirectional switch needs a gate driver to turn on and off the switch. The gate driver component that is used to drive the bidirectional switches is MC33153P. The gate driver circuit also consists of optocoupler TLP 350 which isolates the voltages and currents on the bidirectional switch and DSP. Some other zener diodes, resistors, capacitors and LEDs are used in this driver circuit. The schematic of the driver circuit is shown in Figure F.1 and also the top and bottom layers of diptrace design are shown in Figure F.2 and Figure F.3 respectively. The circuit board is printed and the components are soldered on the printed circuit board (PCB) and the picture of the driver circuit while it's turned on is shown in Figure F.4.
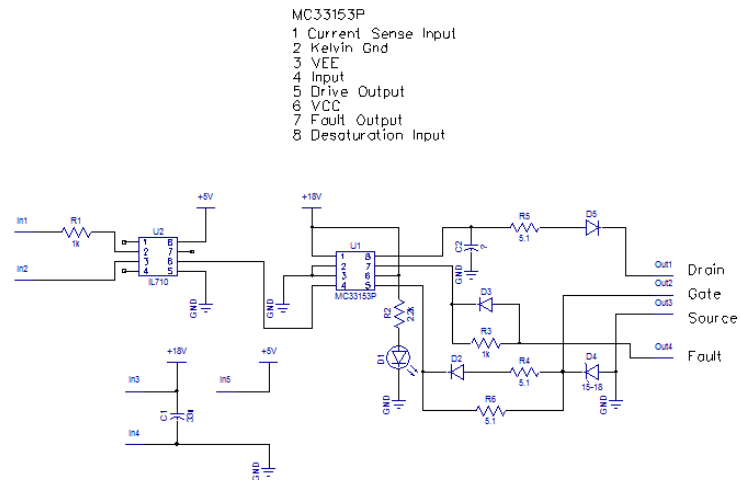


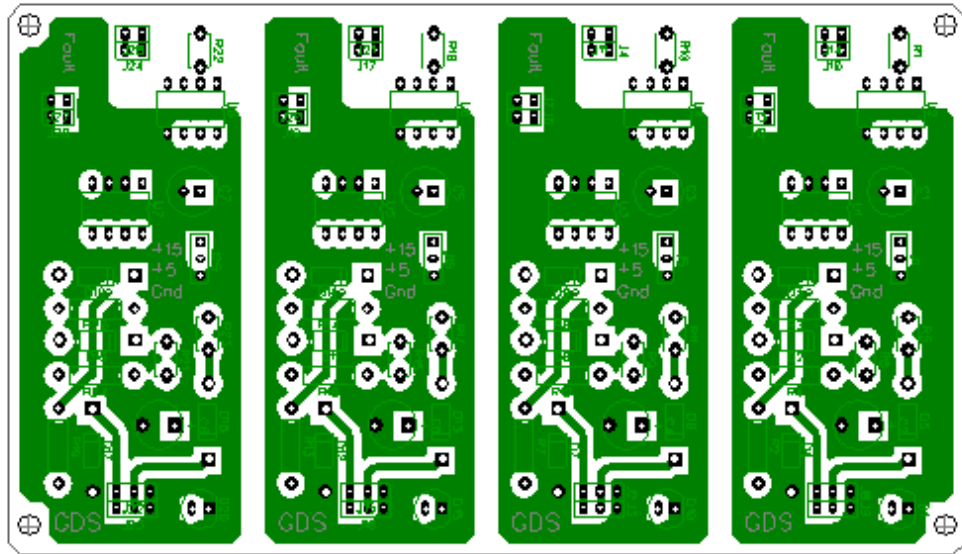Figure F.1 Schematic of driver circuit

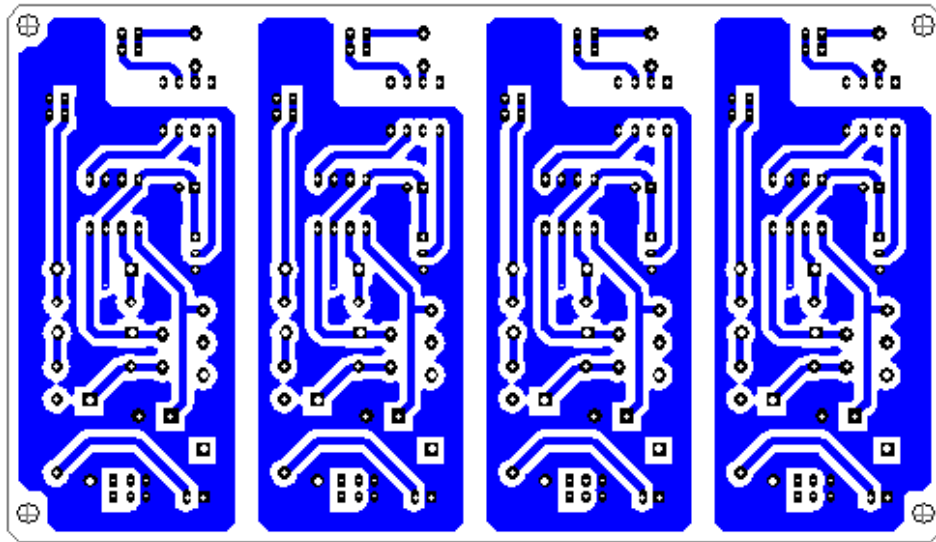Figure F.2 Top layer of Diptrace design of driver circuit.



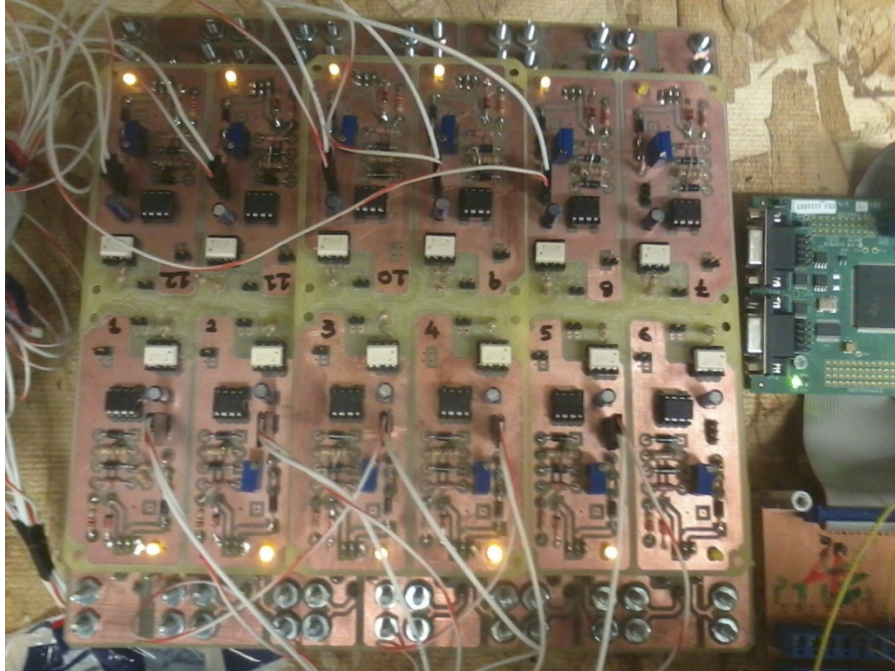Figure F.3 Bottom layer of Diptrace design of driver circuit

Figure F.4 Laboratory setup of driver circuit.

## ISOLATED DC POWER SUPPLY

Each driver circuit requires a minimum of 15V and it can work up to the maximum voltage of 24V. In order to make these switches work independently, for each switch an isolated power supply is needed. Since it would be difficult to get many individual DC power supplies, an isolated power supply circuit is built to supply DC voltage to the driver circuit. The schematic of isolated power circuit is shown in Figure F.5. The diptrace design of isolated power circuit is shown in Figure F.6 and the laboratory prototype is shown in Figure F.7.
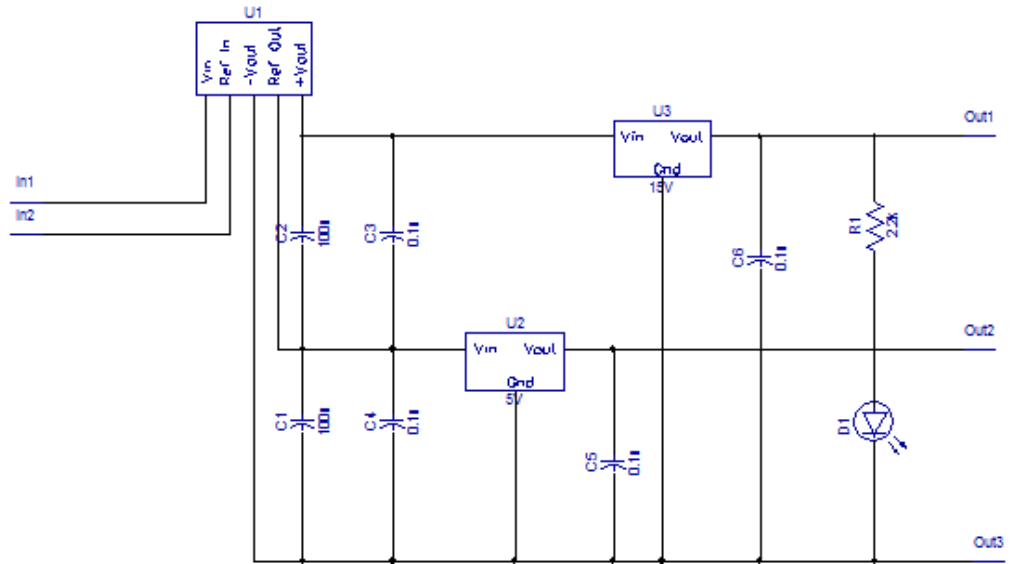
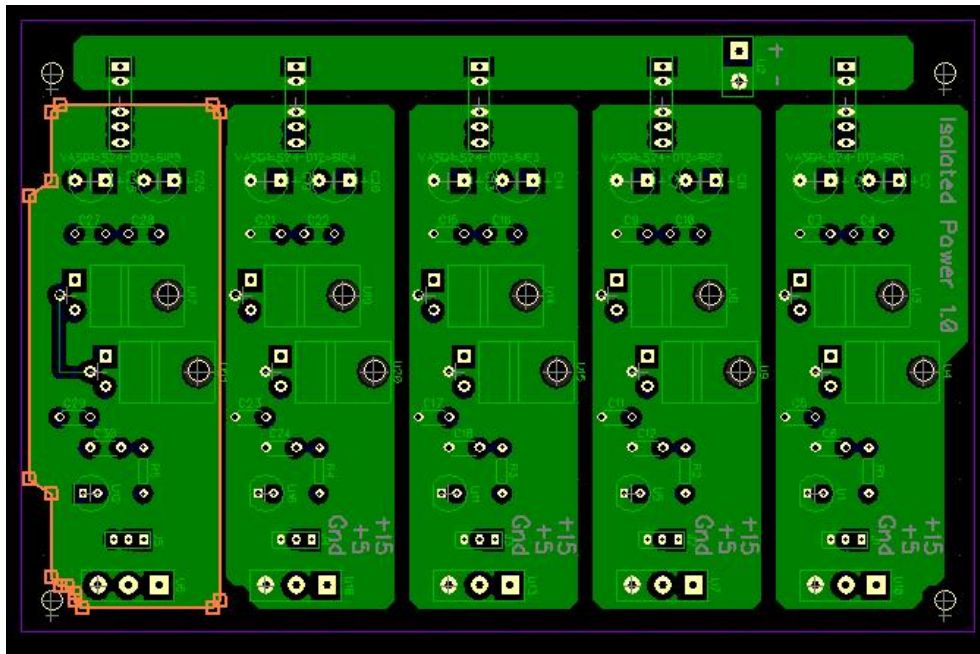Figure F.5 Schematic of isolated power circuit.



Figure F.6 PCB design of top layer of isolated power circuit

Figure F.7 Laboratory prototype of isolated power circuit.

## *POWER CIRCUIT FOR MULTILEVEL INVERTER*

The main circuit of switches is shown in the diptrace design in Figure F.8. Each switch is built individually so that they can be used to any circuit later. All these circuits driver circuit, power circuit and isolated power circuit are connected together and are shown in laboratory prototype in Figure F.9.
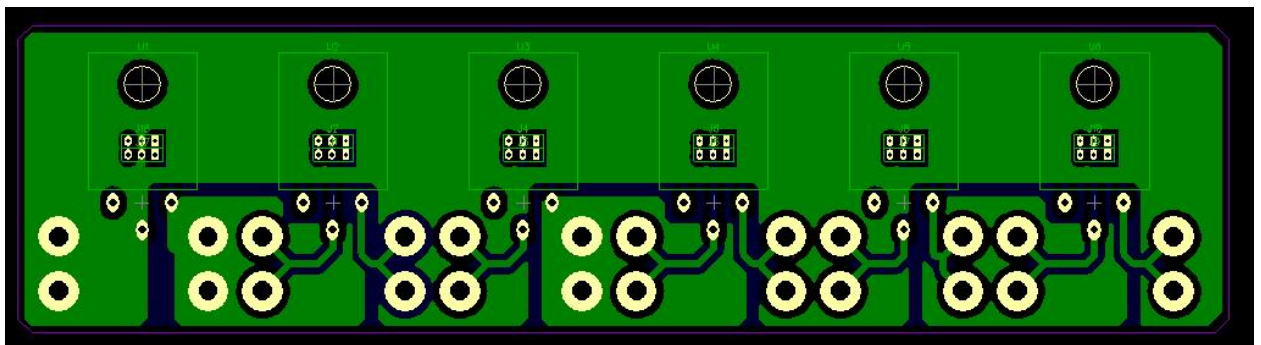


Figure F.8 Diptrace PCB design of power circuit.

Figure F.9 Overall circuit of multistring multi-level inverter

### SENSOR DESIGNS:

The AC current and voltage sensors are designed for the getting closed loop feedback signals. These signals will be sent in the Analog to Digital Converter (ADC) of the DSP. The printed circuit board design is done using Novarm Diptrace software and the designs of both the current and voltage sensors are shown in Figure F.10 and Figure F.11 respectively.
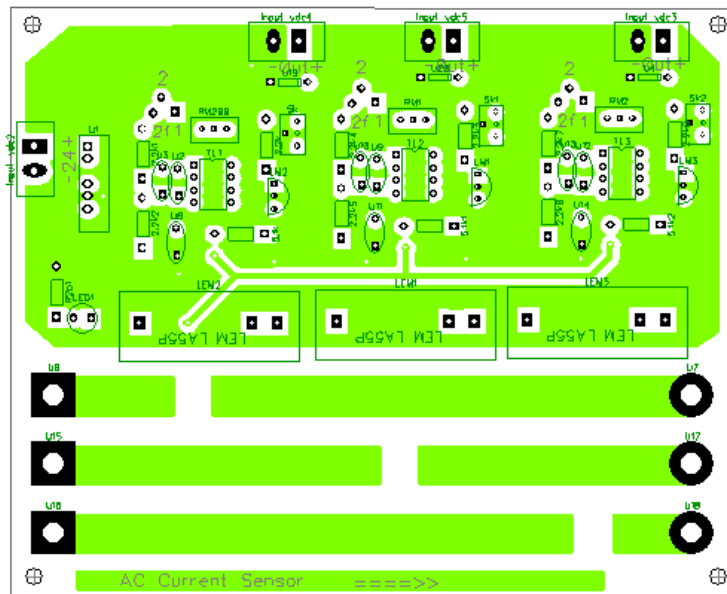
Figure F.10. Diptrace design of three AC current sensors
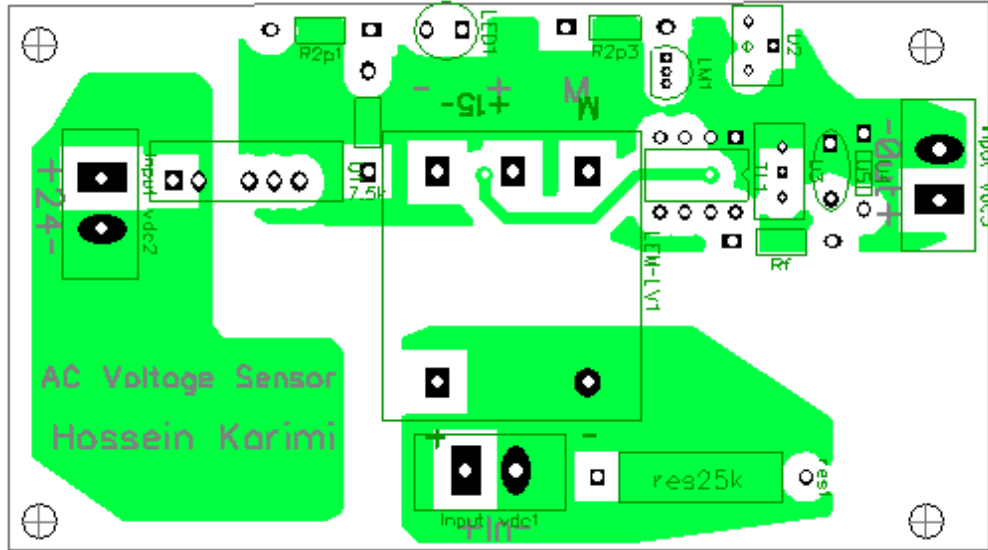


Figure F.11 Diptrace design of Voltage sensor.

## DEAD TIME CIRCUIT

The importance of the dead time circuit is that it generates a short delay between the two complementary switches. This is to make sure that the complementary switches are not turning on together at any point of time. The schematic of dead time circuit is shown in Figure F.12 and the printed circuit board design using Novarm's diptrace software is shown in Figure F.13.



Figure F.12 Dead time circuit schematic

Figure F.13 Dead time circuit diptrace PCB design.

## *COMPLEMENTARY CIRCUIT:*

The DSP has few general purpose input ouput (GPIO) pins to generate PWM signals. The four cell cascaded converter requires 16 PWM signals and DSP F28335 can generate maximum of 12 PWM signals. Hence complementary circuit is designed so the signals that needs to be complemented can be sent through this circuit. The schematic of the complementary circuit is shown in Figure F.14 and the printed circuit board design using Novarm's diptrace software is shown in Figure F.15.

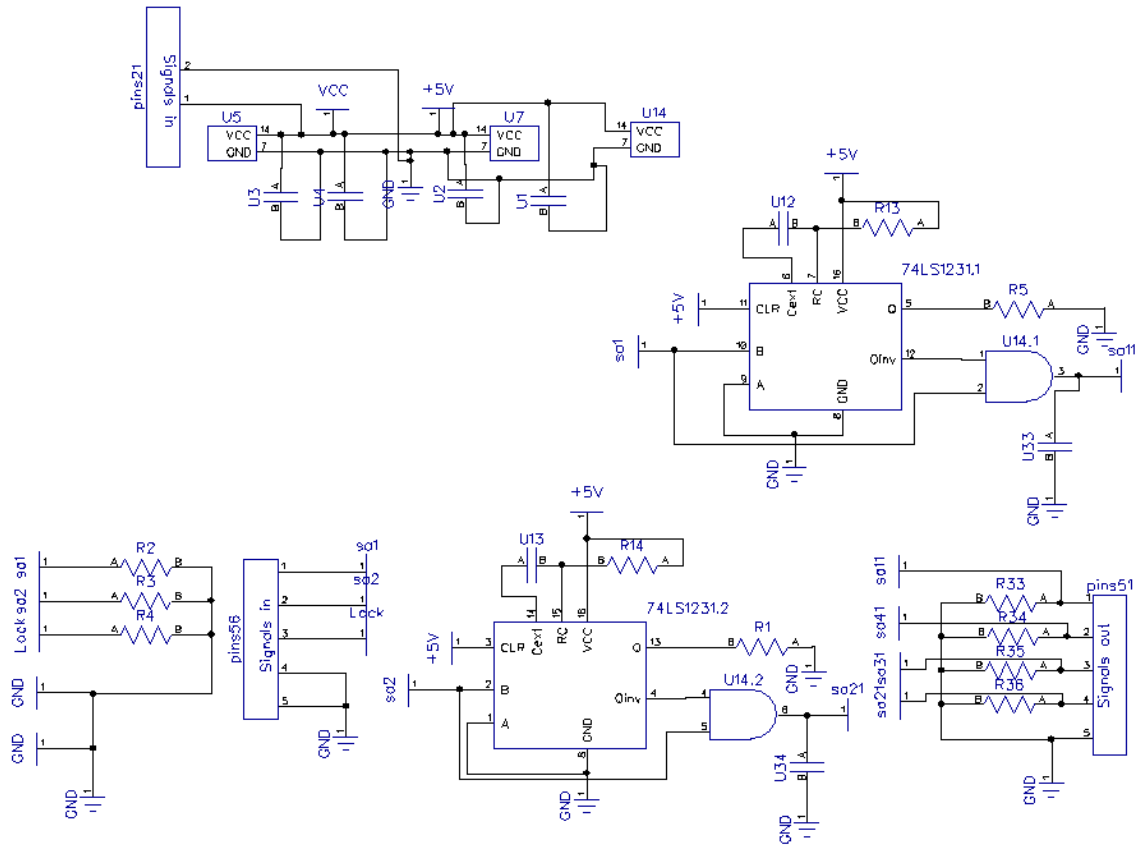Figure F.14 Schematic of the complementary circuit
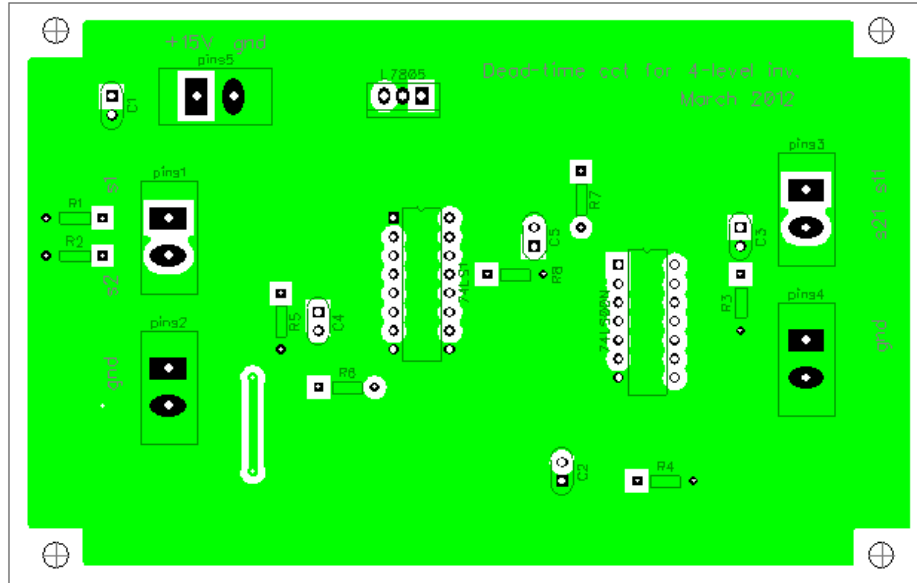


Figure F.15 Diptrace PCB design of complementary circuit.

## CANCELLATION OF ODD CARRIER AND ASSOCIATED HARMONICS AS WELL AS EVEN BASE BAND AND SIDE BAND HARMONICS

The harmonic spectrum of a general carrier-based PWM wave can be expressed in its most general form as:

$$f(x, y) = \frac{A_{oo}}{2} + \sum_{n=1}^{\infty} \{A_{on} \cos(ny) + B_{on} \sin(ny)\} + \sum_{m=1}^{\infty} \{A_{mo} \cos(my) + B_{mo} \sin(my)\}$$
$$+ \sum_{m=1}^{\infty} \sum_{\substack{n=-\infty \\ (n \neq 0)}}^{\infty} \{A_{mn} \cos(mx + ny) + B_{mn} \sin(mx + ny)\}$$

Where $m$ and $n$ represent multiples of the carrier frequency and multiples of the fundamental frequency. The coefficients can be expressed as:

$$x = \omega_c t + \theta_c$$
$$y = \omega_o t + \theta_o$$

And the complex coefficients are given as:

$$A_{mn} + jB_{mn} = \frac{1}{2\pi^2} \int_{-\pi}^{\pi} \int_{-\pi}^{\pi} \{f(x, y)e^{j(mx+ny)}\} dx dy$$

The Fourier series representation of the voltage between point $a$ and $o$ can be expressed as:

$$V_{ao} = \frac{V_{dc}}{2} + \frac{V_{dc}}{2} M \cos y + \frac{2V_{dc}}{\pi} \sum_{m=1}^{\infty} \sum_{n=-\infty}^{\infty} \frac{1}{m} J_n(\frac{m\pi}{2} M) \sin\left(\frac{\pi}{2}(m+n)\right) \cos(mx + ny)$$

Similarly, between $b$ and $o$ is,

$$V_{bo} = \frac{V_{dc}}{2} + \frac{V_{dc}}{2} M \cos(y - \pi) + \frac{2V_{dc}}{\pi} \sum_{m=1}^{\infty} \sum_{n=-\infty}^{\infty} \frac{1}{m} J_n(\frac{m\pi}{2} M) \sin\left(\frac{\pi}{2}(m+n)\right) \cos(mx + n(y - \pi))$$

The line to line voltage between $a$ and $b$ is calculated to be

$$V_{ab} = V_{az} - V_{bz} = V_{dc} M \cos y + \frac{2V_{dc}}{\pi} \sum_{m=1}^{\infty} \sum_{n=-\infty}^{\infty} \frac{1}{m} J_n\left(\frac{m\pi}{2} M\right) \underbrace{\sin\left(\frac{\pi}{2}(m+n)\right)}_{*} \underbrace{\left(\begin{array}{c} \cos(mx+ny) \\ -\cos(mx+n(y-\pi)) \end{array}\right)}_{**}$$

From the above expression lets notice on the following two terms,

$$\cos(mx+ny) - \cos(mx+n(y-\pi)) = \cos(mx+ny) - \{\cos(mx+ny)\cos(n\pi) + \sin(mx+ny)\sin(n\pi)))\}$$

$$= \cos(mx+ny) - \cos(mx+ny)\cos(n\pi)$$

$$= \begin{cases} 2\cos(mx+ny), & n-odd \\ 0 & n-even \end{cases}$$

This implies there are no even base band and side band harmonics in the line to line

voltage

Since the n must be odd to have a non-zero value and considering the terms

$$\sin\left(\frac{\pi}{2}(m+n)\right) = \begin{cases} 1/-1, & m-even \\ 0, & m-odd \end{cases}$$

This implies there are no odd carrier harmonics in the line to line voltage

**Note:**

- Odd carrier and associated side harmonics are completely cancelled in the output line-to-line voltage.
- Only odd sideband harmonics around the even carrier groups presents in the line-to-line voltage

The expression can be simplified as:

$$V_{ab} = V_{dc} M \cos y + \frac{4V_{dc}}{\pi} \sum_{m=2}^{\infty} \sum_{n=-\infty}^{\infty} \frac{1}{m} J_n(\frac{m\pi}{2} M) \sin\left(\frac{\pi}{2}(m+n)\right) \cos(mx+ny)$$

**Cascaded-single phase converters Fourier series**

Converter 1

$$x = \omega_c t = \theta_c + \gamma_1 \qquad\qquad M = M_1$$
$$y = \theta_e + \theta_1 \qquad\qquad V_{dc} = V_{dc1}$$

$$V_a = V_{dc1} M_1 \cos(\theta_e + \theta_1) + \frac{4V_{dc1}}{\pi} \sum_{m=2}^{\infty} \sum_{n=-\infty}^{\infty} \frac{1}{m} J_n(\frac{m\pi}{2} M_1) \sin\left(\frac{\pi}{2}(m+n)\right) \cos(m(\theta_c + \gamma_1) + n(\theta_e + \theta_1))$$

Converter 2

$$x = \omega_c t = \theta_c + \gamma_2 \qquad\qquad M = M_2$$
$$y = \theta_e + \theta_2 \qquad\qquad V_{dc} = V_{dc2}$$

$$V_b = V_{dc2} M_2 \cos(\theta_e + \theta_2) + \frac{4V_{dc2}}{\pi} \sum_{m=2}^{\infty} \sum_{n=-\infty}^{\infty} \frac{1}{m} J_n(\frac{m\pi}{2} M_2) \sin\left(\frac{\pi}{2}(m+n)\right) \cos(m(\theta_c + \gamma_2) + n(\theta_e + \theta_2))$$

Converter 3

$$x = \omega_c t = \theta_c + \gamma_3 \qquad\qquad M = M_3$$
$$y = \theta_e + \theta_3 \qquad\qquad V_{dc} = V_{dc3}$$

$$V_c = V_{dc3} M_3 \cos(\theta_e + \theta_3) + \frac{4V_{dc3}}{\pi} \sum_{m=2}^{\infty} \sum_{n=-\infty}^{\infty} \frac{1}{m} J_n(\frac{m\pi}{2} M_3) \sin\left(\frac{\pi}{2}(m+n)\right) \cos(m(\theta_c + \gamma_3) + n(\theta_e + \theta_3))$$

Converter 4

$$x = \omega_c t = \theta_c + \gamma_4 \qquad\qquad M = M_4$$
$$y = \theta_e + \theta_4 \qquad\qquad V_{dc} = V_{dc4}$$

$$V_d = V_{dc4} M_4 \cos(\theta_e + \theta_4) + \frac{4V_{dc4}}{\pi} \sum_{m=2}^{\infty} \sum_{n=-\infty}^{\infty} \frac{1}{m} J_n(\frac{m\pi}{2} M_4) \sin\left(\frac{\pi}{2}(m+n)\right) \cos(m(\theta_c + \gamma_4) + n(\theta_e + \theta_4))$$

Generally for the $k^{th}$ cell,

$$x = \omega_c t = \theta_c + \gamma_k \qquad\qquad M = M_4$$
$$y = \theta_e + \theta_k \qquad\qquad V_{dc} = V_{dc4}$$

$$V_k = V_{dck} M_k \cos(\theta_e + \theta_k) + \frac{4V_{dck}}{\pi} \sum_{m=2}^{\infty} \sum_{n=-\infty}^{\infty} \frac{1}{m} J_n(\frac{m\pi}{2} M_k) \sin\left(\frac{\pi}{2}(m+n)\right) \cos(m(\theta_c + \gamma_k) + n(\theta_e + \theta_k))$$

The total voltage can be expressed as:

$$V_o = V_a + V_b + V_c + V_4$$

The fundamental component of the output voltage is given as:

$$V_{o,fund} = V_{dc1} M_1 \cos(\theta_e + \theta_1) + V_{dc2} M_2 \cos(\theta_e + \theta_2) + V_{dc3} M_3 \cos(\theta_e + \theta_3) + V_{dc4} M_4 \cos(\theta_e + \theta_4)$$

The harmonic component of the output voltage is given as:

328

$$V_{o,harmonic} = \frac{4V_{dc1}}{\pi} \sum_{m=2}^{\infty} \sum_{n=-\infty}^{\infty} \frac{1}{m} J_n(\frac{m\pi}{2} M_1) \sin\left(\frac{\pi}{2}(m+n)\right) \cos(m(\theta_c + \gamma_1) + n(\theta_e + \theta_1)) +$$

$$\frac{4V_{dc2}}{\pi} \sum_{m=2}^{\infty} \sum_{n=-\infty}^{\infty} \frac{1}{m} J_n(\frac{m\pi}{2} M_2) \sin\left(\frac{\pi}{2}(m+n)\right) \cos(m(\theta_c + \gamma_2) + n(\theta_e + \theta_2)) +$$

$$\frac{4V_{dc3}}{\pi} \sum_{m=2}^{\infty} \sum_{n=-\infty}^{\infty} \frac{1}{m} J_n(\frac{m\pi}{2} M_3) \sin\left(\frac{\pi}{2}(m+n)\right) \cos(m(\theta_c + \gamma_3) + n(\theta_e + \theta_3)) +$$

$$\frac{4V_{dc4}}{\pi} \sum_{m=2}^{\infty} \sum_{n=-\infty}^{\infty} \frac{1}{m} J_n(\frac{m\pi}{2} M_4) \sin\left(\frac{\pi}{2}(m+n)\right) \cos(m(\theta_c + \gamma_4) + n(\theta_e + \theta_4))$$

The first and third harmonics around the second carrier can be considered as the dominant frequencies and determined as follows.

The first harmonics in both sides of the second carrier is given as

$$V_{o1}^+ = -\frac{2V_{dc1}}{\pi} J_1(\pi M_1) \cos(2(\theta_c + \gamma_1) + (\theta_e + \theta_1)) - \frac{2V_{dc2}}{\pi} J_1(\pi M_2) \cos(2(\theta_c + \gamma_2) + (\theta_e + \theta_2)) -$$

$$\frac{2V_{dc3}}{\pi} J_1(\pi M_3) \cos(2(\theta_c + \gamma_3) + (\theta_e + \theta_3)) - \frac{2V_{dc4}}{\pi} J_1(\pi M_4) \cos(2(\theta_c + \gamma_4) + (\theta_e + \theta_4))$$

From the following identity property

$$J_{-n}(x) = (-1)^{-n} J_n(x)$$

$$V_{o1}^- = \frac{2V_{dc1}}{\pi} J_1(\pi M_1) \cos(2(\theta_c + \gamma_1) - (\theta_e + \theta_1)) + \frac{2V_{dc2}}{\pi} J_1(\pi M_2) \cos(2(\theta_c + \gamma_2) - (\theta_e + \theta_2)) +$$

$$\frac{2V_{dc3}}{\pi} J_1(\pi M_3) \cos(2(\theta_c + \gamma_3) - (\theta_e + \theta_3)) + \frac{2V_{dc4}}{\pi} J_1(\pi M_4) \cos(2(\theta_c + \gamma_4) - (\theta_e + \theta_4))$$

Similarly two third harmonics around both sides of the second carrier is given as

$$V_{o3}^+ = -\frac{2V_{dc1}}{\pi} J_3(\pi M_1) \cos(2(\theta_c + \gamma_1) + 3(\theta_e + \theta_1)) - \frac{2V_{dc2}}{\pi} J_3(\pi M_2) \cos(2(\theta_c + \gamma_2) + 3(\theta_e + \theta_2)) -$$

$$\frac{2V_{dc3}}{\pi} J_3(\pi M_3) \cos(2(\theta_c + \gamma_3) + 3(\theta_e + \theta_3)) - \frac{2V_{dc4}}{\pi} J_3(\pi M_4) \cos(2(\theta_c + \gamma_4) + 3(\theta_e + \theta_4))$$

$$V_{o3}^- = \frac{2V_{dc1}}{\pi} J_3(\pi M_1) \cos(2(\theta_c + \gamma_1) - 3(\theta_e + \theta_1)) + \frac{2V_{dc2}}{\pi} J_3(\pi M_2) \cos(2(\theta_c + \gamma_2) - 3(\theta_e + \theta_2)) +$$

$$\frac{2V_{dc3}}{\pi} J_3(\pi M_3) \cos(2(\theta_c + \gamma_3) - 3(\theta_e + \theta_3)) + \frac{2V_{dc4}}{\pi} J_3(\pi M_4) \cos(2(\theta_c + \gamma_4) - 3(\theta_e + \theta_4))$$

## VITA

Bhanu Naga V Angirekula was born in Vijayawada, Andhra Pradesh, India. He received his Bachelor of Science degree in Electrical and Electronics Engineering from Jawaharlal Nehru Technological University (JNTUHCEH), Hyderabad, India in April 2011. In September 2011, he joined the Master's program at Tennessee Technological University and by January he has published 3 articles in well reputed peer-reviewed conferences. He worked as an Electrical Engineering Intern with Bloom Energy while doing his Master's program and he is now towards completing his Master's Degree in Electrical and Computer Engineering in May 2014. His research interests include Power Electronics Converters, Renewable Energy Systems and Control Systems.